Adaptive design of flood defence systems

Incorporating adaptive design methods to cope with sea level rise uncertainty in a system-to-structure approach in the Rhine-Meuse estuary

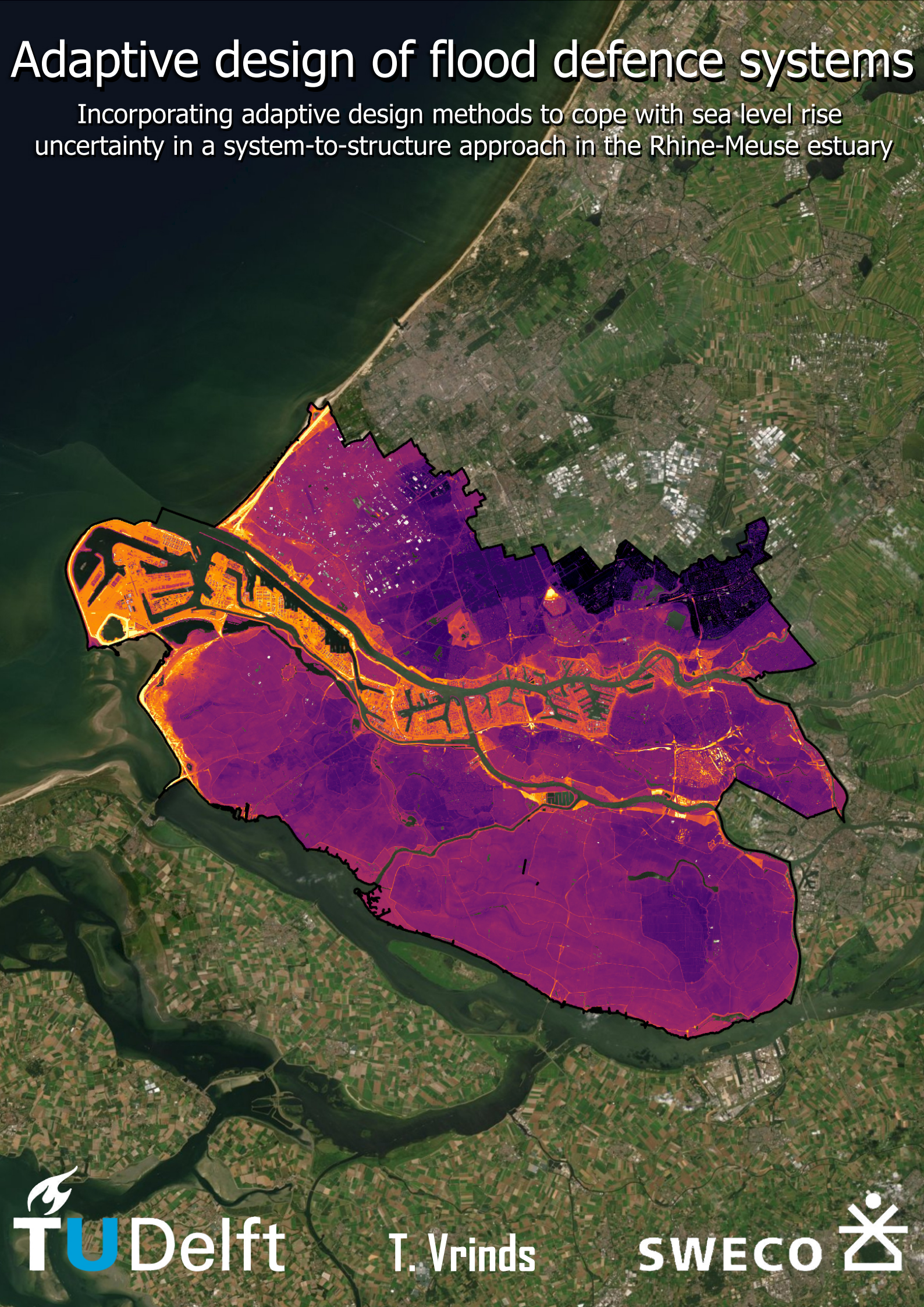

TU Delft

T. Vrinds

SWECO

ADAPTIVE DESIGN OF FLOOD DEFENCE SYSTEMS

by

T. Vrinds

to obtain the degree of Master of Science in Civil Engineering
at the Delft University of Technology
to be defended publicly on October 29, 2021

Student number:	4298608	
Date:	October 18, 2021	
Thesis committee	Prof. Dr. Ir. S. N. Jonkman	TU Delft (Chair)
	Dr. ing. M.Z. Voorendt	TU Delft
	Dr. Ir. J.S. Timmermans	TU Delft
	Ir. R. P. Roggeveld	Sweco

An electronic version of this thesis is available at: `https://repository.tudelft.nl/`.

Preface

This Msc. thesis concludes my masters in Structural Engineering with a specialisation in Hydraulic Structures at the faculty of Civil Engineering and Geosciences at the Delft University of Technology. During both the bachelor and master I gained a broad understanding of a wide variety of engineering aspects which eventually narrowed down to a focus on flood defences. Working part time at a consultancy company during my last year of my bachelors and first year of my masters opened an abstract way of thinking. Having enjoyed thinking outside of the box lead to a preference to no be hindered by instated rules, which coincides my natural stubbornness, and is symbolised by a great part of my thesis work.

Moreover, I would like to thank Sweco for offering me their support throughout the project and special thanks to Richard Roggeveld for his enthusiastic, supportive and abstract way of thinking, providing me and each other, with interesting, both (non-)related to the subject at hand, matter to discuss.

Furthermore, I would like to thank Mark Voorendt, Bas Jonkman and Jos Timmermans for being in my committee, providing me with their support, critical comments and helping me along the way. Thank you for your far reaching interest and time.

Lastly, I would like to thank my friends, roommates and, especially, my parents for their ever lasting support.

- T. Vrinds, October 18, 2021, Rotterdam -

Summary

Climate change is increasingly becoming more impactful on our society. Recent events such as the extreme rainfall in the summer of 2021 in Germany, Belgium and The Netherlands and hurricane Ida in Mississippi (USA), caused severe floodings and damages in these areas. Climate change, in turn, leads to an increase in sea level rise, making flood prone areas more at risk for floodings. As is shown in both the Fifth and Sixth Assessment Reports of the IPCC, sea level will continue to increase over the coming decades and centuries (IPCC (2014a) & IPCC (2021)). However, the magnitude of rise in sea level is of an uncertain nature. This bolsters the idea of applying adaptive designing methods on flood defence systems to tackle the uncertainties decision makers and engineers face in the wake of climate change, whilst finding a balance between safety and expenditures. Thus, the main goal reads:

"Develop an adaptive flood defence system in the Rhine-Meuse estuary under the influence of an uncertain sea level rise balancing between structural safety and costs"

The process is guided by three design loops which converge towards a preliminary design of a hydraulic structure in the Rhine-Meuse estuary. In the first loop, a system, in which the structure is to take form, is derived with the Dynamic Adaptive Policy Pathways approach from Haasnoot et al. (2012). With the method a set of measures and preferred pathways for the system, concerning flood protection structures like barriers and locks, are designed. A number of viable pathways are derived and analysed based on required expenditures of various measures, e.g. dike heightening, salt intrusion reduction and managed retreat measures, under a variety of sea level rise scenarios (5th, 50th -and 95th-percentiles of IPCC sea level rise scenario RCP8.5 (IPCC, 2014a)). The performance of these systems is strongly correlated with the rate of sea level rise and largely balance between required expenditures for dike heightening and strengthening projects for systems that include barriers and economical damages for the shipping industry for systems that include locks. Following the highest level of confidence of RCP8.5, an open system with an open/closable barrier is preferable and the pathway, with the activated measures in opaque, is visualised in Fig. 0.1.

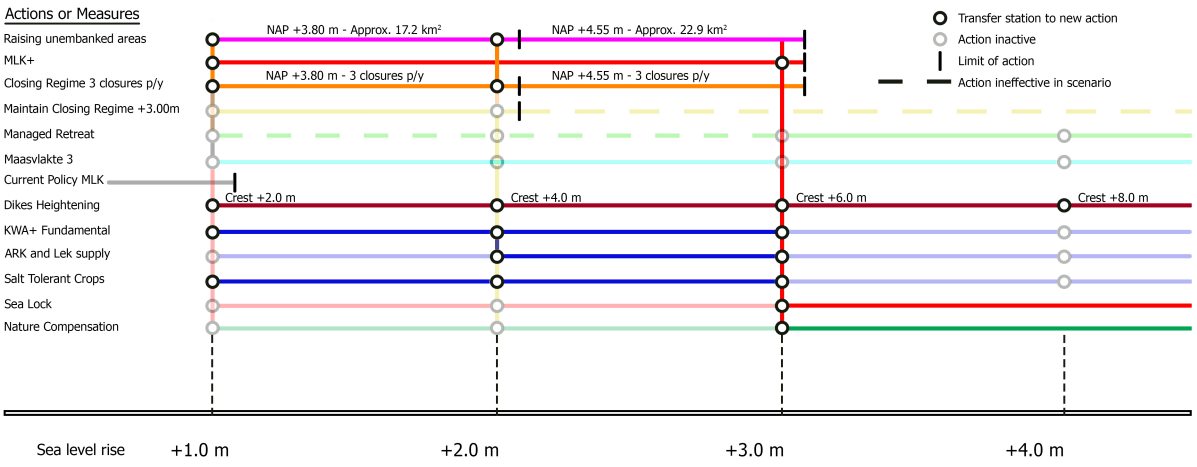

Figure 0.1: Pathway A. Continuation of the open strategy in combination with changing the closing regime and raising unembanked areas. Transparent lines indicate the inactivity of the measures, full coloured lines are active measures.

In the second design loop the location and type of the flood protection structure are determined through the application of a multi-criteria analysis. As derived with the analysis of the adaptive pathways, the most influential criteria, amongst others concerning the location, are the hindrance of the shipping industry and dike heightening projects. The analysis resulted in a preference for a new storm surge barrier to be constructed near Maasdijk in the New Waterway, south of the current Maeslant barrier. Subsequently, a multi-criteria analysis is performed to derive a preferable open/closable barrier type. A sector gate barrier, similar to the current Maeslant barrier, is determined as the preferable barrier type. For further research a cost-benefit analysis, in addition to the multi-criteria analysis, could be added to incorporate the construction costs aspect.

In the third design loop, it is determined what (adaptive) design strategy, on a structural level, is applicable for the storm surge barrier to account for the uncertainty surrounding that of sea level rise. To do so, a reliability model is developed to stress test different designs. The model computes the progression of the failure probabilities of the individual main components, in 10,000 sea level rise scenarios between 2100-2200, of the barrier. Four designs in total are inserted into the model, Static robust and Dynamic robust designs, and these should adhere to instated failure probability threshold norms, only then are they considered as robust. The static and dynamic robust definitions follow from Walker et al. (2013) and are defined as:

- "Static robustness: a design that performs satisfactorily under a wide variety of future conditions."
- "Dynamic (adaptive) robustness: a design that leaves options open and can be adapted to changing future conditions such that the design continues to perform satisfactorily."

In the dynamic robust designs the main components are initially 'smaller' and require a lower investment compared to the static counterpart. The components are then, where possible, adapted when the loading conditions, influenced by sea level rise, exceed the resistance of the component. This adaptation requires an additional investment. The difference between the initially required investments for the dynamic designs and the static designs are computed and denoted as 'costs savings'. These savings are funds that are able to compound over the course of time and, when an adaptation of a component is required, the additional investment is subtracted from the compounded 'cost savings', resulting in either positive or negative benefits. In Fig. 0.2 the ranges of possible negative and positive benefits for two adaptations of two components for three different Dynamic robust design strategies are provided. The figure shows, as an example, when following the means in the left figure of Fig. 0.2, that the adaptation for increasing the bearing capacity of the foundation (wedge soil improvement) is highly likely to result in positive benefits.

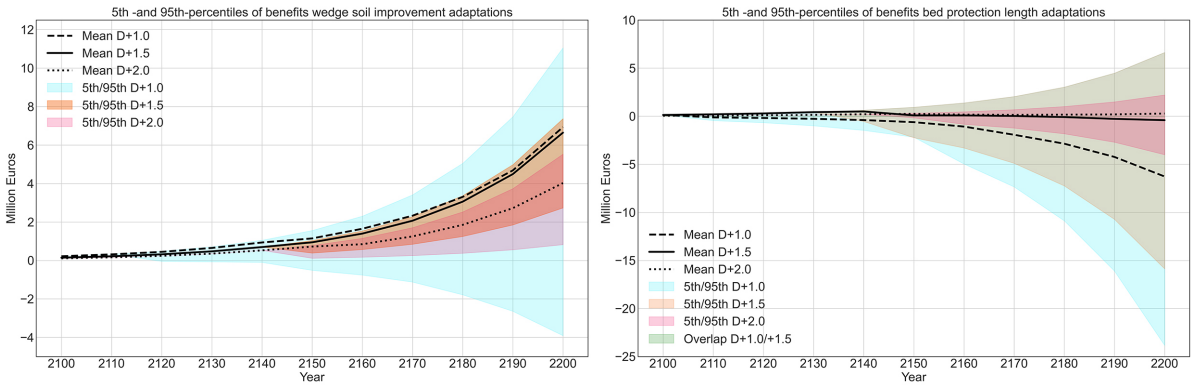

Figure 0.2: 5th -and 95th-percentiles of benefits of the (foundation) wedge soil improvement (left) and bed protection length (right) adaptation for all three dynamic robust design strategies.

Reviewing all the results provided by the reliability model, resulted in a preferable design strategy where two types of adaptations are considered as economically beneficial, i.e. an increase in bearing capacity of the foundation (wedge soil improvement) and an extension of the height of the gates. However, as sea level rise is of an uncertain nature, the exact benefits are difficult to predict and, although, these adaptations provide a high level of confidence to net positive benefits, there is no guarantee they will do so.

Overall, the discussed adaptive designing methods provide a method to understand, and in some cases quantify, what adaptability can provide to cope with the uncertainties surrounding that of climate change and sea level rise. And, although, the applied methods are still far from perfect, it could provide insights in developing alternative designing methods that provide guidance to tackle the uncertainties in the wake of climate change. Thus, to develop the adaptive designing methods further, it is important to apply the approaches in other, quantitative, case studies and also other policy domains, which might lead to a verified approach for both policy makers and engineers to design for uncertainty.

Contents

1 Introduction

1.1. Motivation of the study

Globally, low-lying coastal zones are increasingly prone to uncertain developments considering flood risk. According to Hanson et al. (2011), 13 out of the 20 most populated cities being situated near such zones. The current predictions for sea level rise are spacious in range, and hence challenges decision-makers planning for the future keen on protecting social and economic values in and around these cities. Flood risk is not only influenced by sea level rise, it is also driven by urbanisation, economic developments, land subsidence and developments in the technological fields. Generating strategies to prepare these complex coastal zones, involves not only the consideration of the risk at hand, but as well as economic, political and technical developments. Thus, making decisions should integrate adaptive management practices accepting uncertainty by applying scenario based planning (Brugnach et al., 2008).

Being particularly prone to the effects of climate change and valuable to The Netherlands, the Rhine-Meuse estuary will have to face these prior mentioned challenges in the future. The estuary directly connects the densely populated municipality of Rotterdam to the North Sea and contributes a significant sum to the GDP, estimated at 8% (CBS, 2019), underlining the necessity to reduce flood risk. The region is currently protected by two vital hydraulic structures, the Maeslant and Hartel storm surge barriers, in combination with dikes and artificially heightened areas. The Maeslant barrier is designed to reach its functional lifespan by the end of the 21st century, however, due to projected sea level rise, peak discharges and land subsidence, it is uncertain whether the barrier is able to fulfil its designated lifespan.

1.2. Problem analysis

The continuously increasing emission of greenhouse gasses is leading to a global warming of the climate, resulting in a rise in global sea level and extreme precipitation events (IPCC, 2014a). This change is paired with a high amount of uncertainty and is linked with the path the world takes on global CO_2-reduction. Numerous countries have made pledges to significantly reduce their CO_2 emissions in order to slow global temperature rise. Nevertheless, it has to be seen whether these countries will uphold their pledges and if the effect of these pledges are significant enough to reduce global warming.

According to Ministerie van Infrastructuur en Waterstaat (2019) an acceleration of the rate of sea level rise could occur around 2050, changing the anticipated rate of increase from 5-8 mm/year in 2050 to 5-13 mm/year in 2100 (KNMI, 2019). Currently, the "Delta Programme" by the Ministry of Infrastructure and Water Management takes a maximum of one metre sea level rise, by the end of this century, into account. However, a higher value can not be simply ruled out, depending on the different scenarios introduced by the IPCC.

A probable consequence of sea level rise is an increase of the closing frequency of the Maeslant storm surge barrier, its location visualised in Fig. 1.1. The barrier is currently instigated to close, when water levels are anticipated to reach NAP +3.0 m and +2.9 m, roughly every 10 to 12 years, in Rotterdam and Dordrecht respectively. The closing procedure is quite lengthily and inflicts economic damage for the transportation sector utilising the Nieuwe Waterweg, which is an important shipping route for the port of Rotterdam. In Deltares (2018), economic and technical tipping points

for the barrier are introduced, which are reached with a closing frequency of once and three times a year, respectively. This limit is underlined by Kind et al. (2019), but suggests that a frequency of 4 a 5 times per year could be achieved. Additionally, it has to be noted that the economic tipping point for the transportation sector is suggestive and has not been substantiated. The same report states that these closing frequencies occur for a sea level rise of NAP +0.75 m and +1.00 m, respectively. When this exact rise occurs is debatable and differs with quite some years, dependent on the different climate scenarios, but could lead to an earlier end of life of the structure than initially designed. Additionally, the Maeslant barrier was designed with a closing failure probability of once every 100 closures, however, after research it appears that the actual probability is around once every 10 closings. This is largely due to the closing procedure and complex operating systems (Vrancken et al., 2008), resulting in a closing failure probability of 1:1,000, with a return period of once every 10 years in the present. It therefore is likely, that the increase in closing frequency will lead to an increase of the failure probability. Comparing the failure probability of the Maeslant barrier to the surrounding dikes, with updated norms of 1:30,000 and 1:100,000 year, makes this structure a critical element in the primary flood defence of the hinterland.

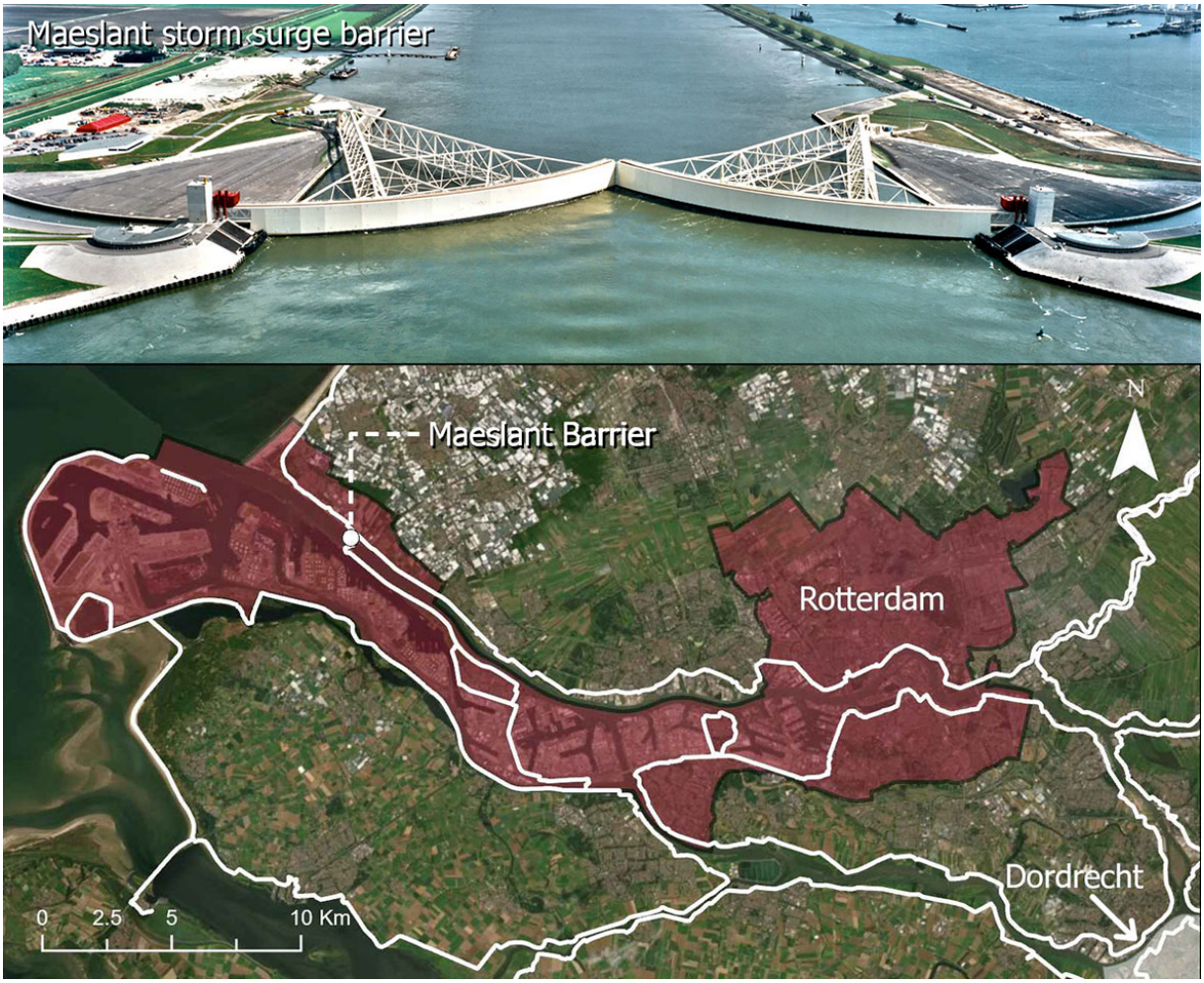

Figure 1.1: An overview of the municipalities of Rotterdam and Dordrecht, existing dikes and location of the Maeslant storm surge barrier. Top figure retrieved and modified from Hollandia Services (nd).

Besides a rise in mean sea level, an increase of the peak river discharge from the Rhine is expected during the winter and a decrease during the summer. By 2100, the maximum design discharge for the Rhine is estimated at 18.000 m^3/s compared to 16.000 m^3/s in 2008 (Deltacommissie 2008,

2008). Therefore, the probability of the simultaneous occurrence of high river discharge and a storm surge is likely to increase. During a closure of the Maeslant barrier the Rhine flow is unable to discharge into the North Sea, leading to an accumulation of water and thus, a rise in backwater level. The Maeslant barrier is designed to open during low tide to discharge the accumulating water behind the barrier and close again during high tide, this 'double-function' makes the barrier quite complex. The storage capacity of the delta has its limits and floodings might occur due to the simultaneous occurrence of a high river discharge and storm surge Zhong et al. (2012). Delta21 aims to simplify the functioning of the barrier. By installing pumping capacity in the delta the accumulating water during a closure could be diverted to a storage lake. In addition, the decrease in river discharge throughout the summer, in combination with the anticipated sea level rise and a fairly recent deepening of the New Waterway, is leading to a farther salt intrusion into the mainland. Causing problems for the fresh water supply and salinization of the soil in the region (Deltares, 2018).

The high amount of uncertainties that are difficult to predict for the far future poses a challenge for the governing parties to maintain the level of flood risk safety in the Rijnmond-Drechtsteden area. Previously mentioned conditions like socio-ecological and economical developments, can change over the course of decades and even after the implementation of new infrastructural projects, which calls for an adaptive delta management approach. In which various pathways or scenarios are designed and applicable depending on the actual development of the uncertainty, like sea level rise, to support decision-making on water policy, planning and infrastructural investments (Deltares, 2014).

1.3. DESIGN OBJECTIVE

This thesis aims to provide a 'dynamic robust', elaborated in Section 1.5, flood protection replacing the Maeslant storm surge barrier under the influence of changing conditions near the end of the 21st century. Incorporating adaptive pathways in the form of scenario-based uncertainties leading to various strategies to cope with the perceived uncertainties, leading to a promising pathway for which a 'robust' hydraulic structure is designed. The adaptive pathways approach, elaborated in Section 1.5, so far has been applied in a holistic policy integration for water systems (Haasnoot et al., 2012), and on a constructive level creating pathways for adapting marine locks (Huijsman, 2021). Within this thesis, the adaptive policy decisions for the Rhine-Meuse system are combined with a constructive design of a flood protection. Thus, the design objective reads:

"Develop an adaptive flood defence system in the Rhine-Meuse estuary under the influence of an uncertain sea level rise balancing between structural safety and costs"

To derive the main objective of this thesis a set of sub questions are introduced which guide the process. Sub questions:

- *"Is the adaptive pathways approach a suitable method to derive flood protection systems with sea level rise uncertainty?*
- *"In what manner is the reliability model, computing failure probabilities and benefits for varying design strategies of a hydraulic structure, applicable and beneficial for the determination of dimensions of the structure with sea level rise uncertainty?"*

1.4. REPORT OUTLINE

The structure of the report follows the structure elaborated in the approach. In Fig. 1.2 the approach is visualised through a flow chart in which the three design loops are colour coded.

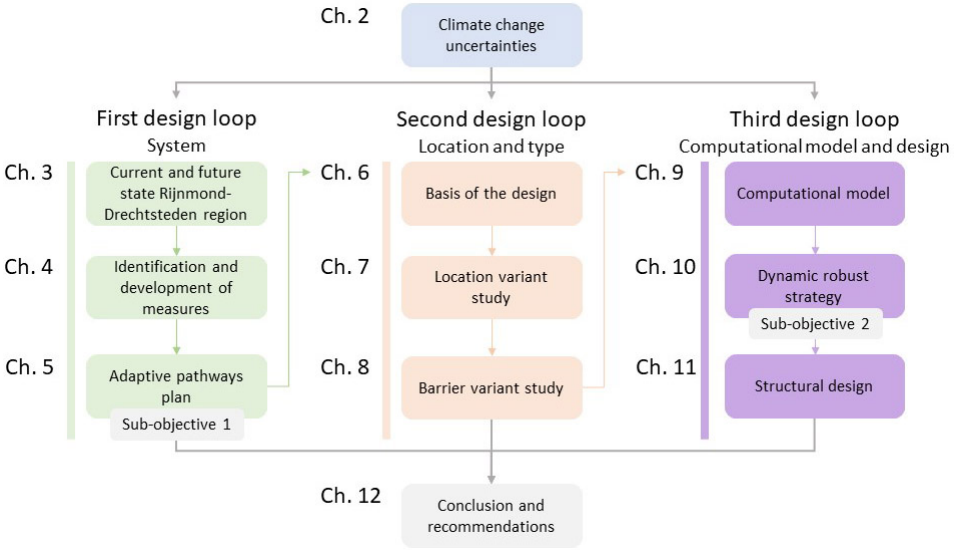

Figure 1.2: Outline of the report.

1.5. APPROACH

To derive a robust and technical solution for the replacement of the current Maeslant barrier, the approach to reach this robustness is defined. According to Walker et al. (2013, p. 2) four types of approaches exist that may result in the development of infrastructural designs which include the desired robustness:

1. "Resistance: design for the worst possible case or future situation. This comes at high costs and the potential of substantial over investments."
2. "Resilience: whatever happens in the future, make sure that the design can quickly recover."
3. "Static (conservative) robustness: a design that performs satisfactorily under a wide variety of future conditions."
4. "Dynamic (adaptive) robustness: a design that leaves options open and can be adapted to changing future conditions such that the design continues to perform satisfactorily."

Due to the changing and uncertain conditions over time, i.e. sea level rise, a dynamic robustness approach is opted for. In contrast, a static robust or conservative design is designed as such that it performs adequately at the end of its lifespan and, depending on the sea level rise scenario, might be over-engineered at start of its lifespan. Leading to an over-investment at this stage. With the dynamic robust approach it is tried to minimise this initial investment. When loading conditions increase, due to an increase of sea level, and surpasses that of the resistances of the flood protection, an additional investment is made to adapt or strengthen certain components of the barrier to adhere to the instated robustness criteria. The idea behinds this is that due to the delay of certain investments or the development of a less severe sea level rise costs can be reduced compared to the static robust design. The robustness criteria for both approaches is equal and is defined as the structural failure probability of the flood protection and should stay below 1:10,000 p/y.

To derive a dynamic flood protection, the system, location and type of hydraulic structure have to be defined. Therefore, three design loops within this thesis are considered and correspond with the outline in Section 1.4, see Fig. 1.3. Within the design loops the Hydraulic Engineering Design Method, a specific form of systems engineering, is integrated. (Molenaar and Voorendt, 2020) An iterative process of the detailing loops occurs and increase in detailing level.

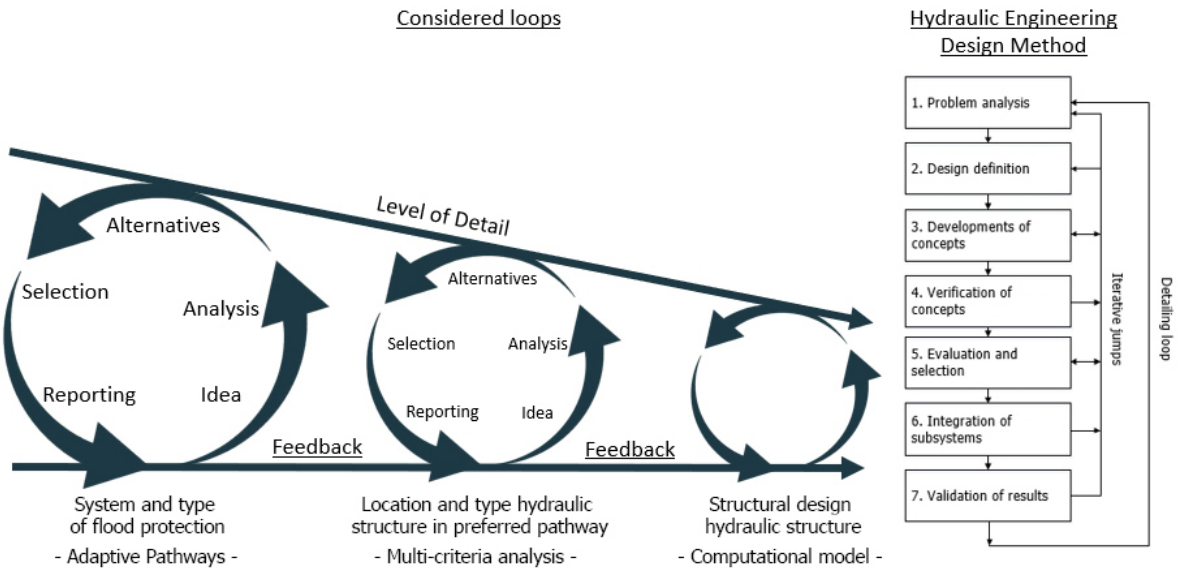

Figure 1.3: Visualisation of the detailing loops to derive a dynamic robust design for flood protection with sea level rise uncertainty and the applied method per loop on the left. On the right the 7 steps of the Hydraulic Engineering Design Method are shown.

The first loop concerns the determination of the system and type of flood protection, e.g. an open/-closable barrier or a lock, which aims to replace the Maeslant barrier. To integrate the dynamic robustness aspect, the system in which the flood protection is to function, is created through the development of an Adaptive Pathways Plan, a visual representation of such a plan is provided in Fig. 1.4. In the plan a wide array of pathways are generated for the Rijnmond-Drechsteden region.

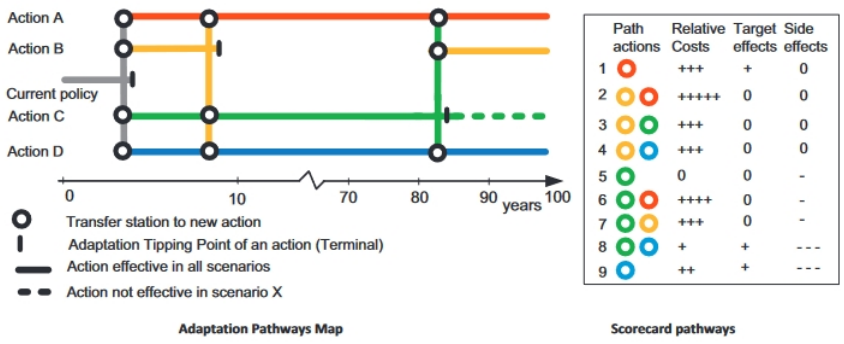

Figure 1.4: Example of adaptation pathways for flood risk. Modified from Haasnoot et al. (2012, p. 488).

Pathways can reach certain tipping points, which marks the end of the applicability of the pathway and adaptive measures are needed to ensure the functioning of the system. The required steps to develop the Adaptive Pathways Plan are elaborated:

- To initiate the first design loop a problem analyses, Section 1.2, is conducted. Whereafter the consequences of climate change uncertainties are analysed in Chapter 2, followed by an analyses of the regional situation in Chapter 3. These parts provide insight in possible uncertainties under uncertain future developments.
- Thereafter the identification or development of measures or actions that provide solutions for the problems follow suit. Subsequently these measures are assessed based on sea level rise, costs, vulnerabilities and opportunities. Both are integrated into Chapter 4.

- Followed by the identification of measures, an Adaptive Pathways Plan is able to take form. In Chapter 5 the various measures, identified or developed in Chapter 4, are integrated into an overall plan. The adaptive plan is considered robust if the varying pathways are able to reach to a desired outcome of results under varying uncertainties and assumptions.

- Lastly, the selection of a preferred pathway, for which the flood protection is developed further, is made through comparing the economic performance of the various pathways under varying sea level rise scenarios and their respective (dis)advantages in Section 5.3 and Section 5.4.

After selecting the preferred pathway in which a new flood protection is developed, the second loop is started. This loop determines the most suitable location and type of the new hydraulic structure and the steps from the Hydraulic Engineering Design Method, Fig. 1.3, are repeated. The selection of both the location and type of structure is substantiated with a Multi Criteria analysis. After which the third loop is initiated. In the third loop static and dynamic robust design strategies are developed to derive a preferable design adhering to the uncertainty of sea level rise. To incorporate the uncertainty of sea level rise a reliability model is developed, the function of the model is elaborated along the flow chart of the model (Fig. 1.5).

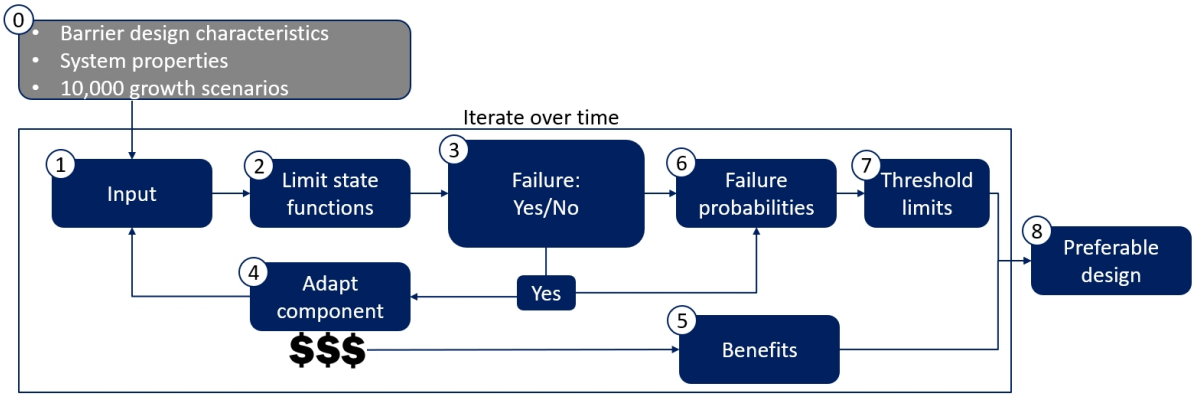

Figure 1.5: Simplified flow chart representation of the reliability model in the third design loop.

In the model distributions of sea level rise scenarios, over a span of 100 years, are sampled and integrated, denoted as 'growth scenarios' (0). Together with the design characteristics of a flood defence structure and the system derived in the adaptive pathways the input parameters for the model are formed (1). With a number of limit state functions (2), connected to the main components of the structure, it is determined whether the design characteristics of said component are able to withstand the acting loading conditions (3). If failure is true for the relative limit state, and a possible adaptation of the component is available, the component is adapted (4). This leads to an extra investment moment at a certain point in time. The model computes the benefits gained from the respective design strategy (5). The total number of failures, over all the integrated growth scenarios, of a design strategy and individual components is computed and defines the failure probability of the structure (6). This probability should stay below a certain instated threshold (7), and if this is verified, the design strategy is designated as suitable. Comparing multiple design strategies, based on the relative gained benefits over all the growth scenarios and the uncertainty thereof, determines which strategy is preferred (8). After selecting the preferred design strategy or a combination of certain components, a preliminary design, with the defined design parameters inserted into the model, is supplied and marks the end of the third design loop.

1.6. SCOPE

The scope of the thesis includes:

- The focus of this thesis is primarily on an alternative (partial-)system-plan and Maeslant storm surge barrier and preliminary design thereof. Therefore, options without implementation of an barrier or lock are disregarded.
- The analytical framework and analyses are quite broad, however, as this is a technical design project, the focus lies on the technical aspects that matter for a design, e.g. economic and socio-ecological prospects are included but not evaluated into thorough detail.

The aspects that are excluded:

- The system beyond the Rijnmond-Drechtsteden area is kept out of scope, see Fig. 3.1.
- Design of the mechanical systems of an alternative hydraulic structure.
- Thorough salt infiltration analysis.
- Consequential impacts on the morphology of an alternative hydraulic structure.
- The consideration of land subsidence, which is currently present, is neglected due to lack of estimations that are provided beyond 2050.
- The design of mechanical systems required for movable gates is kept out of scope.

Furthermore, the design of the adaptive pathways and hydraulic structure are considered within the implementation of Delta21. The plan potentially contributes to the flood risk protection of the Rijnmond-Drechtsteden region, the ecological condition in this area and energy transition currently ongoing in The Netherlands. Delta21 consist out of several components:

- Energy storage lake: As represented in Fig. 1.6, the lake functions as a battery, in which excesses of solar and wind energy can be stored. In critical conditions, accumulating water behind the barriers can be pumped into the sea with the activation of pumps up to a capacity of 10,000 m^3/s.
- Tidal lake: the tidal like is situated between the energy storage lake and the Haringvliet sluices and is in open connection with the North Sea.
- Storm surge barrier. A new storm surge barrier has to be constructed, located between the tidal lake and North Sea, see Fig. 1.6, to protect the hinterland from flooding. The exact layout of this barrier is undefined and is left out of the scope of this thesis project.

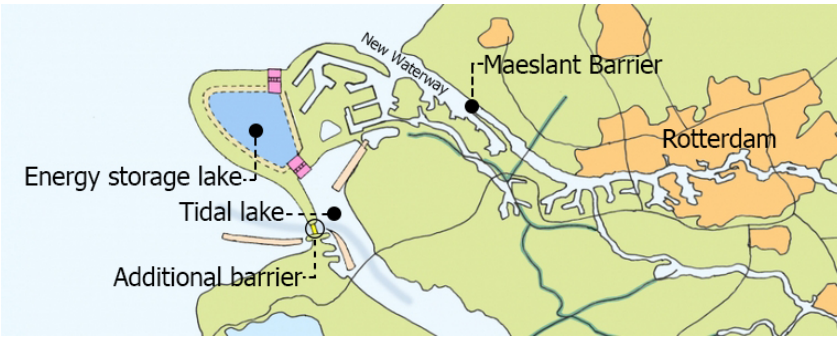

Figure 1.6: Delta21 system overview. Retrieved and modified from Delta21 (2019, p. 12).

2 | Exploration of climate change uncertainties

This chapter marks the start of the first design loop and, together with Chapter 3, forms the problem analysis considering sea level rise uncertainty. Therefore, the range of sea level rise in respect to different scenarios is outlined in Section 2.1. The changing climate has a further effect on river discharges, Section 2.2, and salt intrusion into the estuary, Section 2.3. In Section 2.4 the effects on the Maeslant barrier are summarised. By stating these uncertainties and possible developments due to climate change a basis is provided for the adaptive pathways in Chapter 5.

2.1. Sea level rise

The predictions in sea level rise vary over a wide range and the uncertainty range increases further in the future due to the nature of the models. The IPCC attempts to predict the mean sea level rise through the establishment of four Representative Concentration Pathways (RCPs): RCP2.6, RCP4.5, RCP6 and RCP8.5. These RCPs indicate the increase in radiative forcing that is expected at the end of the 21st century compared to 1750, i.e. pre-industrial time. The radiative forcing is the difference between the received power per unit area or solar irradiance and the energy radiated outwards to space in W/m^2, and is highly influenced by the amount of greenhouse gasses emitted (IPCC, 2014b) & (Vuuren et al., 2011). In Fig. 2.1, the four RCPs are represented as the amount of total greenhouse gasses emitted in CO_2 equivalent emissions. Subsequently, the RCPs lead to predictions, with an uncertainty margin, for sea level rise, till the end of the 21st century on the right side of the figure. It has to be noted that the distribution of sea level rise is not uniform over the surface of the Earth. The distribution is influenced by the differences in the strength of the gravitational pull between the ice sheets in the poles, e.g. ice sheet loss in the South Pole leads to a relative higher sea level rise in the northern hemisphere than near the South Pole and vice versa (Mitrovica et al., 2001). Logically, the values represented in Fig. 2.1, are not necessarily representative for the Rhine-Meuse estuary and thus the Royal Netherlands Meteorological Institute (KNMI) provides predictions regarding sea level rise.

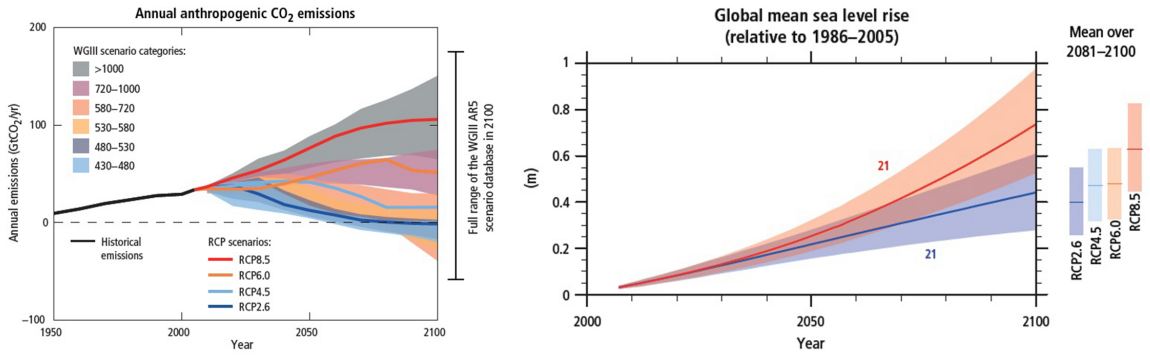

Figure 2.1: The four RCP scenarios represented as annual anthropogenic CO_2-emission in the left figure. Retrieved and modified from IPCC (2014b, p. 9). These RCPs develop in their own prediction for sea level rise with a range of uncertainty, which is visualised in the right figure. Retrieved and modified from IPCC (2014b, p. 11).

The scenarios sketched by the KNMI'14, visualised in left side figure of Fig. 2.2, also referred to as the Deltascenario, are based on two combinations of diverging values for global temperature rise: 'Warm' and 'Gematigd' (Dutch for moderate), and two possible distinctions in airflow patterns: 'Low' and 'High'. When comparing the results for 2100 to the previously mentioned RCP pathways from Fig. 2.1, it can be deducted that the results are quite similar. However, according to Vermeer and Rahmstorf (2009) and Grinsted et al. (2010), the predictions following from the RCPs of Fig. 2.1, might have underestimated the range of potential sea level rise by the end of the 21st century. Recent concerns about the instability of the Antarctic and Greenland ice sheets emphasises these claims (Nicholls et al., 2011). The mass loss of these ice sheets could lead to an acceleration of sea level rise in this and the coming centuries (DeConto and Pollard, 2016). According to Deltares (2018), the predictions that do account for an acceleration are quite similar up to 2050 (Haasnoot et al., 2020), whereafter the predictions start to deviate considerably. The comparison is clearly noticeable when comparing the KNMI'14 predictions (left figure) to the predictions that include an acceleration (right figure) in Fig. 2.2.

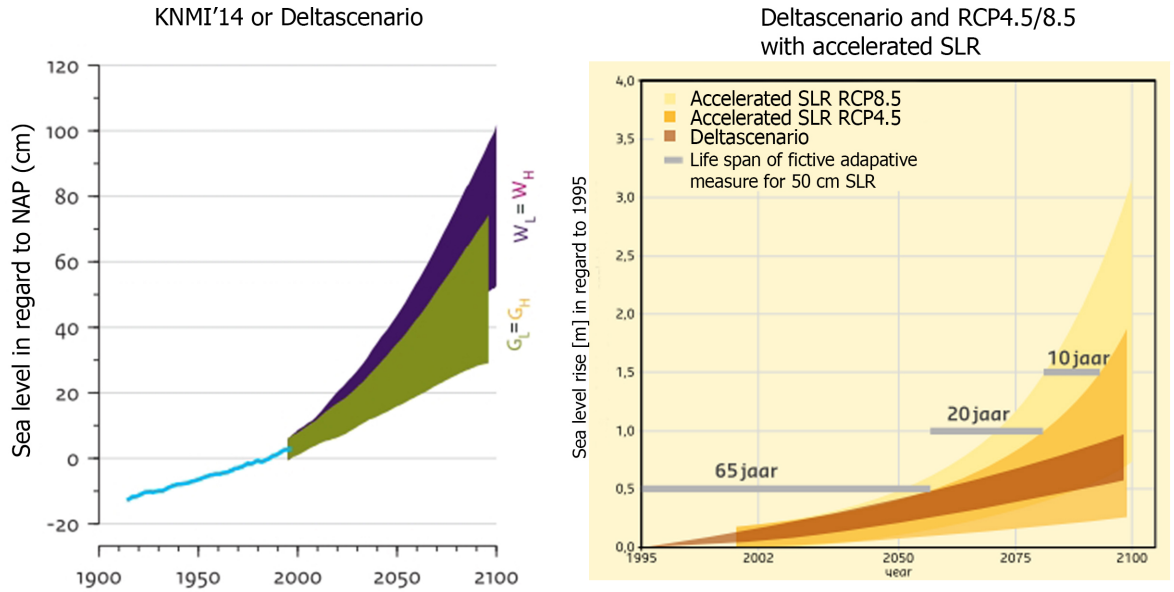

Figure 2.2: Left figure: Sea level rise scenarios by KNMI'14. Retrieved and modified from KNMI'14 (2015, p. 15). Right figure: Sea level rise predictions that include an acceleration (RCP4.5 and RCP8.5). Retrieved and modified from Deltares (2018, p. 46).

The current rate of sea level rise for The Netherlands is estimated at 1.82 ± 0.12 mm/year (Baart et al., 2018). According to le Bars (2019), this value could accelerate up to 5-8 mm/year in 2050. From this point the rate of sea level rise starts to deviate quite heavily, dependent on the respective RCP scenario. Due to the high amount of uncertainty and probable acceleration of ice sheet losses, "the low-probability, high-consequence rise of sea-level rise of more than 1 m cannot be ruled out during the twenty-first century" (Nicholls et al., 2011, p. 162). It is evident that, the development of sea level rise, both with and without the expectation of acceleration, varies considerably up to the end of the 21st century. As most hydraulic structures in The Netherlands are constructed with an estimated life span of 100 to 200 years (Haasnoot et al., 2020), a need arises to look beyond the end of the 21st century. In Fig. 2.3, two different scenarios, with considerable uncertainties due to the large timescale, are visualised.

It is difficult to predict when exactly in time a certain sea level rise occurs. Therefore, the timescales for the adaptive pathways in Chapter 5 are replaced by absolute values of sea level rise, indicating

which measures work for the respective sea live rise. As hydraulic structures are designed to last between 100 and 200 years, and the Maeslant barrier is anticipated to no longer be able to fulfil its main functions around the end of the century, an absolute sea level rise ranging between NAP +0.0 m and +5.4 m could be adopted.

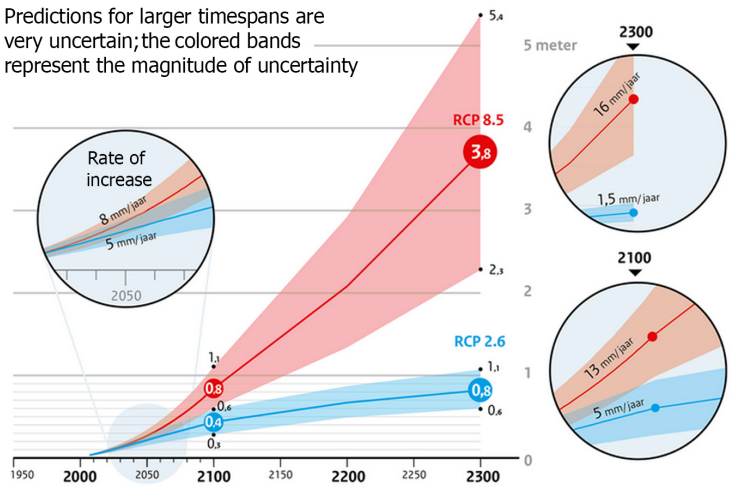

Figure 2.3: Predicted sea level rise up to 2300 and rate of sea level increase per year for 2050, 2100 and 2300 according to le Bars (2019). It has to be noted that these estimates are very uncertain due to the large timescale. Retrieved and modified from le Bars (2019).

2.2. RIVER DISCHARGES

Besides sea level rise, the river discharge contributes to flood risk of the Rhine-Meuse estuary. This risk especially rises in the event when the Maeslant and Hartel barriers are forced to close due to high water of the North Sea. In the eventuality that both the barriers are closed, water flowing from the rivers accumulate behind the barrier causing a rise in backwater level (Zhong et al., 2012). This parameter adds to the complexity of the barriers, as these are not only intended to retain high water from the North Sea but also discharge the accumulated water to the North Sea during lower water levels. Due to global warming these river discharges are subjected to change (Ritzema and van Loon-Steensma, 2017) & (de Wit et al., 2015).

The inflow of water into the Rhine-Meuse estuary is governed by the discharge of the Rhine and Meuse rivers. The Rhine enters the Netherlands at Lobith with an average discharge of 2.200 m^3/s and is currently characterised with a design discharge (1/1.250 p/y) of 16.000 m^3/s (Klijn et al., 2018). After entering The Netherlands the Rhine breaks off into three branches: the IJssel, Nederrijn-Lek and Waal-Merwede. During the flood stage of the Rhine river, the discharge is distributed between the three to the respective ratio of 1:2:6. The Meuse enters The Netherlands in the province of Limburg with an average discharge of 230 m^3/s and is characterised with a design discharge (1/1.250 p/y) of 3.800 m^3/s (Klijn et al., 2018). A report by de Wit et al. (2015), recommends to increase these design discharges, Rhine and Meuse Rivers to 18.000 m^3/s for the Rhine at Lobith and 4.600 m^3/s for the Meuse at Borgharen, before the end of the 21st century to cope with likelihood of an increase in extreme river discharges under the influence of climate change. The extreme discharges are more likely to occur throughout the winter and spring periods for high discharges and during the summer for low discharges (Klijn et al., 2015). In Fig. 2.4 an estimation for the river discharge of the Rhine at Lobith for the years 2050 and 2085 is provided, which visualises this pattern.

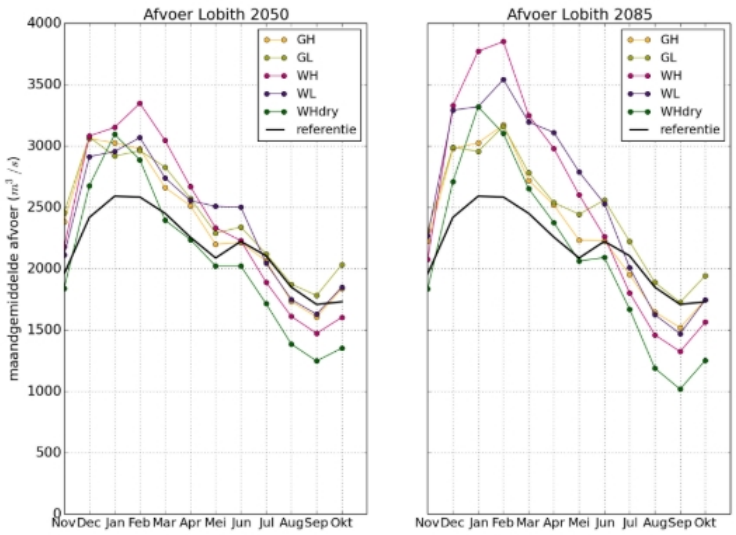

Figure 2.4: Discharge regime of the Rhine River measured at Lobith in respect to the KNMI'14 scenarios from Section 2.1. Retrieved from Klijn et al. (2015, p. 9).

2.3. SALINISATION

Salinisation is the process in which fresh water reservoirs or supplies become increasingly saltier which can lead to fresh water scarcity and may negatively impact agriculture and the availability of drinking water in the vicinity. In the Rhine-Meuse estuary the process is influenced by both the present sea level and relative river discharges. The salty water of the North Sea is able to penetrate deeper into the estuary when the sea level is at a high and the river discharge at a low, when the sea level retreats and the river discharge increases, the salt water retreats. Due to the prospects of a rising sea level and more extreme river discharges, especially during the summer period (April-September), it is likely that salt intrusion will increasingly become more evident in the region. In Fig. 2.5 the prospected salt water intrusion into the estuary is visualised for three different values of sea level rise and a constant river discharge at Lobith of 2.200 m^3/s.

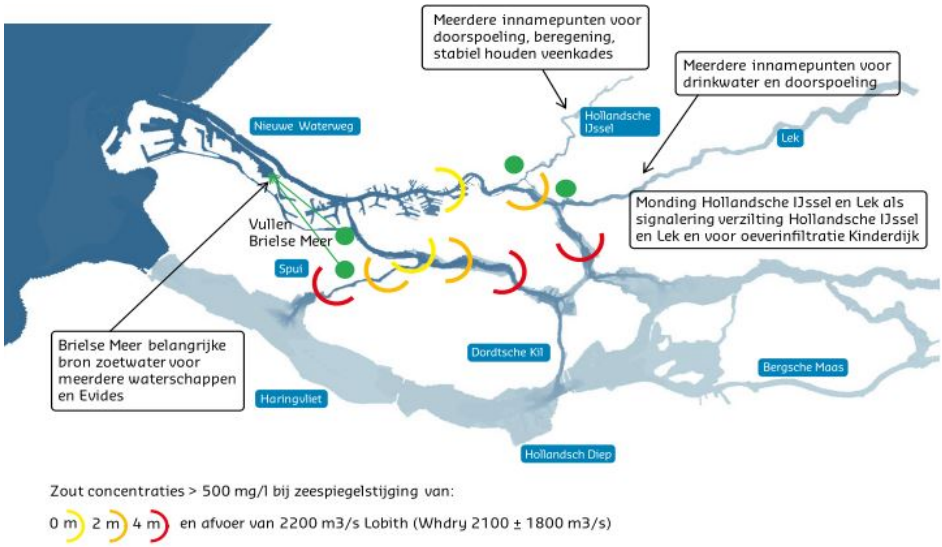

Figure 2.5: Salt intrusion due to sea level rise with a river discharge of 2.200 m^3/s at Lobith. Retrieved from Deltares (2018, p. 63).

2.4. INFLUENCE ON THE MAESLANT BARRIER

The mentioned prognosed changes have consequential effects on the functioning of the Maeslant storm surge barrier. Firstly, due to sea level rise the closing frequency of the barrier is likely to increase, see Fig. 2.6. Two tipping points for the barrier are suggested, regarding the closing frequency, an economical one due to the hindrance for shipping, which is reported to occur at a frequency of 1x p/y, and a technical one due to required maintenance and unavailability of the barrier, which occurs at a frequency of 3x p/y (Deltares, 2018). These tipping points are estimated to be reached with a sea level rise of NAP +0.75 m and +1.00 m, respectively.

Second, the increase in river discharges through the winter and spring periods, in combination with the increased probability of closure occurrences throughout this period, might pose a problem for flooding of the hinterland behind the barrier. If the barrier malfunctions, when it is instigated to open, the water level will continue to rise behind the barrier, resulting in flooding of areas in Rotterdam and Dordrecht. The water level increase behind the barrier can be computed with (Zhong et al., 2012):

$$h_{basin} = h_{basin,c} + \frac{(\frac{8}{9} \cdot Q_{Rhine} + Q_{Meuse}) \cdot \Delta T}{B_{basin}} \tag{2.4.1}$$

In which:

- h_{basin} is the water level in the estuary behind the barrier
- $h_{basin,c}$ is the water level in the estuary behind the barrier directly after closure
- B_{basin} is the surface storage capacity, estimated at 152,000,000 m^2 (Zhong et al., 2012)
- ΔT is the closure period

Thirdly, due to the open-closable nature of the Maeslant barrier, the effects of salt intrusion become increasingly noticeable with sea level rise and a decrease of river discharge in the summer period. A thorough analysis of this problem is not undertaken as it lies beyond the scope of this thesis. However, the manner in which measures positively or negatively influence salt intrusion can be incorporated when a measure is introduced that is a continuation of the current one.

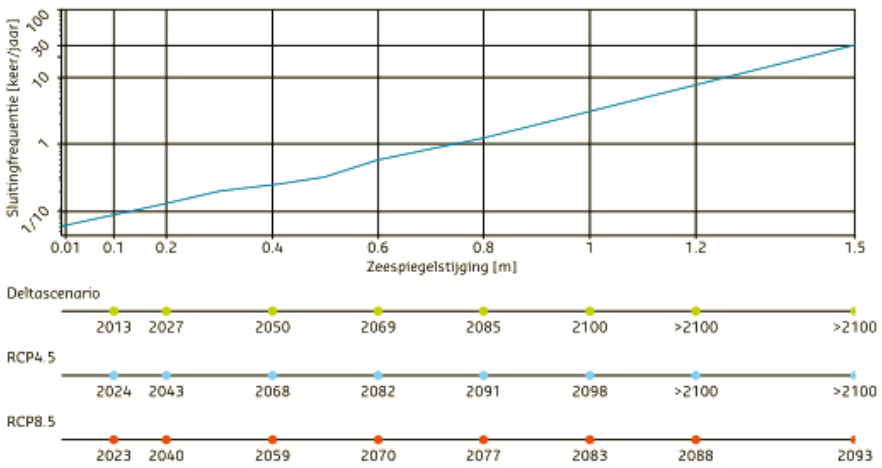

Figure 2.6: The closing frequency (y-axis) coupled to sea level rise (x-axis) for the Maeslant storm surge barrier visualised for different scenarios till the year 2100. Retrieved and modified from Deltares (2018, p. 51).

3 | Exploration of the Rijnmond-Drechtsteden region

The analysis of climate change uncertainties is followed by a regional analysis of the Rijnmond-Drechtsteden in this chapter and is part of the problem analysis. To gain understanding of this highly dynamic region this chapter dives into the current state of the region in Section 3.1, the Maeslant and Hartel barriers in Section 3.2, dikes in Section 3.3 and prospects onto future developments. To get acquainted with non-technical aspects of the regions largest city, Rotterdam, and the Port of Rotterdam are highlighted in Section 3.4 and Section 3.5.1, respectively. Analysing the region in combination with the uncertainties induced by climate change in Chapter 2, will yield a definition of success for the region in which the adaptive pathways in Chapter 5 should be able to take form and marks the end of the first design loop.

3.1. Rijnmond-Drechtsteden region

The Rijnmond-Drechtsteden region envelopes roughly 1.6 million inhabitants of The Netherlands (Programmateam Rijnmond-Drechtsteden, 2014) and is situated in the south of the highly urbanised and dynamic environment of the province South-Holland, see Fig. 3.1. The largest port of Europe, with an open connection to the North Sea, is situated in the municipality of Rotterdam. Together with the industrial complex, these two play an important role in the Dutch and European economy (Programmateam Rijnmond-Drechtsteden, 2014). The New Waterway connects the scattered ports in Rotterdam with the North Sea and shipping via inland rivers. The municipalities in the Rijnmond-Drechtsteden region are protected by the Europoort barrier, Section 3.2, and various dike lines, Section 3.3. These flood defences provide a matter of flood risk safety with varying flood risk exceedance probabilities ranging between 1:2,000 and 1:10,000 year, see Fig. 3.1, adjusted to their relative worth.

The municipality of Rotterdam, as an example, can be divided into three different zones, as is shown in Fig. 3.2. Whereas zones A and B are quite unique, these areas, with an accumulated surface of 24,000 ha, have been heavily urbanised over the past decades. Approximately 60,000 inhabitants reside in 31,000 residences and contains a large cluster of companies outside the primary flood defences (Rijkswaterstaat, 2013). From Fig. 3.2 it can be deducted that, both zones A and B have been artificially heightened to reduce flood risk. According to Rijkswaterstaat (2013), the urbanisation of old port and industrial areas, outside the primary flood defences, is likely to intensify in the future and is further elaborated in Section 3.4.

3.2. The Europoort barrier

The Europoort barrier entails three flood defences and is able to close off the Rhine-Meuse estuary to protect the hinterland from flooding. Together with the Maeslant and Hartel storm surge barrier, Section 3.2.1 and Section 3.2.2, a dike connecting the two and crossing various parts of the port of Rotterdam, visualised as the blue dike in the top figure of Fig. 3.2, forms the Europoort barrier. The Europoort barrier decreases the amount of kilometres of dikes in direct contact with the North Sea by roughly 57.6 kilometres as measured in GIS, based on data by Rijkswaterstaat (2020). This allows for lower crest heights to be designed in the region protected by the Europoort barrier.

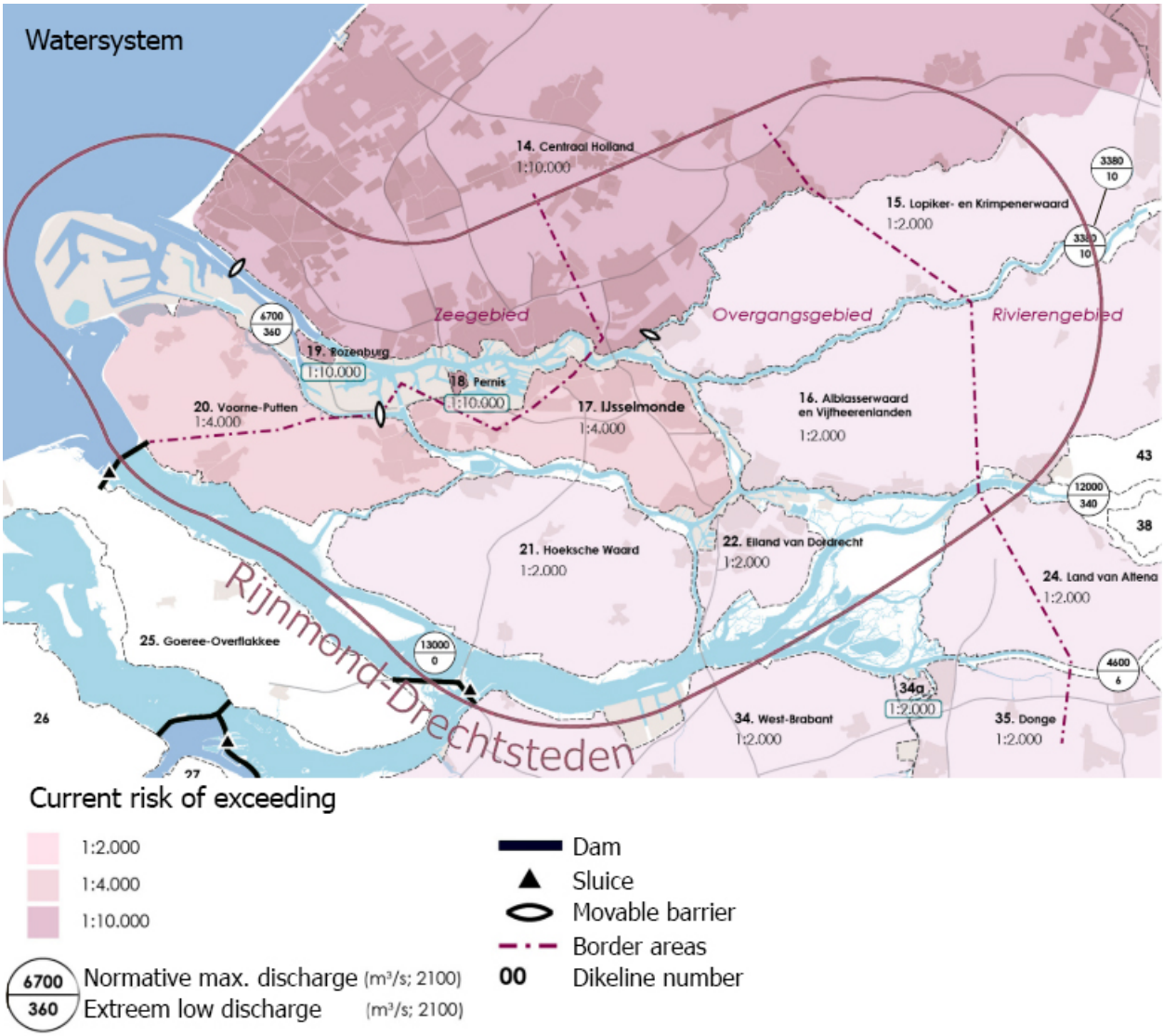

Figure 3.1: The Rijnmond-Drechtsteden area with respective exceedance norms due to flooding and the dominant sub-ares based on hydrodynamic processes. "Zeegebied" is sea dominant area, "Overgangsgebied" is the transition area and "Rivierengebied" is river dominant area. Retrieved and modified from Programmateam Rijnmond-Drechtsteden (2014, p.).

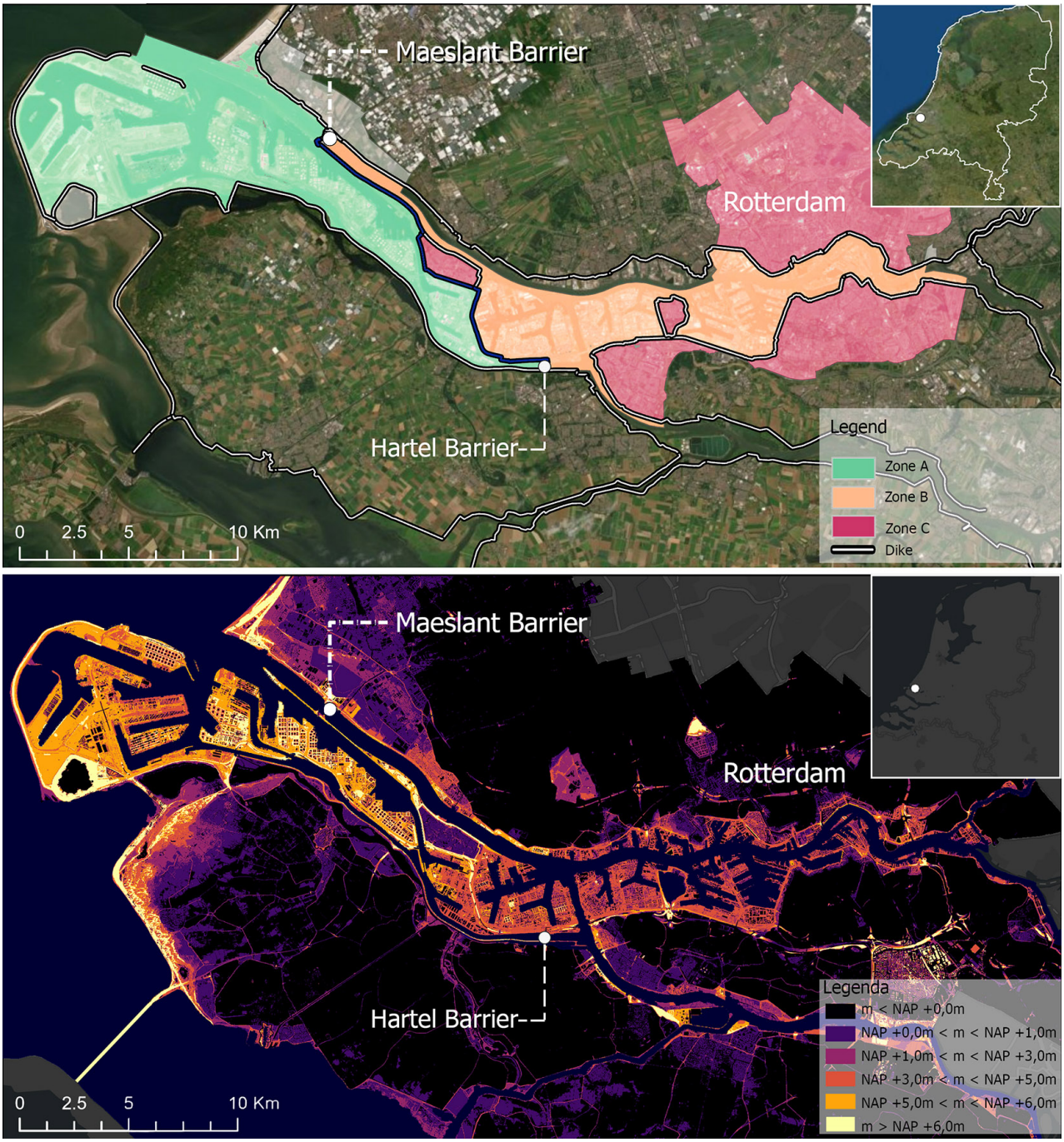

Figure 3.2: In the top figure the respective zones are visualised as well as the location of the Maeslant and Hartel barriers. Together with the blue marked dike they form the Europoort barrier. Zone A is attributed to the western part of the port, mainly ranging between NAP +4,0m and +6,0m, which is not within the protection of the Maeslant barrier. Its artificially elevated height provides protection against floodings for this area. Zone B is attributed to a combination of the eastern part of the port and residential areas ranging between NAP +4,0m and +1,5m. This zone is directly protected by the Maeslant barrier if needed. Zone C is attributed to the remaining part of Rotterdam, accounting for mostly residential and industrial areas. The greater part of this zone is below sea level and is protected by both the Maeslant barrier and a primary dike with a crest level of NAP +5,25m. Division of zones within the municipality of Rotterdam and elevation of the surrounding areas.

3.2.1. THE MAESLANT STORM SURGE BARRIER

The Maeslant storm surge barrier is classified as an open-closable barrier and is part of the Delta Works. It was one of the last major hydraulic structures of the Delta Works, constructed throughout the period of 1991-1997, estimated to cost M€ 656 (Jonkman et al., 2013), extrapolated to 2009 price levels. The open nature of the barrier was adopted, to minimise obstruction and hindrance for the Port of Rotterdam and shipping over the New Waterway. The two main functions of the barrier are therefore contrary, retention of water and enable shipping over the New Waterway. However, complete absence of obstruction can not be guaranteed as the barrier will close if high water of the North Sea threatens to reach certain water levels near Rotterdam and Dordrecht, this roughly occurs once every 10 to 12 years in the present, and once a year for the testing procedure.

The Maeslant barrier is initially designed to last a 100 years, reaching its end of life near the end of the 21st century. The barrier is able to prevent water from flowing into the New Waterway with two massive floating and movable crescent doors, Fig. 3.3, each 216 metres in length, and is able to resist storm surges of up to NAP +5.0 m. Throughout most of the year, the crescent doors are stored alongside the river where the structure can be accessed and maintained. Maintenance is exclusively done throughout the summer period, to avoid the stormy season of autumn and winter. The first functional closure of the barrier occurred on November the 8th of 2007 (Odé, 2007), during the 15 hours closure, the water level behind the Maeslant and Hartel barriers rose from NAP +0.70 m to +1.12 m at Rotterdam. The rise in water level is due to the river discharges of the Rhine (1,171 m^3/s) and Meuse (148 m^3/s) (Zhong et al., 2012).

The closure procedure of the Maeslant barrier operates in coalescence with the Hartel barrier and basically functions as one automated system. The operating system, BOS (dutch for 'Beslis -en Ondersteunend System', roughly translated to Decision -and Supportive System), computes the anticipated water levels and river discharges in the Rhine and Meuse. The system alerts a operational team when water levels are indicated to reach NAP +2.6 m in Rotterdam. If the water levels are anticipated to increase towards NAP +3.0 m in Rotterdam or NAP +2.9 m in Dordrecht the BOS will automatically start the closing procedure of both barriers. The operational team stands by for any malfunctions throughout the procedure. A flow chart and further explanation of the operational control of the barrier can be seen in Fig. A.1.

As previously mentioned in Section 1.2, the barrier is designed with a failure probability of 1:1,000 closings, this results in a total failure probability of the barrier of 1:10,000 years, with a closing frequency of 1:10 years in the present. Which categorises the barrier inline with the flood risk probabilities in the region, visible in Fig. 3.1. However, after revising the closing failure probability, it is estimated that the barrier will fail to close once every 100 closures due to the closing procedure and complex operating systems (Vrancken et al., 2008), resulting in a failure probability of 1:1,000 years, making it a critical link in the Rhine-Meuse delta.

3.2.2. THE HARTEL STORM SURGE BARRIER

The Hartel storm surge barrier is comparable to the Maeslant storm surge barrier, both operational and function wise. The structure is quite different, the barrier is able to retain water flowing from the North Sea with two elliptical lift gates, see Fig. 3.3, with differing lengths, 49 and 98 metres respectively. The size of vessels able to pass underneath the gates is limited, as the gates hover 14 metres above the sea level. To circumvent this limitation, a navigational lock is constructed next to the barrier, providing passage for vessels unable to adhere to the height limitation. The construction costs of the Hartel barrier is significantly lower when compared to the Maeslant barrier, Jonkman et al. (2013) estimates the costs at M€ 143, extrapolated to 2009 price levels.

Figure 3.3: The Maeslant (left) and Hartel (right) storm surge barriers. Retrieved from ANP (nd) and Swart (2015), respectively.

3.2.3. FUNCTION ANALYSIS

The Maeslant storm surge barrier is an iconic project and a well known flood defence worldwide. It therefore provides a cultural value to The Netherlands as underlines the Dutch knowledge and expertise in hydraulic engineering and history of constructing efficient flood defences. The barrier fulfils several functions, classified into three groups: principal, preserving and additional. The principal function follows from the motive to create the desired system. The preserving functions embodies the functions the new system should take into account, as the principal functions could interfere with existing functions. The additional functions do not directly derive from the motive, but are opportunities that could be implemented due to the new system. In the list that follows the functions for the three categories for the Maeslant barrier are listed, in Appendix A.2 an elaboration of these functions can be found:

Principal functions

- Flood protection
- Enable shipping between stretches of water, e.g. the North Sea, New Waterway and New Meuse River
- River discharge (the Double-Function)

Preserving functions to maintain present systems

- Tidal flow
- Reduce salt water intrusion in the fresh water stretch
- Accessibility between Spijkenisse, Rozenburg and the Botlek harbour
- Preserving ecology
- Sediment and debris discharge
- Tourism

Additional functions

- Generation of electricity, although the structure it self is not able to produce energy, plans like Delta 21, see Section 4.4.1, propose that the river discharge could be utilised for an aqua battery able to produce energy and contribute to the sustainable energy goals laid down by the government.
- Cultural values

3.3. DIKES

A distinction between dikes in the Rijnmond-Drechtsteden area can be made. The area consists out of three areas based on the dominant hydrodynamic processes: dominated by the sea, rivers and a transition between the two, represented in Fig. 3.1. For the consideration of the adaptive pathways only the dikes in the sea dominated area are considered. A further distinction between the dike segments in this area is made: dikes in direct contact with the sea and dikes behind the storm surge barriers, zones A and B&C respectively in Fig. 3.2, as these two need to adhere to different design values. The required crest height of the sea dikes is computed with 3.3.1 and is dominated by the significant wave height and wave run-up (Jonkman et al., 2013) based on the respective flooding probability norms attributed to the segment:

$$H_{dike} = H_{design\,WL} + H_{wave\,run-up} \tag{3.3.1}$$
$$\text{In which: } H_{wave\,run-up} = 8 \cdot H_s \tan\alpha$$

The dikes behind the protection of the Maeslant and Hartel barriers adhere to different design values. In theory, if both the barriers do not malfunction, the maximum design water level is equal to roughly NAP +3.0 m, as the barriers are then prompted to close. Therefor, the dike crest height behind the barriers is lower then the sea dikes in front of them, top figure in Fig. 3.4. However, it should be noted, that the allowable failure probabilities of these segments are lower and thus the significant wave height determined is relatively higher then for the sea dikes when compared to the maximum water levels. Additionally, extra height is included to compensate for the likelihood of failure of the Europoort barrier. The failure probabilities in Fig. 3.4 are defined in the Dutch 'Waterwet' (Water Law) as: "the probability of a loss of water retaining capacity of a dike stretch, in which the dike stretch will flood in such extent that fatalities and substantial economical damages occur" (Rijkswaterstaat and Stowa, 2017, p. 36). The allowed probability are mostly determined by the hydraulic or flood characteristics, economic activity and inhabitants in the area (Haasnoot et al., 2012). As an example, the flood probability of a dike with a norm of 1:10,000 per year, results in a flooding probability of 0.01% each year, it however does not mean only one flooding can occur in 10,000 years.

Dikes, as any hydraulic structure, have several failure mechanisms that can occur due to hydraulic loading or instability of the foundation. In Fig. 3.5 the most relevant failure mechanisms for dikes, and hydraulic structures alike, are presented. The mechanisms are elaborated in Appendix A.4.1.

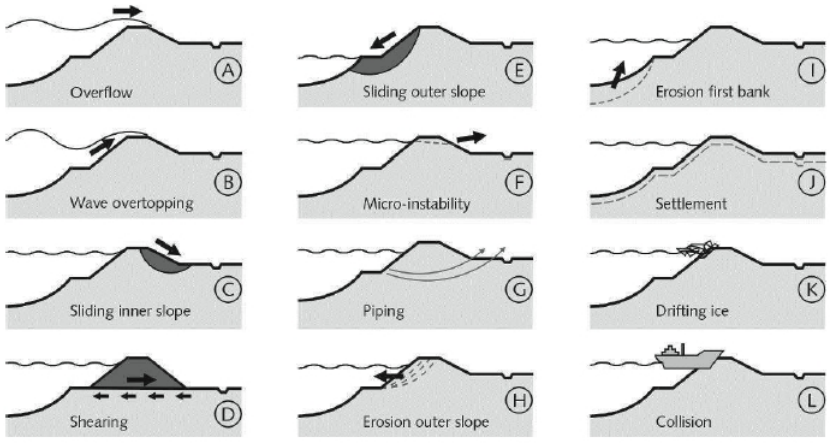

Figure 3.5: Schematic overview of the most relevant failure mechanisms of flood defences. Retrieved from Jonkman et al. (2018, p. 20).

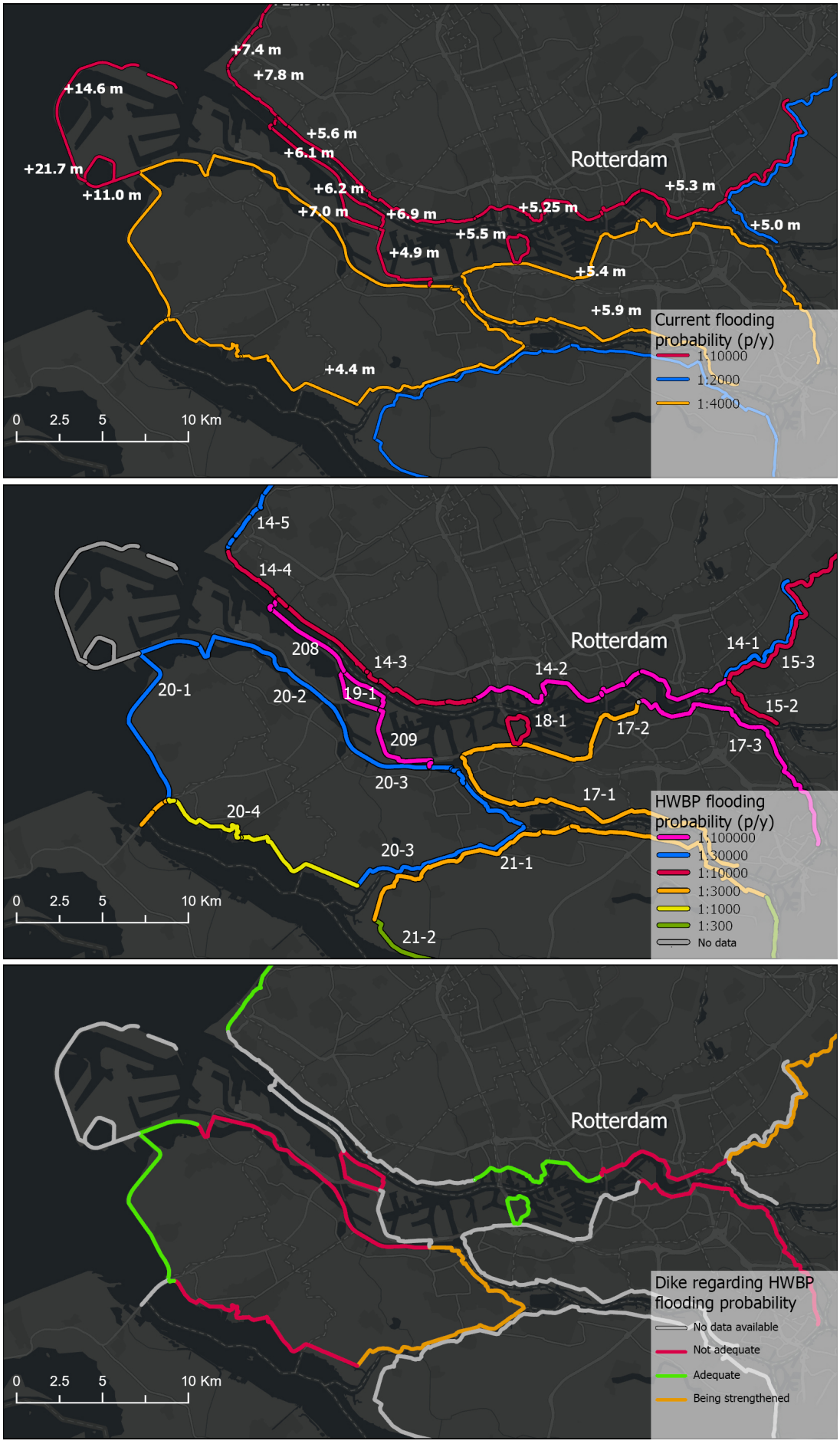

Figure 3.4: Top figure: current dike flooding probabilities and averaged NAP dike height, respective to NAP, for specific dike segments. Middle figure: updated dike design flooding probabilities of the 'Hoogwaterbeschermingsprogramma' (HWBP), in English: 'High water protection programme'. Including the dike-ring stretches. Bottom figure: current (2020) status of the dikes in regard of the HWBP flooding probabilities.

3.4. CITY OF ROTTERDAM

With over 620,000 inhabitants Rotterdam is the second largest city in The Netherlands. Due to its open connection with the North Sea and the New Meuse River the location is strategic, providing a highly efficient and accessible transportation hub in the form of the Port of Rotterdam, the largest in Europe. The city is split into two segments by the New Meuse River, which are connected by bridges, tunnels, a railway and taxi boats. The majority of the residential areas are protected by a primary dike line, zone C in Fig. 3.2, whereas a combination of port segments and residential areas can be found outside the primary dike line on an artificially elevated ground level behind the Europoort barrier, zone B Fig. 3.2 and Section 3.2. Over the course of decades the city and the surrounding region have been steadily urbanising due to an increasing population and growing industries. This process is visible in Fig. 3.6, where the city has been continuously expanding around and over the New Meuse River and towards the North Sea. This process is expected to continue, the municipality plans to further develop 50,000 residences by the year 2040 and aims to supply a stable and continuous building process of residences (Municipality of Rotterdam, 2019) & (Booister and Hekman, 2021). The further rise in population and economic values reiterates the importance of the region and thus the high standard of flood risk safety has to be preserved. Therefore, a scenario, integrated in the adaptive pathways, Chapter 5, is introduced that takes into account the process of urbanisation of the areas in zone B, denoted as Scenario Urbanisation. In this scenario the importance of zone B is considerable in terms of socio-economical prospects and can not be ignored.

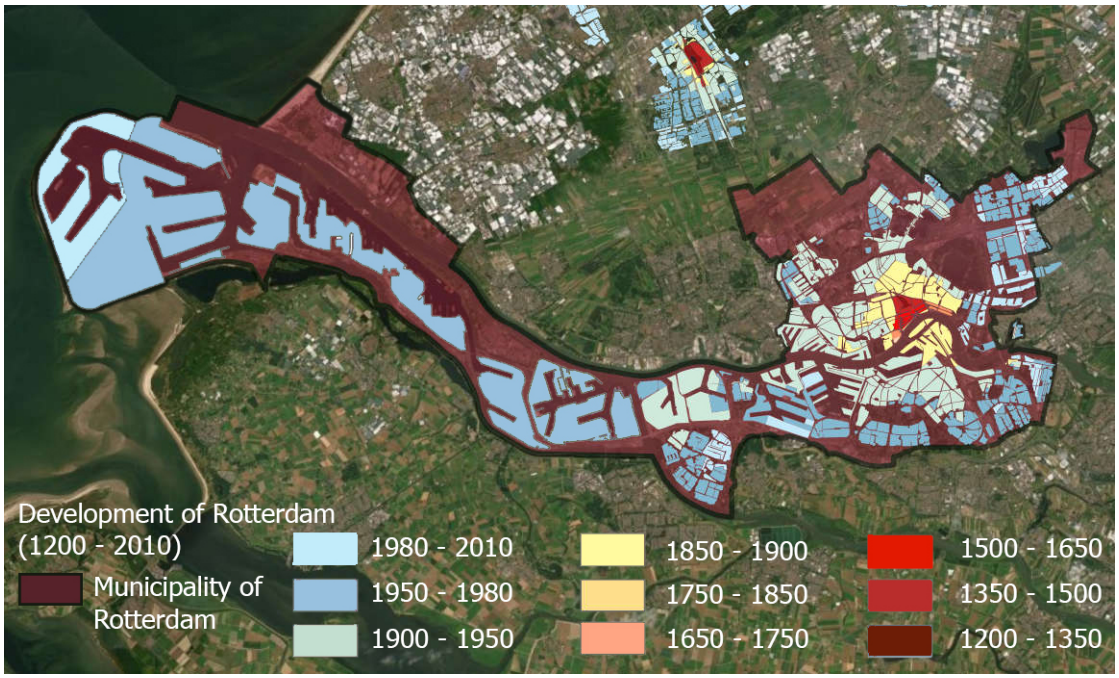

Figure 3.6: Developments and urbanisation in the municipality of Rotterdam over the period of 1970 to 2020. Retrieved and modified from Nationaal Georegister (2020).

3.5. PORT OF ROTTERDAM

In this section some general information about the Port of Rotterdam is provided. In Section 3.5.1 the lay-out of the harbour segments and cargo handling is discussed followed by the distribution of vessels utilising the New Waterway in Section 3.5.2Lastly, in Section 3.5.3 future developments are discussed.

3.5.1. GENERAL INFORMATION PORT OF ROTTERDAM

The Port of Rotterdam has been gradually expanding, from its initial establishment around the year 1400 in the centre of Rotterdam, towards the North Sea, with the newest additions of the Maasvlakte 1 and 2. The increase of global transportation is leading to larger seagoing vessels with larger draught, which in turn led to the deepening of the New Waterway, to a depth of 24 metres, allowing these vessels to make port in segments situated further inland, bolstering the position of the Port of Rotterdam. A total of 29,491 seagoing vessels and 85,969 inland vessels arrived and departed in the port in 2019, accumulating to a total cargo/bulk handling of 469.4 million tonnes. The port provides, both a direct and indirect added value, of 45.6 billion Euros to the GDP (6.2%) of The Netherlands (Port of Rotterdam, 2019). Various types of industries are situated in the port, ranging from cargo handling to chemistry and oil refineries, scattered throughout the entire proximity of the port, as can be seen in Fig. 3.7. In the same report, the total amount of bulk transported for the energy sector equals to 179.5 million tonnes (38.2% of total) in 2019, reporting a continuous decrease over the past 2 years. Although, this is reported over a small time frame, it potentially visualises the transition towards alternative energy sources, which is further elaborated in Section 3.5.3.

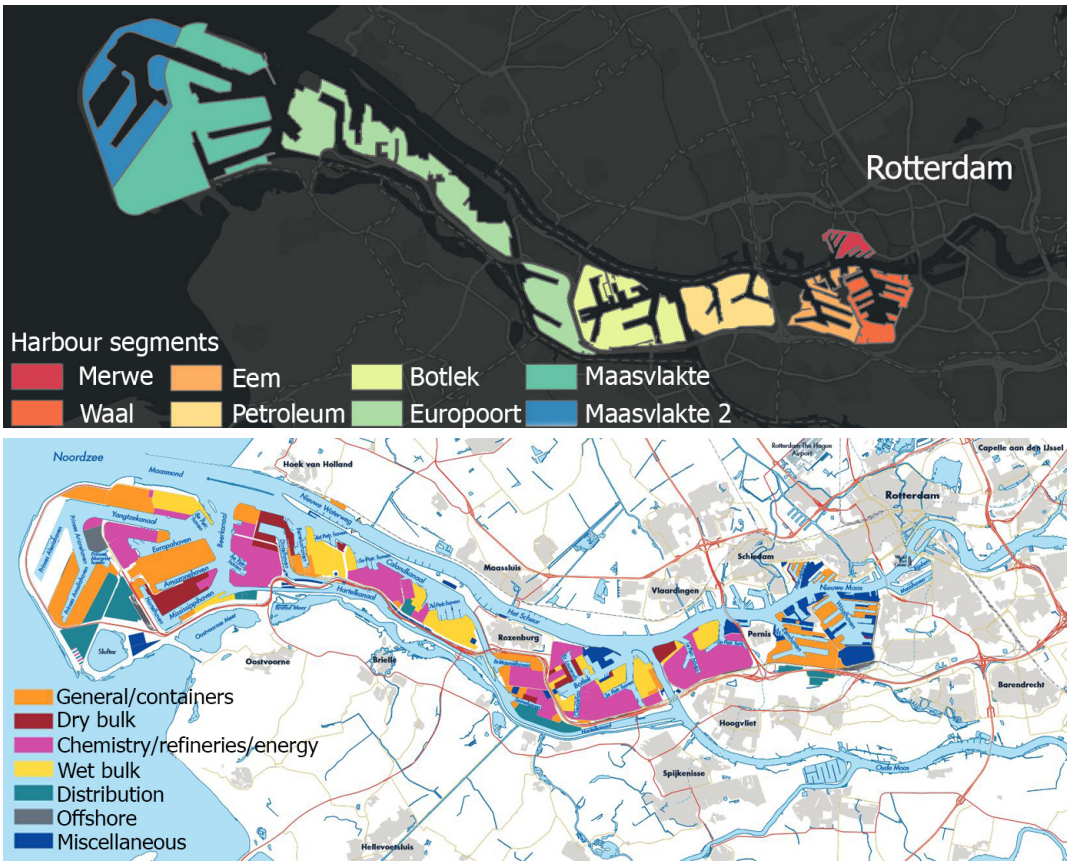

Figure 3.7: Top figure: segments of the Port of Rotterdam.
Bottom figure: type of industry attributed to respective areas of the port of Rotterdam. Retrieved and modified from Port of Rotterdam (2019, p. 6).

3.5.2. DISTRIBUTION OF SHIPPING OVER THE WATERWAYS

The distribution of shipping is of relevance for any adaptation of the flood risks safety strategies, as different strategies lead to different accumulation of costs for the shipping industry and the Port of Rotterdam. In Ecorys and Deltares (2012) some very rough distributions of the different class vessels passing the New Waterway and Calandcanal can be retrieved. However, no exact percentages

can be found, thus these are deducted from the visualisations. In Table 3.1 the distributions for maritime vessels are stated for the year 2010 and 2050. Furthermore, the prognoses for 2050 distinguishes two economic scenarios: GE and LG. GE is the prognoses with the expectation of a high economic growth scenario and LG is the prognoses with the expectation of a low economic growth scenario.

Table 3.1: Distribution of vessel classes over the New Waterway and Calandcanal. Values retrieved from Ecorys and Deltares (2012, p. 12-16).

	New Waterway Volumes			**Calandcanal Volumes**		
	2010	**2050 (GE)**	**2050 (LG)**	**2010**	**2050 (GE)**	**2050 (LG)**
Volume maritime vessels (Total)	57,504	87,802	60,076	13,587	19,327	14,513
Class (Length ; Draught)	Distribution of vessel classes					
1 (<120 m)	14,606	23,024	15,753	1,638	2,668	2,004
2 (120 - 200 m)	17,884	29,121	19,925	4,831	7,205	5,410
3 (200 - 300 m)	10,581	14,609	9,996	2615	3,280	2,463
4 (>300 m ; <14.3 m)	1,898	1,927	1,318	1,993	2,051	1,540
5a (>300 m ; 14.3 - 15.5m)	-	-	-	170	258	194
6 (>300 m ; >17.4 m)	-	-	-	377	290	218
8 (215 m ; 7 m)	57,447	19,121	13,083	1,966	3,570	2,681

It has to be noted that the estimated distribution of vessel classes are very rough estimates, as no definitive value is supplied or can be found other than this technical report. Furthermore, for the determination of the 2050 (LG) prognoses in Table 3.1, no estimate of distribution of vessels classes is supplied. Therefore, the assumption is made that the distribution is the same as 2050 (GE). This is deemed acceptable for the adaptive pathways in Chapter 5, as the costs should visualise overall costs and can not be determined exactly. In Table 3.2 the total amount of inland vessels for the years 2010 and 2050 (GE and LG) for eight locations are supplied, no distribution of vessel classes are supplied in Ecorys and Deltares (2012). Additionally, the numbers from Port of Rotterdam (2019) in Section 3.5 and Ecorys and Deltares (2012) are not identical. The numbers from Port of Rotterdam (2019) are retrieved in 2019 and based on total amount of vessels arriving and departing from the port, whilst the numbers of Ecorys and Deltares (2012) are based on total number of passages for maritime vessels and inland vessels in 2010. The probably cause is that the numbers supplied by Ecorys and Deltares (2012) are counted twice, arrivals and departures, at the same point of reference. If the total maritime vessel passages for 2010 is computed for arrivals, the passages amounts to 28,752 which is lower than the value (29,491) computed by Port of Rotterdam (2019), this difference is most likely due to economic growth of the port and thus the distribution from Ecorys and Deltares (2012) are assumed to be fitting.

3.5.3. FUTURE DEVELOPMENTS

The Dutch government pledged to reduce CO_2-emissions by 49% in 2030 and further down to 95% in 2050 (Rijksoverheid, 2020). The government is trying to do so by transitioning the traditional energy sector, producing energy from coal and gas, towards more sustainable options like wind -and solar energy. In Section 3.5 the figures attributed to energy related bulk are stated, from this figure it is concluded that the energy sectors contribution to the total amount of bulk handled is deemed as considerable. This contribution represents itself in the amount of space utilised by the energy industry in the port, in Fig. 3.7 it can be seen that the purple areas, attributed to the chemistry/refineries/energy sector, encompasses a fair amount of space in the port.

Table 3.2: Amount of inland vessels passing specific points in the region. Retrieved from Ecorys and Deltares (2012, p. 37).

Telpunt	2010	2050-GE	Groei per jaar	2050-LG	Groei per jaar[3]
Nieuwe Waterweg (Hoek van Holland)	76.691	153.309	2,3%	90.169	0,5%
Hartelkanaal oost	71.556	142.542	2,3%	83.836	0,5%
Oude Maas ten oosten Spui	88.201	175.700	2,3%	103.338	0,5%
Dordtsche Kil	101.880	173.029	1,8%	119.365	0,5%
Nieuwe Maas (Krimpen a/d IJssel)	111.621	189.573	1,8%	130.777	0,5%
Hollandsche IJssel	23.355	25.656	0,3%	27.363	0,5%
Noord	97.039	164.807	1,8%	113.693	0,5%
Beneden Merwede	89.109	151.339	1,8%	104.402	0,5%

Bron: RWS, Havenbedrijf Rotterdam, Ecorys (prognoses en groeicijfers).

In 2015 the foundation Urgenda, a platform initiated by civilians focusing on developments and measures to prevent climate change, went to court to force the Dutch government to undertake action to actively reduce CO_2-emissions. The court dictated in favour of the foundation, ordering the government to take more immediate actions to reduce CO_2-emissions (De Rechtspraak, 2015). Two of the three largest coal-fired power stations, contributing roughly 7% of the total CO_2-emissions in The Netherlands, are situated on the Maasvlakte 1 and 2. In a recent article, the minister of Economic Affairs and Climate, E. Wiebes, had made an offer for these three power stations to prematurely halt producing energy to adhere to the Urgenda court ruling (NOS, 2020).

The transition towards more sustainable options and the anticipated decrease of global energy consumption provides opportunities for the region and areas currently in use by the energy sector in the port of Rotterdam. Locations currently in use by coal-fired power stations can be transformed for other types of bulk and refineries. The same could be realised for the large petroleum industry, i.e. the oil refinery of Shell in the Petroleum port, and could be utilised as the basis for future hydrogen power but also residential areas or as an location to transfer the eastern parts of the port, e.g. Merwe and Waal, over time out of the inner part of Rotterdam. The latter, is already occurring in the Merwe-Vier port, where the old fruit industry is making way for various businesses and new residential areas (Port of Rotterdam, nd) & (M4H Rotterdam, 2019).

However, various stakeholders are at play, each with differing intentions and ambitions, the Director Commercial Delivery at the Port of Rotterdam Authority, S. van Els, stated in an interview: "Over the past 150 years, the port has continued to expand from east to west, steadily developing into the port it is today. In the years ahead, this expansion will hopefully reverse its course, spreading the innovation of the Maasvlakte port area back east – and covering the hinterland in the process" (Port of Rotterdam, 2019, p. 3).

These potential transitions can take decades to be finalised and are coherent with uncertainty at this stage. Therefore, the intensification of shipping over the New Waterway and in the Waal-, Eem- and Petroleum harbour segments is integrated as a scenario, denoted as Scenario Intensification Shipping, under which certain measures are ineffective in the adaptive pathways in Chapter 5. A decline in shipping and usage of the aforementioned three harbour segments could bolster the development of Scenario Urbanisation, as mentioned in Section 3.4, and thus, is not introduced as a separate scenario but could provide more flexibility in terms of measures that result in hindrance for the shipping industry in the adaptive pathways. The scenario of a third Maasvlakte is introduced as an individual measure in Chapter 4.

4 | Identification and development of measures

In this chapter existing strategies that are applicable to the Rijnmond-Drechtsteden area are stated in Section 4.1. Followed by the identification and development of measures in the open/closable, Section 4.2, and closed, Section 4.3, strategies. In Section 4.4 measures that can be categorised in the remaining two strategies from Section 4.1, but do not contain the implementation of a hydraulic structure, are stated. Additionally, miscellaneous measures needed to adhere to the framework established in Section 4.5 are also stated in Section 4.4. The framework provides aspects on which the measures can be rated and which combinations are necessary for the development of the pathways in Chapter 5. Lastly, some concluding remarks concerning the developed measures in Section 4.6. This chapter, together with Chapter 5, envelopes the development of concepts phase.

4.1. Outlined strategies

In Haasnoot et al. (2019), four strategies for the Dutch deltas under a rising sea level are presented, see Fig. 4.1. In Appendix B.1 the characteristics attributed to these distinctive strategies are supplied. In the following sections measures within the closed protection and open protection are identified, as these contain the application of a hydraulic structure. Some supplementary measures, in Section 4.4, align themselves with the other two strategies: sea wards expansion and planned retreat.

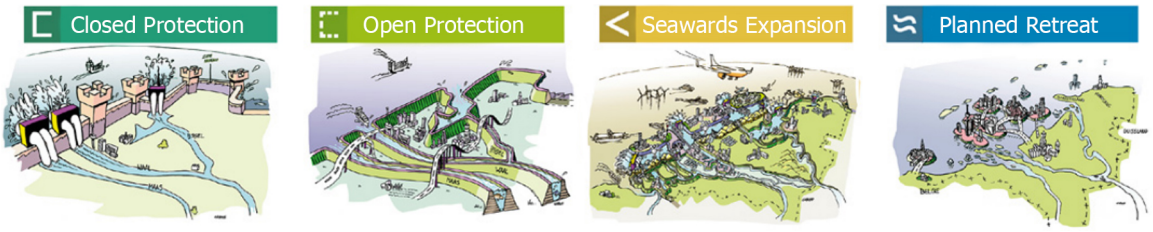

Figure 4.1: Four solution strategies for adaptation to sea level rise in the Dutch Deltas. Retrieved and modified from Haasnoot et al. (2019, p. 21).

4.2. Open/closed strategy

The open/closed strategy is in fact a continuation of the current strategy with the Maeslant storm surge barrier. In the following subsections, measures that are encompassed by the continuation of the open/closed strategy are stated and elaborated.

4.2.1. MLK+

The current Maeslant barrier reaches its technical limit around three closures per year, Kind et al. (2019) states that this limit could be stretched to 4 or 5 times per year. According to Fig. 2.6, this would roughly occur with 1.05 m and 1.10 m sea level rise, respectively. Compared to the limit of three closures per year, this extension is fairly limited and would extent the technical lifetime of the barrier with some years, dependent on the actual rate of sea level rise.

In Kind et al. (2019) the effects of a new Maeslant storm surge barrier, denoted as MLK+, are re-

viewed and the implementation of a new barrier could very well be possible with adjustments to the closing regime and/or technical feasibility, regarding the closing frequency. The current technical limit leads to the expenditure of the Maeslant barrier, however, if the design for MLK+ is properly designed for frequent closure of the barrier, the open-closable strategy continues to be a viable option for the region. As an example, The Hollandse IJssel barrier currently closes three times per year and this frequency is likely to increase to six times per year with a sea level rise of 0.5 m. Further increase in sea level will increase the closing frequency till a sea level rise of 2.0 m to 3.0 m is reached, then the barrier will be permanently closed. This does not result in technical failure of the barrier as it is designed for frequent closures, however, the problem lies with the hindrance of shipping and drainage of the Hollandse IJssel (Kind et al., 2019). The MLK+ option can be designed similarly as long as the economic interests of the Port of Rotterdam are incorporated, thus the scenario in which the MLK+ is permanently closed is not an option and the effectivity of the measure ends at this stage. Furthermore, the barrier type largely depends on the functional requirements following from e.g. shipping dimensions and required feasible closing frequency.

Estimated construction costs of MLK+

The construction costs of an open-closable barrier is very dependent on the type of structure, technical requirements and hydraulic head in which it is build. In Table 4.1 a comparison between different barriers in Europe is made. According to Jonkman et al. (2013), the costs ranges between M€0.5 and M€2.7 per meter width. For the implementation in the adaptive pathways, Chapter 5, the construction costs, M€656 in 2009 price level, for the Maeslant barrier is assumed to be valid for MLK+. Furthermore, the management and maintenance costs of such barrier amount to approximately 3% per year (Jonkman, 2021).

Table 4.1: "An overview of storm surge barriers around the world"(Jonkman et al., 2013, p. 1218). Retrieved from Jonkman et al. (2013, p. 1218).

Name of Barrier	Type	Year[a1]	Width (m)	Height (m)	Head (m)	Construction Costs (M€)	Construction Costs, 2009 Price Level (M€)	Unit Cost Process (M€/m width)
The Netherlands								
Maeslant barrier (New Waterway, Rotterdam)	Floating sector gate	1997	360	22	5	450	656	1.82
Hartel barrier (Hartel channel)	Vertical lifting gates	1997	170	9.3	5.5	98	143	0.84
Eastern Scheldt Barrier	Vertical lifting gates	1986	2400	14	5	2500	4021	1.68
Ramspol (near IJssel Lake)	Bellow barrier	2001	240	8.2	4.4	100	132	0.55
Europe								
Ems (Germany)	Sector gates	2002	360	8.5	3.8	290	368	1.02
Thames (Great-Britain)	Sector gates	1984	530	17	7.2	800	1449	2.73
St. Petersburg (Russia)	Floating sector gate	2011	200	16	4.2	n.a.	—	—
	Vertical lifting gate		100	7	4.2			
Venice MOSE project (Italy)	Flap gates	2012	3200	15	3	4678	4678	1.46
New Orleans								
Seabrook barrier	Vertical lifting gates and sector gates	2012	130	8	4	114.7	115	0.88
IHNC barrier—only gates (excl. floodwall) [a]	Sector gates	2011	250	8	4	518	518	2.07

[a] Remarks: (1) Year when the barrier is or is expected to be commissioned; (2) For the IHNC/storm surge barrier, only the parts containing the gates have been considered, and the floodwall costs were excluded.

Economic consequences closure

During a closure of the Maeslant and Hartel barrier no shipping is able to reach the inner port segments resulting in economic damage for the sector. In Ecorys and Deltares (2012), a first estimate of the economic consequences for the year 2050 in two scenarios, GE and LG as mentioned in Section 3.5.2, is supplied under the assumption that the barriers are due to close once every three years. For the Maeslant barrier this results in: GE M€3.4/y and LG M€2.2/y and for the Hartel barrier: GE

M€0.8/y and LG M€0.5/y. Contrary to Ecorys and Deltares (2012), Vos et al. (2014) suggests that the economic damages, in whichever scenario, due to a closure of the Maeslant barrier are "negligible". However, it is unknown what is considered as "negligible", therefore, the economic damages from Ecorys and Deltares (2012) are considered.

4.2.2. CHANGING THE CLOSING REGIME

Under the consideration that MLK+ adheres to the technical limit of three closures per year, the current closing regime could be altered to lengthen its technical lifetime and limit hindrance for shipping. In Table 4.2 the necessary adjustments considering the closing regime are stated. It has to be noted: increasing the closing level for Rotterdam means the closing level for Dordrecht rises with the same amount of metres and leads to higher hydraulic loads for flood defences behind the barrier, e.g. dikes. For the time being, it is assumed that dikes segments behind the protection of a barrier need to be heightened with the same magnitude as the increase in the closing regime, contrary to the adopted heightening of sea dikes by 2 metre with +1.0 m sea level rise, Section 4.4.5. Additionally, Kind et al. (2019) states that maintaining the current closing regime of NAP +3.0 m at Rotterdam with a sea level rise of NAP +2.0 m is not realistic, as the barrier is essentially closed permanently. The decision to change the closing regime and thus limit the closing frequency lies in the consideration of the economic development of the Port of Rotterdam.

Table 4.2: Closing regime considering Rotterdam and frequencies of MLK+. Retrieved from Kind et al. (2019, p. 7).

Tabel 2.1 Gehanteerde sluitpeilen en sluitfrequenties voor de MLK bij verschillende zeespiegelstijgingen

Zeespiegelstijging (m)	Faalkans MLK kering	Sluitpeil Rotterdam (m+NAP)	Sluitfrequentie (per jaar)
0 (huidig)	1/100	3,00	1/15
1	1/1.000	3,00	3
2	1/1.000	3,80	3
3	1/1.000	4,55	3

4.2.3. DOUBLE IMPLEMENTATION

Theoretically, with the implementation of MLK+ in series with the current Maeslant barrier, as suggested in Kind et al. (2019), the two barriers would work in turns, reducing the amount of closures for the barriers. If the closing regime of the present and technical limit of three closures per year per barrier are maintained, the technical tipping point of the double implementation would occur at six closures per year (three for each barrier), this approximately coincides with a sea level rise of NAP +1.13 m, see Fig. 2.6. The double implementation would lead to a lower failure probability of this system (Kind et al., 2019). This pathway could function under the assumption that the current Maeslant barrier is structurally sound to operate beyond its designed life time of 100 years. Although this is dependent on the fatigue of the structure due to sequential loading throughout its operational lifetime and is difficult to measure. The other option is to construct MLK+ twice. The extension of the technical tipping point to 1.13 m sea level rise is deemed insufficient and thus should be combined with other measures, e.g. changing the closing regime see Section 4.2.2. This option is exempted from the adaptive pathways, considering the amount of costs and uncertainty whether the current Maeslant barrier is able to function beyond its designated lifespan.

4.2.4. RAISING UNEMBANKED AREAS

Raising unembanked areas is the process in which the elevation of low-lying land or a riverbed is elevated to reclaim the land for other purposes. The process can also be undertaken by pumping out water in an enclosed area, which is known as poldering. The demand for raising these unembanked areas is likely to increase in demand over the future due to a growing population, sea level rise and

growth in global trade (Gatto, 2014).

In Section 4.2.2 the measure in respect to the closing regime of MLK+ is discussed. Altering the closing regime will impact some areas outside the primary dike defences, both in Rotterdam and Dordrecht, Fig. 4.2 and Fig. 4.3 respectively, and make these more prone to flooding. To provide flood risk safety, these areas could be artificially heightened in coalescence with the closing regime. Adjusting to the new closing regimes might prove to be difficult for the historical centre of Dordrecht. It is essential to plan ahead when considering this measure as rearrangement of these areas are required. In Table 4.4 costs estimations for raising industrial areas and harbours are stated in 2009 price levels.

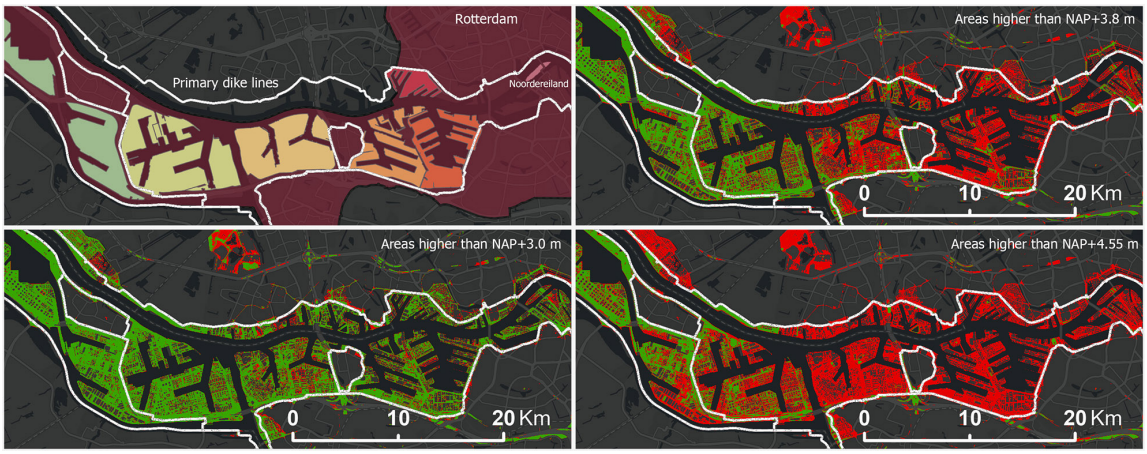

Figure 4.2: Areas in and near the municipality of Rotterdam below (red) or above (green) suggested closing regime water levels from Table 4.2. The white lines represent primary dike defences.

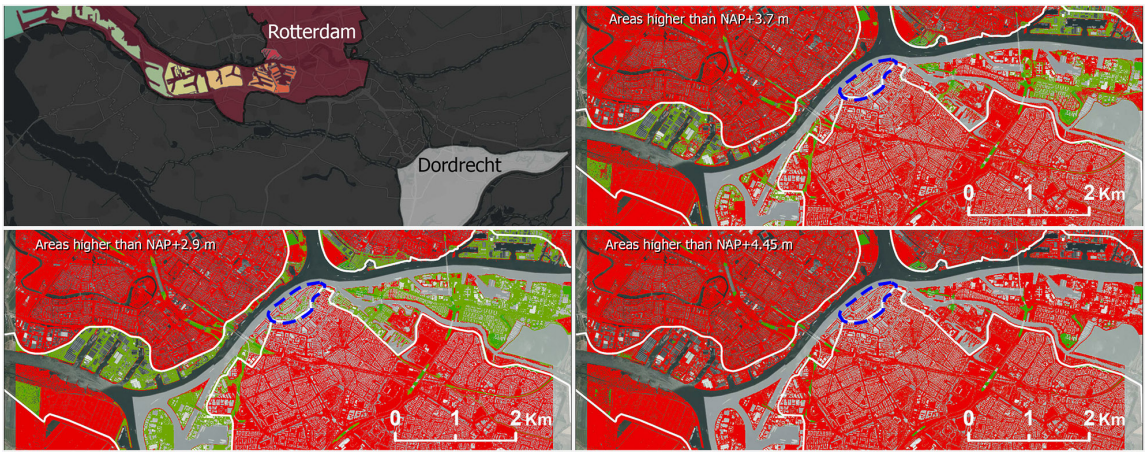

Figure 4.3: Areas in and near the municipality of Dordrecht below (red) or above (green) suggested closing regime water levels from Table 4.2 minus 0.1 metre to adjust for the closing levels in Dordrecht. The blue dashed line represents the historical centre of Dordrecht and the white lines represent primary dike defences.

4.3. CLOSED STRATEGY

A solution contrary to the open strategy presented in Section 4.1 and Section 4.2.1, is the closed strategy. This strategy closes off most of the estuary, dependent on the location of the hydraulic structure, with the implementation of a lock and dam complex. In the following subsections, measures that are directly attributed to this strategy are discussed.

4.3.1. SEA LOCKS

In this subsection the consideration of a sea lock is discussed and where possible quantified. From Ministry of Infrastructure and Environment (2016), Vos et al. (2014) and van Waveren et al. (2015) it is obvious that the overall preference of the involved institutions is to avoid the implementation of locks in the Rhine-Meuse estuary, especially in the New Waterway, due to the hindrance it implicates for the Port of Rotterdam. Nonetheless, this option is kept open to establish independent adaptive pathways in Chapter 5. To ease the process of evaluating this measure, the implementation is based on previously concluded research and assumptions. Reports by Ecorys and Deltares (2012), Vos et al. (2014) and van Waveren et al. (2015), the latter being conclusive report based on 'Plan Sluizen', consider a lock complex that includes three chambers. With the support of the literature an estimation of construction costs, Section 4.3.1, and economic damages for shipping, Section 4.3.1, are retrieved.

Estimated construction costs lock complex

To determine the estimated construction costs of a lock complex in the New Waterway the technical reports by Vos et al. (2014) and van Waveren et al. (2015) are compared. In Vos et al. (2014) the estimations are based on the assumption that the sea lock in IJmuiden, with chamber dimensions of 500 m by 70 m by 18 m, has to be applied three times to adequately minimise hindrance for shipping and balancing costs. The investment costs of the lock in IJmuiden are estimated to range between M€750 - 848. Multiplying this by three results in the nominal investment costs of M€2,250, 2013 price levels (Vos et al., 2014). Furthermore, the report provides additional information on expected lifetime costs:

- Management and maintenance costs determined as yearly averages over a period of 100 years: 0.4% equals to M€9.0 p/y
- Exploitation costs determined as yearly averages over a period of 100 years: 0.1% equals to M€2.3 p/y

In van Waveren et al. (2015) the investment costs for a sea lock situated in New Meuse River, with chamber dimensions 270 m by 37 m by 19 m, which is significantly smaller than the chamber of IJmuiden, is estimated at M€223. Reviewing the distribution of shipping in 2010 from Section 3.5.2 states that over 1,900 ships with length larger than 300 metres sailed over the New Waterway. It is likely that if the lock complex is constructed in the New Waterway these dimensions prove to be insufficient. Therefore the costs are extrapolated to match the dimensions of the chamber in IJmuiden and multiplied by three (number of assumed chambers) results in an estimated investment cost:

$$\text{Cost} = \frac{M€\,223}{270 \cdot 37 \cdot 19} \cdot 500 \cdot 70 \cdot 18 = M€740 \tag{4.3.1}$$

This value roughly matches that of Vos et al. (2014) and thus deemed to be suiting for a rough cost estimation of a lock complex situated in the New Waterway.

Economic consequences

The economic consequences of locks are based on the total delay for the passing ships. According to Ecorys and Deltares (2012) the waiting time for ships is estimated at 85 minutes in GE scenario and 43 in LG scenario in 2050 throughout the year. This results in economic damages of up to M€319.7 and M€95, GE and LG respectively. In Plan Sluizen the estimated economic damages for shipping is somewhere in between M€22 - 88 p/y in 2050. However, this is regarded as an underestimation based on expert judgement. For 2100 the additional costs vary between a reduction of M€18 and an increase of M€140 (van Waveren et al., 2015).

Furthermore, closing off the estuary will negatively impact the natural habit on three fronts: diver-

sity, connectivity and naturalness (Vos et al., 2014). According to the European Framework Directive on Water the loss of the habit should be compensated for. Albeit, most of the Rhine-Meuse estuary is not designated as a Nature 2000 protected area, a small stretch along the Old Meuse river between Spijkenisse and Dordrecht however is (European Commission, 2019). Thus, a measure compensating for the loss of ecology is introduced in Section 4.3.2.

Besides negative economic consequences the lock has the potential to reduce salt induced damages in the region. According to Vos et al. (2014), the lock has a reduction effect on salt induced damages and is assumed to be equal to approximately M€10 p/y by the year 2050. Due to lack of further research this value is assumed to be constant when adding the benefit in cost comparison.

4.3.2. NATURE COMPENSATION

The implementation of almost any infrastructural measure impacts surrounding nature. As mentioned in Section 4.3.1, the implementation of a sea lock will coincide with negative effects for nature: with the closure of both the New and Old Meuse rivers, the last open fish migration route, the New Waterway, is sealed and the tide behind the locks disappears, resulting in fresh water behind the locks (van Waveren et al., 2015) & (Vos et al., 2014). According to European law the loss of nature should be compensated for. In van Waveren et al. (2015), the application of a fish migration river, similar to the Afsluitdijk, could provide a way to reduce the negative impact of a lock, but does not completely prevent loss of nature in the area. van Waveren et al. (2015) estimates that this measure would costs M€50, in 2015 price levels. Moreover, it is unclear what the total costs are and whether it is possible to completely compensate the loss of nature due to the implementation of Plan Sluizen (Vos et al., 2014).

4.4. SUPPLEMENTARY STRATEGIES AND MEASURES

In this section measures that combine the open/closed and closed strategy, Section 4.4.2, managed retreat strategy, Section 4.4.3, seawards expansion, Section 4.4.4, and miscellaneous measures are discussed.

4.4.1. DELTA21

Delta21 is aimed at providing development in three aspects: improve flood risk protection, contribute to the ongoing energy transition and improve ecological situation. Basis of the plan is to construct a basin south of the Maasvlakte II, which functions as a energy storage lake providing a means to contribute to the energy transition. By installing a pumping capacity of up to 10,000m3/s, river discharge in critical coinciding conditions, as mentioned in Section 1.2, is diverted towards the sea via the energy storage lake. Diverting the surplus river discharge to the North Sea via the energy storage lake practically removes the Double Function of the Maeslant barrier, potentially decreasing its failure probability. Additionally, for the consideration of the sea locks in Section 4.3.1, the necessity of additional pumps or pumping stations is deducted due to the implementation of Delta21. Due to the scope of this thesis, this measure is assumed to be implemented in all scenarios and thus is not integrated as a separate measure in the adaptive pathways in Chapter 5.

4.4.2. MLK+ AND LOCK COMBINATION

To reduce economic damages during a closure of the MLK+, a lock can be integrated into the complex, providing a manner of passage for shipping. In Ecorys and Deltares (2012) the approximate waiting time during a closure of the Maeslant barrier with one integrated lock chamber is estimated with the use of a 'Kooman' model. This resulted in a computed waiting time of 444 minutes, which is the maximum the model is able to compute, and it is likely that the actual waiting time surpasses this value. Furthermore, the question is whether the lock, parallel to the MLK+, is able to provide

passage for ships during a storm surge. Throughout the first enforced closure of the Europoort barrier in 2007, the 'Grote Hartelsluis', the sluice adjacent to the Hartel barrier, was unable to provide passage for shipping (Staatscourant, 2007). Additionally, the amount of research conducted on the combination is limited, it is therefore difficult to quantify and truly include all effects, thus this measure is neglected.

4.4.3. MANAGED RETREAT

Besides increasing the flood risk safety of areas outside the primary dike defences the decision could be made that it is more cost-efficient to plan the abandonment of these areas over the period of many decades, gradually retreating behind the safety of flood defences. Costs of this measure are difficult to predict as these are dependent on the socio-economical development of these areas. In Aerts (2018) the costs of re-locating an average residential building is estimated at $353,537 in 2016 price levels. However, this figure does not represent the costs for The Netherlands and additional damages to socio-economic aspects of the inhabitants but supplies somewhat of a basis to estimate costs of the measure.

4.4.4. MAASVLAKTE III

An increase in hindrance for shipping leads to an increase in economic damage for the Port of Rotterdam and shipping in general via the New Waterway. Additionally, the urge to develop more residences in the outside dike areas, zone B in Fig. 3.2, could lead to an increase in pressure to displace the Eem-, Waal- and Petroleum harbour segments. To circumvent this issue, a third Maasvlakte could be constructed somewhere along the coast north of Hoek van Holland. South of the current Maasvlaktes could prove to be difficult as this area is designated as a Nature 2000 protected area. These three harbour segments have a combined surface area of 12.8 km^2, whereas Maasvlakte II encompasses over 9.6 km^2 and is estimated to cost M€2,900, excluding necessary infrastructural investments, in total. Displacing the inner harbour areas towards the sea positively reduces nuisance and pollution in the city of Rotterdam.

4.4.5. DIKES

The location and the rate of sea level rise dictate the amount of kilometres of dikes that should be strengthened and to which height. As stated in Section 3.3 the crest height can be computed with Eq. (3.3.1). For the adoption of this measure into the adaptive pathways in Chapter 5, the required increase of crest height due to sea level rise is determined based on Table 4.3 and the respective costs with Table 4.4. This should provide a rough estimate of costs and required space of this measure for the different pathways.

Table 4.3: "Effects of sea-level rise on changes in height, width, and cross section for a typical Dutch sea dike" (Jonkman et al., 2013, p. 1222). Retrieved from Jonkman et al. (2013, p. 1222).

Sea-Level Rise (m)	Δ Height[a], m (%)	Δ Width, m (%)	Δ Cross Section, m^2 (%)
0	basis = 10m	basis = 80m	basis = 425m
0.5	1 (10)	7 (9)	81 (19)
1	2 (20)	14 (18)	169 (40)
2	4 (40)	28 (35)	366 (86)
5	10 (100)	70 (88)	1125 (265)

4.4.6. FRESH WATER MEASURES

Measures to mitigate or reduce the negative effects of a deeper and lengthier salt intrusion into the Rhine-Meuse estuary vary between the aspects of water supply and water demand. As the focus lies

Table 4.4: "A comparison of unit costs as determined by IPCC CZMS (1990) and Hoozemans, Marchand, and Pennekamp (1993) with cost estimates from this study for The Netherlands (in 2009 prices)" (Jonkman et al., 2013, p. 1219). Retrieved from Jonkman et al. (2013, p. 1219).

	Previous Studies			This Study, 2009 price level (€)[a]
Adaptation Measure	Study	Original Price Level ($)	2009 Price Level (€)[a]	
Construction of sea dike (1 m high)	IPCC CZMS	M$0.4/km With maintenance: M$0.6/km	M€0.6/km With maintenance: M€1.0/km	-
Raising low sea dikes by 1 m in rural areas	IPCC CZMS	M$0.5/km	M€0.8/km	M€4.5–12.4/km per m raising
Raising high sea dikes by 1 m in rural areas	IPCC CZMS	M$1/km	M€1.6/km	
Stone protected sea dike[b]	Hoozemans, Marchand, and Pennekamp	M$4.5–8.5/km	M€6.8–12.8/km	
Clay-covered sea dike	Hoozemans, Marchand, and Pennekamp	M$2.5/km	M€3.8/km	
Raising sea dikes by 1 m in urban areas	IPCC CZMS	M$10/km	M€16.2/km	M€15.5–22.4/km per m raising
Closure dams	IPCC CZMS	M$15–25/km	M€24.3–40.6/km	-
Beach nourishment	IPCC CZMS	$3–6/$m^3$	€4.9–9.7 /m^3	€7–8/m^3
Sand dune	Hoozemans, Marchand, and Pennekamp	M$4.5/km	M€6.8/km	-
Raising industrial areas and harbours by 1 m	IPCC CZMS	M$15/$km^2$	M€20/km^2	-
Raising island elevation by 1 m	IPCC CZMS	M$12.5/$km^2$	M€16.7/km^2	-

[a] The original data has been converted to 2009 prices (in Euros [€])with a discount rate of 4% and an exchange rate of €1 =US$1.35.
[b] Depends on the depth of the toe on outer slope of the dike (see Figure 7).

more on the technical aspects of the flood defences in the estuary, one measure of each aspect is briefly discussed in Section 4.4.6 and Section 4.4.6. Stating only the basis of these measures should yield enough matter to represent the differences of the 'main' adaptation options for the Maeslant barrier, i.e. the manner of salt intrusion in an open strategy is likely to be more drastic than in a closed strategy and thus more measures are applied to mitigate this effect. In respect to salinisation, the general demand of maximum allowable chloride concentration varies between 150 to 450 mg/l and is considered as fresh (Klijn et al., 2012). According to Klijn et al. (2012), the maximum allowable chloride concentration for the three most important water inlet locations in the Rijnmond-Drechtsteden region are:

- Bernisse: 150 mg/l
- Beerenplaat (Drinking and industry): 150 mg/l
- Gouda: 250 mg/l

KWA - Water supply

Adopted in the late '80s, KWA (Kleinschalig Wateraanvoer) is a measure to prevent the intrusion of salt water into the Hollandsche IJssel at Gouda. If the Rhine river discharge dips below 1,100 m^3/s the measure is implemented to prevent damages to nature and agriculture. KWA then supplies an additional 7 m^3/s of fresh water, flowing from Bodegraven, into the river system. In 2003 and 2011 the activation of the measure in its current state was insufficient. Therefor, the volume of the measure is increased to 15 m^3/s by 2021, referred to as KWA+ (Klimaatbestendig Wateraanvoer), and the investment costs are estimated at M€40. (Deltaprogramma, 2015) This excludes additional yearly costs of maintenance and management: M€0.4 p/year, and activation: M€0.3 once every 8 years (van Waveren et al., 2015). To satisfy the anticipated water demand in 2050, the option to further increase this volume to a total of 24 m^3/s is discussed in H20 (2016), estimated to cost M€45 and added yearly costs of M€0.6 p/y with activation costs of M€0.3 twice every 8 years (van Waveren et al., 2015). These costs are included in the adaptive pathways, due to the fact that these measures are needed under the current strategy, open-closable barrier MLK, and are likely to maintain this

position if MLK+ is adopted. Although, no further indications of yearly costs and further development of the measure to cope with far future climate change is retrieved.

It is likely that due to climate change, increase in fresh water demand, more frequent and extreme drought events throughout the summer, the measure will be activated more often (Jeuken et al., 2012b). Additionally, according to Klijn et al. (2012), the current strategy alone is not future proof regarding climate change. Furthermore, according to Haasnoot et al. (2019) KWA+ becomes a fundamental measure active throughout most of the year with +1.0 m sea level rise and the measure is no longer sufficient when sea level rise reaches +2.0 m. It is probable that permanent fresh water supply from the ARK (Amsterdam-Rhine canal) and Lek are necessary. Other options like the POA (Permanente Oostelijke Aanvoer), in which water via Bodegraven and/or the Waaijers sluices is pumped towards the Rijnland to satisfy the current water demand, exists (HydroLogic BV, 2018). However, none of these options present estimates of costs and preliminary figures for the end and beyond the 21st century.

Salt tolerant crops - Water demand

Numerous agricultural companies are situated in and near the Rijnmond-Drechtsteden region, see left figure of Fig. 4.4. On the northern side of the municipality of Rotterdam most of these are horticulture and areas designated for livestock grazing. On the southern side of the municipality a mix of industry types can be found where agriculture is the most common type. In Table 4.5 the chloride concentration thresholds for different crops are stated. Deducting from Table 4.5 the thresholds for horticulture, greenhouses and various crops are considerably low and thus prone to economic damages due to salinisation. Changing the type of crop harvested in the Rijnmond-Drechtsteden region might reduce future economic damages in the agricultural sector in case of severe salt intrusion and droughts. The determination of the costs and benefits lies beyond the scope of this thesis, however, the measure is incorporated as an unquantifiable value.

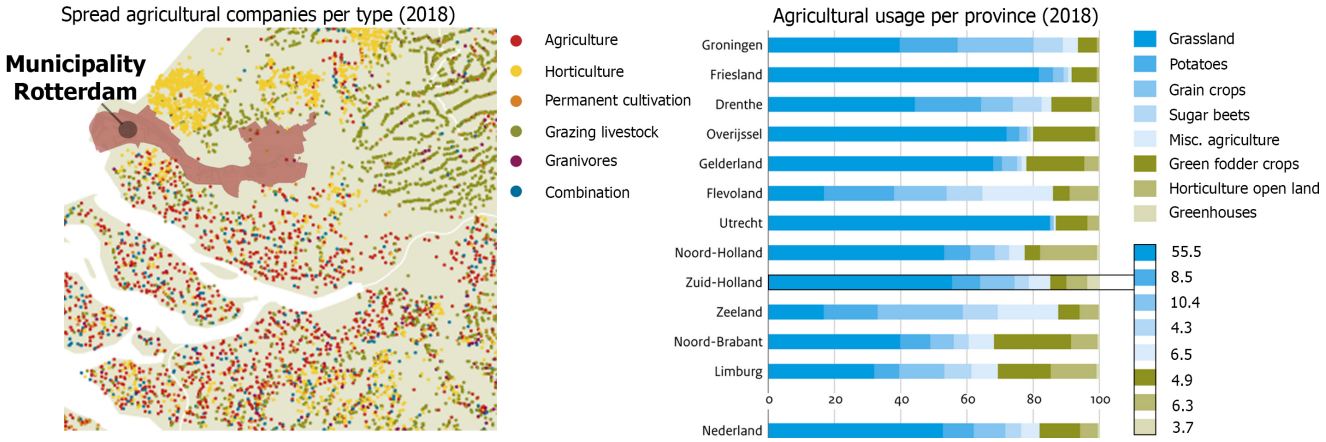

Figure 4.4: Left figure: Distribution of agricultural companies in the province of South-Holland.
Right figure: Percentages of different agricultural usage per province. Modified from CBS, PBL, RIVM and WUR (2018).

Table 4.5: Chloride concentration threshold for different crop types. Retrieved and modified from Jeuken et al. (2012a, p. 49).

Crop cluster	Soil solution Chloride concentration		Irrigation water Chloride concentration	
	threshold mg/l Cl	slope %/mg/l Cl	threshold mg/l Cl	slope %/mg/l Cl
Potato	750	0.016	200	0.061
Grass	3600	0.008	950	0.029
Sugar beet	4850	0.006	1300	0.021
Fodder maize	800	0.009	200	0.034
Grain crops	4850	0.006	1050	0.022
Fruit trees	650	0.026	150	0.099
Horticulture	400	0.189	100	0.709
Vegetables	900	0.016	250	0.059
Greenhouses	500	0.014	150	0.053
Flower bulbs	150	0.018	50	0.068

4.5. DEVELOPMENT OF THE FRAMEWORK FOR THE ADAPTIVE PATHWAYS

In the optimal form of success, no flooding will ever occur. However, financial aspects have to be taken into account as well. Overdimensioning structures enhances the loading capabilities of the structure as well as the costs and material use, financial funds and materials that could be designated for other valuable purposes for society. Although the focus of this thesis is of a technical nature and economical prospects of the region shall not be balanced to the available funds for flood risk safety, a comparison in costs between measures is taken into account. Furthermore, the framework might change over time, as mentioned in Chapter 2 the boundary conditions are set to change in the future, conditions to which it might be difficult to protect ourselves against. Besides physical conditions the potential developments in the Rijnmond-Drechtsteden alter the framework as well, creating a complex situation as multiple aspects are uncertain. As the eventual goal of this thesis is to design an alternative for the Maeslant barrier, through the establishment of adaptive pathways, the sea level rise is taken as the driving force for the different measures to take shape. The pathways determined in Chapter 5 should uphold and/or balance various aspects, retrieved in Chapter 2 and Chapter 3, and are listed:

- Dynamic robustness: Provide flood risk safety under a variety of sea level rise scenarios through adaptive measures balancing between safety and expenditures dynamic robustness
- Minimise economical consequences for shipping and the Port of Rotterdam where possible
- Consider the influence of salt infiltration
- Consider development of the Port of Rotterdam
- Consider socio-economical changes

Scorecard of the measures within the framework

The aforementioned measures in this chapter are summarised in a scorecard, Table 4.6, highlighting their impact and rated between + + and - -, representing the relative impact on the aspect of the measure, on the five aspects from the framework. Additionally, where possible the measures are quantified under the following columns:

- 'Sell-by SLR (m)', which represents the moment on which the measure should be activated in regard to the metres of sea level rise
- (Yearly) costs, which represents the estimated construction and exploitation costs
- Economic effects, which represents the economic consequences of the measure to e.g. shipping and salt induced damages/compensation

Table 4.6: Measures and assessment of their respective impact in terms on flood risk safety, shipping, fresh water, ecological, socio-economical and costs based on Chapter 2, Chapter 3 and Chapter 4.

Action or Measure	Impact					Sell-by SLR (m)	Costs (M€)	Yearly costs (M€)	Economic effects (M€)
	Flood risk safety	Shipping	Fresh water	Ecological	Socio-economical				
MLK+	+	+ +	-	0	0	+1.0	1,009.9	30.3	Per Closure: - 10.2 (GE) - 6.6 (LG)
Sea lock	+ +	- -	+	-	0	+1.0	2,250	11.3	Salt dmg red.: + 10 Shipping: - 319.7 (GE) - 95 (LG) - 31 (position)
Dikes heightening	+	0	0	-	-	p/m SLR	13.0-29.2 p/km /ΔH	0.6 p/km /ΔH	N.A.
Changing closing regime (NAP +3.8m)	-	+ +	-	0	-	+1.0	N.A.	N.A.	
Changing closing regime (NAP +4.55m)	- -	+ +	-	0	-	+2.0	N.A.	N.A.	
Current closing regime (NAP +3.0m)	0	-	0	0	0	+1.0	N.A.	N.A.	
Raising unembanked areas (NAP +3.8m)	+	+	0	0	+	+1.0	424.2	N.A.	
Raising unembanked areas (NAP +4.55m)	+	+	0	0	+	+2.0	529.0	N.A.	
Managed retreat 7,432 (+4.55 m)	+	+	-	0	- -	p/m SLR	5,414 (+3.80 m)		
	N.A.								

Table 4.6 continued from previous page

Action or Measure	Impact					Sell-by SLR (m)	Costs (M€)	Yearly costs (M€)	Economic effects (M€)
Maasvlakte 3	0	+	0	-	+	Any	2,900	N.A.	Reduces neg. effects on hindrance
KWA+ (15 m^3/s)	0	0	+ +	+	+	+0.0	40	0.5	Salt dmg red.: + 10
KWA+ (24 m^3/s	0	0	+ +	+	+	+0.0	40	0.8	Salt dmg red.: + 10
KWA+ (fundamental)	0	0	+ +	+	+	+1.0	45	2.2	Salt dmg red.: + 10
Additional supply ARK and Lek	0	0	+ +	+	+	+2.0	N.A.	N.A.	Salt dmg red.: + 10
Salt tolerant crops	0	0	+	+	+	Any			
Nature compensation	0	0	0	+ +	0	N.A.	N.A.	N.A.	N.A.

4.6. CONCLUDING REMARKS

Now that a broad scalar of measures are identified and, in most instances, quantified, the measures can be integrated to form an adaptive pathways plan that adheres to the instated criteria from the framework in Section 4.5. The scorecard in Section 4.5 helps inserting the quantitative values and (dis)advantages of the measures into the adaptive pathways that follow in Chapter 5. However, it should be considered that not all possible measures are identified in this chapter as most measures follow from retrieved literature and surround the functioning of hydraulic structures like the barrier and locks.

5 | Development of the adaptive pathways plan

Successive to the identification of the measures stated in Chapter 4, the formation of the adaptation pathways follows in this chapter. To enhance the understanding of the adaptive pathways, the considered flood defence system is reiterated in Section 5.1. Whereafter the adaptive pathway plan is explained in a phased fashion and two main pathways are elaborated in Section 5.2. Subsequently, these main pathways are compared under various sea level rise scenarios in Section 5.3. Lastly, a preferred pathway is chosen in Section 5.4 and marks the end of the first design loop. This chapter, together with Chapter 4, envelopes the development of concepts, verification, evaluation and selection of these concepts.

5.1. Flood defences system overview

Before visualising the adaptive pathways in Section 5.2 an overview of the considered system is supplied in Fig. 5.1. The figure includes the locations of both the current Maeslant and Hartel barriers, the municipalities of Rotterdam and Dordrecht and the dike-ring stretches that are incorporated for the expenditures computation in Appendix C.2 and Appendix C.4. Furthermore, an overview of the number of kilometres of rural and urban dike segments is supplied in Table C.13 and the changing number of kilometres, regarding four varying locations, is supplied in Table C.14.

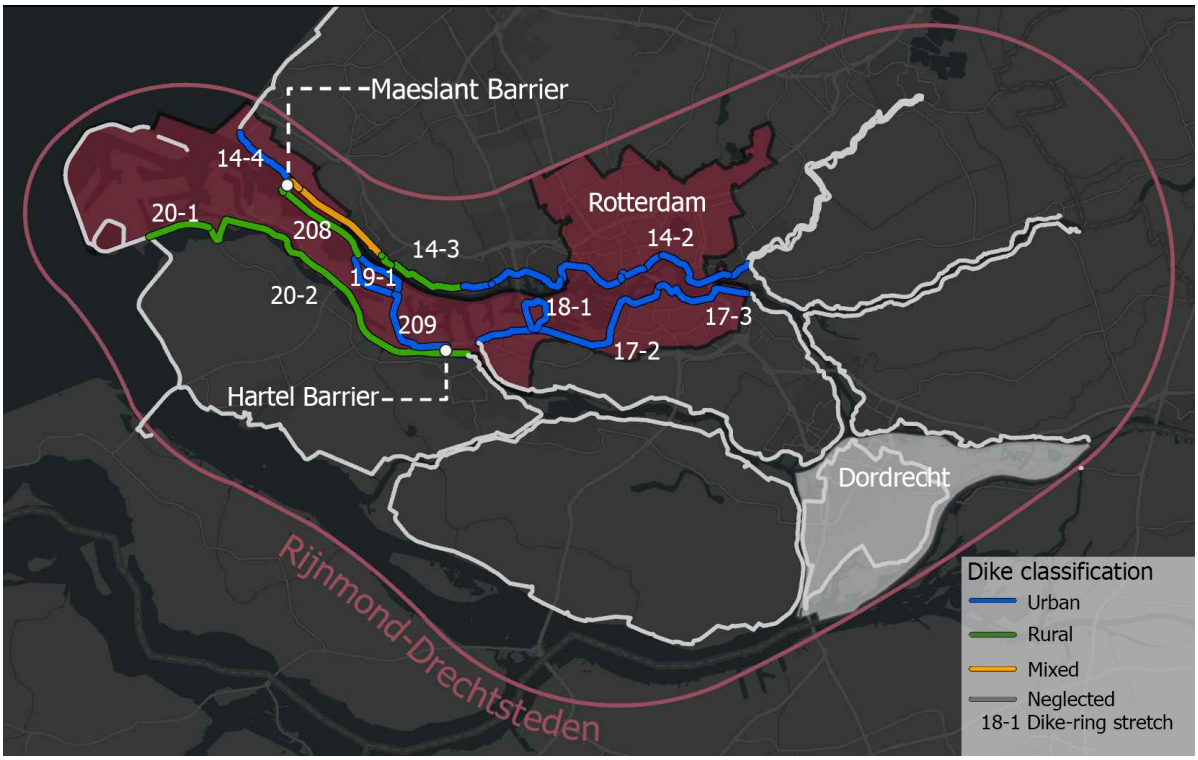

Figure 5.1: Overview of the system taken into account for the adaptive pathways in Section 5.2.

5.2. ADAPTIVE PATHWAYS

After analysing and linking the measures to values of sea level rise from Chapter 4 the adaptive pathways plan is developed. To understandably elaborate on the plan, a phased explanation of the plan is provided in this section. In Fig. 5.2 the first phase of the plan is presented. In this phase the layout of the plan, sea level rise on the x-axis, a legend and the actions or measures on the left side are presented. Additionally, the two main hydraulic structures, open/closed and closed from Chapter 4, are integrated and are presented as red lines, which form the core of the plan. The plan originates in the middle at 'Current policy MLK', which is the policy currently present in practice. At +1.0 metre sea level rise, coinciding with the limit of the current Maeslant barrier regarding the maximum number of closures within a year, the 'Current policy MLK' branches off into the two main strategies, namely 'MLK+' and 'Sea lock'. The measure of MLK+ has a limit at +3.0 metre sea level rise, as determined in Section 4.2.1. A red vertical line, originating form this point, can be seen to connect the measures of MLK+ and a Sea lock, indicating the necessity for a different strategy as the limit of the MLK+ has been reached.

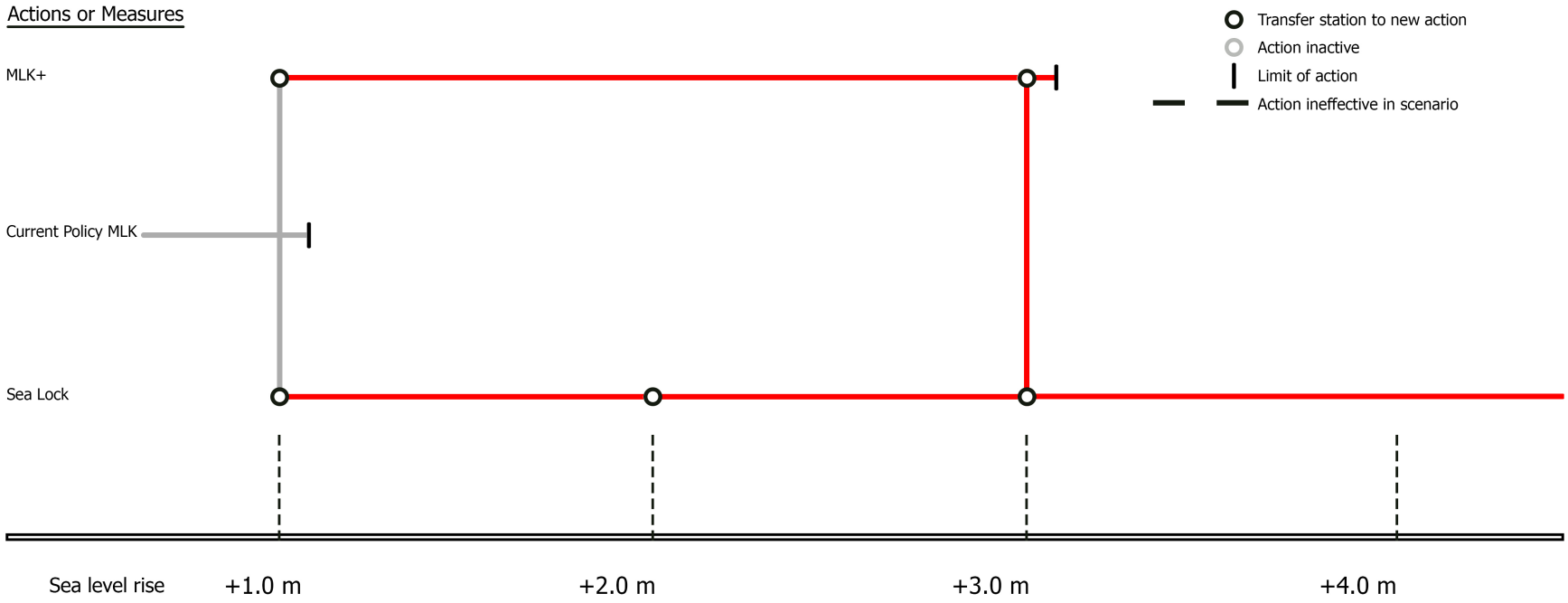

Figure 5.2: Basis layout of the adaptive pathways with the two main considered flood defence structures for the Rhine-Meuse estuary.

In the subsequent phase the measures 'Raising unembanked areas' (purple), 'Managed retreat' (green) and 'Dikes heightening' (dark red) are added. These measures influence the matter of flood risk safety in the system and are therefore grouped into this phase's explanation. As visible in Fig. 5.3, the measure 'Managed retreat' is presented as a striped line between values of +1.0 and +3.0 metre sea level rise. This represents the ineffectiveness of the measure under the occurrence of 'Scenario urbanisation'. With this measure the the unembanked areas, as stated in Section 4.2.4, are yielded to the rising closing regime in accordance with the sea level, substantiated in Fig. 5.6. If large amount of investments have been made in the unembanked areas the effectiveness of the measure drops, i.e. in 'Scenario urbanisation'.

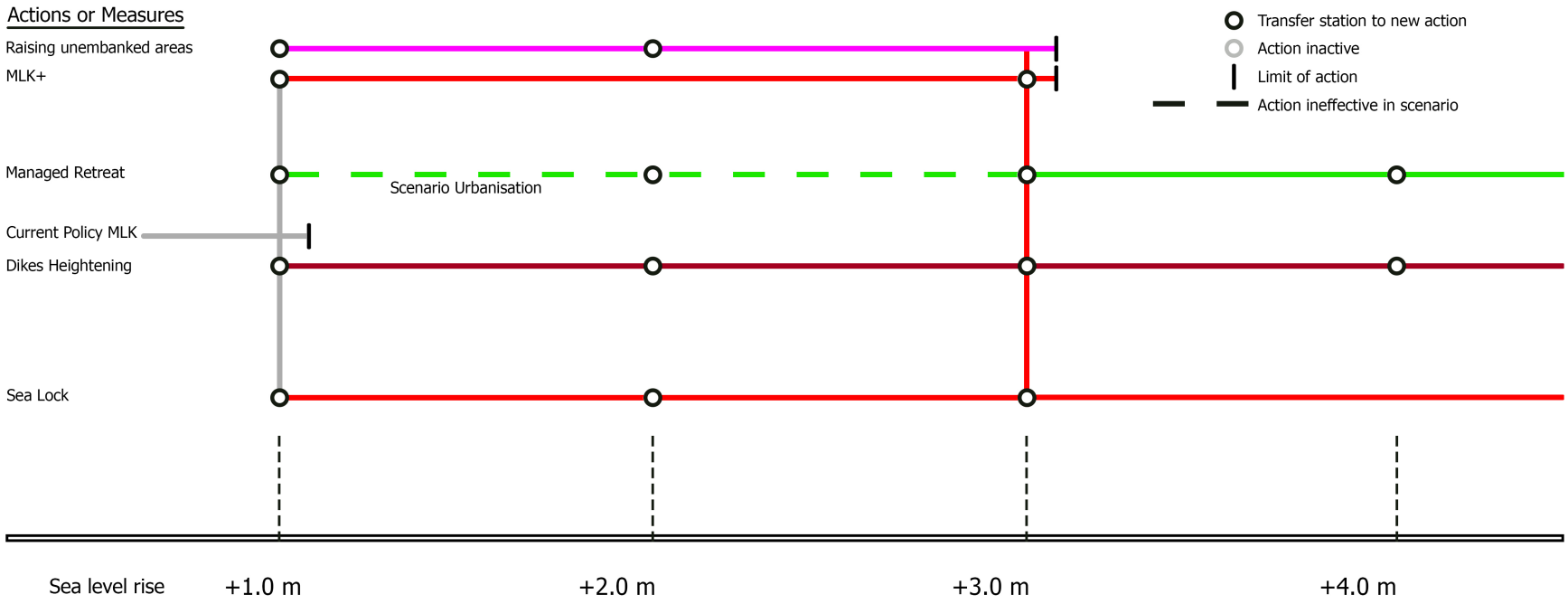

Figure 5.3: Continuation of the adaptive pathways from Fig. 5.2, where the measures 'Raising unembanked areas'(purple) and 'Managed retreat' (green) are added.

Further along, the measures 'Closing regime' (orange) and 'Maintain closing regime' (yellow), influencing the operational aspect of the closable barrier MLK+, are introduced. The measure 'Closing regime' is adaptable and has to be increased with increasing sea level to limit the maximum amount of closures per year to 3 times. The second measure influencing the operational aspect is in fact a continuation of the current policy in regard to the closing regime, closure of the barrier if water levels rise to NAP +3.0 metre. With this measure the amount of closures increases greatly with an increasing sea level and is substantiated in Fig. 5.6. Comparable as in Fig. 5.3, a striped line originating from the 'Maintain closing regime' at +2.0 metre sea level rise can be seen, indicating the ineffectiveness of this measure when 'Scenario intensification shipping' occurs. Under this scenario, an increases of traffic via the New Waterway is expected. Shipping utilising the waterway could be severely hindered under the expectation that the amount of closures of the barrier is to increase with increasing sea level, resulting in hefty economical damages for the Port of Rotterdam. Furthermore, it can be noted that two vertical lines, originating from the measure 'Closing regime', are connected to the other present measures. This is to indicate that the measure has to be combined with other measures at the same time and is further elaborated in Section 5.2.1 and Section 5.2.2.

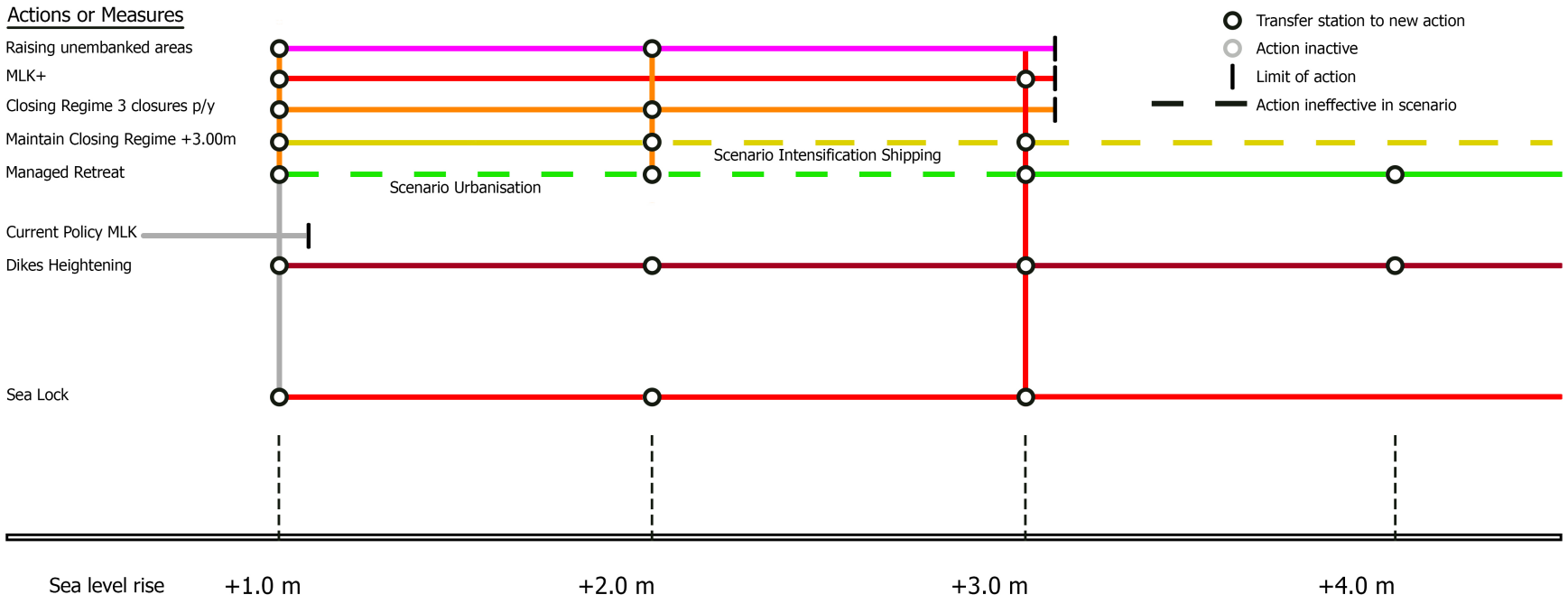

Figure 5.4: Continuation of the adaptive pathways from Fig. 5.3, where the measures that influence the operational aspects of the MLK+ are added, 'Closing regime 3 closures p/y' (orange) and 'Maintain closing regime'(yellow), respectively.

Second to last, the remaining measures, 'Maasvlakte 3' (bright blue), 'KWA+ fundamental', 'ARK and Lek supply', 'Salt tolerant crops' (all blue) and 'Nature compensation' (green), are added to the adaptive pathways. Various vertical lines originating from different measures and starting points can be noted, indicating the need of additional measures to be active. However, the lines overlap with each other, which reduces readability. In Appendix C.1 the various main pathways are identified, from these pathways the connectivity of these vertical lines become more clear.

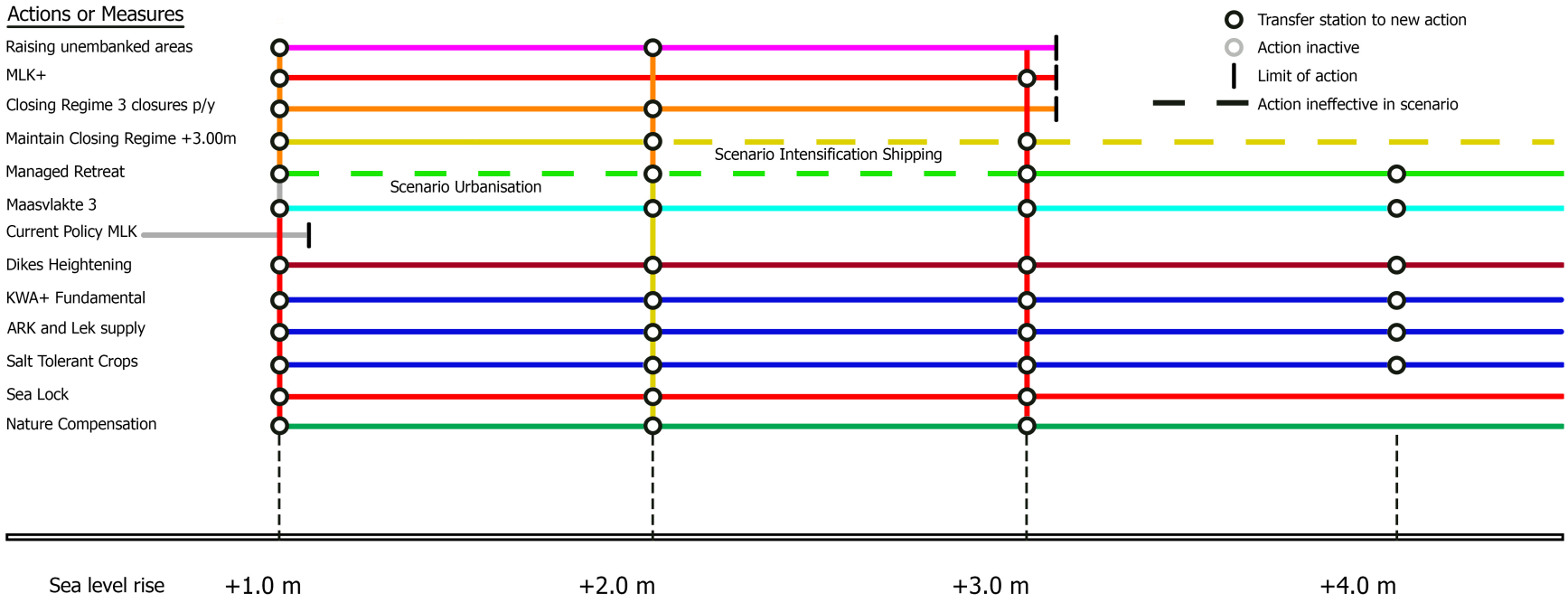

Figure 5.5: Adaptation pathways for the Rhine-Meuse estuary and Maeslant storm surge barrier.

Lastly, the measures, where possible, are substantiated and additional information is attached to the respective measures as well as a few tipping points. The tipping points for the individual measures are elaborated in Chapter 4, and can be found with the same name of the measure in this chapter. In Section 5.2.1 and Section 5.2.2, the two most complicated, out of four in total, main pathways are elaborated, providing a better distinction with different measures that can be undertaken and quantifying these strategies in economic values over the long-term. In these subsections, measures are either active, visualised by the lines being bright and starting with a circle with a black outline, or inactive when the colours are opaque or transparent and starting with a circle with a grey outline. These strategies all adhere to the definition of success in their own way as defined in Section 4.5. In Appendix C.1 all four of these main pathways are viewable.

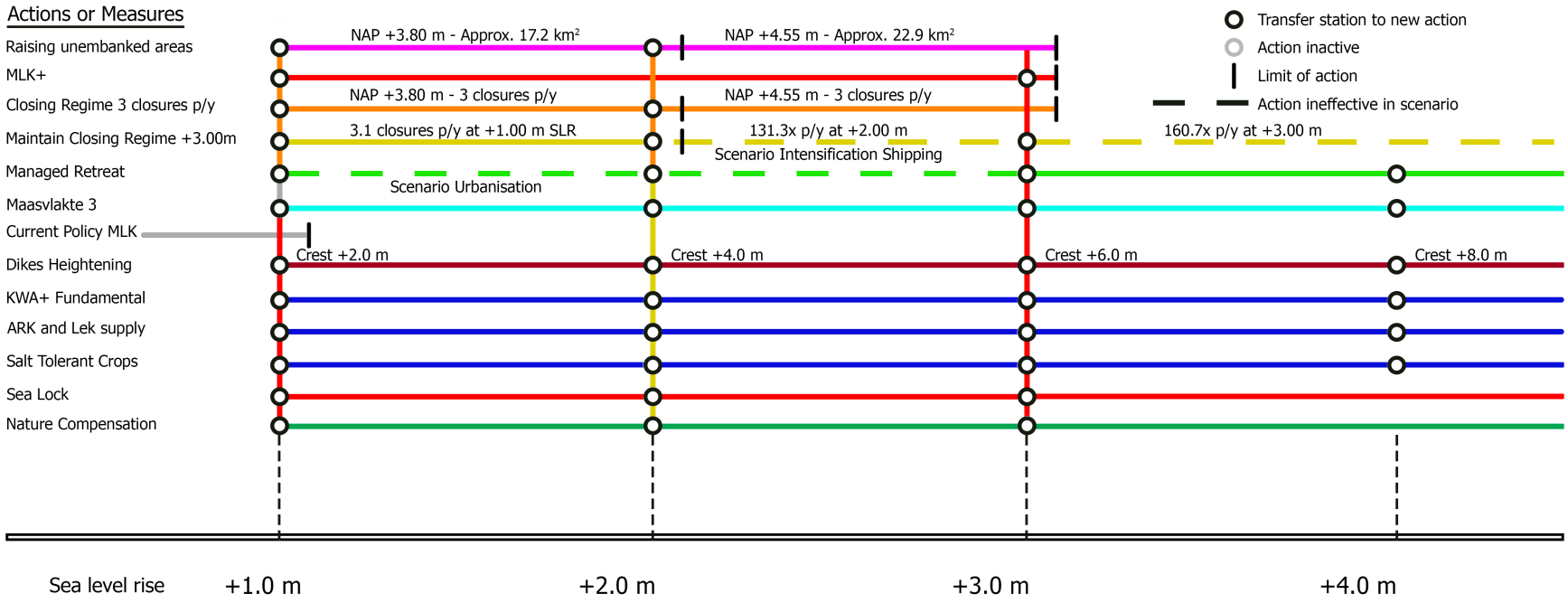

Figure 5.6: Adaptation pathways for the Rhine-Meuse estuary and Maeslant storm surge barrier.

5.2.1. Pathway A with MLK+ and raising unembanked areas

Pathway A, Fig. 5.7, represents the continuation of the current policy with a new hydraulic structure, MLK+, in combination with altering the closing regime, as envisioned in Section 4.2.2, to limit the number of closures per year. With +1.0 metre SLR this measure is combined with the first step of raising the unembanked areas, as envisioned in Section 4.2.4, elevating approximately 17.2 km^2 of surface area to NAP +3.80 m. This process is repeated at +2.0 m SLR for approximately 22.9 km^2 that lies below the new closing regime of NAP +4.55 m. To tackle the problem of salt intrusion, measures like KWA+ becomes fundamental and is probable that the amount of fresh water diverted towards the estuary increases along the x-axis. At +2.0 m SLR this measure is combined with additional fresh water supply via the ARK and Lek. At +3.0 m SLR the possibilities in terms of keeping the estuary 'open' narrows down towards the adoption of a sea lock, closing off the last open estuary of The Netherlands. This measure results in a loss of ecology and should be compensated for, and thus the nature compensation becomes active. Measures to reduce salt intrusion are deactivated at this point.

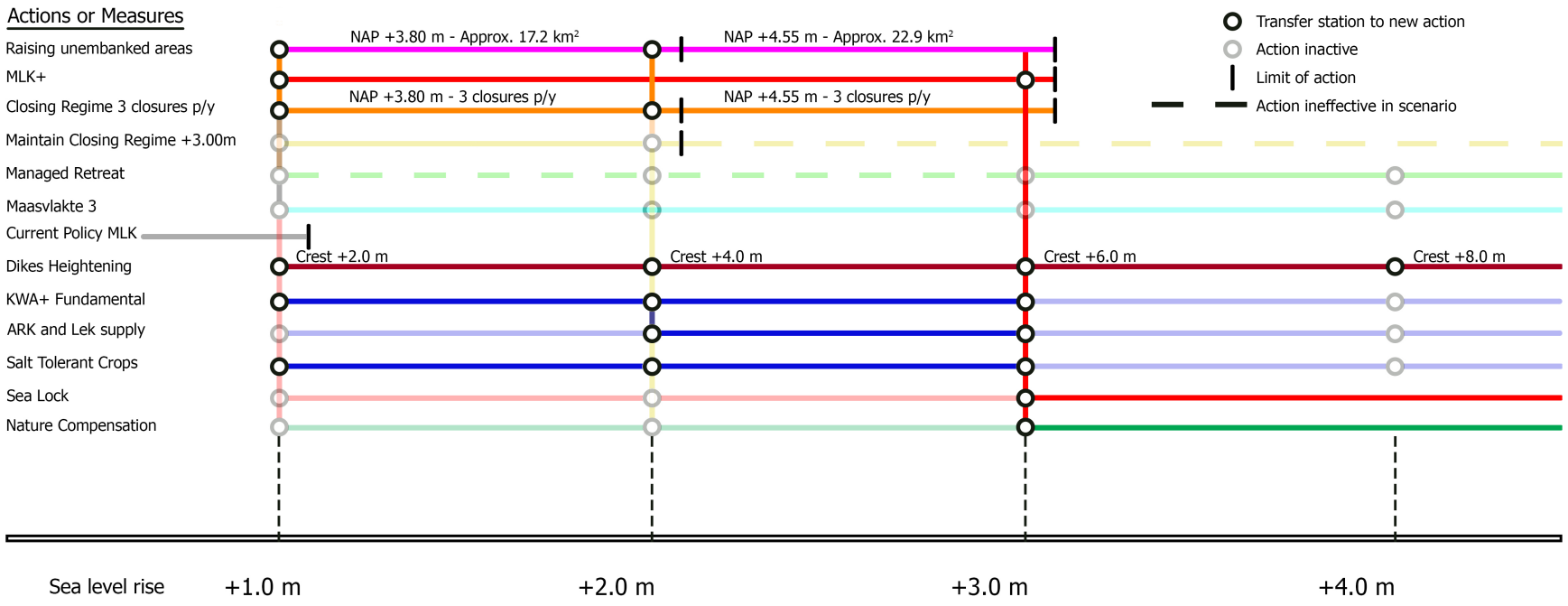

Figure 5.7: Pathway A. Continuation of the open strategy in combination with changing the closing regime and raising unembanked areas. Transparent lines indicate the inactivity of the measures, full coloured lines are active measures.

5.2.2. PATHWAY B WITH MLK+ AND MANAGED RETREAT

Pathway B, Fig. 5.8, is quite similar to pathway A, Section 5.2.1, however, one major difference is the activation of the managed retreat measure in combination with the changing closing regimes. Outside dike areas, as envisioned in Section 4.4.3, are abandoned in two steps, similar as the land reclamation measure in Section 5.2.1. It has to be noted that such a drastic measure can only be introduced under the right circumstances, as it could result in resistance from the general population and hinder (socio-)economic development in the region and should be incorporated with long-term planning (Haasnoot et al., 2019). Therefore, Managed Retreat is ineffective in case Scenario urbanisation, Section 3.4, develops.

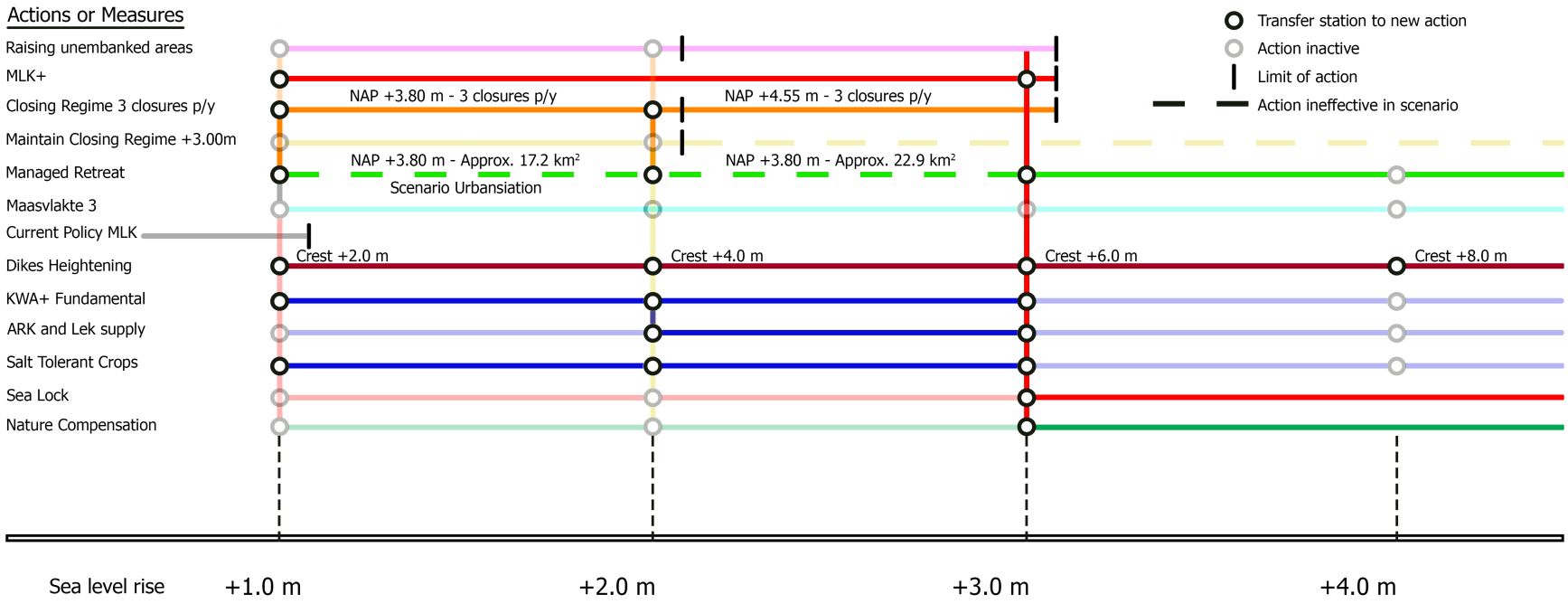

Figure 5.8: Pathway B. Continuation of the open strategy in combination with changing the closing regime and managed retreat. Transparent lines indicate the inactivity of the measures, full coloured lines are active measures.

5.3. COMPARISON OF THE MAIN PATHS

In this section, the economic performance of three promising pathways are presented under four sea level rise scenarios: the lower, median and upper boundary value of RCP8.5 from Fig. 2.3 and a hypothetical extreme sea level rise scenario, where the upper boundary value of RCP8.5 is multiplied with an additional factor (1.4 - 7.5 metre SLR by 2200). Additionally, two economic growth scenarios, LG (low) and GE (high), are integrated to present the differences of the pathways bearing the development of economic aspects of The Netherlands in mind. To increase the readers understanding on the method applied to compute the costs for each individual pathway under several sea level rise scenarios, a detailed elaboration for one pathway is supplied in Section 5.3.1.

Moreover, the implementation of several measures, e.g. salt tolerant crops (Section 4.4.6, KWA+ (Section 4.4.6) and nature compensation (Section 4.3.2), might not be properly quantified or unquantified due to unavailability of research considering these topics for the region. Furthermore, the economic consequences due to hindrance for shipping in case of a sea lock are quite normative, and dependent on the low or high economic growth scenario, dominant in the overall cumulative expenditure graphs which are discussed further on.

Furthermore, after pre-analysing all the pathways, pathways D and D2 - MLK+ with closing regime NAP +3.0 m, are withdrawn from the analyses in this section due to heavily under-performing in comparison to the other pathways. Nonetheless, the performance and calculations of these pathways are viewable in Appendix C.2 and Appendix C.3.4. In Table 5.1 the overall positive and negative effects of each pathway are stated:

Table 5.1: Side-effects for each of the four pathways in regard to varying values of SLR that represent certain tipping points.

Pathway A - MLK+ and raising unembanked ares

SLR +1.0 m - 3.0 m	**SLR > +3.0 m**
+ Open connection with the sea is maintained + Minimises hindrance for shipping and the Port of Rotterdam + Compensation for nature is delayed + Continuation of current preference strategy (excluding the closing regime)	+ Flooding probability due to high water at sea reduced to almost zero + Salt intrusion greatly reduced + Probable that harbour competitors in Europe disappeared behind locks, no loss in competitive position
- Salt intrusion increases with increase in SLR - Salt intrusion increasingly more problematic during summer and drought periods - Additional measures needed to counteract salt intrusion over SLR - Elevation of outside dike areas needed, coordinated planning in advance required - Historic centre of Dordrecht might be difficult to elevate - Heightening of dikes necessary due to change of closing regime, problematic for urban areas	- Hindrance for shipping is severe - Natural tide disappears - Severe nature loss, unknown whether full compensation is possible and costs - Investments in salt intrusion reduction measures are partly binned - Increase in salt intrusion over time

Pathway B - MLK+ and managed retreat

SLR +1.0 m - 3.0 m	**SLR > +3.0 m**
+ Similar to A, with additions: + Increases flood risk safety + No additional costs of area elevation	Similar to A, with addition: + Outer dike areas can be utilised again
- Similar to A, with additions: - Retreat of the outside dike areas will lead to resistance from the public - Restrictions on urbanisation of e.g. Rotterdam, challenge for growing housing shortage - Historic centre of Dordrecht might be difficult to yield	Similar to A

Pathway C - MLK+ and continuation of current closing regime

SLR > +1.0 m	
+ Flooding probability due to high water at sea reduced to almost zero + Salt intrusion greatly reduced + Maasvlakte III provides option to minimises economic losses for shipping and Port of Rotterdam	No additional effects
- Hindrance for shipping is severe - Port of Rotterdam losses in competitive position - Natural tide disappears - Severe nature loss, unknown whether full compensation is possible and costs - Increase in salt intrusion over time	No additional effects

Pathway D - Sea lock

SLR +1.0 m - 3.0 m	**SLR > +2.0 m**
+ Open connection with the sea is maintained + Minimises hindrance for shipping and the Port of Rotterdam + Compensation for nature is delayed + Continuation of current preference strategy + Dike heightening behind barrier not necessary + Possibility to make MLK+ less complicated than current MLK + Maasvlakte III provides option to minimises economic losses for shipping and Port of Rotterdam with increasing of closing frequency	+ Flooding probability due to high water at sea reduced to almost zero + Salt intrusion greatly reduced + Probable that harbour competitors in Europe disappeared behind locks, no loss in competitive position
- Increase in hindrance for shipping and Port of Rotterdam with increase of SLR - Could result in rapid transition towards locks - Scenario Intensification Shipping limits this Pathway - Salt intrusion measures needed, similar to Pathway A	- Hindrance for shipping is severe - Natural tide disappears - Severe nature loss, unknown whether full compensation is possible and costs - Investments in salt intrusion reduction measures are partly binned - Increase in salt intrusion over time - Investment made in MLK+ could prove to be inefficient due Scenario Intensification Shipping

5.3.1. ELABORATION ON COMPUTATION OF COSTS OF THE PATHWAYS

In this subsection the method of costs computation of the adaptive pathways is elaborated on the basis of pathway A - MLK+ with raising the unembanked areas in RCP8.5 upper boundary value sea level rise. What follows is a list of the various included expenditures, these are then inserted into Table 5.2 where the costs are determined between the period 2100 and 2200. The costs are then inserted in a cumulative expenditure graph, Fig. 5.9. Important to note is that all computed costs are in 2020 price levels, with constant values over the indicated period, and are computed with Eq. (5.3.1) where the net present value is computed with a discount rate of 4%.

$$NPV2020 = Cost_{year\ X} \cdot €1 \cdot (1 + \frac{4\%}{100})^{(2020 - year\ X)} \tag{5.3.1}$$

Expenditures:

- MLK+ construction costs: M€1,010 in 2020 price level, from Section 4.2.1 in 2009 price level
- MLK+ maintenance and management costs: approximately 3%, Section 4.2.1 equals to M€30 p/y in 2020 price level
- Raising unembanked areas NAP +3.80 m: approximately 14.2 and 3.1 km^2 in Rotterdam and Dordrecht, respectively, by 1 metre equals to M€424.2 in 2020 price level
- Raising unembanked areas NAP +4.55 m: approximately 19.1 and 3.8 km^2 in Rotterdam and Dordrecht, respectively, by additional metre equals to M€529 in 2020 price level
- KWA+ construction costs: combined costs of KWA+ incidental and increase to KWA++, M€48.7 and 54.7 in 2020 price levels, from Section 4.4.6 in 2015 price level
- KWA+ fundamental exploitation costs: equals to 2.2 M€p/y in 2020 price level, as determined in Section 4.4.6
- Sea lock construction costs: M€2,250 as determined in Section 4.3.1
- Sea lock maintenance and management costs: approximately M€11.3 p/y, as determined in Section 4.3.1
- Sea lock salinisation damage reduction: added benefit of -M€10 p/y, as determined in Section 4.3.1

Computation of dikes heightening costs, note: the current location of the Maeslant barrier is taken as reference in the computation of the amount of kilometres of dikes in need to be heightened:

- 28.1 (Rural) km and 16.65 (Urban) km of dikes in direct contact with the sea, see Table C.14, raising these dikes by 2 metres per 1 metre sea level rise, as determined in Section 4.4.5
- Multiplying amount of km of rural dikes with M€13.0 in 2020 price levels, average of Table 4.3
- Multiplying amount of km of urban dikes with M€29.2 in 2020 price levels, average of Table 4.3
- 3.8 (Rural) km and 51.32 (Urban) km of dikes in need for heightening by 1 metre, see Table C.14, regarding Closing regime, see Section 4.2.2, and Raising unembanked areas, see Section 4.2.4, measures
- Multiplying amount of km of rural dikes with M€6.9 in 2020 price levels, lower boundary value of Table 4.3 for the construction costs
- Multiplying amount of km of urban dikes with M€23.9 in 2020 price levels, lower boundary value Table 4.3 for the construction costs

Added damages

- MLK+ closures: 3 closures p/y due to Closing regime and Raising unembanked areas measures, economic consequences for shipping is estimated at M€20 and M€31 p/y in 2020 price levels, LG and GE respectively, as determined in Section 4.2.1
- Sea lock hindrance: economic consequences for shipping is estimated at M€95 and M€320 p/y in 2020 price levels, LG and GE respectively, as determined in Section 4.3.1
- Sea lock Competitive Position (CP): CP is the economic consequences for the Port of Rotterdam due to a decrease in the competitive position of the port, estimated at M€31 p/y in 2020 price levels, as determined in Section 4.3.1

Inserting the construction costs, which are assumed to be constant over the year, and yearly costs multiplied with the respective period results in Table 5.2. A complete overview of costs computations for each individual adaptive pathway is available in Appendix C.3.

Table 5.2: Cumulative costs calculation for Pathway A in RCP8.5 upper boundary sea level rise situation in M€.

Pathway A - Closing Regime and Raising unembanked areas										
Expenditures						**Switch to Lock**				
MLK+	Constr.	1,010	1,010	1,010	1,010	1,010	1,010	1,010	1,010	1,010
	p/y	30	757	1,515	2,272	3,030	3,030	3,030	3,030	3,030
	Total	**1,040**	**1,767**	**2,525**	**3,282**	**4,040**	**4,040**	**4,040**	**4,040**	**4,040**
Raising unembanked areas		**424**	**424**	**953**	**953**	**953**	**953**	**953**	**953**	**953**
Dikes	Constr.	2,908	2,908	5,816	5,816	7,473	7,473	9,130	10,787	10,787
	p/y	29	720	1,439	2,159	2,879	3,598	4,318	5,038	5,758
	Total	**2,937**	**3,628**	**7,255**	**7,975**	**10,352**	**11,072**	**13,448**	**15,825**	**16,545**
KWA+	Constr.	103	103	103	103	103	103	103	103	103
	p/y	2	55	109	164	219	219	219	219	219
	Total	**106**	**158**	**213**	**268**	**322**	**322**	**322**	**322**	**322**
Locks	Constr.	0	0	0	0	2,250	2,250	2,250	2,250	2,250
	p/y	0	0	0	0	11	283	565	848	1,130
	Salinisation	0	0	0	0	-10	-250	-500	-750	-1,000
	Total	**0**	**0**	**0**	**0**	**2,251**	**2,283**	**2,315**	**2,348**	**2,380**
Added damage										
Closures	LG	20	495	990	1,485	1,980	1,980	1,980	1,980	1,980
	GE	**31**	**765**	**1,530**	**2,295**	**3,060**	**3,060**	**3,060**	**3,060**	**3,060**
	Diff	**11**	**270**	**540**	**810**	**1,080**	**1,080**	**1,080**	**1,080**	**1,080**
Locks	LG	0	0	0	0	95	2,375	4,750	7,125	9,500
	CP	0	0	0	0	31	775	1,550	2,325	3,100
	LG + CP	0	0	0	0	126	3,150	6,300	9,450	12,600
	GE	**0**	**0**	**0**	**0**	**320**	**7,993**	**15,985**	**23,978**	**31,970**
	Diff	**0**	**0**	**0**	**0**	**194**	**4,843**	**9,685**	**14,528**	**19,370**
Cumulative	LG + CP	20	495	990	1,485	2,106	5,130	8,280	11,430	14,580
	GE	**31**	**765**	**1,530**	**2,295**	**3,380**	**11,053**	**19,045**	**27,038**	**35,030**
	Diff	**11**	**270**	**540**	**810**	**1,274**	**5,923**	**10,765**	**15,608**	**20,450**
	Total LG	**4,527**	**6,472**	**11,130**	**14,822**	**21,810**	**26,550**	**31,579**	**35,481**	**41,314**
	Total GE	**4,537**	**6,742**	**11,670**	**15,632**	**23,084**	**32,473**	**42,344**	**51,089**	**61,764**
RCP8.5 Upper bound	year	2100	2125	2150	2175	2200	2225	2250	2275	2300
	SLR (m)	1	1.6	2	2.45	2.9	3.5	4.2	4.8	5.4

The costs, as calculated in Table 5.2, are then presented in a cumulative expenditure graph over the period 2100 to 2200. In Fig. 5.9 the costs of MLK+, dikes and, around the year 2200, a sea lock are shown. It can be seen that the expenditures for dikes, as an example, contain certain hikes, these represent the necessary heightening of dike segments due to sea level rise, and lead to a sharp increase in expenditures. Further along, in Fig. 5.10, the expenditures of the other measures and hindrance to shipping, for both LG (low) and GE (high economic growth), are presented. It is worthwhile to notice, that around 2200, which coincides with the implementation of a sea lock, the economic damages to shipping increase sharply. This is due to the fact, that a lock has to be implemented as the MLK+ reaches its limit with +3.0 metre sea level rise and the economic consequences of a lock are higher in comparison to the consequences of MLK+.

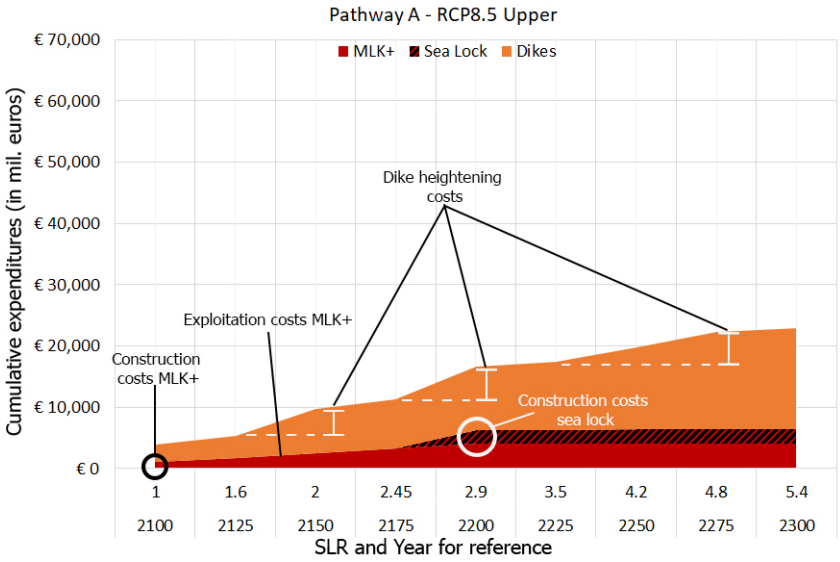

Figure 5.9: Cumulative expenditures graph for Pathway A considering MLK+, dikes and a sea lock, in RCP8.5 upper boundary scenario.

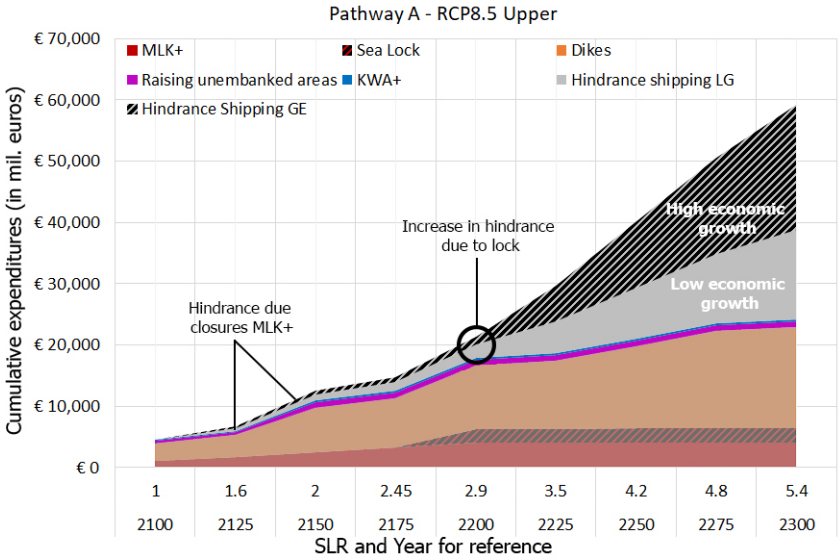

Figure 5.10: Cumulative expenditures graph for Pathway A considering all the appropriate measures in RCP8.5 upper boundary scenario.

The total cumulative expenditures graph, from Fig. 5.10, is then translated to a minimalistic presentation used to determine the relative performance of the pathway, Fig. 5.11, creating a distinction between the two economic scenarios (LG and GE) and two sea level rise scenarios (upper and lower boundary of RCP8.5). In which the cumulative expenditures of this pathway are clearly represented, to eventually compare the expenditures to that of other pathways under varying sea level rise scenarios. This process is repeated for the other adaptive pathways under four sea level rise scenarios, i.e the upper, median and lower boundary value of RCP8.5 and a hypothetical extreme sea level rise scenario, between the period 2100 and 2200.

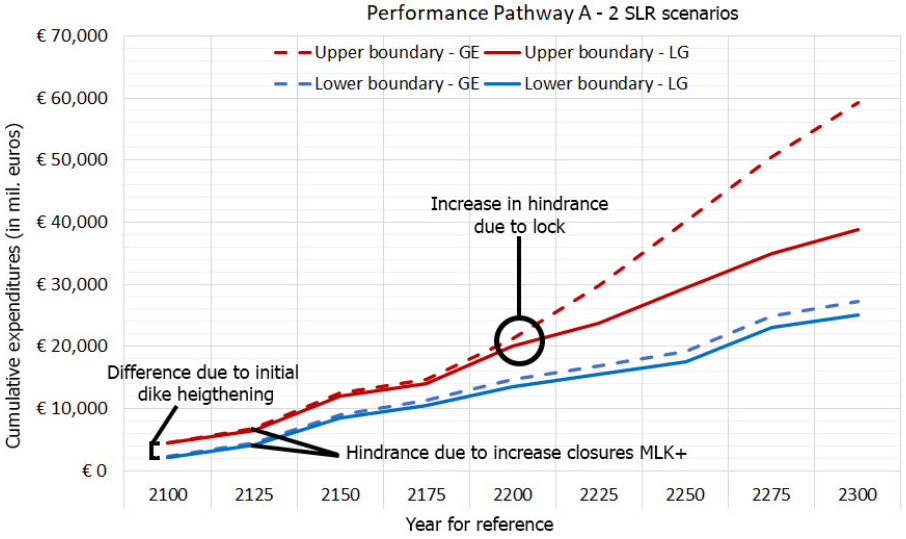

Figure 5.11: Cumulative expenditures graph for Pathway A in RCP8.5 upper and lower boundary SLR scenario.

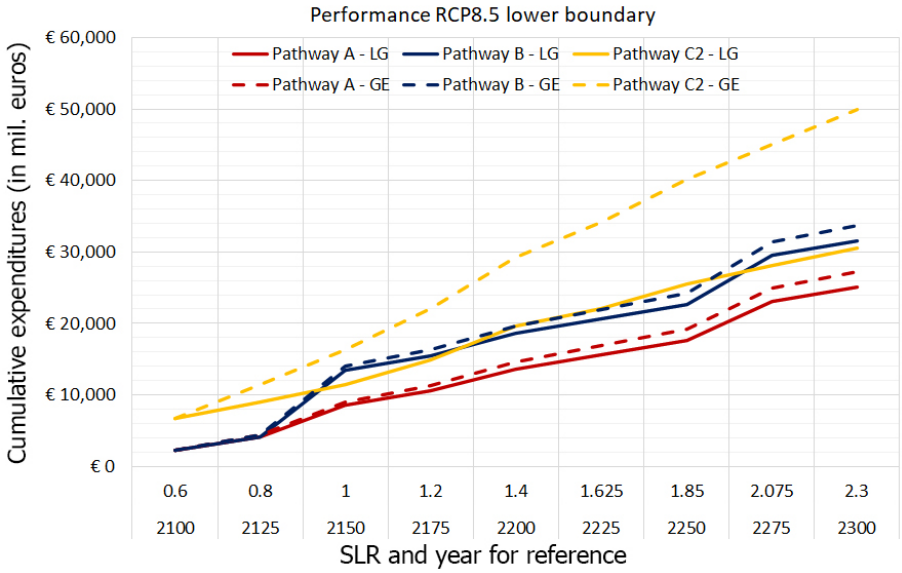

Figure 5.12: Cumulative expenditures for Pathways A, B and C2 under RCP8.5 lower boundary scenario. Cumulative expenditures visible on the y-axis. Sea level rise in metres and year for reference visible on the x-axis.

5.3.2. PERFORMANCE OF THE PATHWAYS IN RCP8.5 LOWER SCENARIO

In Fig. 5.12 the performance of Pathways A, B and C2 are represented in accordance with the lower boundary values of sea level rise scenario RCP8.5. A thorough elaboration of the conducted calcu-

lations can be read in:

- Pathway A: Appendix C.3.1, Fig. C.13 and Table C.3
- Pathway B: Appendix C.3.2, Fig. C.16 and Table C.6
- Pathway C: Appendix C.3.3, Fig. C.19 and Table C.9

When considering low expectation of sea level rise, the three pathways perform quite similarly expenditures wise. However, a rather large deviation in cumulative costs can be observed for Pathway C2 - GE, Fig. 5.12, as hindrance for shipping due to the lock amount over the years. The estimated economic consequences for shipping are quite high in the GE scenario, M€319.7 p/y as stated in Section 4.3.1, and contribute over half of the total cumulative expenditures.

5.3.3. PERFORMANCE OF THE PATHWAYS IN RCP8.5 MEDIAN SCENARIO

In Fig. 5.13 the performance of Pathways A, B and C2 are represented in accordance with the median boundary values of sea level rise scenario RCP8.5. A thorough elaboration of the conducted calculations can be read in:

- Pathway A: Appendix C.3.1, Fig. C.12 and Table C.1
- Pathway B: Appendix C.3.2, Fig. C.15 and Table C.6
- Pathway C2: Appendix C.3.3, Fig. C.18 and Table C.7

When considering the median expectation of sea level rise, the three pathways perform quite similarly in both LG and GE scenarios. In contrary to the performance of the pathways in Fig. 5.12, the cumulative expenditures of Pathways A and B start to increase significantly around 2200, due to the fact that a sea lock is implemented around this time, as the lifespan of MLK+ is assumed to be surpassed. In the eventuality that MLK+ could be designed for 150 years, the adoption of a sea lock can be delayed until further sea level rise (+3.0 m) occurs, reducing economic consequences for shipping.

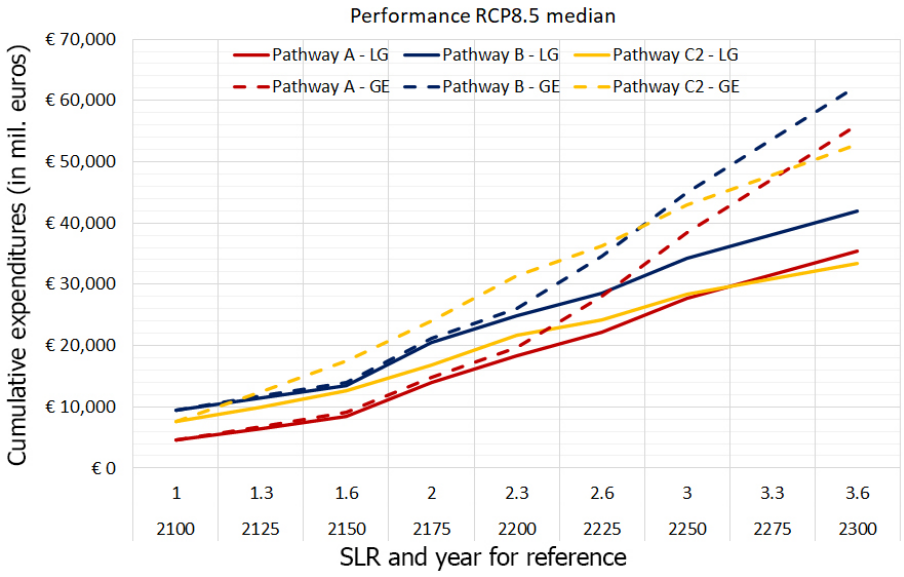

Figure 5.13: Cumulative expenditures for Pathways A, B and C2 under RCP8.5 median scenario. Cumulative expenditures visible on the y-axis. Sea level rise in metres and year for reference visible on the x-axis.

5.3.4. PERFORMANCE OF THE PATHWAYS IN RCP8.5 UPPER SCENARIO

In Fig. 5.14 the performance of Pathways A, B and C2 are represented in accordance with the upper boundary values of sea level rise scenario RCP8.5. A thorough elaboration of the conducted calculations can be read in:

- Pathway A: Appendix C.3.1, Fig. C.14 and Table C.2
- Pathway B: Appendix C.3.2, Fig. C.17 and Table C.5
- Pathway C2: Appendix C.3.3, Fig. C.20 and Table C.8

When considering the upper boundary expectation of sea level rise, the overall performance follows the same pattern as observed in Fig. 5.13. The expenditures are somewhat higher than in the median RCP scenario and this is largely due to the need for higher crests of dikes in the Rijnmond-Drechtsteden area. Additionally, it has to be noted, that investments have to be made earlier in time, compared to the median and lower RCP scenario, which is unbeneficial in general terms, as these funds could be spend on other aspects of society.

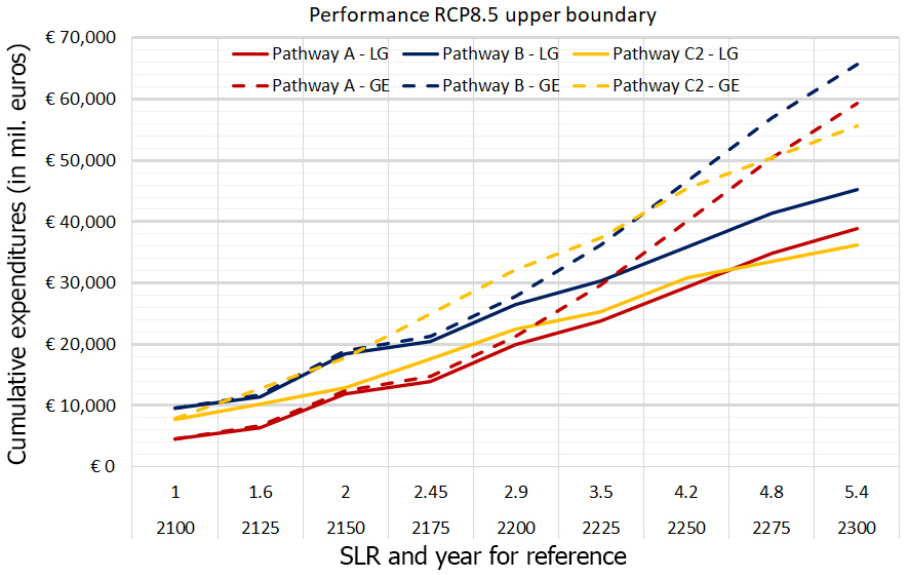

Figure 5.14: Cumulative expenditures for Pathways A, B and C2 under RCP8.5 upper boundary scenario. Cumulative expenditures visible on the y-axis. Sea level rise in metres and year for reference visible on the x-axis.

5.3.5. PERFORMANCE OF THE PATHWAYS IN EXTREME SEA LEVEL RISE SCENARIO

Lastly, the three pathways are compared in a situation that could represent the accelerated sea level rise, from Fig. 2.2 scenarios in Fig. 5.15. In this scenario it becomes evident that Pathway C2, with a third Maasvlakte, out performances the other open/closable pathways. This is largely due to the reduction, by the third Maasvlakte, in hindrance for shipping. Additionally, the MLK+ barrier in Pathway A and B reaches its tipping point around +3.00 m SLR, 2150 in this hypothetical scenario, reaching only half of its intended lifespan, resulting in the necessity to adopt the implementation of a sea lock earlier. This in turn leads to the necessity to replace that lock, if a life span of 100 years is maintained, by 2250, which is included in the expenditure computation.

However, it has to be considered that the implementation of a third Maasvlakte is available for Pathway A and B as well. Thus Pathway C, without a third Maasvlakte, is added to the graph to compare the pathways on an equal basis. Resulting in fairly similar cumulative expenditure paths.

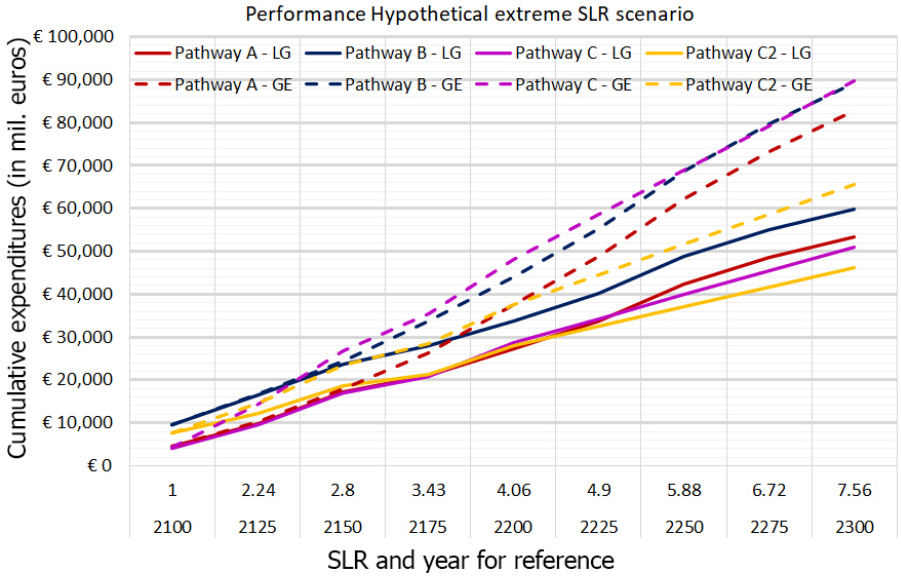

Figure 5.15: Cumulative expenditures for Pathways A, B and C2 under RCP8.5 lower boundary scenario. Cumulative expenditures visible on the y-axis. Sea level rise in metres and year for reference visible on the x-axis.

5.4. CONCLUDING REMARKS

From the comparisons drawn between Pathway A and B it becomes clear that, considering the expenditures and socio-economic aspects, the measure 'raising unembanked areas' has the preference over 'managed retreat', independent from the sea level rise scenario. However, it should be noted that as of yet, the closing failure probability of MLK+ has not been accounted for in the cumulative expenditures calculation, which could lead to damages due to floodings and should be added as a risk for the unembanked areas. On the other hand, retreating from the unembanked areas is likely to lead to resistance from the residents and population in general, this measure could prove to be additionally difficult to implement due to the ongoing urbanisation and growing housing shortages: Scenario Urbanisation. Nevertheless, both pathways can be considered as viable options, in which Pathway A has less expenditures and negative side-effects, as represented in Table 5.1.

When comparing the implementation of MLK+ to a sea lock, Pathway A/B and C (without Maasvlakte III) respectively, it is evident that the most dominant contributor to total expenditures is the hindrance for shipping, independent from economic and sea level rise scenarios. To make Pathway C more consistent with the other two, the measure Maasvlakte III is added and from here on denoted as C2, providing a reduction in hindrance to shipping. In contrast, the same measure could also be adopted in Pathway A and B, which would probably lead to a significant drop in expenditures. When taking a closer look into the hypothetical sea level rise scenario, it becomes evident that Pathway C2, is likely to perform better than the Pathways A and B. This is mostly due to the fact that the needed dike heightening, in-front and behind the barrier and lock, are now equalising or surpassing hindrance for shipping in terms of costs, and also because the lifespan of MLK+ is surpassed within 50 years, which makes it a costly investment in high sea level rise scenarios.

Besides considering the quantified measures from Chapter 4, other aspects that may not have been properly quantified or substantiated, due to lack of completed research, have to be considered. The

economic consequences due to the increasing intrusion of salt into the mainland are not integrated and should definitely be incorporated to establish a complete image of adopting the MLK+ option for the region. Additionally, the ecological impact by closing of the estuary has not been quantified as well. As stated in Section 4.3.2, no estimation of costs are available as of yet, and the question is whether it is even possible to fully compensate. Furthermore, the third Maasvlakte has been discussed, proving to greatly reduce the economic consequences for shipping, although research on the matter is slim. Various factors like the availability of enough sand and other building materials, compensation for ecology, public resistance and willingness of the Port of Rotterdam are not represented in the expenditures figures. Moreover, the future of the port itself is quite uncertain, increasing frequency of draught might hinder the usage of inland river and the transition to durable energy sources might greatly reduce the total amount of cargo handled in the port, nonetheless the ports' importance for the region is present but at this stage uncertain. Furthermore, the closing failure probability of MLK+ can not be neglected, especially in scenarios in which a closing frequency of three times per year is guaranteed, in comparison with the sea lock, which has a failure probability of near to zero.

Concluding, all pathways provide various positive and negative side-effects as presented in Table 5.1, but none, with the exception of Pathway D in median-higher sea level rise scenarios, prove to be inadequate for the region. In most of the scenarios the hindrance to shipping is a major driver in expenditures, it is advisory to correctly assess the exact costs of a closure of MLK+ and consequences of a lock as the economic consequences deviate with quite some margin when comparing two different technical reports, as stated in Section 4.3.1. The third Maasvlakte provides a reduction of these estimates, and could prove to be especially appealing in case Scenario Urbanisation, see Section 3.4, which represents the ongoing urbanisation of the unembanked areas of e.g. Rotterdam, continues under pressure of the growing housing shortage. Considering the level of confidence of the scenarios, the performances yielded from the median RCP8.5 scenario is the most prominent. Looking at a 100 year time span the preferable pathway is A - MLK+ with altercations to the closing regime. This pathway, or system, is developed further for the remainder of this thesis.

6 | Selection of barrier location

In this chapter the second design loop is started and a suitable location for the barrier is selected. Initially, multiple locations are taken into account in Section 6.1, followed by an analysis of these locations, leading to the selection of one location through the utilisation of a Multi Criteria Analysis in Section 6.2. This chapter envelopes the development of location concepts, verification, evaluation and selection of concepts.

6.1. CONSIDERED LOCATIONS

For the implementation of MLK+ in the preferred pathway, four locations are considered, see Fig. 6.1. These locations follow from the analysis of the region in Chapter 3, literature and conducted research. Location Maasdijk, Petroleum -and Delfshaven have been considered in a previously conducted thesis research (Dorrepaal, 2016) for a sluice able to replace the current Maeslant barrier, location Petroleumhaven also coincides with Plan Sluizen (van Waveren et al., 2015). Location Hoek van Holland (HvK) is added as this plan provides the largest reduction of dikes in direct contact with the sea. Additionally, two options for location HvK are considered. One in which MLK+ is situated solely in the New Waterway, similar to the current location of the Maeslant barrier only further downstream, denoted as HvK I, and one in which MLK+ is implemented as such that it also provides flood protection for the port areas that are situated outside any primary flood defence, i.e. Maasvlakte I, II and the Europoort port segments, zone A in Fig. 3.2, and is denoted as HvK II. Worthwhile to note, is that the current Europoort barrier consists out of the Maeslant and Hartel barrier, and a dike connecting the two. Only in case of location HvK II a 'new Hartel barrier' is not needed.

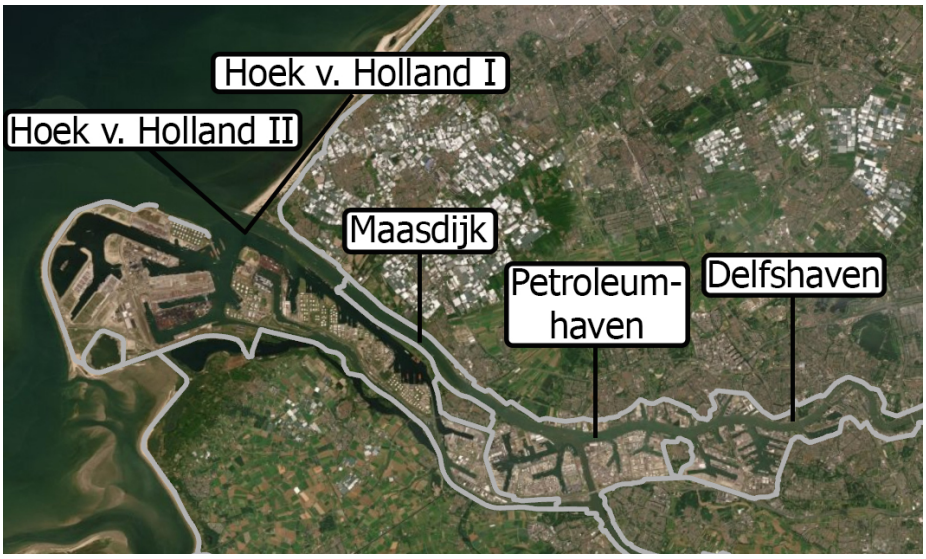

Figure 6.1: Considered locations for both MLK+ and a sea lock.

6.2. MULTI-CRITERIA ANALYSIS

To determine a preferred location for MLK+ poses quite a challenge, as for an initial design a location is needed and simultaneously a location is required to initiate the design. The location is selected by comparing five criteria: hindrance to shipping and flood defence cost reduction (Section 6.2.1), amount of unprotected surface (Section 6.2.2), available construction space (Section 6.2.3) and impact of hydraulic loading in the form of the significant wave heights (Section 6.2.4). The locations are scored through a multi-criteria analysis (MCA) (Section 6.2.5) due to the lack of conclusive demands from the hypothetical client.

6.2.1. HINDRANCE TO SHIPPING AND COSTS FLOOD DEFENCES

The consequential economic effects and construction costs these locations have on hindrance for shipping and the amount of dikes that have to be heightened is thoroughly elaborated in Appendix C.4. From the computations the overall economic costs, considering sea-dike heightening and hindrance to shipping, of each location is retrieved and presented in Fig. 6.2. Evidently, it can be concluded that constructing a hydraulic structure closer into the mainland leads to an increase of dikes segments in direct contact with the sea, increasing the costs for dike heightening under the influence of sea level rise, which explains the increased costs for locations Maasdijk, Petroleum -and Delfshaven. However, the costs of location HvK I surpasses that of Maasdijk, this is due to the fact that an additional dike segment has to be constructed along the New Waterway, connecting dike segment 208 (Fig. 5.1) with location HvK I (6.5 km). Moreover, location HvK II provides the lowest amount of yearly costs, with the implementation of MLK+ and altering the closing regime so that no more than 3 closures per year occur, due to the greatest reduction of dike stretches in direct contact with the sea. However, the Port of Rotterdam becomes completely inaccessible during a closure of the barrier.

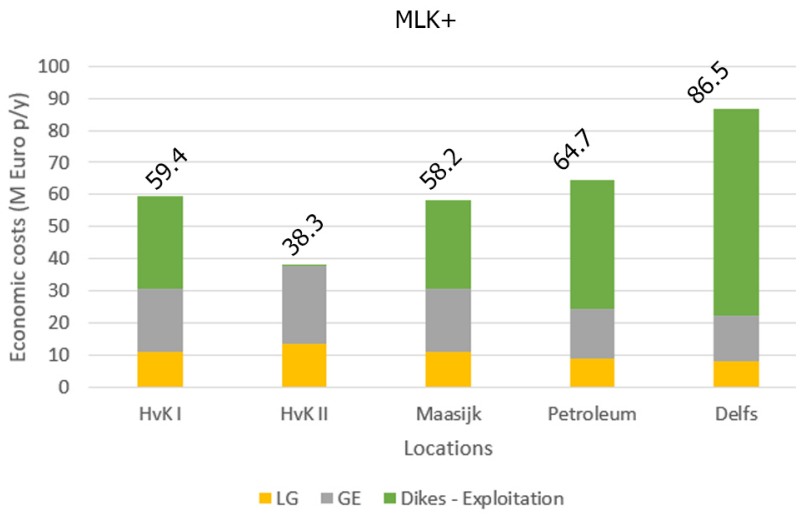

Figure 6.2: Yearly economic costs due to hindrance for shipping, in low (LG) and high (GE) economic growth scenarios, and maintenance costs of the dikes regarding the different locations in 2020 price levels. The costs to shipping due to a closure of MLK+ is based on three closures per year.

What rests is the inclusion of the construction costs of the barriers for the locations. In Table 4.1 the costs of the current Maeslant and Hartel barrier are presented in 2009 price levels, extrapolating these to 2020 price levels result in M€1,010,- and M€220,-, respectively. As an initial estimation it is assumed that twice the length of the current Maeslant barrier is required to provide flood protection for location HvK II and the construction cost is multiplied by two: M€2,020,-. This results in

Table 6.1:

Table 6.1: Construction cost estimation for the various locations, in 2020 price levels.

Location	MLK+	Hartel+
HvK I, Maasdijk, Petroleum -and Delfshaven	M€1,010	M€220
HvK II	M€2,020	-

6.2.2. UNPROTECTED SURFACE

Moreover, under increasing sea level rise it is not unthinkable that artificially elevated port segments, i.e. Maasvlakte I, II and Europoort segments, have to be elevated accordingly. As of yet, this is not incorporated into the costs indication of Fig. 6.2, and thus, a supplementary indication is provided in Table 6.2. The figures, in terms of costs, of each location are relatively close to each other, with the exception of locations HvK II in which the barrier is constructed in such a manner that is able to fully protect all of the unembanked areas.

Table 6.2: Total amount of unprotected surface area of the Port of Rotterdam respective to the various locations and an indication of costs per metre of raising.

	Total unprotected surface (km^2)	**Indicated costs per metre raising (M€)**
Location HvK I	67.07	2,065
Location HvK II	0	0
Location Maasdijk	67.07	2,065
Location Petroleumhaven	74.97	2,308
Location Delfshaven	89.16	2,653

6.2.3. AVAILABLE SPACE

Most barrier types require available space to store the gates when opened as is the case with the current Maeslant barrier. The current Maeslant barrier roughly accounts for 0.10 km^2 on each side of the riverbank. It is therefore reviewed whether all four locations provide enough available space to store an equivalent type of structure. Worthwhile to mention, some barrier types, i.e. lift gates and rotary segments, do not necessary require the same amount of available space as the gates do not have to be stored on the riverbanks.

In Fig. 6.3 an overview of the four locations and available space is supplied. Usable spaces are coloured, with a distinction between space directly available for the structure (blue and dark green at locations HvK and Maasdijk) and storage of building material (yellow and light green) if necessary. It can be deducted from Fig. 6.3 that locations Petroleumhaven and Delfshaven are situated in a dense urban and/or industrial areas, making it more difficult and costly to reserve the required space on the river banks. Locations HvK and Maasdijk do provide such available space. However, for option HvK II an immense barrier is needed, one that does not limit shipping in any matter, as the length of the waterway at this location is roughly 1.3 kilometres, in comparison, the current Maeslant barrier spans just over 360 metres. This could prove to be an impossible challenge without constructing piers in the waterway and thus creating hindrance for shipping. Resulting in the deduction of this option.

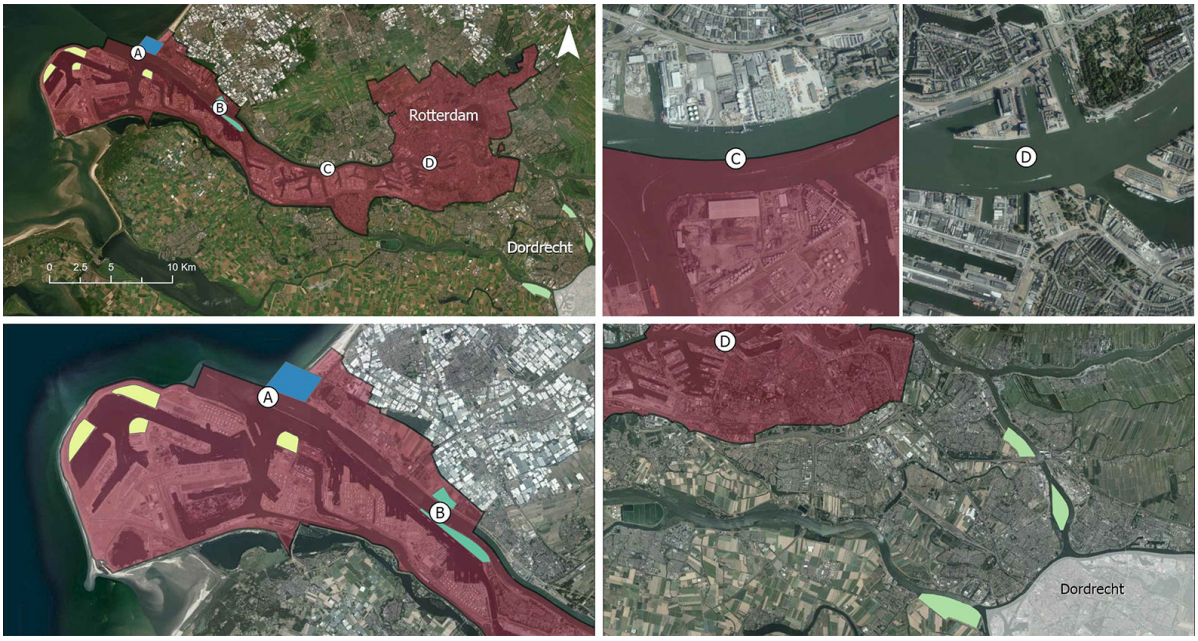

Figure 6.3: Overview of the four locations where the available space for the structure (blue and dark green) and potential space for the storage of building materials are marked (yellow and light green). A: HvK, B: Maasdijk, C: Petroleumhaven and D: Delfshaven.

6.2.4. EXPOSURE TO ENVIRONMENTAL LOADING

The location has an influence on the magnitude of hydraulic loading. For instance, if the significant wave height were to be calculated by computing a first estimation, in accordance with Breugem and Holthuijsen (2006) and Young and Verhagen (1996), as in Appendix F.1, based on the fetch of the wind, the highest significant waves (H_s) would occur closer to the mouth of the estuary. In Appendix F.1 the significant wave height is calculated for location Maasdijk, with a fetch of 10.3 kilometres, and results in a height of approximately 1.0 metre, compared to measured significant waves at Hoek van Holland, waves of up to 6.9 metres can occur (Dorrepaal, 2016). Further upstream, considering locations Petroleum -and Delfshaven, the fetch of the wind decreases and the velocity is also disturbed by surrounding buildings, leading to a likely decrease of the significant wave height. Albeit the hydraulic loading plays a significant less important role than the other integrated criteria, it has to be noted that the decrease in magnitude of significant wave heights, when comparing locations Maasdijk, Petroleumhaven and Delfshaven with location HvK, is of a considerable portion.

6.2.5. MULTI CRITERIA ANALYSIS AND SELECTION

Following from the verification of the alternatives, a multi criteria analysis is performed for the four locations, scoring each of them on five criteria. The weight factors in Table 6.3 are determined based on relative importance that followed from the regional analysis, Chapter 3, and evaluation of the adaptive pathways in Chapter 5. From these chapters it is evident that the hindrance to shipping plays an important role for the region and various stakeholders, followed by the overall state of the flood defences in the region. Furthermore, the criteria of the protection of the unembanked areas and available space for the barrier are ranked equally. The environmental loading could increasingly play a more significant role as sea level rise increases, however, in theory a structure could be designed to withstand these loads if costs are not considered and is rated with the lowest weight. In the multi criteria analysis the alternatives are rated with a score between 1 (least favourable) and 4 (most favourable), multiplied with the weight factor and summed to result in a score for the alter-

native.

From Table 6.3 it can be deducted that locations HvK, Maasdijk and Delfshaven perform quite similar and the differences are minimal. Although, locations HvK and Maasdijk generally score better on the higher weighted criteria, with the exception of the hindrance to shipping. To yield a preferred locations, the yearly economic costs from Fig. 6.2 are compared. From cost estimation, it becomes evident that the amount of costs for location Delfshaven surpasses that of HvK and Maasdijk with quite a margin. This is due to the required strengthening of dikes of areas that are now unprotected in comparison with the current location of the Maeslant barrier. The estimated costs for location HvK and Maasdijk are fairly similar, however, combining the score of the MCA for HvK and Maasdijk with the small margin in economic values, results in the preference for location Maasdijk and thus this location is opted for. As mentioned in Section 6.1, it should be noted that it is likely a 'new Hartel barrier' has to be constructed to continue the function of the current Europoort barrier. With this brief analysis considering the location the second design loop is concluded and the next loop is started in Chapter 7.

Table 6.3: Multi criteria evaluation of the four locations based on the stated criteria in Section 6.2.

Criteria	**Weight factor**	**HvK I**	**Maasdijk**	**Petroleum**	**Delfshaven**
Hindrance shipping	0.4	2	2	3	4
Flood defence costs	0.25	3	3	2	1
Unprotected surface	0.15	3	3	2	2
Available space	0.15	3	3	1	1
Environmental loading	0.05	1	3	4	4
Score		**2.50**	**2.60**	**2.35**	**2.50**

7 | Selection of barrier type

After determining a suitable location for the barrier, a variant study to determine a suitable barrier type is started is this chapter. The varying types and their respective (dis)advantages are stated in Section 7.1. Subsequently, an elaboration of the used criteria, evaluation and selection of a barrier types follows in Section 7.2. Lastly, a general lay-out of the selected barrier is provided in Section 7.3 and marks the end of the second design loop. This chapter envelopes the development of barrier concepts, verification, evaluation and selection of concepts.

7.1. Considered barrier types

A wide range of open/closable barriers exists that can be considered (Mooyaart and Jonkman, 2017). For the current Maeslant barrier six gate concepts where taken into consideration: Pneumatic flap gates, driven sector gates, rolling gates, hydraulic flap gates, barge gates and the winning concept: floating sector gates. With the addition of the inflatable rubber barrier, a consideration from Riteco (2017), seven barrier types in total are taken into consideration. Barriers that obstruct the natural path of the river by constructing structural components in the New Waterway, e.g. rising sector and lift gates, are not considered due to necessity of constructing elements in the New Waterway and this interferes with the demand that obstruction in the waterway is not allowed.

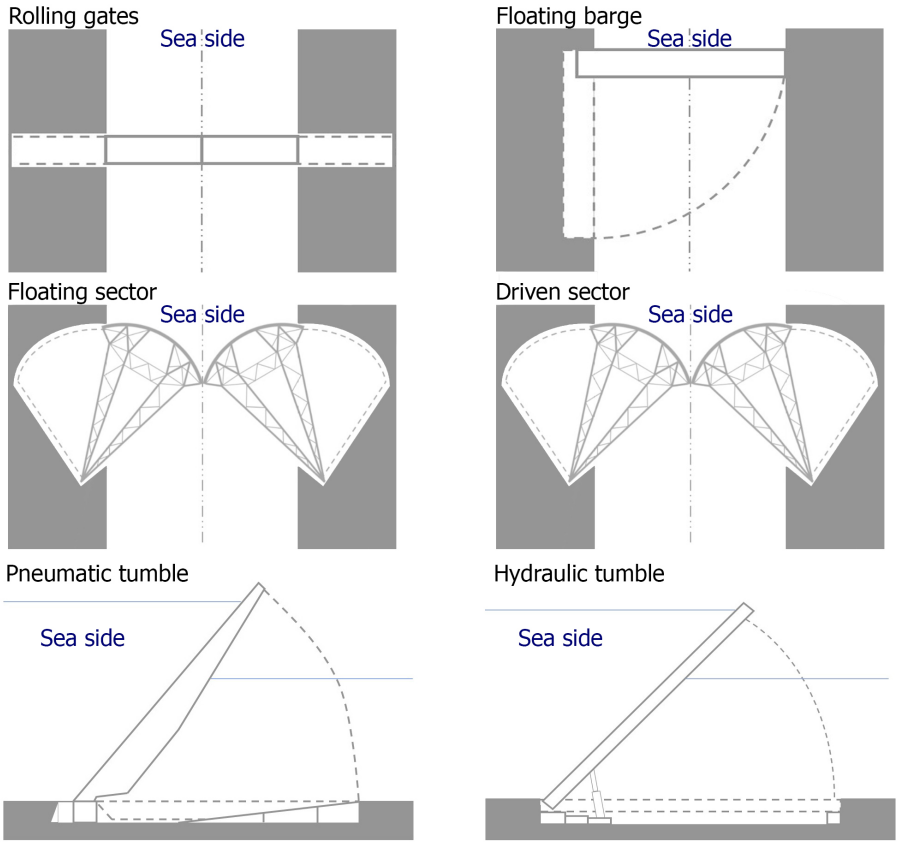

Figure 7.1: Six out of seven considered barrier types.

7.1.1. INFLATABLE RUBBER BARRIER

The inflatable rubber barrier retains water by inflating the rubber membrane so that it rises above the high water level, preventing water to flow into the flood prone region. The largest completed rubber barrier is the Ramspol barrier near the city of Zwolle, see Fig. 7.2. The total length of the barrier is of a considerable smaller size than that would be required to replace the Maeslant barrier, 75 metres compared to roughly 360 metres in width and 10 metres compared to approximately 20 metres in depth. Due to the considerable larger required dimensions, the most significant issue with the barrier would be the peak stresses in the folds of the membranes (Riteco, 2017).

Figure 7.2: Northern segment of the Ramspol inflatable rubber barrier.

7.1.2. THE (DIS)ADVANTAGES OF THE BARRIER TYPES

In Table 7.1 a brief summary of all the (dis)advantages of the seven barriers is provided.

Table 7.1: The (dis)advantages of the different barrier types.

Type	Advantages	Disadvantages
Rolling gates	- Gates protected whilst open - Easily accessible in drained docks - Simple construction, technology - Proven in practice	- Interference with navigation during construction - High transverse and bending forces - Most expensive solution - Requires high amount of available space on the river banks
Floating barge	- Insensitive to silting - Moving parts above water	- Control of the gate during closure difficult - Design loads difficult to define, influences closing procedure
Floating sector	- Gates protected whilst open - Easily accessible in dry docks - Deduction of bending forces - Utilises buoyancy for movement	- Sensitive to negative head - Forces concentrate on ball hinges
Driven sector	- Simple and proven construction - Barrier can be closed during extreme flood event	- Gates are vulnerable to collisions - Sediment deposits on the guidance component can cause closing issues - No dry maintenance - Hindrance to shipping during construction

Table 7.1 continued from previous page

Type	Advantages	Disadvantages
Pneumatic tumble	- Closing mechanism is straightforward - Reliable parallel system - Simple construction	- Sensitive to negative head - Silting of valves and buoyancy chambers - No dry maintenance
Hydraulic tumble	- Independent valves, distribution of gate failure - Space requirement is minimal	- Hard to maintain and obstruction for shipping - Over-dimensioning of components required - Foundation technology complex - Silting can cause failure of the gates
Inflatable rubber barrier	- Costs relatively low - No movable parts - Simple construction - Rubber membrane can be replaced	- Rubber membrane can be damaged - No dry maintenance - Relatively new barrier type, not a proven design for the required size

7.2. MULTI-CRITERIA ANALYSIS

The most suitable barrier is selected through a multi-criteria analysis. The seven types are scored, with a score between 1 and 4, based on six criteria. These scores are then multiplied with their respective weights, based on the importance of the criterion.

7.2.1. CRITERIA

A brief elaboration of the six criteria follows in this subsection.

Maintenance

The barrier types are scored based on the general complexity to perform required maintenance. For instance, maintenance in the wet is more costly and difficult to perform when compared to performing maintenance in a dry dock. Sufficient and qualitative maintenance is an important contributor to obtain a consistent functioning of the barrier, it is therefore attributed with a weight of 0.2 out of 1.0.

Hindrance to shipping

The construction and maintenance of the barriers could result in hindrance to vessels utilising the New Waterway. Barriers that require maintenance to be performed with equipment on the New Waterway score less on this criterion. Although the economic importance of free shipping via the New Waterway is of importance, it is of lesser importance when compared to criteria influencing the function of the barrier. It is therefore attributed with a weight of 0.1 out of 1.0.

Experience and knowledge

Gained experience and overall knowledge of a specific structure can enhance the ease of designing and/or operation of said structure. Some barriers are relatively new, i.e. inflatable rubber barrier, or are generally constructed less. As a less significant criterion, as new methods or structure can always be developed/researched, this criterion is weighted with 0.1 out of 1.0.

Distribution of forces

Differences in how the barrier distributions the acting forces to the foundation but also within the gates influences the dimensions of the various components. As an example, barriers with large horizontal gates without a foundation block connecting in the middle will result in high transverse and bending forces, as is the case with the rolling gates barrier. Albeit this criterion signifies the

ability of the barrier how the structures distributes the acting forces, it plays a less significant role. It is therefore weighted with 0.1 out of 1.0.

Complexity achieving reliability demand
The complexity achieving reliability demand, denoted further as reliability, criterion is based on how difficult it is to reach the required reliability. As an example: tumble gate systems have a low likelihood of overall failure as the gates function in parallel (easier to achieve reliability demand), a failure of one of the many gates does not necessary lead to a overall failure of the barrier and flooding of the hinterland. And is attributed with the highest weight, 0.3 out of 1.0.

Dynamic robustness
The dynamic robustness criterion signifies the general adaptability of the barrier and its components. The criterion speculates whether the respective barrier type allows to be designed in such way it is adaptable over time. As being part of the objective of this thesis this criterion is attributed with a weight of 0.2 out of 1.0.

7.2.2. EVALUATION AND SELECTION OF ALTERNATIVES

Evaluating and scoring each of the seven barrier types based on the aforementioned criteria is though as the criteria are unquantifiable. Thus, the scores are based on engineering judgement and personal communication with one of engineers of the current Maeslant barrier (van Oorschot, 2021). Having discussed many aspects of the varying barrier types and their respective (dis)advantages, the scores as in Table 7.2 are generated. A thorough elaboration on the performance and score of each of the barrier on each of the criteria can be found in Appendix E. The final scores, which are multiplied with the respective weights, roughly coincide with the preference established during the design process of the current Maeslant barrier. At the time, according to van Oorschot (2021), the floating sector and pneumatic tumble gates had the preference over the other types, however, a clear preference between these two could not be made. Therefore, the decision was made by Rijkswaterstaat and thus a floating sector gate was constructed. Coincidentally, these two barrier types yielded the highest scores, see Table 7.2, with the main differences, in favour of the floating sector gates, attributed to the maintenance, hindrance, experience and dynamic robustness criteria, whilst the reliability criterion in favours the pneumatic tumble gate. For the remainder of this thesis the floating sector gate barrier is developed further, as the potential of the dynamic robustness is derived to be higher.

Table 7.2: Multi Criteria Analysis of the various barrier types.

Criteria	**Weight**	**Rolling gates**	**Floating barge**	**Floating sector**	**Driven sector**	**Pneumatic tumble**	**Hydraulic tumble**	**Inflatable rubber**
Maintenance	0.2	3	3	4	2	2	1	3
Hindrance	0.1	2	2	3	3	2	2	2
Experience	0.1	4	3	4	3	3	2	2
Force dist.	0.1	1	1	3	3	3	2	2
Reliability	0.3	2	2	3	2	4	4	2
Dynamic rob.	0.2	2	2	3	3	2	2	4
Score	**1.0**	**2.3**	**2.2**	**3.3**	**2.5**	**2.8**	**2.4**	**2.6**

7.3. GENERAL LAY-OUT OF THE FLOATING SECTOR GATE

To supply a basic visual understanding of the selected barrier and its main components, a general lay-out figure in Fig. 7.3 is supplied. The figure represents one half of the complete barrier, as two crescent shaped gates are required, and designates its main components.

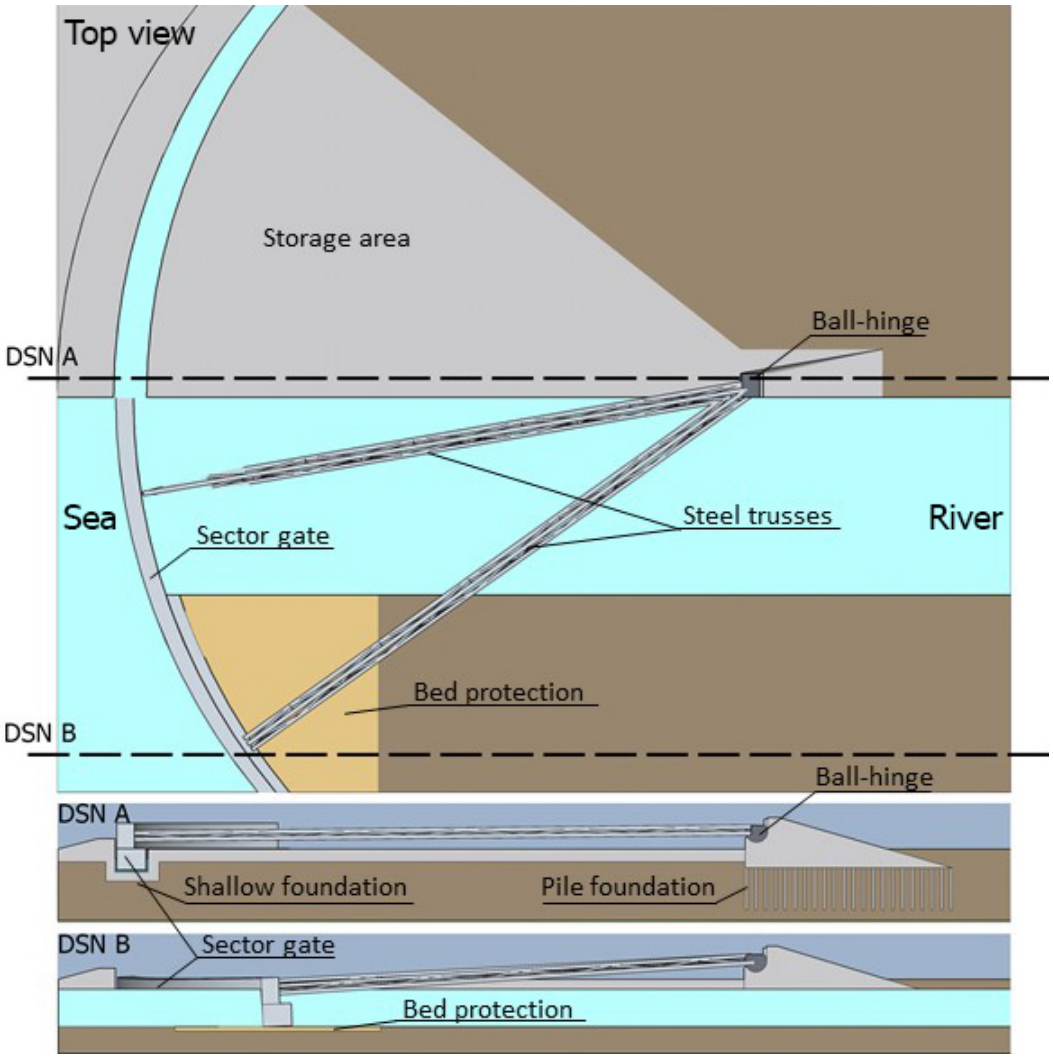

Figure 7.3: General lay-out of the sector gate barrier. Worthwhile to note is that the figure represent one section of a total of two gates.

8 | Development of a reliability model

In this chapter the development of the reliability model is elaborated. In Section 8.1 the approach with the model is elaborated, followed by a description of the fault tree of the barrier in Section 8.2 and the setup, along with the main processes, in Section 8.3.

8.1. Reliability model approach

The reliability model is utilised such that it is able to provide a way to compare static robust and dynamic robust design strategies based on the failure probabilities of individual components and investments or construction costs in multiple sea level rise growth scenarios. It does so by integrating a fault tree, to which the individual components of the barrier are linked, through which the failure probabilities of these components under the influence of a sea level rise distribution is determined. At the same time it is able to yield the required dimensions of certain components of the barrier in order to adhere to an instated failure probability threshold. The difference between static and dynamic robust designs is that the static design performs adequately, based on the instated threshold, over a wide range of scenarios and the dynamic design can be adapted to continuously adhere to the instated threshold, which is in accordance with the definitions in Section 1.5.

Two types of design strategies are inserted into the model and these strategies with their characteristics are elaborated in Section 9.1. The static robust design provides a baseline to which the dynamic robust designs can be compared. Both these designs should adhere to the instated failure probability threshold for the overall structural failure probability (1:10,000 p/y) and that of each component of the barrier (1:80,000 p/y), which is elaborated in Section 8.2. If this is satisfied under a wide range of growth scenarios, the design is considered robust. In case of a static robust design it means that initially the design can be considered as an over-dimensioned one, but over time the loads due to sea level rise increase and thus the failure probabilities along with it. At the end of its lifespan the design should stay below the instated thresholds. When considering a dynamic robust design, it is evident that components are designed as such that they are 'smaller' and/or 'weaker' than the static counterpart. This is to gain an initial economic advantage, as the construction is likely to cost less. However, as sea level increases over time, the failure probabilities are to increase as well. If the probability of a component is anticipated to exceed the instated threshold, an adaptation or strengthening of the component is necessary, leading to additional investments. The reliability model helps to understand when investments have to be made and whether these are beneficial in economic terms and adequate in terms of failure probabilities and is elaborated further in Chapter 9. Comparing varying dynamic robust designs based on the these benefits eventually leads to a preferable design strategy.

8.2. Fault tree of the barrier

The fault tree serves as a basis to determine the failure probability of the barrier applied in the reliability model in Section 8.3. With the fault tree and the reliability model the total failure probability of the top event, *"Exceedance critical water level"*, can be quantified. However, in this thesis the focus is on the structural failure consequence. Three main causes leading to this top event are identified: Structural failure, Closure failure and Backwater level limit exceedance of the unembanked areas during successful closure. In Fig. 8.1 the top event and these main consequences are visualised, the subsequent components leading to each of these consequences is withheld in this figure and these

are elaborated and visualised in Section 8.2.1, Section 8.2.2 and Section 8.2.3. In addition, as can be seen in Fig. 8.1, the consequences are connected with an OR-gate, the difference between these OR-and AND-gates is elaborated in Section 8.3.4.

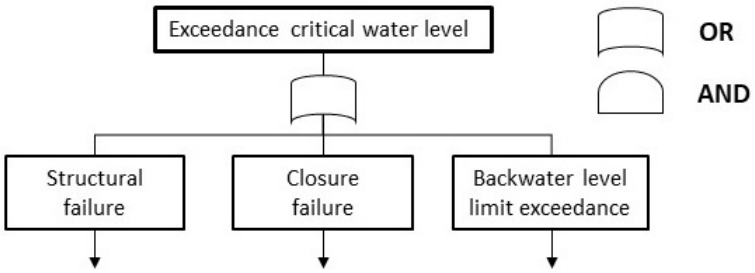

Figure 8.1: Top fault tree branches leading to flooding of the unembanked areas. All three branches are connected with OR gates.

8.2.1. STRUCTURAL FAILURE BRANCH

The *"Structural failure"* branch diverts into three branches: the bed protection, the sub -and superstructure and the gates, Fig. 8.2. Within these branches the main components, from Fig. 7.3, are attributed to their respective branch to which they belong. These components have their own failure mechanisms under which they are assumed to no longer be able to adequately preserve stability or resistance for the barrier. These components, the forcing and their failure mechanisms are discussed in the summation that follows:

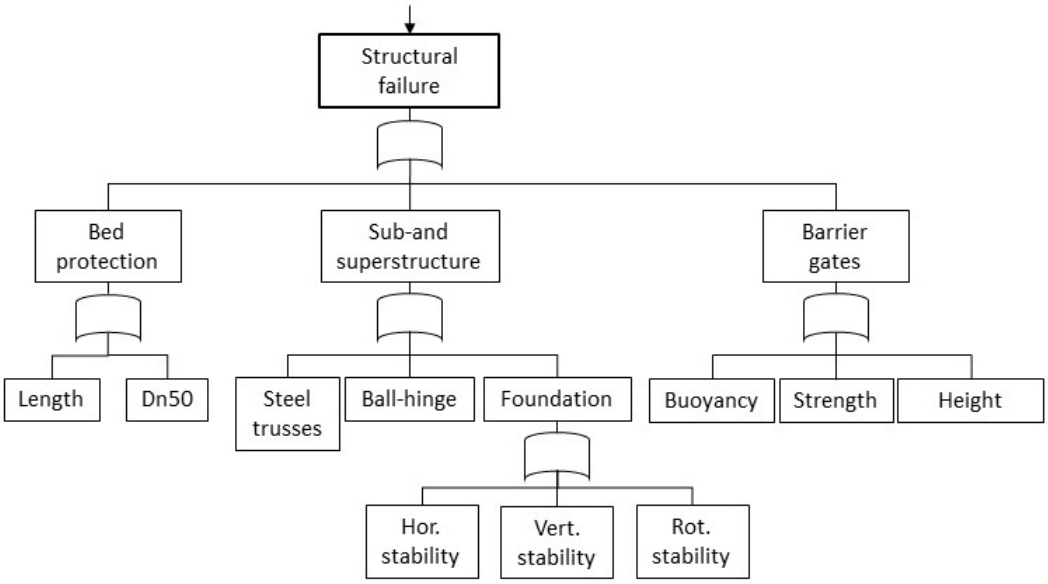

Figure 8.2: Remainder of the Structural failure consequence within the general fault tree of the barrier.

Bed protection

The bed protection provides stability of the bed on which the barrier rests throughout the closure of the barrier. Waves, currents and other flow induced velocities cause erosion of the bed and therefor influences the stability of the barrier. Varying mechanisms impact the stability of the bed and these are identified:

- Plunging jet due to overtopping waves or water

- Underflow due to the opening and closing procedures
- Natural tides and currents
- Waves from both the sea -and riverside of the barrier

These mechanisms result in a critical shear velocity, that influences the stability and movements of sediment of the riverbed, or result in a scour hole at the sill of the barrier. In turn the critical shear velocity determines the required rock dimensions of the bed protection to provide stability and the scour hole determines the required length of this bed protection.

Ball-hinge
The ball-hinge is a crucial component of a sector gate barrier, it provides the necessary movement space in x,y,z-directions, which are needed to properly displace and rotate the gates from a resting position, on the embankments, towards the closed position, from floating on the New Waterway to the bottom of the riverbed. Hydraulic and wind forces acting on the barrier convergence to a single point for each sector gate, i.e. the ball-hinge. A few loading mechanisms impact the ball-hinge:

- Positive head, water level at the sea side is higher than that of the hinterland
- Negative head, water level at the hinterland is higher than that of the sea side
- Wind induced forcing
- Waves from both the sea -and riverside of the barrier

These mechanisms result in compression and tension forces for which the ball-hinge has to account to properly resist the acting forces.

Foundation block
The foundation provides the horizontal, vertical and rotational stability of the barrier. The forces converging on the ball-hinge are transferred to the foundation which can either be a shallow, piled, pneumatic caisson or a combination. Inadequate foundation can result in displacements and misaligned of the gates during closures resulting in a failure of the barrier.

As is the case with the current Maeslant barrier, the loads are supported by a shallow foundation and the soil provides the stability. The foundation can be provided with additional stability through the installation of piles, anchors and soil strengthening methods.

Sector gates
Two crescent shaped sector gates provide water retention during high water levels. To resist the high water these gates must have sufficient strength to cope with the hydraulic forces. Varying mechanisms can lead to the structural failure of the gates:

- Vibrations, due to overtopping water
- Buoyancy of the gates, allowing the sinking or uplift of the gate
- Strength of the gates, considering the loading conditions

These loading conditions determine the required height, strength and way of designing to provide buoyancy of the gates.

Steel trusses
The steel trusses transfer the acting forces on the gates to the ball-hinge and the foundation. Logically, the same forces that converge on the ball-hinge influence the dimensions of the steel trusses supporting the gates.

- Positive head, water level at the sea side is higher than that of the hinterland
- Negative head, water level at the hinterland is higher than that of the sea side
- Wind induced forcing

- Waves from both the sea -and riverside of the barrier

8.2.2. CLOSURE FAILURE BRANCH

Although being not the focus of this thesis it is important to consider the overall failure probability of the barrier and thus the *"Closure failure"* is elaborated. The Maeslant barrier in the current state is attributed with a closure failure probability of 1:100 per closure, and with an anticipated closure of once every 10 years results in a closure failure probability of 1:1,000 p/y. In contrast, for MLK+ with the implemented system in which the closing water level is increased with sea level rise, Section 4.2.2, three closures are expected every year. According to Vrancken et al. (2008), a closure failure probability of 1:1,000 for every closure is preferable and reachable thus, for the time being, this is assumed to be the closure failure probability of the new barrier. This would result in an annual Closure failure probability of 1:333, with an approximate of three closures per year. The various components leading to this consequence are visualised in Fig. 8.3 and are distinguished between control and mechanical failure, these components are not discussed further.

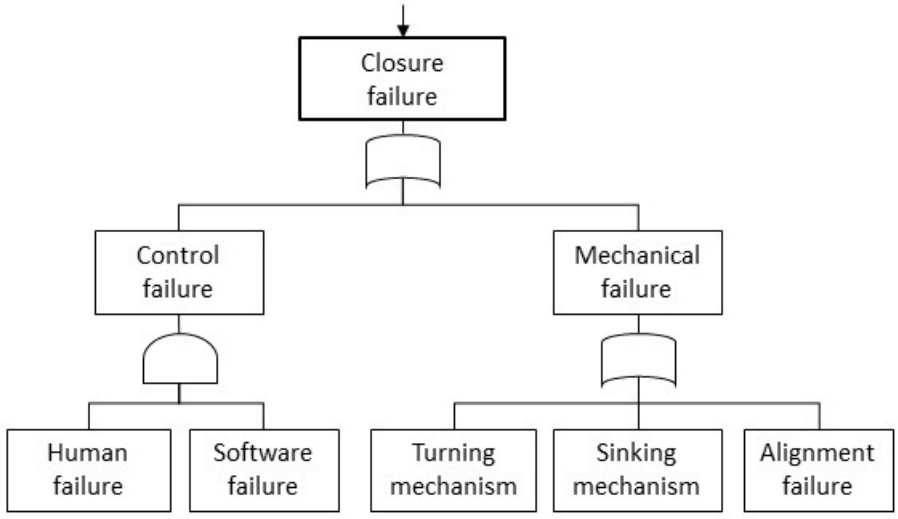

Figure 8.3: Remainder of the Closure failure consequence within the general fault tree of the barrier.

8.2.3. BACKWATER LEVEL LIMIT EXCEEDANCE

The *"Backwater level limit exceedance"* branch symbolises the probability of flooding when water levels in the basin, protected by the barrier, exceed the water level limits of the unembanked areas throughout a successful closure of the barrier. This is the case when a combination of factors, listed below, are unfavourable. A fault tree elaborating further on these factors is neglected from this thesis, as this part of the overarching fault tree requires a thorough examination of the system and how these factors play their role.

- Volume of water inflow into the basin behind the barrier
- Volume of water pumped out of the basin behind the barrier (Delta21)
- Duration of barrier closure
- Opening failure of the barrier

8.3. SETUP OF THE RELIABILITY MODEL

The setup of the reliability model is described with the flow chart provided in Fig. 8.4. When considering a static robust design strategy a few segments of Fig. 8.4 are deducted. A description of this method is provided:

The model is saturated with input from design parameters concerning the dimensions of the barrier, the system in which the barrier is to take function and sea level rise distributions, this saturation is represented by step 1. Then a wanted number of scenarios is taken from the sea level rise distribution, these are named 'growth scenarios', as these grow over the anticipated time horizon, and are denoted as N,i...m. The anticipated time horizon is divided in time steps of 10 years, denoted as T,j...n. After the model has been saturated with these growth scenarios the loading conditions acting on the individual components are computed and checked against the resistance attributed with the design parameters, as presented in Fig. 8.4. This check represents the Limit State Function and is elaborated in Section 8.3.2. With the Limit State Function the number of failures in all of the growth scenarios in a single time step per individual component is computed and this results in a failure probability of the component. The failure probabilities are then inserted into the fault tree of the barrier from which a probability for the structural failure branch is retrieved. When considering static robust or conservative design strategies the application of the model ends here.

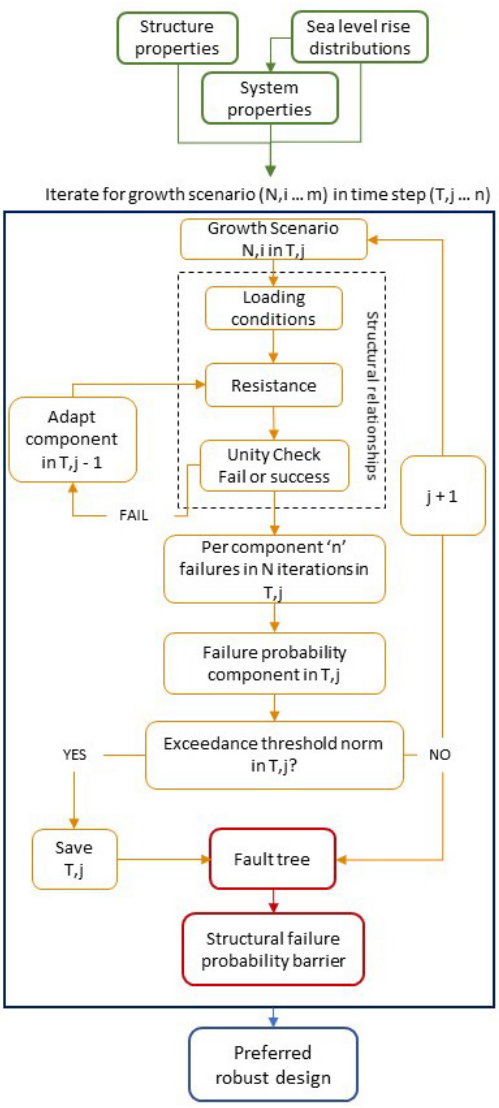

Step A: Input
Initial dimensions of the barrier and system properties are extracted from the requirements, boundary conditions and first estimates from calculations. The sea level rise distributions follow from the anticipated sea level rise predictions over the period 2100 (T,0) – 2200 (T,11), roughly between 0.4 and 3.5 metres.

Step B: Unity Check
N number of values are drawn from the sea level rise distribution (N,i) for T,j. N,i is growth scenario, which progresses over the selected period thus N,i progresses over T,j+1 ... n. In which 'n' are the steps in time over the period. The sea level rise scenario leads to loading conditions which are checked against the resistance of the various components: the Unity Check. The amount of Unity Checks above 1.0 are counted and divided by the amount of scenarios per time step, leading to the failure probability of the component in T,j. This process is repeated for the subsequent time step: T,j+1.
If a component fails the Unity Check it should be adapted leading to an investment moment in the previous timestep. This then increases the resistance of that component. The failure probability of an individual component over all the growth scenarios is aimed to stay below an exceedance threshold norm. Additionally, when the component is adapted, it is computed whether the adaptation is beneficial in economic terms. The failure probabilities of each of the components are inserted into the fault tree which computes the global structural failure probability.

Step C: Fault tree
The failure probabilities of each of the components are inserted into the fault tree, through which the total failure probability of the barrier is computed with the mathematical expressions for the OR –and AND-gates.

Step D: Dynamic robust design
In the final the benefits of varying design strategies are compared and especially those that contain adaptable components. All design strategies should adhere to the threshold norms of the failure probabilities. Thus, the preferred design flows from the global benefits of the design strategy. This is elaborated in Chapter 9.

Figure 8.4: Flow chart of the reliability model.

8.3.1. INPUT PROPERTIES

For the reliability model some initial design parameters or barrier and system properties along with the sea level rise scenarios have to be stated and follow below.

Barrier and system properties

A brief summary of the barrier and system base properties:

- Depth of the sill is NAP -17.0 metres
- Arc length of the barrier is 200 metres
- Concerning the closing regime, which is adjusted with an absolute sea level rise value, in accordance with Chapter 5, to limit the anticipated number of closures to 3 p/y:
  - 0 metre of sea level rise: NAP +3.00 metres (≈ 1/10 closures p/y to 3 p/y)
  - 1 metre of sea level rise: NAP +3.80 metres (≈ 3 closures p/y)
  - 2 metre of sea level rise: NAP +4.55 metres (≈ 3 closures p/y)

Sea level rise distribution

Normal distributions for scenario RCP8.5 from Fig. 2.3 are computed and from these distributions N random values per timestamp are drawn. Scenario RCP8.5 is taken as it is the most severe climate change scenario at the time, to reduce the overall workload this thesis limits itself to this single scenario. The distributions are then inserted into Fig. 8.5 and thus N scenarios are created. Each growth scenario influences the loading factors or hydraulic boundary conditions with its corresponding rise in sea level. Appendix G provides an in-depth elaboration of this method. Worthwhile to note, the progression of the growth scenarios likely do not match a 'realistic' sea level rise and this is due to the setup of the Python script. The idea is, if enough scenarios are generated the results will globally match that of a 'realistic' sea level progression and a comparison is supplied in Fig. G.4.

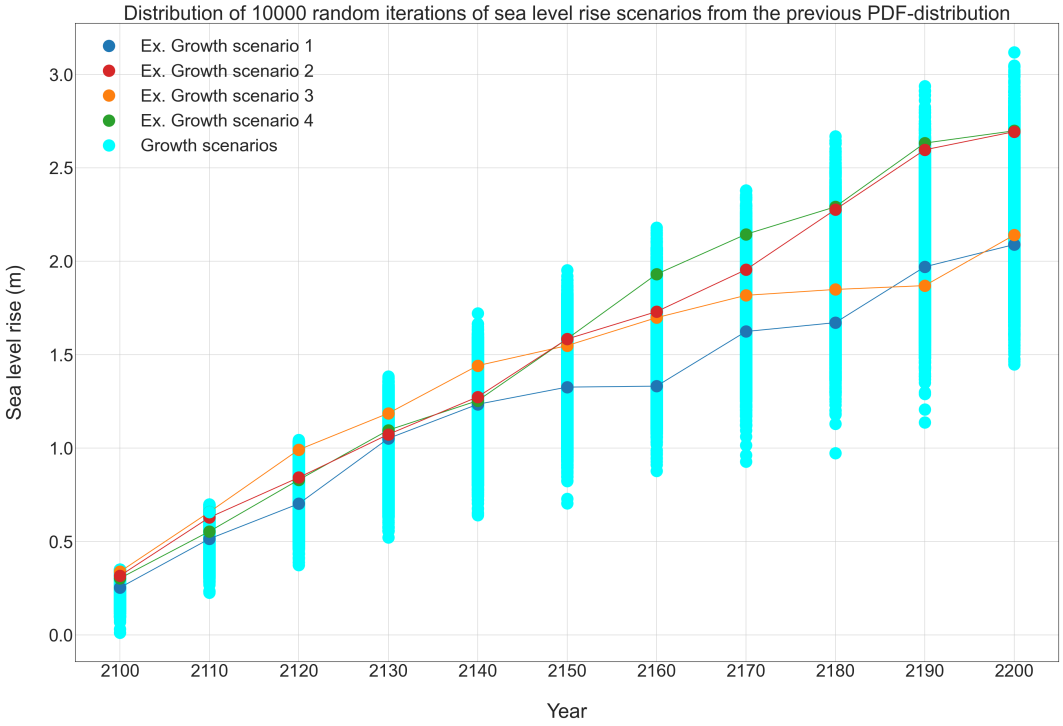

Figure 8.5: Visualisation of the N random generated sea level rise scenarios for each timestamp in accordance with the PDF-distributions.

8.3.2. LIMIT STATE FUNCTIONS

To determine whether a component has the capability to resist the acting loading condition(s), limit state functions for each individual component are introduced. The limit state functions, presented in Eq. (8.3.1), follows the form supplied in (Jonkman et al., 2017). The R represents the Resistance of the component and S the Solicitation, in most cases it is referred to as the load on the component. In case the load exceeds the resistance of a component, Z becomes negative and signifies the failure of the component. Table 8.1 presents the limit state functions for the components included in the model. For most of the components the limit state functions are defined by their dimension, however, for the steel trusses and the ball-hinge no direct dimensions in relation to the resistance of the component were retrieved and are therefore defined as: R equals the desired load bearing capacity and S the acting load.

$$Z = R - S \tag{8.3.1}$$

Table 8.1: The considered limit state functions for each component.

Component	Limit state function	Appendix
Foundation	$Z_{Horizontal} = Q - \sum H$	Appendix F.7.1
	$Z_{Vertical} = p'_{max} - \sigma_{k,max}$	Appendix F.7.2
	$Z_{Rotational} = \frac{1}{6}L - \frac{\sum M}{\sum V}$	Appendix F.7.3
Bed protection	$Z_{dn,50} = u_{*r,Res} - u_{*r}$	Appendix F.5.1
	$Z_{Length} = L_{bed} - (6 - \beta_{ratio}) \cdot h_{scour\ hole}$	Appendix F.6
Steel trusses	$Z = F_{Res,Comp./Tens.} - (F_{hydro,Hor} + F_{waves})$	Appendix F.3
Ball-hinge	$Z = F_{Res,Comp./Tens.} - (F_{hydro,Hor} + F_{waves})$	
Gates	$Z_{gate\ height} = 0.2\ m^3/s/m - q_{overflow/overtopping}$	Appendix F.4.1
	$Z_{strength} = 10\ mm - f_{deflection}$	Appendix F.4.3

8.3.3. FAILURE PROBABILITY THRESHOLD LIMITS

For the structural failure consequence it is retrieved that the structure should be able to resists 1:10,000 p/y occurring storm surge. This is translated to two threshold limits that can not be exceeded by the imposed designs: one for the structural failure branch and one for each individual component as visualised in Fig. 8.2. The maximum allowable yearly failure probability due to structural failure is set at 1:10,000 p/y. To derive the threshold for each component, an assumption is made that all the components equally contribute to the structural failure. The threshold for the components is then computed with Eq. (8.3.2), where $P_{f,structural} = 1:10,000$ p/y, which results in a maximum allowable failure probability of 1:80,000 p/y for individual components.

$$P_{f,structural} = 1 - ((1 - P_{f,component,1}) \cdot (1 - P_{f,component,2}) ... (1 - P_{f,component,8})) \tag{8.3.2}$$

8.3.4. FAULT TREE COMPUTATION

When the failure probabilities for each component with their respective failure mechanisms and the loading conditions have been computed, the failure probability for the barrier is derived. The fault tree is structured in such a manner that it portrays the connectivity of the components and their influence to each other through the connection of OR-and AND-gates. The OR-gate implies that if one of the listed components fails the upper consequence will fail as well. The AND-gate implies that all of the listed components are required to fail to lead to a failure of the upper consequence.

As an example: *the failure probabilities of components B, D and E from Fig. 8.6 are equal to 0.3, 0.1 and 0.2, respectively. The governing equations for independent components from Table 8.2 result in failure probabilities of 0.02 for C and 0.314 for A, see Eq.* (8.3.3) *and Eq.* (8.3.4) *respectively.*

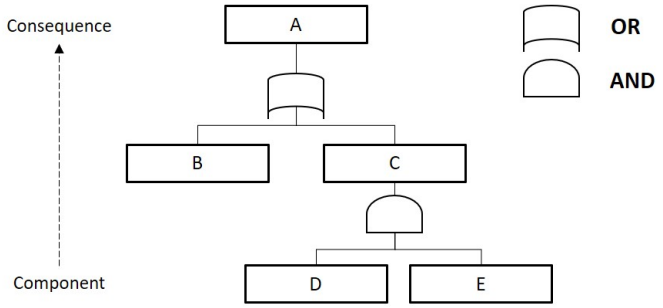

Figure 8.6: Example of a fault tree.

Table 8.2: OR-and AND-gates usage. Retrieved from Jonkman et al. (2017, p. 218).

Gate	Mutually exclusive	Independent	Fully dependent
OR	$\sum_{i=1}^{n} P_i$	$1-\prod_{i=1}^{n}(1-P_i)$	$\max(P_i)$
AND	0	$\prod_{i=1}^{n} P_i$	$\min(P_i)$

$$P_f(C) = P_f(D) \cdot P_f(E) = 0.02 \tag{8.3.3}$$

$$P_f(A) = 1 - [1 - P_f(B)] \cdot [1 - P_f(C)] = 0.314 \tag{8.3.4}$$

The fault tree of the structural failure branch is computed in the same manner, with the assumption that the events/components can be regarded as independent.

9 | Selection of preferred design strategy

In this chapter the reliability model from the previous chapter (Chapter 8) is utilised to determine the reliability and performance of varying design strategies of the barrier. In Fig. 9.1 a flow chart, representing the outline of Chapter 9, is provided. In Section 9.1 the various design strategies are elaborated. Subsequently, utilisation of the reliability model on these strategies is elaborated in Section 9.2. Followed by the identification of possible adaptations for the components in Section 9.3 and the filtering of these options in Section 9.4. An analysis of the design strategies and their components is provided in Section 9.5, which eventually leads to a preferable design strategy in Section 9.6. Lastly, some concluding remarks follow in Section 9.7.

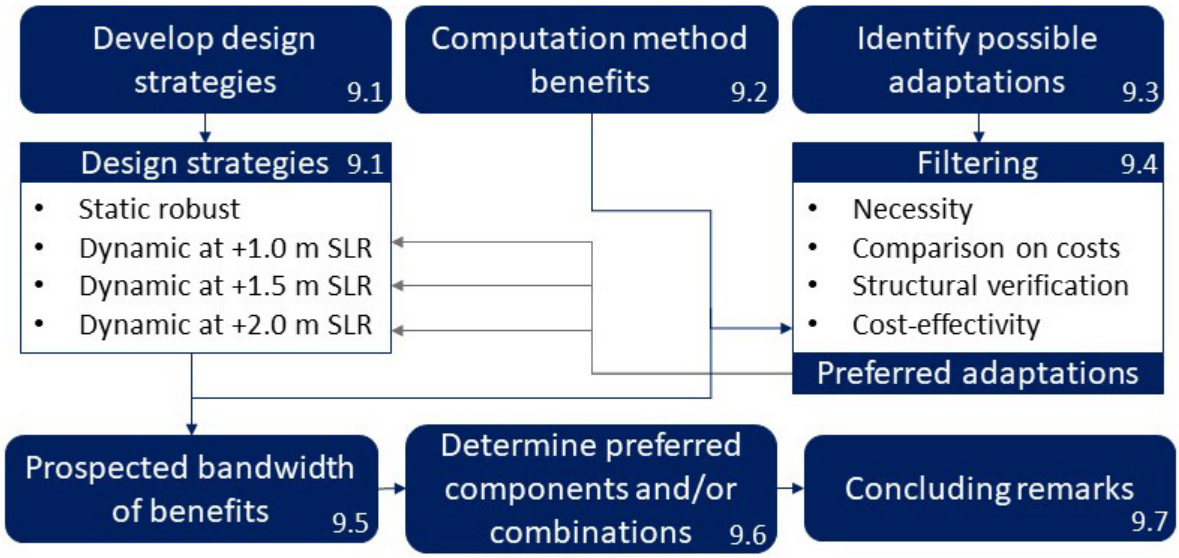

Figure 9.1: Flowchart representation the outline of Chapter 9.

9.1. Development static and dynamic robust design strategies

The design parameters of the components for the static design strategy are determined through iteratively using the reliability model until the criteria of robustness are met. When concerning the static robust design strategy, design parameters for the components are designed as such that, over its lifespan, the failure probabilities stay below the threshold limits (Section 8.3.3). Deriving the parameters for the dynamic design strategies is approached differently. Initially, the design parameters of the components are determined for three absolute values of sea level rise: +1.0, +1.5 and +2.0 metres. The required resistances, and thus design parameters, for these values are derived with the verification of the reliability model in Appendix F. The design parameters of components, that are initially identified as adaptable see Section 9.3, of all four strategies are listed in Table 9.1. Other relative design parameters determined as non-adaptable are stated in Appendix I. How the dynamic design strategies and their adaptations are handled is elaborated with an example:

Table 9.1: Broad dimensions outline of the components that are identified as possibly adaptable (Section 9.3) for the different design strategies.

	Substantial Adaptability Minor			
Component	**Dynamic+1.0**	**Dynamic+1.5**	**Dynamic+2.0**	**Static robust**
Shallow foundation	50x53	50x55	50x56	50x59 m (LxB)
Bed protection	d_{n50}: 1.18 m Length: 55.0 m	d_{n50}: 1.18 m Length: 56.0 m	d_{n50}: 1.18 m Length: 57.0 m	d_{n50}: 1.44 m Length: 58.5 m
Steel trusses	N_{Rd}: 130 kN	N_{Rd}: 130 kN	N_{Rd}: 135 kN	N_{Rd}: 141 kN
Gate height	22.8 m	23.2 m	23.5 m	24.2 m

In Fig. 9.2 the failure probabilities for the Dynamic+2.0 robust design strategy over a time span of 100 years is visualised. In the figure it can be seen that the failure probabilities for the individual components might exceed the instated threshold limit, initiating an adaptation, if available, of the component (red dot). Logically, in a real-world project the adaptation has to be applied before the loading conditions exceed the resistances, thus the computation of the benefits of the adaptations are always made one time stamp earlier than the anticipated failure of the component. The progression for all of the design strategy are elaborated in Appendix I.2.

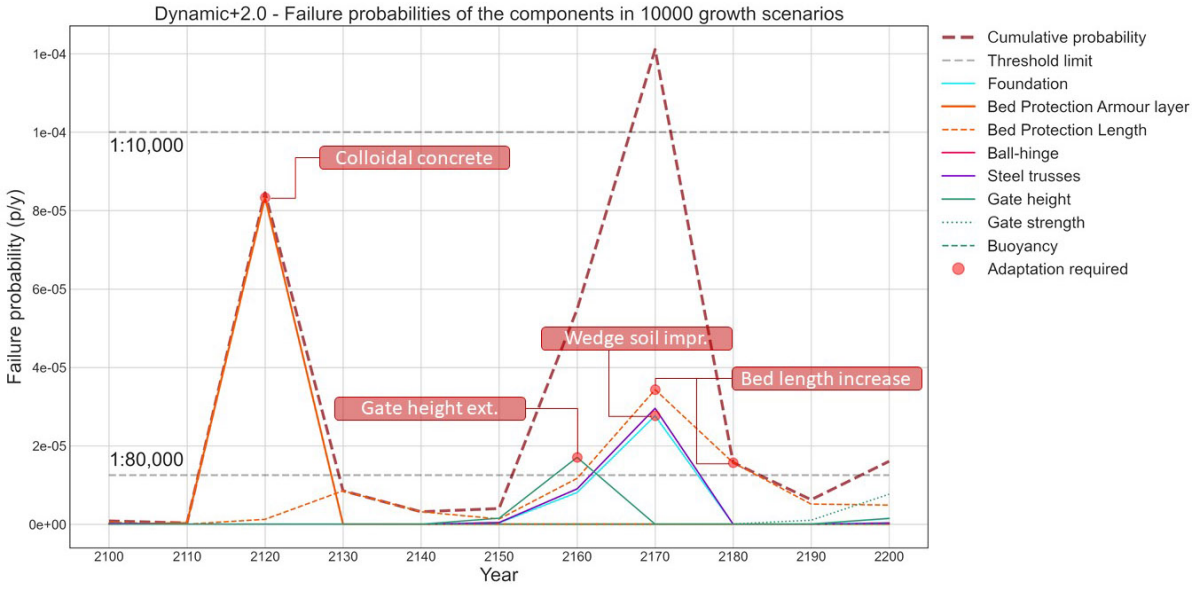

Figure 9.2: Example of the progression of the failure probabilities of the components for Dynamic+2.0 design strategy with possible adaptations of the components. The adaptations follow from the identification of suitable adaptations in Table 9.2. However, the cost-effectiveness of these adaptations still is to be determined and serves as an example.

9.2. ANALYSIS OF THE DESIGN STRATEGIES

The static robust design serves as a baseline to which the dynamic robust designs are compared to in terms of relative construction costs differences of the various components between the dynamic and static designs. These differences are denoted as savings and are computed in Appendix H. All four design strategies should adhere to the instated failure probability threshold: 1:10,000 p/y for global structural failure and 1:80,000 p/y for individual components (Section 8.3.3). The components of the dynamic designs are dimensioned as such that they are adequately able to resist loading conditions occurring at +1.0, +1.5 and +2.0 m sea level rise (Section 9.1) and, if the need arises, the components can be adapted to adhere to the threshold limits. The possible adaptations identified in Section 9.3 are filtered based a number of 'sieves' to exclude non-beneficial adaptations. The

effectivity of these adaptations are based on the initial savings, multiplied with a discount rate of 4% (Appendix H.3), versus the necessary additional investment, multiplied with an inflation rate of 2% (Appendix H.3), over time of the adaptation. An example is supplied to elaborate:

In Fig. 9.3 three different sea level rise (growth) scenarios affecting the same component with the same adaptation are visualised. Hypothetically, the moment when a component has to be adapted depends on the input from the sea level rise distribution and thus can vary for different growth scenarios, this in turn leads to varying moments in ***time*** *when this adaptation is necessary:* ***A*** *to* ***D*** *in Fig. 9.3. If a closer look is taken at Scenario 3 (green) and A, it can be concluded that the adaptation is resulting in a negative benefit. This is due to relative value of the savings vs investment, in Eq.* (9.2.1) *the equation that determines the benefit is stated. With Eq.* (9.2.1) *one could deduct that the adaptation is required too soon in order to yield a positive benefit, thus the adaptation is considered as in-effective in this scenario.*

$$\text{M€12.5 (Savings)}_{t=0} \cdot 1.04^X - \text{M€15.0 (Costs Adaptation)}_{t=0} \cdot 1.02^X \tag{9.2.1}$$

Now consider Scenario 2 (red), it can be seen that the first adaptation (first dip near C) is delayed enough to net a positive benefit. However, whilst progressing in time towards B, when a second adaptation of the component is necessary, the effectiveness of the adaptation becomes negative. One could argue that the years between the first and second adaptation, provided to be insufficient to yield a positive benefit. Lastly, consider Scenario 1 (blue) and C and D in time, from this scenario it can easily be conducted that both adaptations yield a high positive benefit. In this hypothetical example, it can be concluded that the first adaptation is cost-effective in 2 out of 3 scenarios and the second adaptation is effective in 1 out of 3 scenarios.

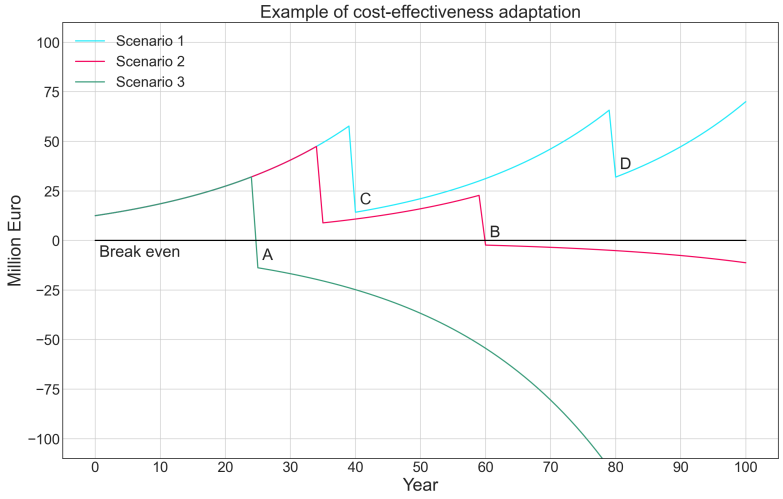

Figure 9.3: Computed benefits of one adaptation of one components in three growth scenarios, Eq. (9.2.1) utilised.

Important to note is that the reliability model is able to produce the failure probability of a component over all growth scenarios and thus determines when a component fails for individual growth scenarios with the expected year of failure. The failure probability over all growth scenarios of a component determines the likeability whether a component needs to be adapted, however, in a 'real-world' situation the component is adapted when it is no longer able to adequately resist the loading conditions, this could vary time-wise, and is dependent on the sea level. Thus, the cost-effectiveness or benefits of the adaptations are computed for the individual growth scenario and with the timestamp indicating failure of said component. This yields a general idea of the benefit potential of the adaptation and, when including the benefits over all growth scenarios, a bandwidth or range of possible benefits from the adaptation and/or design strategy.

9.3. IDENTIFICATION OF SUITABLE ADAPTATION OPTIONS

In this section a table of suitable adaptation options for the components are stated, see Table 9.2. In Section 9.4 it is elaborated how these adaptations are selected through the application of a number of filters in order to eliminate non-beneficial or unnecessary adaptations.

Table 9.2: Remaining verified adaptations for the components

Component	Adaptation	Description
Foundation (Horizontal stability)	Wedge Soil improvement	Replacing the soil behind the foundation block by a heavier soil type providing additional horizontal stability
Bed protection (Armour layer)	Colloidal concrete penetration	Penetrating the armour layer with colloidal concrete improves resistance to erosion and movement of stones
Bed protection (Length)	Length increase	Adding additional length prevents structural instability of the barrier due to the formation of a scour hole
Sector gate (Overtopping/flow)	Gate extension	Extending the height of the sector gates reduces the volume of overtopping/overflowing water

9.4. FILTERING OF AVAILABLE ADAPTATIONS

In this section a range of possible adaptations for the individual components are identified. These adaptations are stated in Table 9.3 and are retrieved from literature, i.e. Huijsman (2021), and generally known applications. To derive suitable adaptations of the components for the design strategies, a series of filters are introduced (Section 9.4.1). Followed by the application of the filters in Section 9.4.2, Section 9.4.3, Section 9.4.4 and Section 9.4.5.

9.4.1. APPLIED FILTERS

The filtering of adaptations helps determining which adaptations, and their relative characteristics, are suitable and through the filters adaptation options are eliminated. The identified adaptations in Section 9.3 are filtered through the following filters in chronological order:

- Necessity of the adaptation: verify whether adaptation is needed
- Comparison of costs between adaptations of the same component
- Mechanical/structural verification
- Cost-effectivity of the adaptations (where possible with varying characteristics of the adaptation

Table 9.3: List of identified possible adaptation options for the varying main components of the barrier.

Component	Adaptation	Description
Foundation	Compression piles	By installing compressive piles at the shallow foundation additional horizontal, vertical and rotational stability is provided.
	Tension anchors	By installing tension anchors at the shallow foundation additional resistance against negative head is provided.
	Soil improvements	By injecting, i.e. grout, or replacing the subsoil, the bearing capacity of the soil is increased leading to additional vertical and rotational stability.
	Increase in shallow foundation surface	By increasing the dimensions of the existing shallow foundation the horizontal, vertical and rotational stability is increased.

Table 9.3 continued from previous page

Component	Adaptation	Description
Bed protection	Replacement	By replacing the top layer of the bed protection, and if required the underlying filter layers, by a larger d_{n50} the erosion with increasing shear velocities is reduced.
	Colloidal concrete	Colloidal concrete increases the resistance of the bed protection to erosion. The grains of the colloidal concrete are small and can be poured into the pores of the top layer of the bed protection, preventing erosion of the layer.
	Length increase	Increasing the length of the existing bed protection to provide sufficient stability considering the slope resulting from a scour hole at the toe of the protection.
Steel trusses	Additional truss	Installation of an additional truss providing an increase in resistance against hydraulic forces.
	Replacement	Replacing existing trusses.
Sector gate	Gate extension	Extension of the existing sector gates.
	Replacement	Replacement of the entire sector gates to increase the height and strength of the gate.
	Buoyancy increase	Applying components that increase buoyancy of the gates.
Ball hinge	No options identified	-

9.4.2. NECESSITY OF THE ADAPTATION

Deriving the relationship between the loading conditions and resistances of the components with sea level rise yields an estimation whether a components needs to be adapted over time due to increasing loading conditions. In Appendix F the loading conditions acting on the component with a range of sea level rise are computed, from the verification the following is concluded:

- Bed protection seaside: Underflow velocities during the opening procedure decrease with an increase in sea level rise as the water level behind rises in accordance with the closing regime (Fig. F.24)
- Steel trusses and foundation under negative head: horizontal forces following from negative head are set to decrease with an increase in sea level rise (Appendix F.2.2)
- Compression piles and tension anchors: the bearing capacity of the subsoil of the foundation provides sufficient resistance to the loading conditions as determined in Fig. F.30 (horizontal) and Fig. F.31 (rotational).
- Buoyancy of sector gates: it is unlikely that the buoyancy causes issues (Appendix F.4.2)

9.4.3. RELATIVE COSTS

Following the necessity filter, a comparison is made between available adaptations for the same component. Logically, if the adaptation results in a similar increase of the resistance, the adaption with the lower costs has the preference. In Appendix H the costs of the adaptations are stated and summarised:

- Bed protection: Replacement of the armour layer (≈ M€4.72, see Table H.5) is considered cost-inefficient compared to colloidal concrete (≈ M€2.12, see Table H.5)
- Sector gate: Replacement of the sector gates (≈ M€194.7 Table H.3) is considered as highly cost-inefficient compared to extension (≈ M€9.92 Table H.7)

- Steel trusses: Replacement of the steel trusses is considered as highly cost-inefficient as the derived cost of a gate (≈ M€185, Table H.3) dwarfs that of an extension (≈ M€5 - 10, Appendix H.2.3)

9.4.4. MECHANICAL/STRUCTURAL VERIFICATION

In accordance with the verification in Appendix F, a closer look into the installation of an additional truss to increase the bearing capacity of the superstructure is conducted. The sector gates are shaped as an arch, the idea behind an arch-like structure is to minimise the formation of bending moment forces in the structure, see Fig. 9.4. However, installing an additional truss could lead to a different flow of forces.

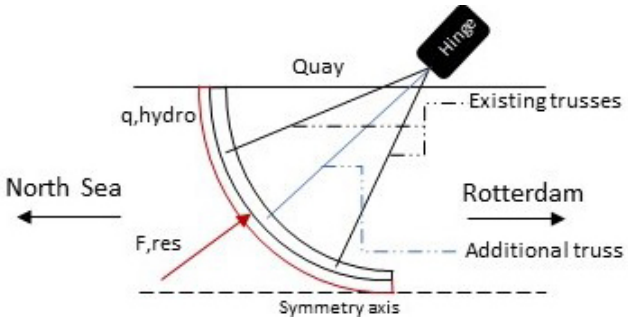

Figure 9.4: Schematised overview of the structure with an additional truss.

In Appendix F.3.1 the adaptation is verified and from the verification it is concluded that the adaptation is likely to lead to a counter productive result. Instead of decreasing the compressive force on the two existing trusses, it leads to an increase of these forces. Therefore, this adaptation is excluded from further analysis and no remaining adaptations for the steel trusses are available. The remaining adaptations are viewable in Table 9.2 and are analysed further based on the benefits of the adaption.

9.4.5. BENEFITS OF ADAPTATIONS WITH VARYING DIMENSIONS

What rests from the applied filters, is determining which adaptations, and dimensions thereof, are the most suitable for the individual design strategies. This last filter is conducted through determining the positive/negative benefit ratio of the adaptations, where variance of the dimension (metres) of the adaptation for the component is possible, for each individual design strategy. The possible variances are identified and stated in Table 9.4. The costs of these variances are derived in Appendix H.2 and these increase linearly with the amount of metres of the adaptation. The variances are chosen as such that an adaptation of component is required two times at maximum.

Table 9.4: Variances in dimensions of adaptations for the individual dynamic design strategies.

Adaptation	Unit indicator	Dynamic+1.0	Dynamic+1.5	Dynamic+2.0
Bed length increase	Metre(s)	+3.0 & +4.0 & +5.0	+2.0 & +3.0	+1.0 & +2.0
Gate extension	Metre(s)	+1.0 & +1.5 & +2.0	+1.0 & +1.5	+0.5 & +1.0

The performance of these variances are elaborated along the results retrieved from the bed protection length increase adaptation for the Dynamic+1.0 design strategy. In Fig. 9.5 the performance of these variances based on the anticipated benefits are visualised. With the figure it is seen that these adaptations are likely to yield a negative benefit. Although, in some instances the adaptation could result in positive benefits. The likelihood, however, is slim as the mean of the adaptations are well

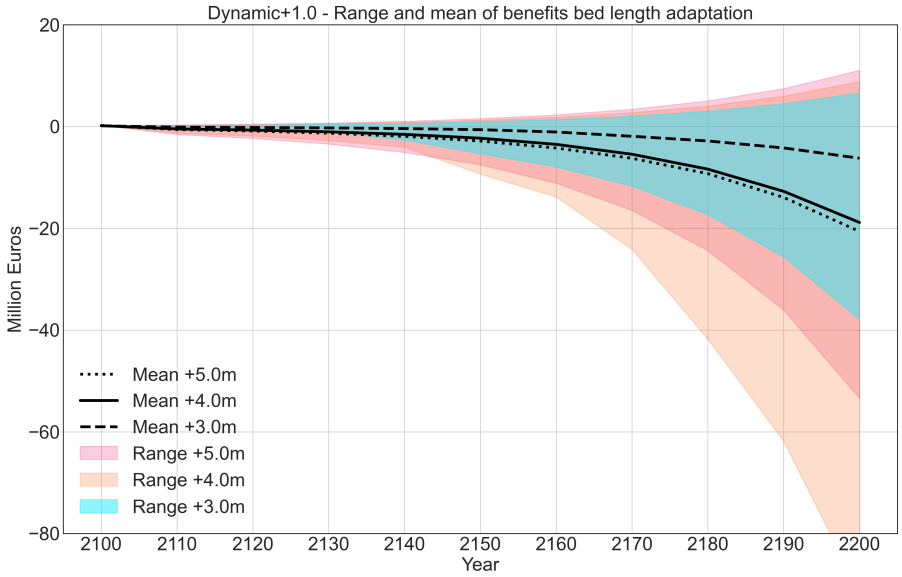

Figure 9.5: Performance of the adaptation bed length increase with varying characteristics in three dynamic designs.

below the break-even line of 0 by the end of the 22nd century. In Appendix I.3 an in-depth analysis of the remaining components in the same manner is provided and with the analysis the preferred dimensions of these adaptations for each individual design strategy are determined, see Table 9.5. Along with the wedge soil improvement, these adaptations are applied to the design strategies and analysed further in Section 9.5.

Table 9.5: Overview of advised dimensions of the adaptations with varying characteristics.

Bed protection length	**Dynamic+1.0**	**Dynamic+1.5**	**Dynamic+2.0**
Advised length adaptation	+3.0	+3.0	+1.0
Estimated costs in 2021 price levels	€531,000	€531,000	€178,000
Gate height	**Dynamic+1.0**	**Dynamic+1.5**	**Dynamic+2.0**
Advised height adaptation	+1.0	+1.5	+1.0
Estimated costs in 2021 price levels	M€9.92	M€14.88	M€9.92

9.5. GLOBAL COST-EFFECTIVITY ANALYSIS DYNAMIC DESIGN STRATEGIES

Now that most of the adaptations are filtered and the preferred characteristics of these adaptations are determined, a global analysis, where the performance of the adaptations in the respective design strategy are compared, remains. This analysis follows a similar procedure as is conducted in Section 9.4.5 and is elaborated along an example. In the left figure of Fig. 9.6, the performance of the gate height extension adaptation, as determined in Table 9.5, based on the anticipated benefits is visualised. As one can deduct from the figure, it is likely that the adaptation yields a positive benefit for all three dynamic designs. However, the range of the benefit is of a considerable size and gives no guarantee of a positive benefit, although the odds are slimmer. When reviewing the 5th -and 95th-percentiles of benefits (Right figure in Fig. 9.6), one could see that the ranges reduce significantly. This confirms that, for Dynamic+1.0 and +2.0, the likelihood of this specific adaptation to yield negative benefits are considerably small.

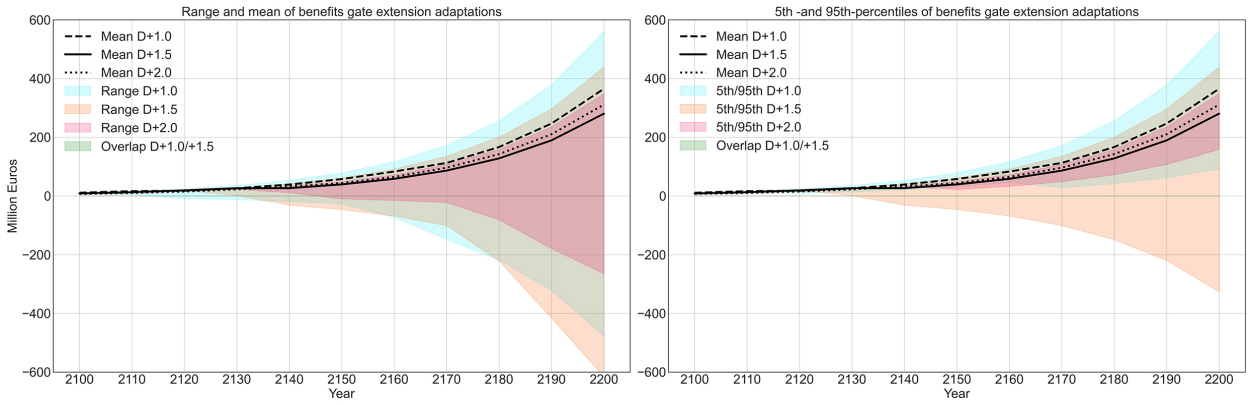

Figure 9.6: Left: Mean and range of the gate extension adaptation benefits for all three dynamic design strategies. Right: 5th -and 95th-percentiles - D+1.0 stands for the Dynamic+1.0 design strategy.

An in-depth analysis of the wedge soil improvement and bed protection length increase is provided in Appendix I.4.1 and Appendix I.4.2, respectively. In Fig. 9.7 the 5th -and 95th-percentiles of the benefits of these adaptations are provided. With these results it is deducted that the wedge soil improvement has a moderate to high confidence yielding positive benefits when considering the Dynamic+1.5 and +2.0 design strategies. Whilst the range of benefits for the Dynamic+1.0 is considered as too uncertain, which could result in negative benefits. In contrast, it is highly likely that the bed protection length adaptation will result in a negative benefit for all three design strategies. Thus, the latter adaptation is excluded and designed as in the static robust design.

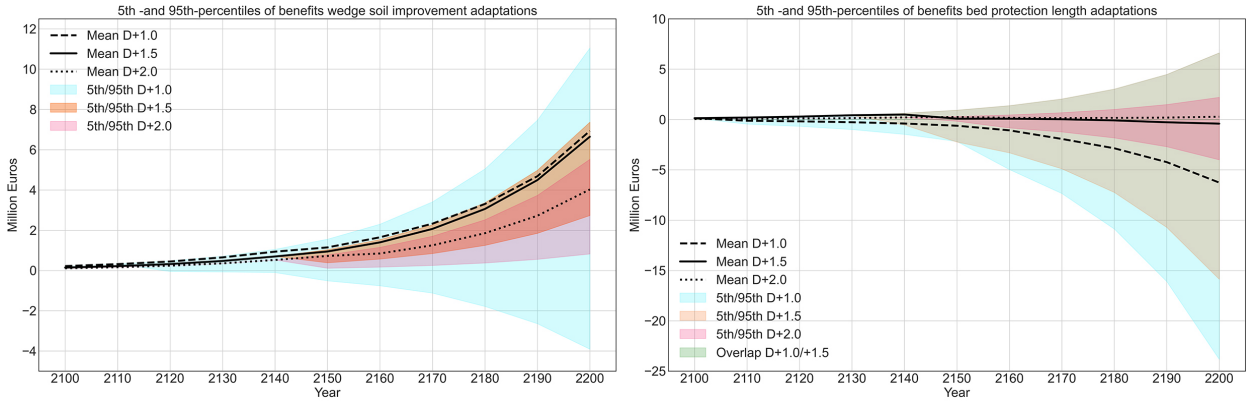

Figure 9.7: 5th -and 95th-percentiles of benefits of the soil improvement (left) and bed protection length (right) adaptation for all three dynamic design strategies.

9.6. PREFERABLE DESIGN STRATEGY

Lastly, a preferable design strategy is determined by combining the most beneficial characteristics of the components and their adaptations. With the analysis provided in the previous section (Section 9.5) it is determined to not include the adaptation for the bed protection length. Furthermore, the adaptations of the wedge soil improvement and gate height extension are included, where the initial dimensions follow from the Dynamic+1.5 and Dynamic+2.0 design strategies, respectively. The Dynamic+1.5 characteristics for the foundation block are chosen due to the fact that the potential benefits of the adaptation are attributed with a positive 5th -and 95th-percentiles spread and a relatively high mean, see left figure of Fig. 9.7. The Dynamic+2.0 characteristics for the gate height are chosen for a similar reason, see right figure of Fig. 9.6. The characteristics of the preferred design

for (non-)adaptable components are summarised in Table 9.6 and these are applied in the structural design (Chapter 10).

Table 9.6: Overview of the characteristics of the components for the preferred design strategy.

From	Component	Parameter	Dimensions	Adaptation or comment
Dynamic+1.5	**Foundation**	LxBxH	50x55x4 m	Wedge soil improvement
Static	**Bed protection**	$d_{n50,river}$	1.44 m	Or 1.18 m with colloidal concrete
		L_{river}	58.5 m	No adaptation
		$d_{n50,sea}$	0.59 m	No adaptation
		L_{sea}	28.0 m	No adaptation
Static	**Steel truss**	N_{Rd}	141 MN	No adaptation
Static	**Ball-hinge**	N_{Rd}	141 MN	No adaptation
Dynamic+2.0	**Sector gates**	H_{gate}	23.5 m	Gate height extension (+1.0 m)

9.7. CONCLUDING REMARKS

Concluding, options to design certain components of the barrier in an adaptable manner are available and according to the analysis could prove to be beneficial. As the range of sea level rise is of an uncertain nature, it is difficult to precisely predict to what boundary conditions the barrier should adhere too. This, from a traditional point of view, could lead to a very conservative design if the rate of sea level rise is less severe than anticipated. The dynamic robust design strategies could provide some initial reduction of these construction costs, and as sea level rises, can be adapted to withstand rising loading conditions. However, one has to consider that for all cases analysed in this chapter, there is no guarantee of yielding positive benefits, although the likelihood for some adaptations are higher than for others. Moreover, the computations with the reliability model is performed with input from the RCP8.5 SLR scenario and the results could differ when the other, less severe sea level rise scenarios, are also included. In general, the potential benefits of the adaptions follows the principle of high risk, high reward. This becomes evidently clear when comparing the ranges of benefits for all adaptations between Dynamic+1.0 and +2.0. Dynamic+1.0 design strategy produces the highest possible positive benefits but also is joined with the highest possible negative benefits, as was shown in Fig. 9.6 and Fig. 9.7, whilst these maxima and mimima decrease significantly for the Dynamic+2.0 design strategy. Therefore, the design strategies are combined, as readable in Table 9.6. In Chapter 10 an elaboration of the defined dimension parameters of the components is supplied along with visualisations of the barrier.

10 | Structural elaboration of preferable design strategy

In this chapter the derived preliminary characteristics of the components and the respective Limit State Functions are briefly defined and elaborated. In the first section (Section 10.1) an conceptual overview of the barrier is provided, along with the performance of the design in the reliability model. Whereafter, the elaboration of the main components follow. In Section 10.2 the foundation blocks of the barrier are addressed, followed by the design for the bed protection (Section 10.3), steel trusses (Section 10.4), the sector gates (Section 10.5) and ball-hinge (Section 10.6).

10.1. Overview

A visualisation of the barrier and the main components is provided in Section 10.1.1. In Section 10.1.2 the performance, considering the failure probabilities in 10,000 growth scenarios, is supplied.

10.1.1. Overview of the barrier

In Fig. 10.1 an overview of the upper segment of the sector gate barrier, drawn in AutoCAD, is provided along with some dimensions.

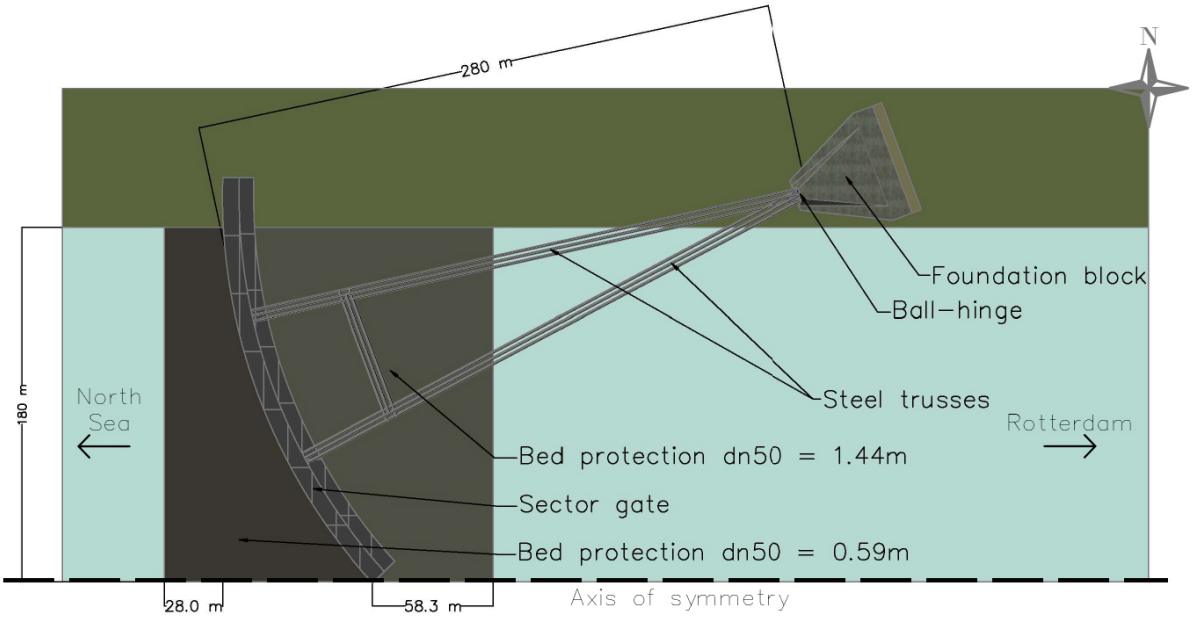

Figure 10.1: Topview of the northern segment of the barrier and its main components.

10.1.2. Performance of the design strategy over time

In Fig. 10.2 the performance, based on the relative failure probability of the components, is provided. From the graph it is deducted that most of the failure probabilities of the components adhere to the instated threshold limits. Some slight exceedance of the threshold limit by the bed protection length and steel trusses components is seen, which is deemed as acceptable for the remainder of

this thesis. Moreover, the introduced adaptations of the foundation (wedge soil improvement) and gate height extension adequately reduce the failure probability. Additionally, the strategy and the adaptations are attributed with a high likeability to yield positive benefits, see the ratio in the red brackets in Fig. 10.2. Furthermore, the structural failure probability stays well below the instated limit of 1:10,000 p/y, this is due to the fact that some of the identified components, in Section 8.2.1, rarely fail and contribute to the structural failure. This is discussed further in Chapter 11.

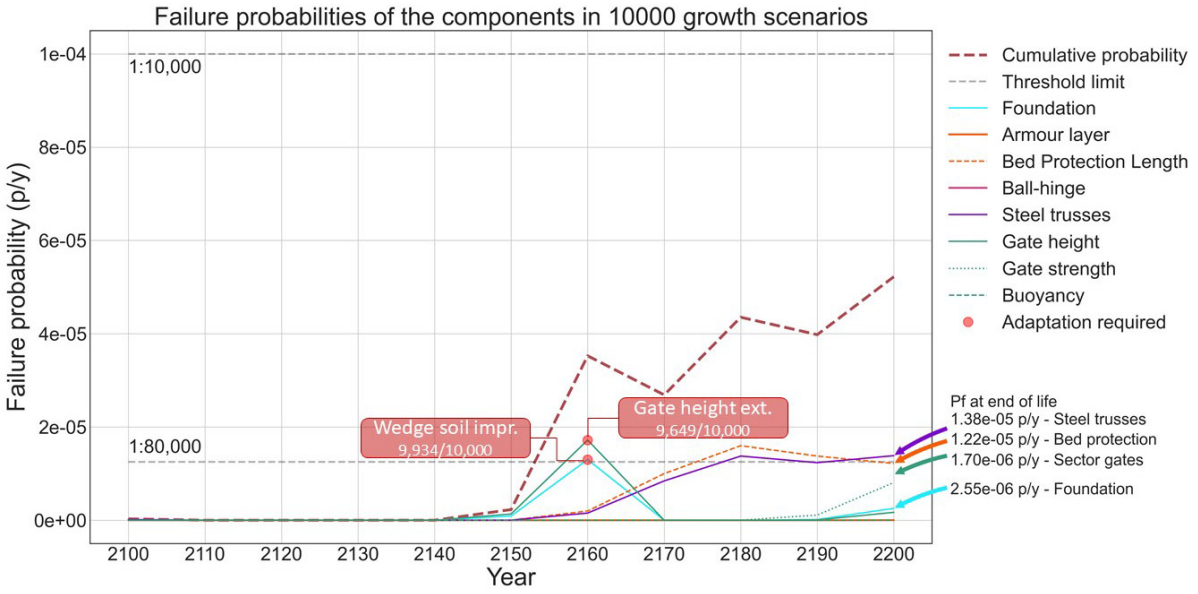

Figure 10.2: Failure probability progression over time in 10,000 growth scenarios of the components for the preferred design strategy with indicative cost-effectiveness ratio of the two applied adaptations.

10.2. FOUNDATION BLOCK

In Fig. 10.3 a top -and sideview of the foundation block that supports, the sector gates and steel trusses, is provided. The wedge, providing additional horizontal stability as defined in Appendix F.7.1, is included. The calculations determining whether sufficient horizontal, vertical and rotational stability is provided with the dimensions defined in Table 9.6, as integrated in the reliability model, are briefly discussed in this section.

Vertical stability

To determine whether the foundation block is able to provide sufficient vertical stability, the vertical bearing capacity of the soil is verified. According to CUR (2010), the bearing capacity of densely packed sand can be assumed to be equal to 400 N/mm^2. The Limit State Function for vertical stability reads:

$$Z = 400 - \sigma_{k,max} = 400 - \frac{F_{vertical}}{A_{foundation}} + \frac{M_{Ed}}{\frac{1}{6} \cdot B \cdot L^2} \tag{10.2.1}$$

According to the results of the reliability model, the dimensions viewable in Fig. 10.3, satisfy the instated threshold limits. An elaboration of the vertical stability calculation is provided in Appendix F.7.2.

Horizontal stability

To determine whether the foundation block is able to provide sufficient horizontal stability, the resistance of the block is verified against the horizontal force. The resistance is a combination of the friction of the block on the subsoil (Molenaar and Voorendt, 2019) and the passive pressure of wedge supporting the block (Q) (Vardon, 2020). The Limit State Function for vertical stability then

reads:

$$Z = f \cdot \sum H + Q - F_{Ed,horizontal} \tag{10.2.2}$$

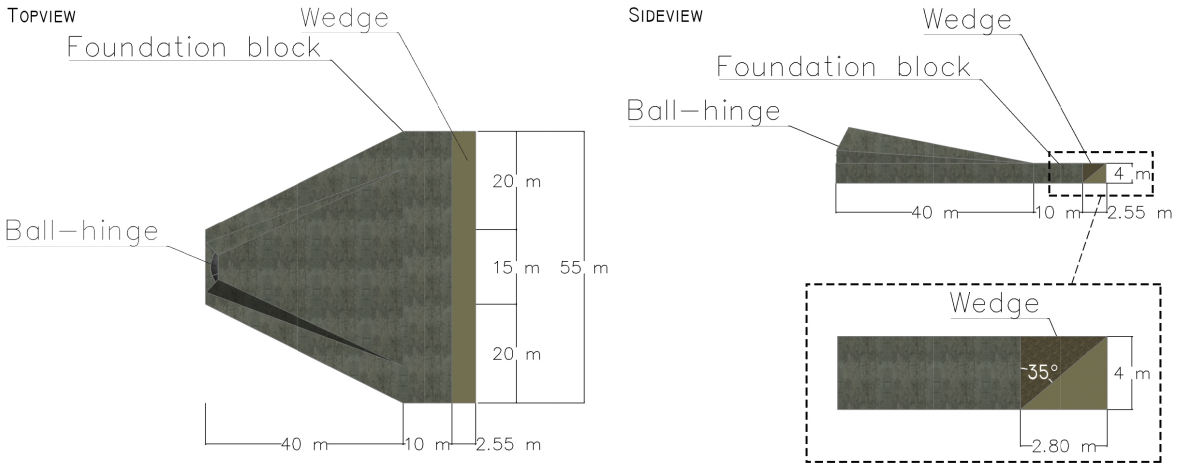

Figure 10.3: Design and dimensions of the foundation block. The wedge is the segment, initially sand ($\gamma = 18$ kN/m^2), that is replaced by gravel ($\gamma = 21$ kN/m^2) as the adaptation.

The dimensions of the block (50x55x4 - LxBxH) initially adhere to the instated threshold limits. However, as sea level rises, it is likely an increase in horizontal resistance is necessary, as is shown in Fig. 10.4. If the horizontal forces surpass the resistance the wedge soil improvement adaptation should be applied and is elaborated further on. In Appendix F.7.1 an elaboration of the calculation is provided.

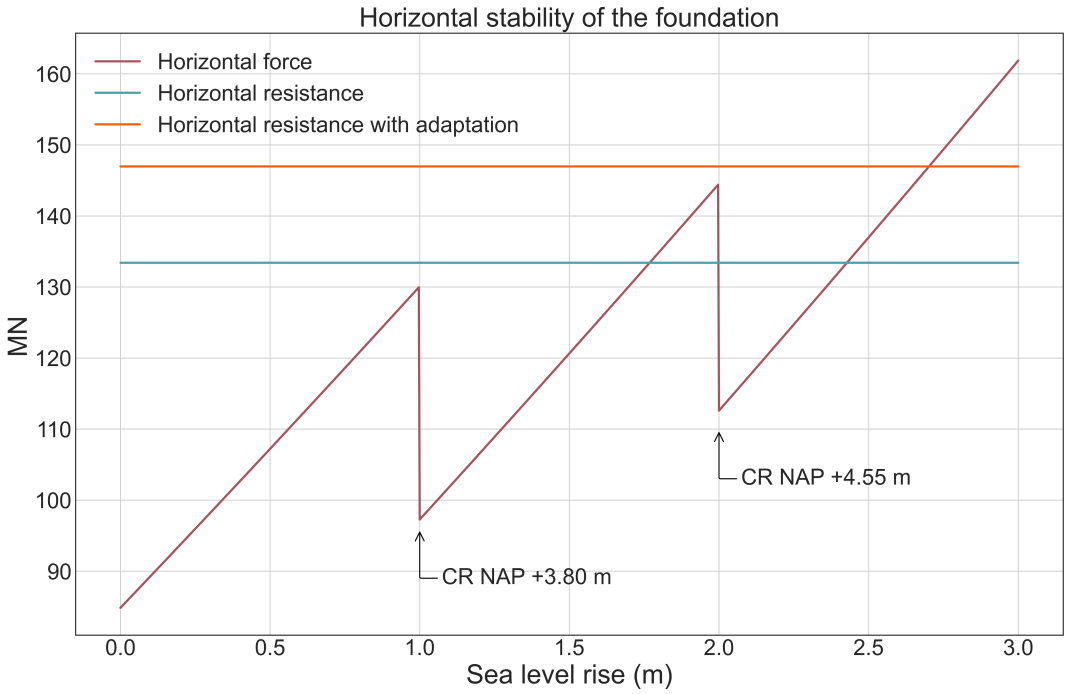

Figure 10.4: Horizontal stability of the barrier in regard to the sea level rise with(out) wedge soil improvement adaptation. 'CR' are the altercations to the Closing Regime of the barrier.

Wedge soil improvement adaptation

The wedge at the back of the foundation block provides additional horizontal resistance due to the passive soil pressure of the wedge (Vardon, 2020). If the horizontal forces surpasses the horizontal bearing capacity of the barrier, the soil wedge is improved by a heavier material, i.e. gravel. Initially, the selfweight of the wedge is equal to that of sand ($\gamma = 18$ kN/m^2) with an angle of internal friction of 32.5 degrees, once replaced by gravel this is increased to $\gamma = 21$ kN/m^2 with an angle of internal friction of 35 degrees. The increase in horizontal resistance is presented in Fig. 10.4. According to Fig. I.6, it is likely the adaptation is required near the year 2160. However, the necessity could occur earlier or later in time and depends on the actual sea level rise scenario. For an elaboration Appendix F.7.4 is provided.

Rotational stability

To determine whether the foundation block is able to provide sufficient rotational stability it is verified whether the soil stresses are solely of a compressive nature. This criteria is met when the resulting force intersects the core of the foundation block (Molenaar and Voorendt, 2019, p. 274). The core of the block is defined as $\frac{1}{6}$ times the length (50 metres). Thus, the equation for the rotational verification reads:

$$e_R = \frac{\sum M}{\sum V} \leq \frac{1}{6} \cdot L \tag{10.2.3}$$

In Fig. 10.5 it is shown that for a range of sea level rise between 0 and 3 metres the demands for rotational stability are satisfied. In Appendix F.7.3 an elaboration of the calculation is supplied.

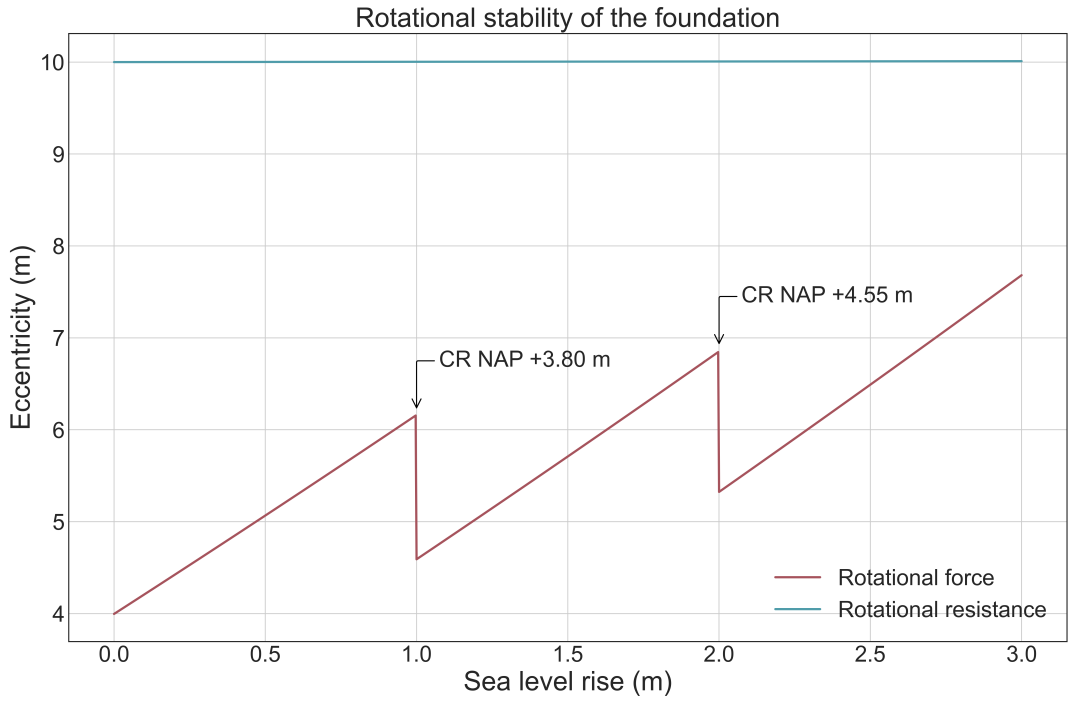

Figure 10.5: Rotational stability of the barrier in regard to the sea level rise. 'CR' are the altercations to the Closing Regime of the barrier.

10.3. BED PROTECTION

In Fig. 10.6 a sideview of the bed protection of the barrier is provided. During the closed position the barrier rests on a concrete sill, but is not elaborated further. The required size of the applied stones of the armour layer and the length thereof, and as computed within the reliability model,

are determined in accordance with Schiereck and Verhagen (2019) and is elaborated along a few equations. The size of the stones of the armour layer are determined by applying Shields where the resistance ($u_{*r,Res}$) is subtracted by the acting flow velocity acting flow velocity (u_{*r}), in accordance with the Limit State Function (Table 8.1). For the Shields parameter (ψ_c) 0.03 is applied as this is considered as "a safe choice for the threshold of motion" (Schiereck and Verhagen, 2019, p. 55). The equation then reads:

$$Z = \sqrt{\psi_c \cdot \Delta \cdot g \cdot d_{n50}} - u_{*r} \tag{10.3.1}$$

According to the computations from the reliability model (Table 9.6) d_{n50} =1.44 m is satisfactory for the riverside protection and d_{n50} =0.59 m for the seaside to adhere to the instated threshold limits. A thorough elaboration of the calculations are readable in Appendix F.5. The thickness of the armour layers are determined in accordance with Schiereck and Verhagen (2019) and equal to $1.5 \cdot d_{n50}$ metres. The required filter layers are not discussed further in this preliminary design and should be included in further designs. The length of the bed protection is computed with:

$$h_s(t) = \frac{(\alpha \cdot \bar{u} - \bar{u}_c)^{1.7} \cdot h_0^{0.2}}{10 \cdot \Delta^{0.7}} \cdot t^{0.4} \text{ (Schiereck and Verhagen, 2019, p. 92)} \tag{10.3.2}$$

Which results in a required length of 58.5 m and 28.0 m at the river -and seaside, respectively. Calculations concerning the length of the bed protection are elaborated in Appendix F.6.

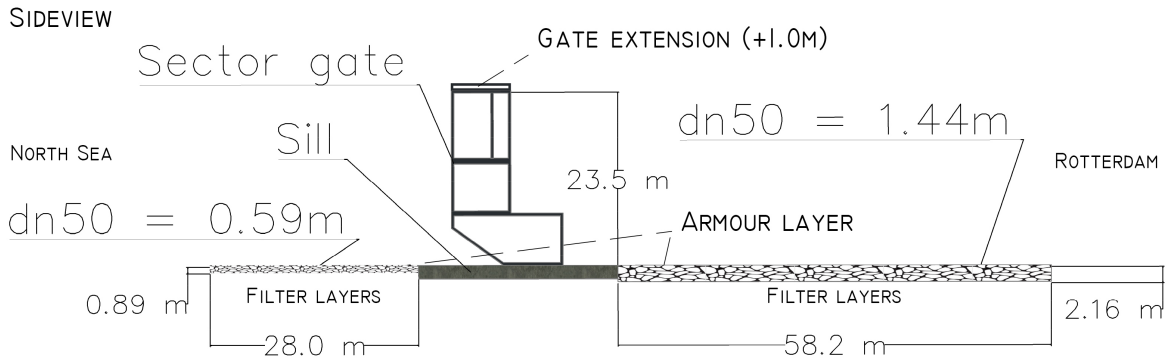

Figure 10.6: Design and dimensions of the armour layer of the bed protection.

10.4. STEEL TRUSSES

As the characteristics of the steel trusses, determined in Section 9.6, are defined as the required resistance to a compressive force, a calculation to derive the required profiles of the main beams is provided. According to the preferred design strategy, the steel trusses of a single sector gate should be able to withstand 141 MN of compressive force. The force is divided over two trusses which each consists out of three main beams supported by girders in the truss, see top left figure of Fig. 10.7. The force on a single main beam is then computed as:

$$F_{Ed,main\,beam} = \frac{F_{Comp,max}}{N_{trusses} \cdot N_{main,beams}} = 23.5\,\text{MN} \tag{10.4.1}$$

To satisfy the demand the required steel cross-sectional surface is computed with steel quality S355 (f_y) and γ_{m0} is equal to 1:

$$F_{Ed,main\,beam} = \frac{A \cdot f_y}{\gamma_{m0}},\ A = 66{,}200\,\text{mm}^2 \tag{10.4.2}$$

The required steel cross-sectional surface is fulfilled by a CHS762/30 hollow section, see Fig. 10.7. The three main beams, similar to the current Maeslant barrier, are installed in a triangular shape. To determine the allowable distance between the girders supporting the main beam, a calculation based on buckling for global instability is applied:

$$F_{cr} = \frac{\pi^2 \cdot EI}{L^2} \tag{10.4.3}$$

In Appendix F.3.2 the computation is elaborated in detail and results in a maximum allowable distance of 18.4 metres, see bottom figure of Fig. 10.7.

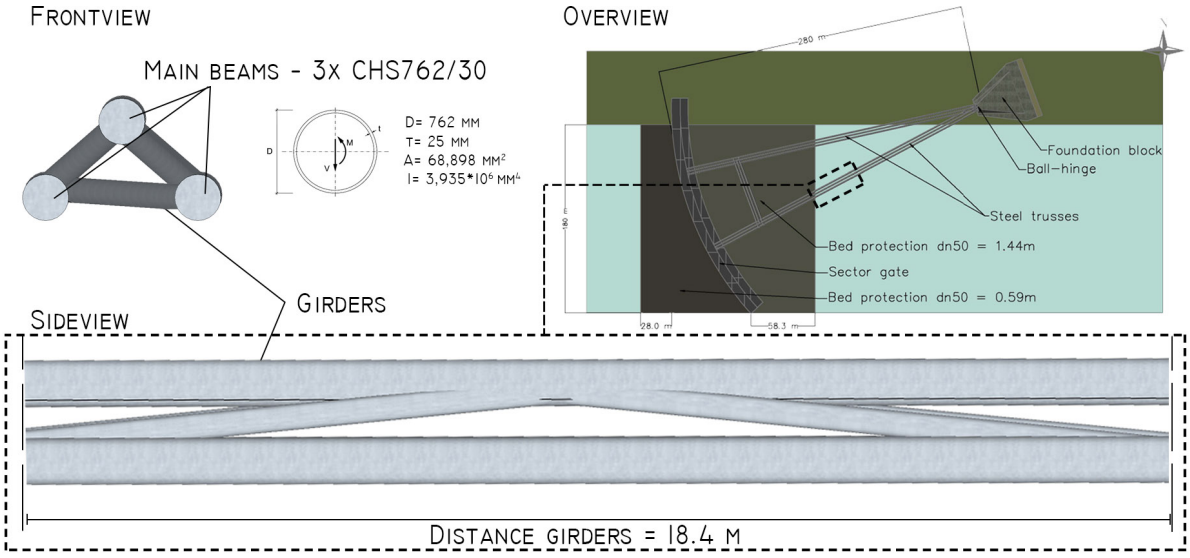

Figure 10.7: Design and dimensions of the steel trusses. Not to scale.

10.5. SECTOR GATES

In Fig. 10.8 a top -and sideview of one sector gate is provided. The dimensions of the gate are determined with the reliability model and are briefly elaborated in this section.

Sector gate height

The required height of the sector gate is determined by the Limit State Function (Table 8.1) where the amount of water overtopping and/or overflowing should stay below an instated value of 0.2 m^3/s per metre width. The limit is based on the Ultimate Limit State (ULS) mean discharge attributed to embankment sea walls and sea dikes (van der Meer et al., 2018), however, this value could prove to be (very) conservative. The amount of volume flowing over the gates depends on the sea level rise, which is added to a 1:10,000 p/y occurring storm surge of NAP +5 metres as defined in Appendix D.1, and whether positive, zero or negative freeboard is present. The Limit State Function then reads:

$$Z = 0.2 - \sqrt{g \cdot H_{m0}^3} \cdot 0.04 \cdot e^{-1.8 \frac{R_c}{H_{m0}}}, \text{ for positive and zero freeboard (Appendix F.4.1)} \tag{10.5.1}$$

$$Z = 0.2 - 0.54 \cdot \sqrt{g \cdot [-R_c^3]}, \text{ for negative freeboard (Appendix F.4.1)} \tag{10.5.2}$$

To initially adhere to the instated threshold limits a gate height of 23.5 metres and, when sea level rises, an additional metre is installed on top of the gates to adhere to future conditions. According to the failure probabilities attributed to the gate height of 23.5 metres from Fig. 9.2, the adaptation is likely to be necessary around 2160. However, the necessity could occur earlier or later in time

and depends on the actual sea level rise scenario. An example of such a modular gate is provided in further on.

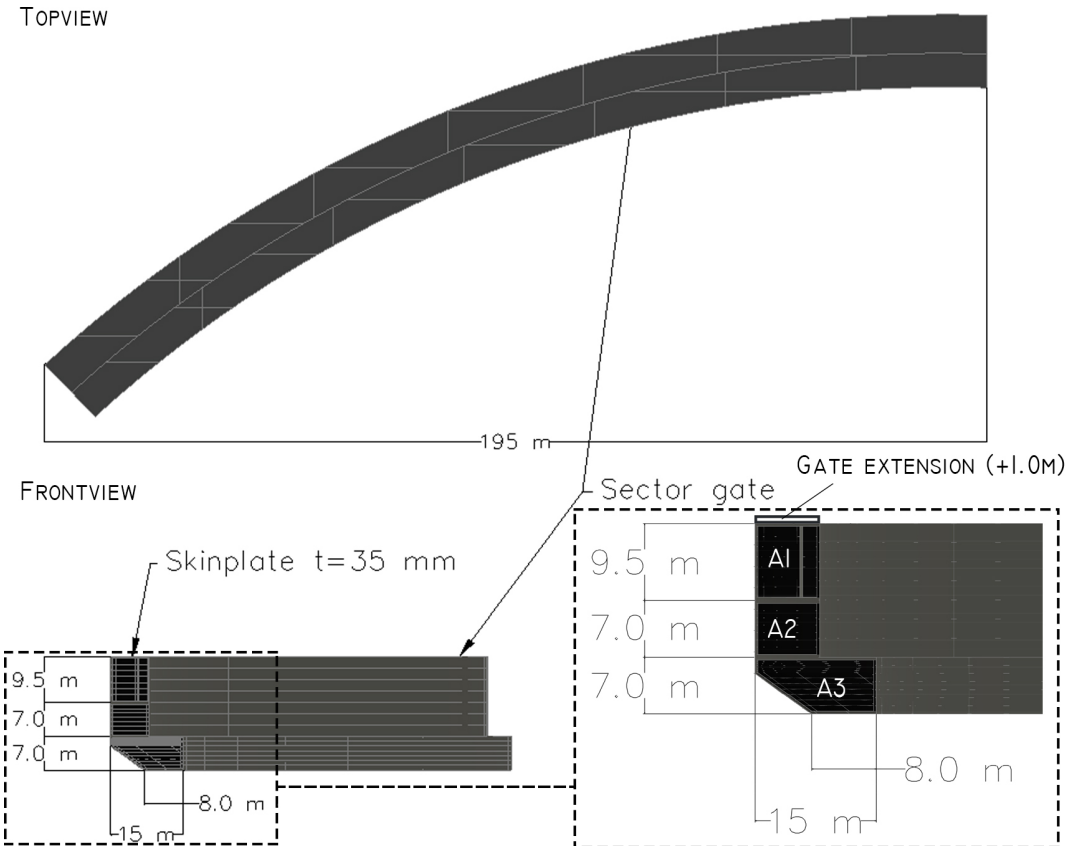

Figure 10.8: Design and dimensions of the sector gates. Including gate extension (+1.0 m) adaptation.

Skinplate thickness

The skinplate of the gate must be able to withstand the loading conditions resulting from the hydraulic loading. To derive the required thickness the resistances to bending and deflection are verified. To limit the bending moment (Eq. (10.5.3)) and deflection (Eq. (10.5.4)), girders, spaced 2 metres apart, in horizontal direction are installed. The required dimensions of these girders is withheld from this thesis. An elaboration of these calculations is readable in Appendix F.4.3. According to the results of the reliability model a thickness of 35 mm with steel quality S355 is sufficient to adhere to the instated threshold limits, see the green dashed line in Fig. I.2.

$$Z = M_{Ed} - M_{Rd} = \frac{1}{10} \cdot q_{hydro} \cdot \text{ Girder spacing} - \frac{1}{6} \cdot \text{ Girder spacing} \cdot t_{steel}^2 \cdot f_y \tag{10.5.3}$$

As a rule of thumb, the deflection should not surpass $\frac{1}{200}$ times the spacing between the girders:

$$Z = f_{limit} - f_{deflection} = 10\text{ mm} - \frac{\alpha \cdot p \cdot a^4}{E \cdot t^3} \tag{10.5.4}$$

Buoyancy

The annotations A1, A2 and A3 in Fig. 10.8 resemble the filling areas providing the buoyancy of the gates and allowing it to sink to the bottom, which is elaborated further in Appendix F.4.2.

Gate extension adaptation

As of yet, no examples, concerning the extension of a sector gate of a storm surge barrier, are re-

trieved. However, modular systems for mitre gates, as supplied in Fig. 10.9, exist or being developed and the application for the gate height extension in this thesis could be designed similarly.

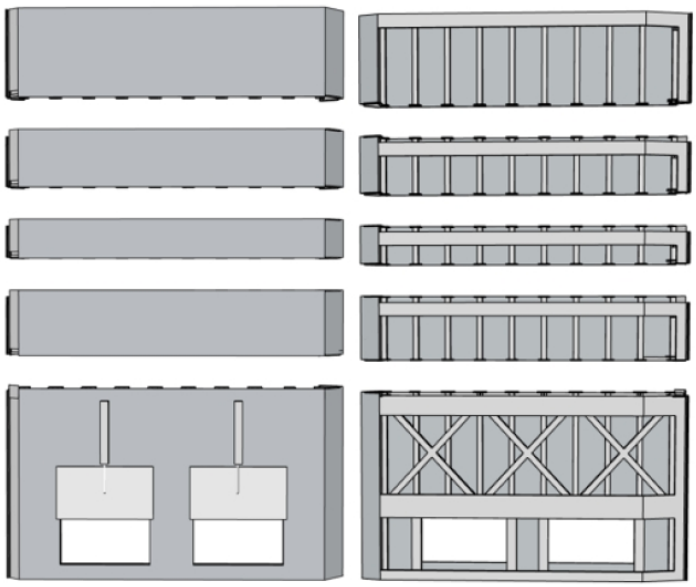

Figure 10.9: Modular rendition of mitre gates serving as an example for the sector gate in this thesis. Retrieved from Levinson (2018, p. III).

10.6. BALL-HINGE

Due to the complexity of the ball-hinge a preliminary design of the ball-hinge is left out of the scope within this thesis. The experience from the current ball-hinge in the Maeslant barrier learns that it is possible to construct such a component. However, at the time it was quite difficult to find a suitable contractor able to produce such an immense object (van Oorschot, 2021), and as forces are likely to increase with sea level rise, the ball-hinge required for this new design is likely required to be of a greater size. This could prove to hinder the constructability of a new barrier. In Fig. 10.10, a schematic of the ball-hinge installed in the Maeslant barrier and a photographed figure of the pre-fabricated object is provided.

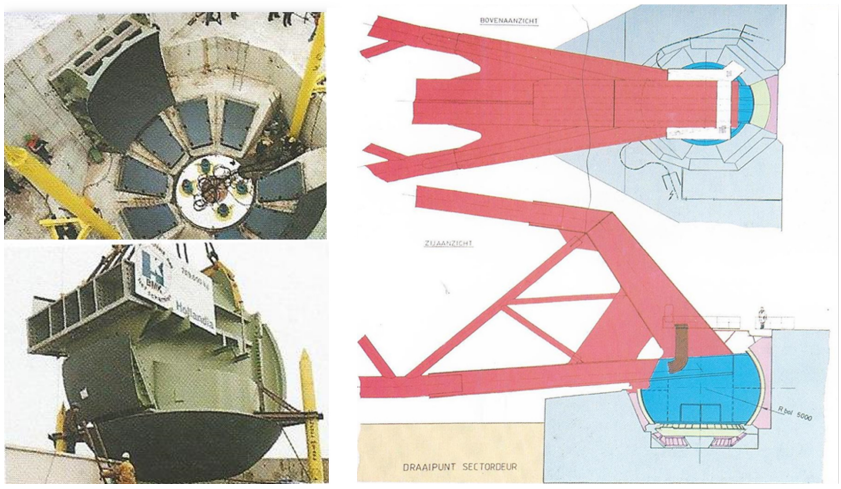

Figure 10.10: Left: Photographed images of the ball-hinge in the Maeslant barrier. Right: Schematised top and cross-sectional view of the ball-hinge. Figures with the courtesy of van Oorschot (2021).

11 | Discussion and reflection

In this chapter a few points open to discussion are discussed in Section 11.1 and include, but not limited to, the adaptive pathways plan, reliability model and the recent publication of the Sixth Assessment Report of the IPCC. Furthermore, a reflection of the approach is supplied in Section 11.2.

11.1. Discussion

Adaptive pathways plan

In this report the adaptive pathways approach from Haasnoot et al. (2012) has been utilised to derive a system in which a dynamic flood protection, i.e. barriers and locks, could take form. The identified measures and pathways mainly surrounded these structure in order to let these be able to function under a range of sea level rise and some socio-economical developments. In addition, the pathways were designed with the assumption that Delta21 would have been developed in the future. This allowed for the deduction of the consequences of river discharges from the Rhine and Meuse. If Delta21 would not come to fruition in the future, the identified pathways could be altered in their functionality and performances. As recent flooding events in Germany, Belgium and The Netherlands have shown, risks of flooding do not solely come from the sea. Moreover, it would be interesting to integrate other regional plans, e.g. river as a tidal park as suggested by Gemeente Rotterdam (2019), and their functionality into the adaptive pathways as these broaden the scope of possible solutions for the Rhine-Meuse estuary.

Reliability model

Some key features of the reliability model are open to discussion and, if researched further, could prove to yield more accurate and desired results. Three major features are discussed below.

- **Fault tree and threshold limits**
  The fault tree and the instated threshold limits, especially the limit dictating the limit for the individual components of the barrier (1:80,000 p/y), heavily influences the likelihood whether, and how often, a component has to be adapted. In the current model all eight identified components are considered as equally important and so the 1:10,000 yearly structural failure limit is divided amongst these components. It is questionable whether all components contribute equally to the structural failure. A key example is the contribution of buoyancy component to the structural failure probability. In Section 9.1 an example of the failure probability performance is provided and the contribution of the buoyancy constantly yields a zero failure probability, all the whilst consuming a portion of the 'available' failure probability.

- **Time steps**
  The reliability model produces results for a time span between the 21st and 22nd century with steps of 10 years, in combination with a number of wanted iterations (N=10,000), resulted in quite some computing time of the model ($\approx$ 3 hours per design strategy). Due to the lack of computing power of available hardware the time steps and number of wanted iterations has not been increased. Running the model with a higher number of iterations and decreasing the time steps between results would yield a more accurate depiction of reality. This especially becomes evident when computing the benefits of the adaptations. As the computation of the benefits is an exponential function, where the savings and costs are multiplied with 1.04^{Years} and 1.02^{Years}, respectively.

- **Interest and inflation rates**
  The benefits computed within the reliability model are based on a 4% interest rate on costs savings, which compound over the years and thus increase in value, and a 2% inflation rate (target of the European Commission (European Central Bank, nd)), which increases the costs of the adaptation over the years and thus increases in costs. In a real world situation, these rates are not fixed and fluctuate in accordance with the present situation of the market. The retrieved benefits are largely dependent on these rates and fluctuations influence the general outcome whether an adaptation is determined as beneficial and could be integrated as an additional uncertainty. The revival of the economy, in the wake of the CoVID-19 pandemic, signals a stark increase in global inflation rates. Inflation rates for the energy, in September 2021, and construction, for the first quarter of 2021, sectors are indexed at 19.4% (CBS, 2021) and 1.1-1.8% (Rats et al., 2021). According to (Rats et al., 2021), considering the inflation rate in the first quarter of 2021 for the construction sector could result in an estimated inflate rate between 4.5-7.4% by the end of 2021. Although, these figures are attributed to the housing sector and, therefore, do not necessarily represent rates that can occur in the hydraulic engineering department. Coincidentally, both are heavily influenced by the steep increase in material costs, which can be attributed to the revival of the worlds economies. Needless to say, these high inflation rates impact whether positive benefits are retrievable from applying adaptive design strategies but are difficult to predict as fluctuations occur.

- **Environmental Cost Index integration**
  The Environmental Cost Index or ECI-values determines the impact of the construction of a structure on the environment by, as an example, monetisation. According to Jonker (2019, p. 16), "The so called shadow costs related to the environmental impact of the product van be included in the price (internalization - polluter pays), making the product sustainable (if this money is spent on reversing the impact of course". The same concept could be applied in adaptive designing strategies, as this bolsters the initial costs savings of adaptive designs, which initially are 'smaller' and thus require less material. As an example, the required volume of reinforced concrete of the foundation block for the static and Dynamic+1.0 could be compared: $V_{Static} = 8{,}680$ m^3 and $V_{Dynamic+1.0} = 7{,}960$ m^3. Translating this to an monetised ECI-value results in: €174,000,- and €159,000,- (without the inclusion of logistics), respectively, see Appendix J for the ECI-value calculations. The difference between these values could be added to the initial costs savings in Table H.1, increasing the amount that can compound over time, bolstering the value of adaptability of a structure, albeit the contribution is slim. Logically, in case an adaptation for the foundation is required, extra costs in the form of ECI-values should also be applied. However, according to Table J.3, the ECI-values for the wedge soil improvement are negligible. Additionally, in most growth scenarios the adaptation is not necessary and, thus, adds to the value of adaptive designing. Including costs saving in the form of monetised ECI-values bolsters the idea of adaptive designing methods.

- **Application exploratory modelling**
  The method and reliability model to derive a preferable design for the barrier with sea level rise uncertainty shares its idea with that of exploratory modelling. Exploratory modelling is generally applicable in policy making decisions and the idea behind it is that the systems in consideration are *"too complex and their context is of an uncertain nature, human reasoning alone is incapable of handling this. We need computer assisted reasoning"* (Kwakkel, 2021, p. 5). Although the reliability model shares the idea of that of exploratory modelling, it still is of a deterministic and iterative nature. The solutions retrieved from this approach might be the most optimal solution within its framework but it lacks the modelling to generate all possible variations.

Adaptation options

The adaptations for the components considered within the dynamic robust strategies might not be complete. Therefore, existing, but unknown adaptations to the author of this paper, might have been left out. In this paper one adaptation for two out of five components have been deemed suitable and beneficial. Identifying an increasing number of adaptations for the components can favour the total amount of suitable adaptations and thus the benefits gained from applying dynamic strategies. Additionally, it would be interesting to compare different barrier types and define their relative performance based on their individual adaptations.

Climate change IPCC report 2021

The Sixth Assessment Report (AR6) of IPCC published in august 2021 contains updated predictions concerning sea level rise. Sea level rise scenarios integrated in this paper are based on the Fifth Assessment Report (AR5) and might deviate from the newly published predictions. In Fig. 11.1 the two are set side-by-side. Worthwhile to note, is that the RCP scenarios are now combined with Shared Socioeconomic Pathways (SSP) and, as an example, SSP5-8.5 is similar to the RCP8.5 pathway anticipated in the AR5. If the predictions in global mean sea level rise of RCP8.5 (left) and SSP5-8.5 (right) are compared, a slight increase can be seen. As reported in IPCC (2021) the rate of sea level rise over the past decades is accelerating. The rate of sea level rise is an important factor in determining adequate adaptive measures, for both the adaptive pathways and the dynamic robust design. Since the rate influences the duration before certain measures need to be taken, e.g. dike heightening and gate heightening of the barrier. Constantly integrating updated predictions is essential, as moving forward in time decreases the ranges of uncertainty, providing more accurate predictions.

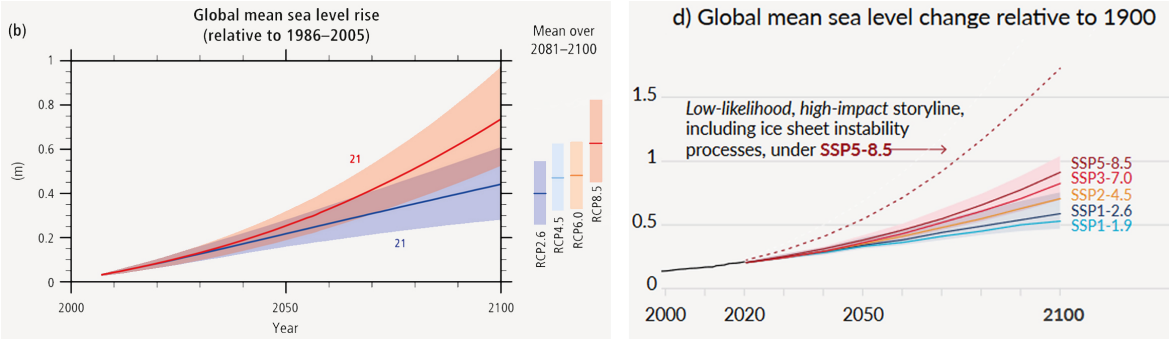

Figure 11.1: Left: Global mean sea level rise as anticipated in the Fifth Assessment report. Retrieved and modified from IPCC (2019). Right: Global mean sea level rise as anticipated in the Sixth Assessment report. Retrieved and modified from IPCC (2021, p. 30).

11.2. REFLECTION

This thesis is based on the idea of applying adaptive designing methods on flood defence systems to tackle the uncertainties decision makers and engineers face in the wake of climate change. In Haasnoot et al. (2012) the Dynamic Adaptive Policy Pathways approach is introduced to account for "deep uncertainties about the future arising from social, political, technological, economic and climate changes." (Haasnoot et al., 2012, p. 485) on a governmental policy level in the Rhine Delta system in The Netherlands. Moreover, in Huijsman (2021), the approach is applied to quantify the benefits of adapting existing lock infrastructure, to prolong the lifespan on a structural level as a function of sea level rise. Following these studies, the aforementioned approaches are combined and modified to form a system-to-structure approach applicable for an adaptive flood defence system in the Rhine-Meuse estuary to cope with sea level rise uncertainty. In this part a reflection on the applied approach in this thesis is provided. Let us initially consider the Adaptive Policy Pathways approach.

The adaptation pathways plan devised in Haasnoot et al. (2012) and this thesis are considered to be largely similar, however, some differences do exist. For instance, for the adaptation pathways plan in Haasnoot et al. (2012), the triggers of the various measures are determined by a set of two climate scenarios: 'Warm' and 'Crowd', as envisioned in Programmateam Rijnmond-Drechtsteden (2012). These scenarios are driven by climate change and define the X-axis of the plan and, thus, these scenarios dictate the activation in time of the measures. In this thesis, absolute values of sea level rise are used as triggering values on the X-axis, which dictate the activation of the measures. In both studies multiple preferred policy pathways are defined, providing different solutions for the system. However, in Haasnoot et al. (2012), no quantification, in terms of expenditures of the preferred pathways, is provided and as stated in the study itself: "The results suggest that it is worth-while to further use and test the approach for a real quantitative case study" Haasnoot et al. (2012, p. 496). This thesis provides such an application. Estimations of required investments for the pathways under a variety of sea level rise scenarios are computed and provide insights in how different sea level rise scenarios influence the overall needed investments of the preferred pathways. The designed adaptive pathways plan provides crucial quantified information for decision makers, connecting short- and long-term goals, considering the uncertainties of sea level rise while "keeping options open for the future" (Haasnoot et al., 2012).

Moreover, the difficulties of sea level rise uncertainty do not solely influence decision making on a system level, the issue also influences the design of a flood protection structure. Overengineering a structure results in an overinvestment, whilst designing for a 'low' sea level rise scenario could result in the failure of the structure if a more severe scenario develops. When considering the development of climate change, the further decision makers or engineers look into the future, the more uncertain the predictions of sea level rise become. This makes it difficult to predict to what boundary conditions the structure should adhere to, whilst balancing between structural safety and costs. Applying an adaptive designing method, partly based on the study of Huijsman (2021), could provide key insights in the performance of multiple (adaptive) designing strategies, whilst considering the structural failure probabilities and possible benefits.

In this thesis a so-called reliability model is developed to stress test different designs. The model computes the progression of the failure probabilities of the individual main components, in 10,000 sea level rise scenarios between 2100-2200, of a barrier. Four designs in total are inserted into the model, Static robust and Dynamic robust designs, and these should adhere to instated failure probability threshold norms, only then are they considered as robust. The static and dynamic robust definitions follow from Walker et al. (2013) and are defined as:

- "Static (conservative) robustness: a design that performs satisfactorily under a wide variety of future conditions."
- "Dynamic (adaptive) robustness: a design that leaves options open and can be adapted to changing future conditions such that the design continues to perform satisfactorily."

In the dynamic robust designs the main components are initially 'smaller' and require a lower investment compared to the static counterpart. The components are then, where possible, adapted when the loading conditions, influenced by sea level rise, exceed the resistance of the component. This adaptation requires an additional investment. The difference between the initially required investments for the dynamic designs and static designs are computed and denoted as 'costs savings'. These savings are funds that are able to compound over the course of time and, when an adaptation of a component is required, the additional investment is subtracted from the compounded 'cost savings', resulting in either positive or negative benefits. With the quantified output from the model, decision makers and/or engineers could make a substantiated decision to what boundary conditions a design, under the influence of sea level rise uncertainty, should adhere to.

Overall, the discussed adaptive designing methods provide a method to understand, and in some cases quantify, what adaptability can provide to cope with the uncertainties surrounding that of climate change and sea level rise. And, although, the applied methods are still far from perfect, it could provide insights in developing alternative designing methods that provide guidance to tackle the uncertainties in the wake of climate change. Thus, to develop the adaptive designing methods further, in accordance with Haasnoot et al. (2012), it is important to apply the approaches in other, quantitative, case studies and also other policy domains, which might lead to a verified approach for both policy makers and engineers to design for uncertainty.

12 | Conclusions and recommendations

12.1. Conclusions

In this section the conclusion of the main objective are summed.

"Develop an adaptive flood defence system in the Rhine-Meuse estuary under the influence of an uncertain sea level rise balancing between structural safety and costs"

To derive the main objective of this thesis a set of sub questions are introduced:

- *"Is the adaptive pathways approach a suitable method to derive flood protection systems with sea level rise uncertainty?*
- *"In what manner is the reliability model, computing failure probabilities and benefits for varying design strategies of a hydraulic structure, applicable and beneficial for the determination of dimensions of the structure with sea level rise uncertainty?"*

The following answers to the sub questions are found:

- The process required to derive an adaptive pathways plan with the approach of Haasnoot et al. (2012) provided key insights of possible solutions to provide flood protection for the region. However, as complexity would increase with the incorporation of more regional developments and the consideration of not only the Rijnmond-Drechtsteden region, the adaptive pathways approach might be difficult to design and interpret.
- The reliability model is able to provide analytical values of failure probabilities of varying design characteristics with integrated distributions of sea level rise over a time span. By doing so, the number of hand-calculations is decreased drastically, providing an indication of when certain design characteristics no longer suffice and incorporates economical benefits of certain design strategies over the time span. This makes the model very usable when applied to a problem that requires substantiated data to make designing decisions. However, it requires thorough understanding of the setup of the model and the problem at hand.

Conclusion of the main objective:

- The preferred adaptive flood defence system is determined by comparing the economical performance of multiple suitable adaptive pathways plans. Large (socio-)economical drivers like the Port of Rotterdam, shipping via the New Waterway, urbanisation of unembanked areas and costs for dike heightening projects are strongly correlated to the rate of sea level rise. Following the highest level of confidence within sea level rise scenario RCP8.5 (median), a system in which the open/closable nature, with the construction of a new barrier, of the Rhine-Meuse estuary is maintained. In this system the closing regime of the barrier is adapted in accordance with sea level rise to limit the amount of anticipated closures to three per year at maximum. To do so, the unembanked areas situated near the centre of Rotterdam have to be heightened or protected accordingly. Thus, the closing regime and unembanked areas are altered/heightened as follows:
  - Present - closing water level NAP +3.00 metres
  - +1 metre sea level rise - Increase to NAP +3.80 metres

  - +2 metres sea level rise - Increase to NAP +4.55 metres
  - +3 metres sea level rise - End of applicability defined system

  The applicability of an open/closable system is anticipated to no longer be suitable at +3 metres sea level rise, at this stage a lock it is advised to adapt to a closed estuary through the construction of a lock.

- The derivation of the preferable location is based on a multi-criteria analysis that incorporates five criteria. The hindrance of the shipping industry and dike heightening are the most influential criteria because of their relatively large contribution to the expenditures. Thus, these are attributed with the highest weights with which the scores are multiplied. This resulted in the preferable location near Maasdijk in the New Waterway south of the Maeslant storm surge barrier.
- A similar type as the current Maeslant storm surge barrier is derived as the preferable barrier type through the application of a multi-criteria analysis. This corresponds with the opinion of van Oorschot (2021). However, solely basing a preference based on a multi-criteria analysis is sub-optimal as construction costs could play a factor.
- Following the likelihood of yielding positive benefits from applying dynamic robust design strategies, two adaptations are considered as economically viable for this specific project: gate extension and wedge soil improvement. However, as sea level rise is of an uncertain nature, the exact benefits are difficult to predict and although these adaptations provide a high level of confidence to yield positive benefits, there is no guarantee they will do so. Following the analysis in Chapter 9 dynamic design strategies that require minor adaptations are preferable over substantial adaptations as the prospected benefits are less uncertain. The design of the barrier consists out of components that are designed as static robust (bed protection, steel trusses and ball-hinge) and components that are designed as dynamic robust (gate height and foundation block). Some basic dimensions of the main components of the barrier are stated below:
  - Trapezoid shaped foundation block: 50x55x4 m (LxBxH) - Adaptation: Wedge improvement with gravel
  - Bed protection:
    - Armour layer: d_{n50} = 1.44 m
    - Length: L_{Bed} = 58.5 m
  - Gate height: H_{Gate} = 23.5 m (ToS NAP +6.5 m) - Adaptation: Extension +1.0 metre
  - Steel truss/Ball-hinge: $F_{Rd,Compressive}$ = 141 MN

12.2. RECOMMENDATIONS

Recommendations are made concerning the three design loops and their method:

- The performance of the adaptive pathways in Chapter 5 are computed with the implementation of Delta21. With Delta21 the influence of the river discharge flowing into the Rhine-Meuse estuary is deducted. It is recommended to verify whether that with the implementation of Delta21 the influence of the river discharge can be completely discarded and review the results without the implementation of Delta21.
- In the adaptive pathways plan system with the implementation of hydraulic structures are considered. To broaden the spectrum of possible solutions for the system, it is recommended

to include, non-structural, plans like room for the river and the river as a tidal park in the development of the adaptive pathways.

- In Chapter 7 a suitable barrier type is solely derived with a multi-criteria analysis. To substantiate an optimal decision a cost-benefit analysis should be included.
- The structural failure probability threshold limit of 1:10,000 p/y is equally divided amongst the identified components. A more optimised design could be derived if a sensitivity analysis is conducted, which determines the relative contribution of the individual components to the structural failure probability. This will likely alter the required dimensions of certain components.
- Applying dynamic designs could safe necessary funding required for other important aspects concerning The Netherlands. However, one should bear in mind that positive benefits are never guaranteed. Thus, lawmakers should consider the consequences of high risk, high reward and low risk, low reward principles.
- Designing with the usage of a computational modelling reduces the amount of iterative calculations by a fair amount. Which allows for the simulation of multiple sea level rise scenarios and its influence on the structural components of the barrier. Applying such models provides quantifiable data for design decision making. It is recommended to continuously develop and improve such methods on a variety of projects as uncertainties are likely to develop increasingly in the future due to climate change.
- Within this thesis an analysis of possible improvements of the Maeslant storm surge barrier is not conducted and might provide essential insights for a similar design. It is, therefore, recommended to perform such an analysis or study to improve future designs.

References

Aerts, J. C. J. H. (2018). A review of cost estimates for flood adaptation. *Water*, 10(11).

Aktis Hydraulics (2018). Voorbeeld wbi voorbeeldboek: toepassen hb havens voor ijmuiden (dutch). Technical report, Rijkswaterstaat.

ANP (n.d.). Maeslantkering gaat waarschijnlijk na jaren weer dicht (dutch). https://www.omroepwest.nl/nieuws/3568124/Maeslantkering-gaat-waarschijnlijk-na-jaren-weer-dicht.

Baart, F., Rongen, G., Hijma, M., Kooi, H., de Winter, R., and Nicolai, R. (2018). Zeespiegelmonitor 2018: De stand van zaken rond de zeespiegelstijging langs de Nederlandse kust (Dutch). Technical report, Deltares.

Boiten, W. (1992). Vertical gates for distribution of irrigation water. In *International conference on protection and development of the Nile and other major rivers, Cairo, Egypt, February 3 - 5, 1992*, number 30 in Rapport / Landbouwuniversiteit, Vakgroep Waterhuishouding. Landbouwuniversiteit Wageningen. International conference on protection and development of the Nile and other major rivers.

Booister, N. and Hekman, A. (2021). Ruimte voor de toekomst. Technical report, Sweco.

Breugem and Holthuijsen (2006). Shallow water formulation. Technical report, Unknown.

Brugnach, M., Dewulf, A., Pahl-Wostl, C., and Taillieu, T. (2008). Toward a relational concept of uncertainty: About knowing too little, knowing too differently, and accepting not to know.

CBS (2019). Regionale economische groei (dutch). https://www.cbs.nl/nl-nl/maatwerk/2020/17/regionale-economische-groei-2019.

CBS (2021). Inflatie stijgt naar 2,7 procent in september (dutch).

CBS, PBL, RIVM and WUR (2018). Land- en tuinbouw: ruimtelijke spreiding, grondgebruik en aantal bedrijven, 1980-2018 (dutch). https://www.clo.nl/en/node/32691.

Cobouw (n.d.). Gww kosten.

CUR (2010). *CUR-publication 166: Damwandconstructies (Dutch)*. Civieltechnisch Centrum Uitvoering Research en regelgeving (CUR), Gouda, 5th edition.

De Rechtspraak (2015). Staat moet uitstoot broeikasgassen verder beperken (dutch). https://www.rechtspraak.nl/Organisatie-en-contact/Organisatie/Rechtbanken/Rechtbank-Den-Haag/Nieuws/Paginas/Staat-moet-uitstoot-broeikasgassen-verder-beperken.aspx.

de Wit, M., Buiteveld, H., van Deursen, W., Keller, F., and Bessembinder, J. (2015). Klimaatverandering en de afvoer van Rijn en Maas (Dutch). *Stromingen*, 14(1).

DeConto, R. M. and Pollard, D. (2016). Contribution of Antarctica to past and future sea-level rise. *Nature*, 531(7596):591–597.

Delta21 (2019). Delta21: Een actualisering van het plan (dutch). Technical report, Delta21.

Deltacommissie 2008 (2008). Working together with water: A living land builds for its future. Technical report, Deltacomissie.

Deltaprogramma (2015). Factsheet west nederland: Capaciteitstoemane kleinschalig wateraanvoer stap 1 (dutch). https://www.deltaprogramma.nl/documenten/publicaties/2015/09/15/factsheet-west-nederland-capaciteitstoename-kleinschalige-wateraanvoer-stap-1.

Deltares (2014). Adaptive delta management. https://www.deltares.nl/app/uploads/2014/11/Brochure-Adaptive-Delta-Management.pdf.

Deltares (2018). Mogelijke gevolgen van versnelde zeespiegelstijging voor het deltaprogramma (dutch). Technical report, Deltares.

DINOloket (n.d.). Data en informatie van de nederlandse ondergrond (dutch).

Dorrepaal, S. G. (2016). Closure of the new waterway. Master's thesis, Technical University Delft.

Ecorys and Deltares (2012). Effecten hoogwater- beschermingsstrategieën voor scheepvaart en havens Rijnmond- Drechtsteden (Dutch). Technical report, Deltares.

Eurocode Applied (n.d.). Table of design properties for steel tubes - circular hollow sections (chs).

European Central Bank (n.d.). Monetary policy.

European Commission (2019). Nature 2000. https://ec.europa.eu/environment/nature/natura2000/index_en.htm.

European Commission (n.d.). Eurocodes:building the future. Technical report, European Commission.

Gatto, M. (2014). Reclamation pays: Assessing the socio-economic effects of reclamation projects. IADC.

Gemeente Rotterdam (2019). Programma rivier als getijdenpark (dutch).

Grinsted, A., Moore, J. C., and Jevrejeva, S. (2010). Reconstructing sea level from paleo and projected temperatures 200 to 2100 AD. *Clim Dyn*, 34:461–472.

Grondverzet (n.d.). Kosten afgraven en afvoeren grond (dutch).

H20 (2016). Nieuwe mogelijkheden voor aanvoer zoet water naar west-nederland bij extreme droogte (dutch). *Tijdschrift voor watervoorziening en waterbeheer (Dutch)*, Unknown(17):6–8.

Haasnoot, M., Diermanse, F., Kwadijk, J., De Winter, R., and Winter, G. (2019). Strategieën voor adaptatie aan hoge en versnelde zeespiegelstijging. Een verkenning. (Dutch)]. Technical report, Deltares.

Haasnoot, M., Kwadijk, J., van Alphen, J., Bars, D. L., van den Hurk, B., Diermanse, F., van der Spek, A., Essink, G. O., Delsman, J., and Mens, M. (2020). Adaptation to uncertain sea-level rise; howuncertainty in Antarctic mass-loss impacts thecoastal adaptation strategy of the Netherlands.pdf. *Environmental research*, 15(3):16.

Haasnoot, M., Kwakkel, J. H., Walker, W. E., and ter Maat, J. (2012). Dynamic adaptive policy pathways: A method for crafting robust decisions for a deeply uncertain world. *Global Environmental Change*, 23(2):485–498.

Hanson, S., Nicholls, R., Ranger, N., Hallegatte, S., Corfee-Morlot, J., Herweijer, C., and Chateau, J. (2011). A global ranking of port cities with high exposure to climate extremes. *Climatic Change*, 104(1):89–111.

H&B grondstoffen (2021). Personal communication.

Hollandia Services (n.d.). Maeslantkering (dutch). `https://hollandia.biz/projecten/maeslantkering/`.

Huijsman, D. (2021). Adaptation of marine locks against sea level rise. Master's thesis, Technical University Delft.

HydroLogic BV (2018). Vervolgonderzoek kosten en effecten permanente oostelijke zoetwateraanvoer voor West-Nederland (Dutch). Technical report, HydroLogic BV.

IPCC (2014a). Climate change 2014: Synthesis report. Technical report, IPCC.

IPCC (2014b). Climate Change 2014 Synthesis Report Summary Chapter for Policymakers. Technical report, IPCC.

IPCC (2019). Programma rivier als getijdenpark (dutch).

IPCC (2021). Climate change 2021: The physical science basis - synthesis report summary for policymakers. Technical report, IPCC.

Jeuken, A., Hoogvliet, M., van Beek, E., and van Baaren, E. (2012a). Opties voor een klimaatbestendige zoetwatervoorziening in laag nederland, tussentijds integratierapport (dutch). *KvK thema Climate Proof Fresh Water Supply (CPFWS)*, page 99.

Jeuken, A., Van Beek, E., Van Duinen, R., Van der Veen, A., Bocalon, A., Delsman, J. R., Pauw, P. S., Oude Essink, G. H., Van der Zee, S. E., Stofberg, S. F., Zuurbier, K. G., Stuyfzand, P. J., Appelman, W., Creusen, R., Paalman, M. A., Katschnig, D., Rozema, J., Mens, M. J., Kwakkel, J. H., Thissen, W., Veraart, J. A., Tolk, L., and De Vries, A. (2012b). Balancing supply and demand of fresh water under increasing drought and salinisation in the Netherlands. Technical Report January, Kennis voor Klimaat.

Jonker, H. M. (2019). *Reader CIE4100: Materials and Ecological Engineerin*. Faculty of Civil Engineering and Geosciences, TU Delft.

Jonkman, S., Hillen, M., Nicholls, R., Kanning, W., and Ledden, M. (2013). Costs of adapting coastal defences to sea-level rise— new estimates and their implications. *Journal of Coastal Research*, 290:1212–1226.

Jonkman, S., Jorissen, R., Schweckendiek, T., and van den Bos, J. (2018). *Flood defences: Lecture notes CIE5314*. Department of Hydraulic Engineering, Faculty of Civil Engineering and Geosciences, Delft University of Technology.

Jonkman, S., Steenbergen, R., Morales-Nápoles, O., Vouwenvelder, A., and Vrijling, J. (2017). *Probabilistic Design: Risk and Reliability Analysis in Civil Engineering*. Faculty of Civil Engineering and Geosciences, TU Delft.

Jonkman, S. B. (2021). Personal communication.

Kind, J., de Bruijn, K., Diermanse, F., Wojciechowaska, K., Klijn, F., van der Meij, R., Nolte, A., and Kees (2019). Invloed Hoge Scenario's voor Zeespiegelstijging voor Rijn-Maas Delta (Dutch). Technical report, Deltares.

Klijn, F., Asselman, N., and Mosselman, E. (2018). Robust river systems : On assessing the sensitivity of embanked rivers to discharge uncertainties, exemplified for the Netherlands ' main rivers. *Flood Risk Management*, page 13.

Klijn, F., Hegnauer, M., and Weiland, F. S. (2015). Wat betekenen de nieuwe klimaatscenario's voor de rivierafvoeren van Rijn en Maas? (Dutch). Technical report, KNMI.

Klijn, F., van Velzen, E., ter Maat, J., and H, J. (2012). Zoetwatervoorziening in Nederland aangescherpte landelijke knelpuntenanalyse 21e eeuw. Technical report, Deltares.

KNMI (2019). Zeespiegelstijging nu en in de toekomst (dutch).

KNMI'14 (2015). klimaatscenario's voor Nederland. Technical report, KNMI.

Kwakkel, J. (2021). Supporting decision making under deep uncertainty. University lecture.

le Bars, D. (2019). Zeespiegelstijging nu en in de toekomst (dutch). *KNMI specials 03*.

Levinson, M. (2018). Standardization of mitre gates. Master's thesis, Technical University Delft.

M4H Rotterdam (2019). Ruimtelijke raamwerk merwe-vierhavens rotterdam: Toekomst in de maak (dutch). https://m4hrotterdam.nl/wp-content/uploads/2019/07/DLA-M4H-17028-Boekwerk-190627-LQ.pdf.

Ministerie van Infrastructuur en Waterstaat (2019). Deltaprogramma 2020. Doorwerken aan de delta: Nuchter, alert en voorbereid. Technical report, Ministry of Infrastructure and Water.

Ministry of Infrastructure and Environment (2016). Tweede Kamer der Staten-Generaal 2. Technical report, Tweede Kamer der Staten-Generaal.

Mitrovica, J. X., Tamisiea, M. E., Davis, J. L., and Milne, G. A. (2001). Recent mass balance of polar icesheets inferred from patterns ofglobal sea-level change. *Letters to nature*, 409:1026–1029.

Molenaar, W. (2019). Lecture 4: Steel structures in hydraulic engineering. University lecture.

Molenaar, W. and Voorendt, M. (2019). *Manual Hydraulic Engineering*. Faculty of Civil Engineering and Geosciences, TU Delft.

Molenaar, W. and Voorendt, M. (2020). *Hydraulic Structures: General lecture notes*. Faculty of Civil Engineering and Geosciences, TU Delft.

Mooyaart, L. F. and Jonkman, S. N. (2017). Overview and Design Considerations of Storm Surge Barriers. *Journal of Waterway, Port, Coastal, and Ocean Engineering*, 143(4).

Municipality of Rotterdam (2019). Rotterdam kiest voor goede en slimme groei (dutch). https://persberichtenrotterdam.nl/blog/persbericht/rotterdam-kiest-voor-goede-en-slimme-groei/.

Nationaal Georegister (2020). Atlas van de verstedelijking in nederland - groeikaarten (dutch). https://www.nationaalgeoregister.nl/geonetwork/srv/dut/catalog.search#/metadata/ff63434f-7b4a-4346-a4e2-2037adfbcf0c.

Nicholls, R. J., Marinova, N., Lowe, J. A., Brown, S., Vellinga, P., de Gusmão, D., Hinkel, J., and Tol, R. S. J. (2011). Sea-level rise and its possible impacts given a'beyond 4○C world' in the twenty-first century. *Phil. Trans. R. Soc. A*, 369:161–181.

NOS (2020). Grote kolencentrale rotterdam kan dicht tegen vergoeding (dutch). https://nos.nl/artikel/2353202-grote-kolencentrale-rotterdam-kan-dicht-tegen-vergoeding.html.

Odé, J. (2007). Eerste daadwerkelijke sluiting maeslantkering goed verlopen. (dutch). https://edepot.wur.nl/343045.

Peters, D. (2020). Hydraulic structures – seismic resistance / dynamic analysis. unpublished.

Port of Rotterdam (2012). Hydrometeobundel nr. 4 (dutch). Technical report, Port of Rotterdam.

Port of Rotterdam (2019). Feiten & Cijfers. Een schat aan informatie. Make it happen. (Dutch). Technical report, Port of Rotterdam.

Port of Rotterdam (n.d.). Merwe-vierhavens. https://www.portofrotterdam.com/en/our-port/our-themes/a-safe-port/water-safety/merwe-vierhavens.

Programmateam Rijnmond-Drechtsteden (2012). Deltaprogramma 2013: Probleemanalyse Rijnmond-Drechtsteden (Dutch). Technical report, Stuurgroep Rijnmond-Drechtsteden.

Programmateam Rijnmond-Drechtsteden (2014). Synthesedocument Rijnmond-Drechtsteden (Dutch). Technical report, Deltaprogramma Rijnmond-Drechtsteden.

Rats, J., van Rooij, M., and Heins-Wundelre, H. (2021). Prijsontwikkelingen en bouwkosten (dutch). Algemeen Bestuur 16 juni 2021.

Rijksoverheid (2020). Klimaatbeleid (dutch). https://www.rijksoverheid.nl/onderwerpen/klimaatverandering/klimaatbeleid.

Rijkswaterstaat (2013). Waterveiligheidrisico's in het buitendijkse gebied van Rijnmond- Drechtsteden (Dutch). Technical report, Rijkswaterstaat.

Rijkswaterstaat (2017). Richtlijnen ontwerp kunstwerken rok 1.4 (dutch). Technical report, Rijkswaterstaat.

Rijkswaterstaat (2020). Dijkringen. https://geo.rijkswaterstaat.nl/services/ogc/gdr/primaire_waterkering/ows?service=WFS&request=GetFeature&version=2.0.0&typeName=primaire_waterkering:dijkring_l&outputFormat=SHAPE-ZIP.

Rijkswaterstaat and Stowa (2017). Water veiligheid Begrippen begrijpen: Ontwikkeling beleid en uitleg begrippen (Dutch). Technical report, Rijkswaterstaat and Stowa.

Riteco, J. (2017). Maeslant barrier: Alternative solution for the upgrading of the maeslant barrier. Master's thesis, Technical University Delft.

Ritzema, H. P. and van Loon-Steensma, J. M. (2017). Coping with climate change in a densely populated delta: A paradigm shift in flood and water management in the netherlands. *Irrigation and drainage*, 67:56–65.

Saville, T. (1954). The effect of fetch width on wave generation.

Schiereck, G. and Verhagen, H. (2019). *Introduction to Bed, bank and shore protection*. Delft academic press/VSSD.

Staatscourant (2007). Nieuwe waterweg, hartelkanaal. maeslantkering,hartelkering. stremming scheepvaart (dutch). *Haven Rotterdam*.

Swart, S. (2015). Hartelkering - hartel storm surge barrier. https://siebeswart.photoshelter.com/image/I0000C.wjRTE54yk.

Sweco Nederland Bv (2021). Personal communication.

van der Meer, J., allsop, N., Bruce, T., de Rouck, J., Kortenhaus, A., Pullen, T., Schüttrumpf, H., Troch, P., and Zanuttigh, B. (2018). Eurotop: Manual on wave overtopping of sea defences and related structures. Technical report, EurOtop.

van Oorschot, J. (2016). Maeslantkering: Havenvereninging rotterdam (dutch). Presentation.

van Oorschot, J. (2021). Personal communication.

van Waveren, H., Kors, A., Labrujere, A., and Osmanoglu, D. (2015). Motie Geurts, Deltaprogeramma: onderzoek naar de effecten van sluizen in de Nieuwe Maas en Oude Maas op de waterveiligheid en de zoetwatervoorziening (Dutch). Technical report, Rijkswaterstaat.

Vardon, P. (2020). Ctb2310 soil mechanics - lecture 24: Lateral stresses. University lecture.

Vermeer, M. and Rahmstorf, S. (2009). Global sea level linked to global temperature. *Sustainability Science*, 106(51):21527–21532.

Verruijt, A. (2005). *Grondmechanica*. VSSD.

Voorendt, M. (2017). *Design principles of multifunctional flood defences*. PhD thesis, Delft University of Technology.

Vos, R. J., Jeuken, A., and Kind, J. (2014). Compilatie van de onderbouwing van de keuze Open of Gesloten Nieuwe Waterweg (Dutch). Technical report, DPRD.

Vrancken, J., Van Den Berg, J., and Dos Santos Soares, M. (2008). Human factors in system reliability: Lessons learnt from the Maeslant storm surge barrier in the Netherlands. *International Journal of Critical Infrastructures*, 4(4):418–429.

Vuuren, D. P. V., Edmonds, J., Kainuma, M., Riahi, K., Nakicenovic, N., Smith, S. J., and Rose, S. K. (2011). The representative concentration pathways : an overview. *Climate Change*, 109:5–31.

Walker, W. E., Haasnoot, M., and Kwakkel, J. H. (2013). Adapt or perish: A review of planning approaches for adaptation under deep uncertainty. *Sustainability*, 5(3):955–979.

Waterveiligheidsportaal (2020). Landelijk veiligheidsbeeld (dutch). https://waterveiligheidsportaal.nl/#/nss/nss/current.

Waterveiligheidsportaal (n.d.). Nationaal basisbestand primaire waterkeringen (dutch). https://waterveiligheidsportaal.nl/#/nss/nss/norm.

Welleman, H. (2020). Load carrying principles: Cables and arches. University lecture.

Young, I. and Verhagen, L. (1996). The growth of fetch-limited waves in water of finite depth. part 1: Total energy and peak frequency. Technical report, Coastal Engineering 29.

Zhong, H., van Overloop, P.-J., van Gelder, P., and Rijcken, T. (2012). Influence of a storm surge Barrier's operation on the flood frequency in the rhine delta area. *Water (Switzerland)*, 4(2):474–493.

A | Exploration of flood defence systems in the Rijnmond-Drechtsteden region

In this appendix chapter an inventory of stakeholders is provided (Appendix A.1) and followed by the functions and processes of the Maeslant storm surge barriers are elaborated (Appendix A.2 and Appendix A.3).

A.1. STAKEHOLDER ANALYSIS

The Rijnmond-Drechtsteden is a highly dynamic region with various (non-)governmental stakeholders each with their respective objectives, wishes and preferences. A brief inventory of stakeholder is made in this subsection. In addition, their respective influence and interests is mapped in a matrix.

Table A.1: Inventory of stakeholders

	Stakeholder	Interests
Governmental		
	Ministry of Infrastructure and Water Management	• Flood protection • Shipping and ports • Water quality • Sustainable energy
	Ministry of Economic Affairs and Climate	• Shipping and ports • Sustainable energy
	Province of South Holland	• Flood protection • Shipping and ports • Water quality
	Municipalities	• Flood protection • Shipping and ports • Water quality
	Regional water authorities	• Flood protection • Shipping and ports • Water quality
	Rijkswaterstaat	• Flood protection • Shipping and ports • Water quality
Companies		
	Harbour of Rotterdam	• Shipping and ports • Flood protection
	Agricultural	• Flood protection • Water quality
	Water purification	• Water quality
	Miscellaneous	• Flood protection
Other		
	NGOs	• Ecology

Table A.1 continued from previous page

Residents	• Flood protection
Recreational river users	• Recreation

A.2. FUNCTION ELABORATION OF THE MAESLANT BARRIER

Flood protection

The Maeslant and Hartel barrier protect the hinterland from high water of the North Sea. If a malfunction of these barriers occurs, the dikes in the hinterland become the primary defence. The primary dike lines behind these barriers are thus based on a combination of their own respective flood probability, elaborated in Section 3.3, and thus the dikes also incorporate the failure probability of these barriers. They are prompted to close when water levels are predicted to reach NAP +3.0 m and +2.9 m in Rotterdam and Dordrecht, respectively. This currently occurs every 10 to 12 years, this frequency is predicted to increase with sea level rise as mentioned in Section 1.2.

Navigation and accessibility

The New Waterway is a vital transportation route, connecting the North Sea with the port of Rotterdam and shipping from inland rivers. The open-closable function of the Maeslant and Hartel barrier preserve this function and allows vessels to navigate over the New Meuse River without the delay navigational locks have. When the barriers are prompted to close due to high water, no navigation to and from the North sea is possible via the New Waterway. The ports situated in Zone A, visible in the top figure of Fig. 3.2, are accessible during such a closure. In addition, the Hartel barrier provides a connection between the mainland near Spijkenisse and residents of Rozenburg and the Botlek. This national road (N218) connects with the highway (A15) near the Botlek port.

River discharge

The open-closable barriers provide the capacity for river discharge flowing from the New and Old Meuse River. If a closed hydraulic structure would have been constructed, measures would have been needed to drain of the excess water flowing from these rivers. However, if the barriers are closed, the region has no capabilities to drain excess water and water level start to rise in the region. Therefor, the Maeslant barrier is adopted with a Double-Function, during a storm surge and coincides low water the barrier is floated up to the current water level to drain excess water stored behind the barrier towards the sea. When, in turn, high tide occurs the barrier is moved to a fully closed position. Whether these water levels will reach critical levels is dependent on the duration of the closure or storm duration the amount of river discharge flowing into the region, see Section 2.2, and the water storage capacity of the region.

Tidal flow

The open nature of the barrier provides to ability to maintain the natural tide in the New Waterway.

Salt water intrusion

Due to the open-closable nature of the barriers, salt water from the North Sea is able to freely flow into the New Waterway, intruding into the freshwater. The manner of intrusion is a dynamic process between the water level of the sea and the amount of river discharge of the New Meuse River and Old Meuse River.

Ecology

The open nature of the barrier does not immediately affect the flora and fauna behind the barrier and is maintained.

Sediment and debris discharge

Due to to the open-closable nature of the barriers, sediment and other debris is able to freely dis-

charge towards the sea. The Hartel barrier, however, has a foundation pier situated in the stream, thus debris and sediment could accumulate behind this pier.

Tourism
Besides the logistical usage of the New Waterway, the canal is also utilised by cruise ships named the America-Holland line, forming a touristic bridge between the mainland of Europe and North-America.

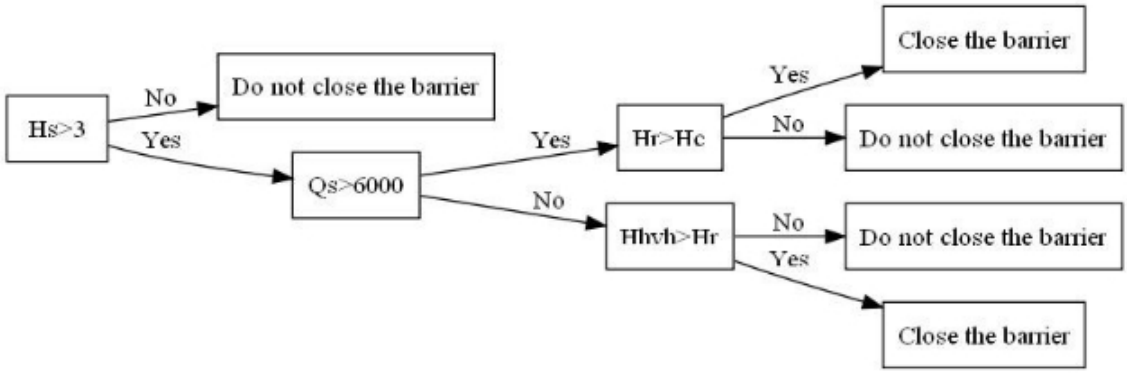

Figure A.1: Flow chart of the operation control of the Maeslant barrier. Hs represents the predicted highest level at Rotterdam, Qs the critical Rhine flow, Hr is the water level at Rotterdam, Hc is the sea level at which the barrier is actually closed and Hhvh is the water level at Hoek van Holland. Retrieved from Zhong et al. (2012, p. 12).

A.3. PROCESS AND FUNCTION ANALYSIS

To create insight in the desired use and behaviour of the future system and structure, the processes and functions of the barrier within the preferred pathway, Chapter 5, are analysed.

A.3.1. PROCESS ANALYSIS

A process is the sequence of various activities. According to Molenaar and Voorendt (2020, p. 53) three types of processes can be distinguished:

1. "Use processes: the activities of the individual users (for instance, vessels sailing in and out of a lock and the work of a maintenance team);"
2. "System processes: the activities of the exploiting system (including management and maintenance);"
3. "Natural processes: the activities of the natural environment (like rainfall, oxidation, scour of sandy river beds)."

The following use processes are identified:

- Vessels passing the barrier via The New Waterway
- Maintenance on the barrier and its components
- Operational team operating the barrier in case of anticipated required closure and opening

Subsequently the systems process are identified:

- Maintenance on The New Waterway, e.g. due to soil sedimentation and quay wall deterioration
- Expansion or decrease in port activities

- Sea level rise, Section 2.1
- Raising of unembanked areas, Section 4.2.4
- Altering of the closing regime, Section 4.2.2
- Dike heightening and strengthening
- Implementation Delta21 affecting the river discharge, Section 4.4.1
- Accumulation of water behind the barrier in case of closure
- Possible strengthening of the barrier, depended on the design strategy, i.e. dynamic robust design

Lastly, the natural processes:

- Sea level rise
- Hydrostatic loads
- Seiches
- Tidal currents
- Waves
- Winds
- Scour

A.3.2. FUNCTIONAL ANALYSIS

Subsequently the desired functions of the new barrier are identified. Worthwhile to notice, most of the functions of the current Maeslant barrier are maintained, however, the double function, as in river discharge, is deducted and the option to adapt the structure, with the goal of a dynamic robust design, is added.

Principal functions

- Flood protection

Preserving functions to maintain present systems

- Enable shipping between stretches of water, e.g. the North Sea, New Waterway and New Meuse River
- Tidal flow
- Reduce salt water intrusion in the fresh water stretch
- Preserving ecology
- Sediment and debris discharge
- Tourism

Additional functions

- Availability to adapt and strengthen the barrier in case of sea level rise if desired
- Generation of electricity, although the structure it self is not able to produce energy, plans like Delta 21, see Section 4.4.1, propose that the river discharge could be utilised for an aqua battery able to produce energy and contribute to the sustainable energy goals laid down by the government.
- Cultural values

A.3.3. FUNCTIONS OF DIKES IN GENERAL

Description of principal, preserving and additional functions of dikes:

Principal functions

- Retaining water

Preserving functions to maintain present systems

- Landscape values
- Cultural values
- Nature values

Additional functions

- Perseverance of land
- Transportation along the crest and/or inland side
- Providing living and working aspects
- Providing agricultural value, e.g. grazing for cattle

A.4. DIKES

In this section some basic information about the failure mechanisms that predominately influence a required heightening of the dikes (Appendix A.4.1) and general information (Appendix A.4.2) about the dike-ring stretches are provided.

A.4.1. FAILURE MECHANISMS OF DIKES

Overflow

Overflow is the mechanisms in which the water, in this case flowing from the North Sea, the New Meuse River and/or Old Meuse River, is able to flow over the crest level without the consideration of waves, i.e. the still water level is higher than the crest level of the dike. If overflow occurs, water is able to flow into the protected area and over the inner slope of the dike. This could lead to flooding of the area and, in process, damage the inner slope which leads to erosion of the dike and in the worst cases to a breach or infiltration. (Jonkman et al., 2018)

Wave overtopping

Overtopping is the process in which waves are able to run up the outer slope of the dike and exceed over the crest level. Critical discharge are usually used to establish the limit state of the dike for the wave overtopping mechanism. The height of the wave run-up is influenced by the roughness of the outer slope, the angle of the attacking waves, the dike design, wave height, breaker type and other factors. (Schiereck and Verhagen, 2019) This failure mechanisms is typically is attributed to sea dikes. (Jonkman et al., 2018)

A.4.2. DIKE-RING STRETCHES

General information about the relative dike-ring stretches in the considered region are readable in Appendix A.4.2.

Table A.2: Informative table for the various dike-ring stretches in the Rijnmond-Drechtsteden area. Based on data supplied by Waterveiligheidsportaal (2020), averaged crest heights measured in GIS based on AHN3 data.

Dike-ring stretch	Current norm	HWBP norm	Status	Average crest height (NAP)	Dominated by
14-1	1:10,000	1:10,000	No data	+5.3 m	River
14-2	1:10,000	1:100,000	Inadequate (D)	+5.3 m	Transition
14-3	1:10,000	1:10,000	No data	+5.6 m	Sea
14-4	1:10,000	1:10,000	No data	+7.8 m	Sea
14-5	1:10,000	1:30,000	Adequate (A)	+12.9 m	Sea
15-2	1:2,000	1:10,000	No data	+5.3 m	River
15-3	1:2,000	1:10,000	Inadequate (D)	+5.3 m	River
17-1	1:4,000	1:3,000	No data	+5.4 m	Sea
17-2	1:4,000	1:3,000	No data	+5.9 m	River
17-3	1:4,000	1:100,000	Inadequate (D)	+5.0 m	River
18-1	1:10,000	1:10,000	Adequate (A)	+5.5 m	Sea
19-1	1:10,000	1:100,000	Inadequate (C)	+6.9 m	Sea
20-1	1:4,000	1:30,000	Adequate (A)	+11.0 m	Sea
20-2	1:4,000	1:10,000	Inadequate (C)	+6.2 m	Sea
20-3	1:4,000	1:30,000	Inadequate (D)	+4.4 m	River
20-4	1:4,000	1:1,000	Inadequate (C)	+5.5 m	River
21-1	1:2,000	1:3,000	No data	+4.6 m	River
21-2	1:2,000	1:300	No data	+4.6 m	River
208	1:10,000	1:100,000	No data	+7.0 m	Sea
209	1:10,000	1:100,000	No data	+7.0 m	Sea

B | Identification of measures for the adaptive pathways

In this appendix chapter the development of the adaptive pathways plan in Chapter 5 outlined.

B.1. Outlined Strategies

In the list below the four strategies mentioned in Section 4.1 are elaborated, information regarding the characteristics is retrieved and translated from Haasnoot et al. (2019, p. 7).

Closed Protection

- Regarding sea level rise:
  - Up to a few metres
  - Rate of rise can interfere with sand replenishment
  - Salt intrusion can not be completely be prevented
- Technical feasibility:
  - Availability of sand for replenishment is unknown
  - Pump capacity and temporarily storage of river discharge needed
- Social feasibility:
  - Closure of Rijnmond-Drechtsteden will lead to resistance of the plan
  - Incremental costs and required free area for dike heightening and strengthening
  - Large consequences for nature
- Adaptability:
  - Upcoming 20 years: free area required for dikes or room for the river
  - Continuation of current strategy leads to this strategy

Open Protection

- Regarding sea level rise:
  - Limited, approximately 1 metre for current barrier, with altering the closing regime between 1 and 2 metres
  - Rate of rise can interfere with sand replenishment
  - Salt intrusion leads to adaptation of land use in coastal and lower river area
- Technical feasibility:
  - Availability of sand for replenishment is unknown
- Social feasibility:
  - Incremental increase of costs for dike heightening and strengthening
- Adaptability:
  - Upcoming 20 years: large amount of free area required for dikes or room for the river
  - Current strategy; eventually leads to Closed Protection

Seawards Expansion

- Regarding sea level rise:
  - Limited, approximately 1 metre with open variant islands
  - Up to a few metres with closed variant
  - Demand for sand replenishment could prove to be too high regarding the rate of sea level rise
- Technical feasibility:
  - Large amount of sand required
  - Large volume of pumping capacity and temporarily storage for river discharge needed
- Social feasibility:
  - Mega investment
  - Large consequences for nature
- Adaptability:
  - Upcoming 20 years: experimentation with islands
  - Hard to adapt
  - Need for socio-economical or international developments needed to trigger this strategy, e.g. Port of Rotterdam Maasvlakte 3 or Schiphol expands in sea

Managed Retreat

- Regarding sea level rise:
  - Limited in case of building on poles or mounds
  - Few cm per year in combination with ground level increase
  - Extensive with floating constructions or abandonment of flood prone areas
- Technical feasibility:
  - Artificially heightening of residential areas required, urge for innovation
  - Natural ground level increase only possible with sufficient sediment transport
- Social feasibility:
  - Local or with future constructions
  - Poles and mounds only allowable with temporarily floodings
  - Planned retreat will likely result in resistance from the inhabitants
- Adaptability:
  - Upcoming 20 years: need to be included in considerations for new construction projects
  - Limited adaptability with ground level increase and buildings
  - Could result in migration
  - Low consciousness of potential flood risk could result in a hard to stimulate population

B.2. SUMMARY OF QUANTIFIABLE MEASURES

To summarise, the following components are integrated in the adaptive pathways in Section 5.3 and Appendix C as follows:

- Location B, as in Fig. 6.1, is taken as reference
- MLK+: 100 year lifespan
- Replacement for the Hartel barrier neglected from expenditures indication
- Sea lock: 100 year lifespan
- Crest heightening sea dikes:
  - +1.0 m SLR, 2 m crest heightening
  - +2.0 m SLR, 4 m crest heightening
  - +3.0 m SLR, 6 m crest heightening
  - +4.0 m SLR, 8 m crest heightening
- Crest heightening dikes behind protection of MLK+ due to altering the closing regime:
  - Closing regime NAP +3.80 m, 1 metre of heightening
  - Closing regime NAP +4.55 m, additional metre of heightening
- Sea level rise RCP8.5 scenario, see Fig. 2.3:
  - RCP8.5 upper boundary: +1.1 m by 2100 and +5.4 by 2300
  - RCP8.5 median: +1.0 m by 2100 and +3.6 by 2300
  - RCP8.5 lower boundary: +0.6 m by 2100 and +2.3 by 2300
- Scenario Urbanisation: Urbanisation of unembanked areas Section 3.4
- Scenario Intensification Shipping: Intensification of shipping over the New Water Way Section 3.5.3
- Activation of the Maasvlakte III measure reduces hindrance to shipping as determined in Appendix C.5

C | Adaptive pathways analysis

In this chapter the four main adaptive pathways are presented, Appendix C.1. This is followed by the relative costs of these pathways under multiple sea level rise scenarios within RCP8.5 (Appendix C.2). In Appendix C.3 the derivation of these costs are elaborated in detail. Furthermore, a brief analysis of the influence of varying locations on the costs is supplied in Appendix C.4 and influence of creating a third Maasvlakte in Appendix C.5

C.1. Main adaptive pathways

In the following subsections, a series of strategies within the overall plan are highlighted and elaborated, providing a better distinction with different measures that can be undertaken and quantifying these strategies in economic values over the long-term. In these subsections, measures are either active, visualised by the lines being bright and starting with a circle with a black outline, or inactive when the colours are opaque or vague and starting with a circle with a grey outline. These strategies all adhere to the definition of success in their own way as defined in Section 4.5.

C.1.1. Pathway A with MLK+ and land reclamation

Pathway A, Fig. C.1, represents the continuation of the current policy with a new hydraulic structure, MLK+, in combination with altering the closing regime, as envisioned in Section 4.2.2, to limit the number of closures per year. With +1.0 metre SLR this measure is combined with the first step of land reclamation, as envisioned in Section 4.2.4, elevating approximately 17.2 km^2 of surface area to NAP +3.80 m. This process is repeated at +2.0 m SLR for approximately 22.9 km^2 that lies below the new closing regime of NAP +4.55 m. To tackle the problem of salt intrusion, measures like KWA+ becomes fundamental and is probable that the amount of fresh water diverted towards the estuary increases along the x-axis. At +2.0 m SLR this measure is combined with additional fresh water supply via the ARK and Lek. At +3.0 m SLR the possibilities in terms of keeping the estuary 'open' narrows down towards the adoption of a sea lock, closing off the last open estuary of The Netherlands. This measure results in a loss of ecology and should be compensated for, and thus the nature compensation becomes active. Measures to reduce salt intrusion are deactivated at this point.

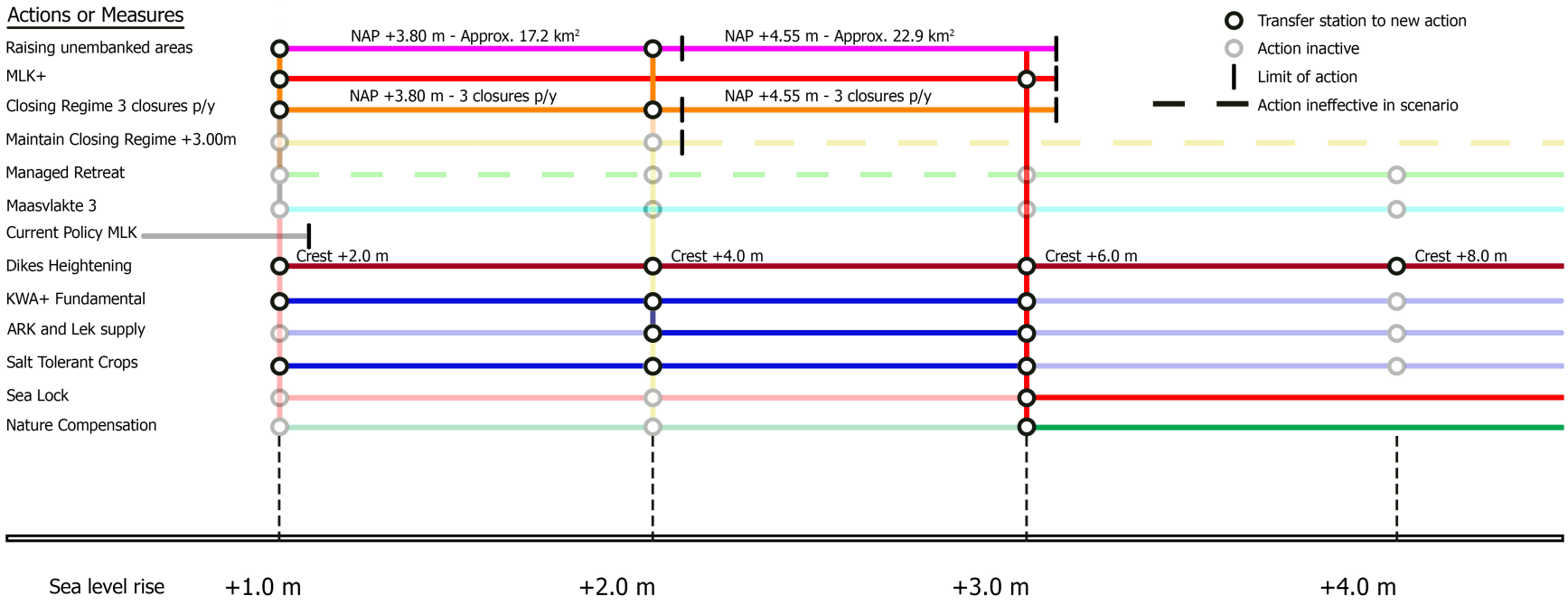

Figure C.1: Pathway A. Continuation of the open strategy in combination with changing the closing regime and elevating areas.

C.1.2. PATHWAY B WITH MLK+ AND MANAGED RETREAT

Pathway B, Fig. C.2, is quite similar to pathway A, Section 5.2.1, however, one major difference is the activation of the managed retreat measure in combination with the changing closing regimes. Outside dike areas, as envisioned in Section 4.4.3, are abandoned in two steps, similar as the land reclamation measure in Section 5.2.1. It has to be noted that such a drastic measure can only be introduced under the right circumstances, as it could result in resistance from the general population and hinder (socio-)economic development in the region and should be incorporated with long-term planning. (Haasnoot et al., 2019) Therefore, Managed Retreat is ineffective in case Scenario A, Section 3.4, develops.

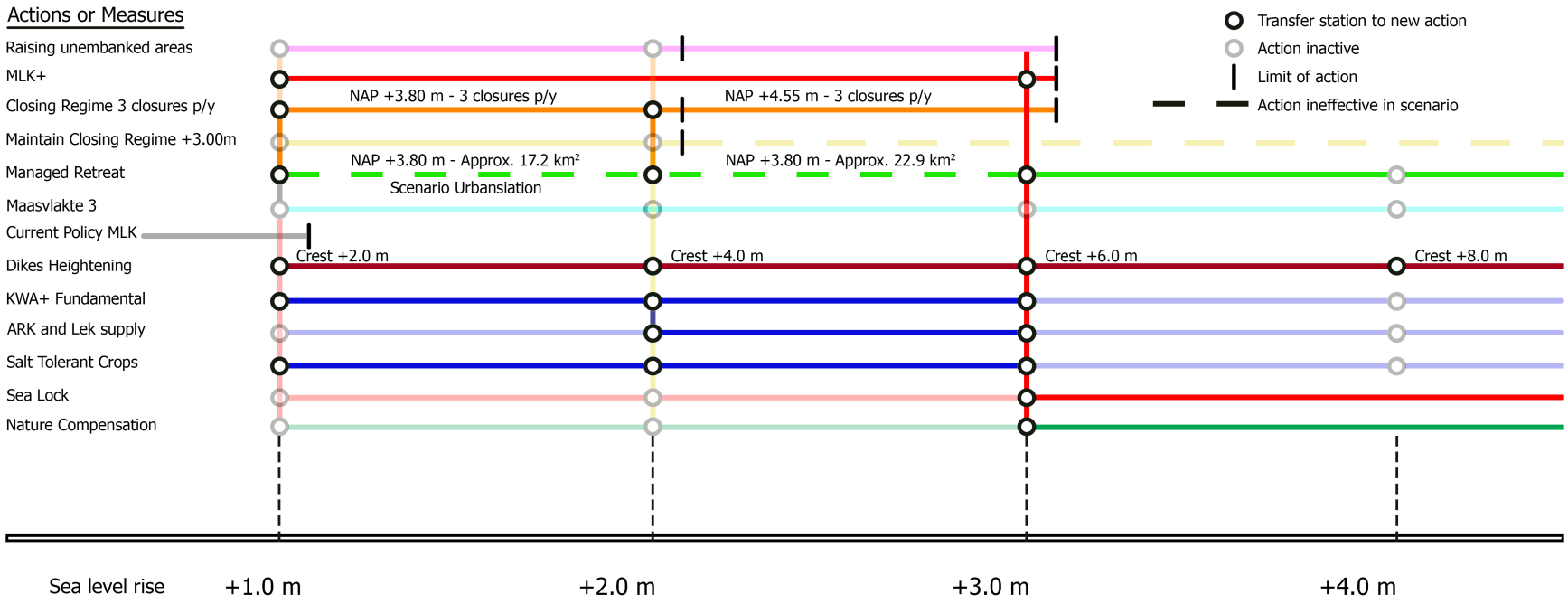

Figure C.2: Pathway B. Continuation of the open strategy in combination with changing the closing regime and managed retreat.

C.1.3. PATHWAY C WITH SEA LOCK

Partway C, Fig. C.3, is fairly straightforward, with the abolishment of the current policy a sea lock is implemented that could be designed over the full range of anticipated sea level rise. The implementation of the lock is simultaneous with the necessary nature compensation as stated in Section 4.3.2 and Section 5.2.1. Furthermore, the option is present to construct the third Maasvlakte, Section 4.4.4, to reduce the amount of hindrance the Port of Rotterdam and shipping in general will face.

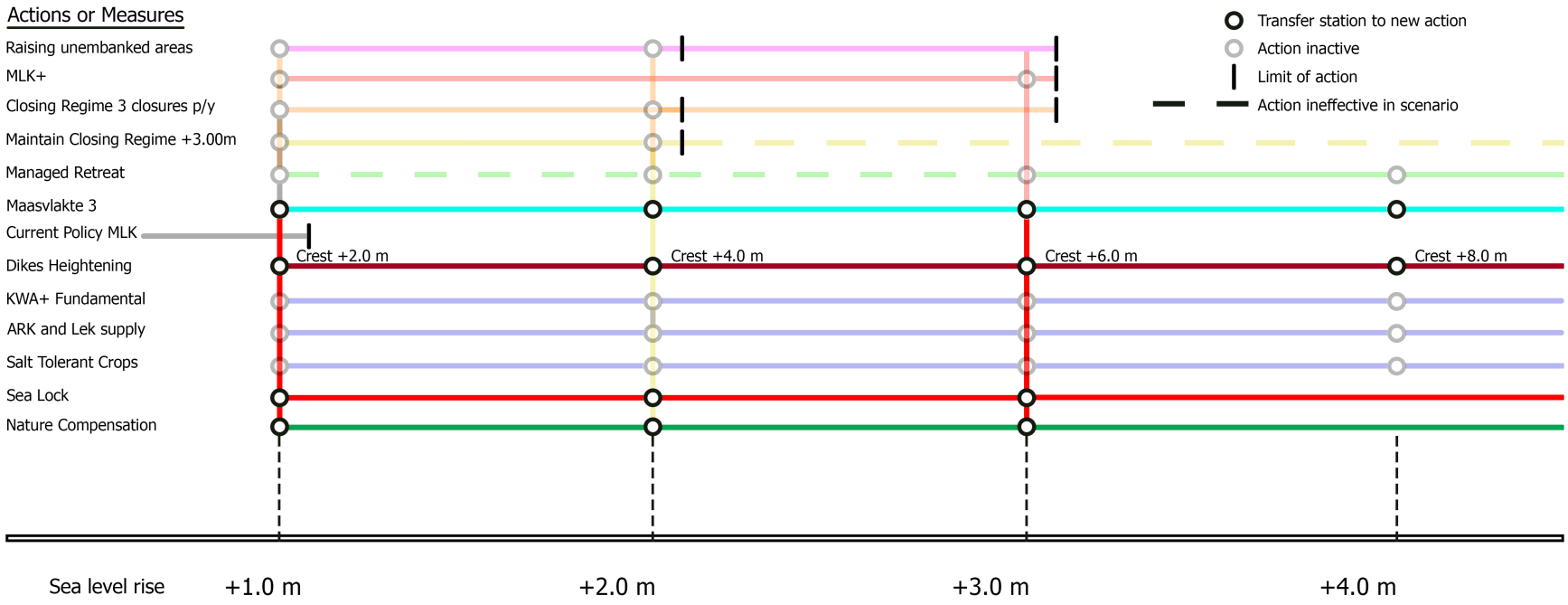

Figure C.3: Pathway C. In which the estuary is closed with the implementation of a sea lock.

C.1.4. PATHWAY D WITH ALTERNATIVE MLK+ BARRIER

Pathway D, Fig. C.4, represents the continuation of the current policy with a new hydraulic structure, MLK+, in combination with maintaining the current closing regime at NAP +3.0 m in which the number of closures throughout the year increase with SLR. The MLK+ in this pathway has to be designed in such a way that numerous of closures is not a significant problem for the structure. At +2.0 m SLR it is estimated that the barrier is forced to close roughly 130 times per year, which makes the inner part of the Port of Rotterdam unreliable and likely results in economic damages for shipping. At this point an additional path develops, one in which the MLK+, as introduced in this pathway, operates adequately and is a continuation of the measure along the x-axis as the yellow stripped line, Fig. C.4, and one in which Scenario B occurs, Section 3.5.3, where the measure is no longer effective. The latter results in the implementation of the sea lock.

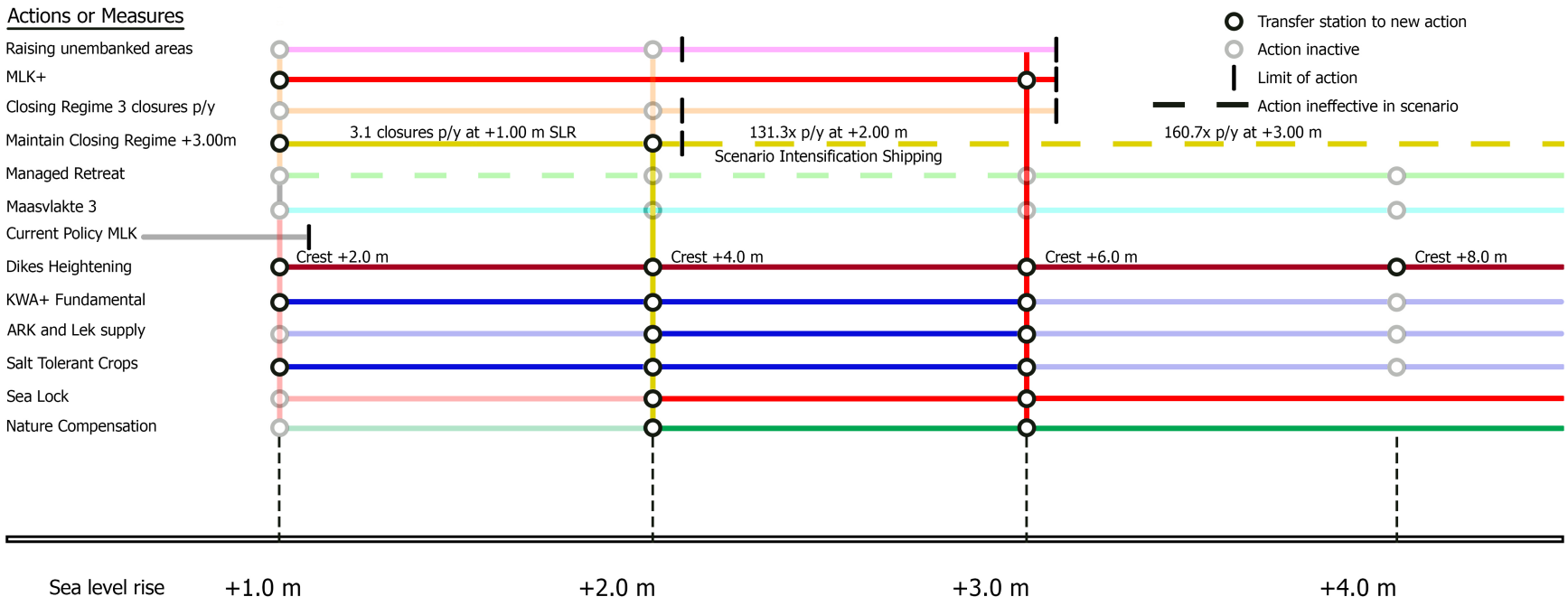

Figure C.4: Pathway D. Continuation of the open strategy with the current closing regime.

C.1.5. Pathway D2 with alternative MLK+ barrier

Pathway D2, Fig. C.5, is quite similar to Pathway D in Appendix C.1.4. However, the option of the third Maasvlakte is introduced, reducing the economical damages that the Port of Rotterdam and shipping in the area should endure.

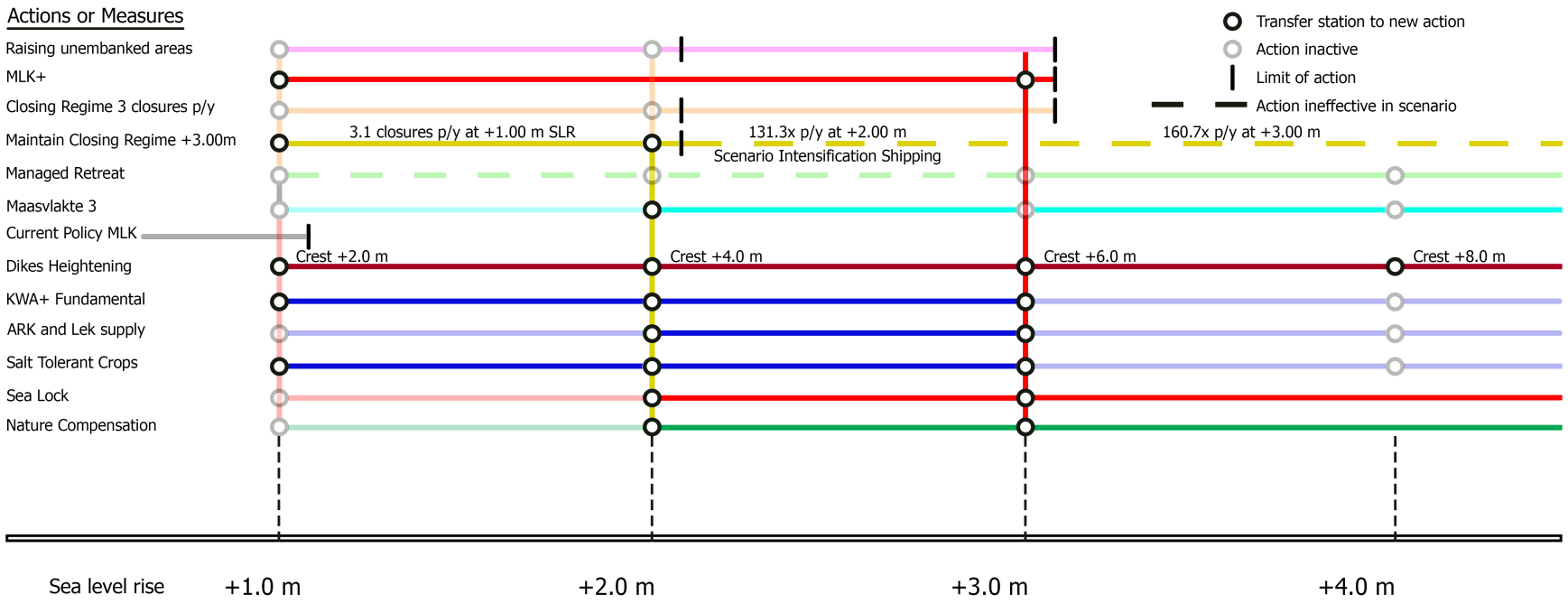

Figure C.5: Pathway D2. Continuation of the open strategy with the current closing regime and the third Maasvlakte.

C.2. PERFORMANCE MAIN PATHWAYS IN RCP8.5

For each of the four main pathways, A, B, C/C2 and D/D2, the cumulative expenditures of the pathways considering three sea level rise scenarios, upper, median and lower boundary values of RCP8.5 from Fig. 2.3, are plotted. This represents the overall performance of the main pathways under varying conditions of sea levels rise. C and D, visible in Fig. C.9 and Fig. C.11, without a third Maasvlakte, are neglected when considered in the three RCP8.5 scenarios, due to the fact that these pathways greatly exceed any other pathway, expenditure wise, by a factor between approximately 1.5 and 2.0. This is due to the fact that the hindrance for shipping in both C and D contributes over half of the total expenditures, when considering the estimated economic consequences of a closure and waiting time for the sea lock from Section 4.2.1 and Section 4.3.1, respectively. However, these pathways do perform quite well with very little sea level rise, +2.3 metre by 2300, due to the fact that these pathways are in fact a continuation of the current preference strategy. If continuing research proves that these costs are exaggerated, these two pathways might prove they are viable options as well. Continuing with the costs determined in Chapter 4 Pathway C and D are considered as unviable under the three RCP8.5 scenarios.

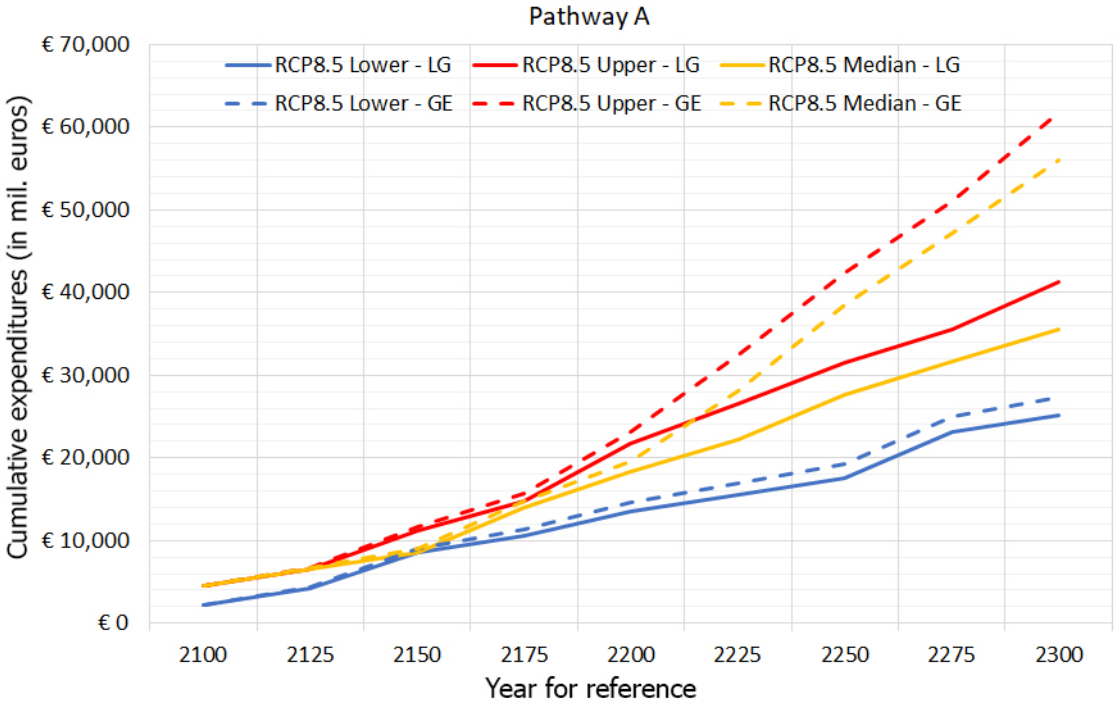

Figure C.6: Cumulative cost graph for all three RCP8.5 scenarios for Pathway A.

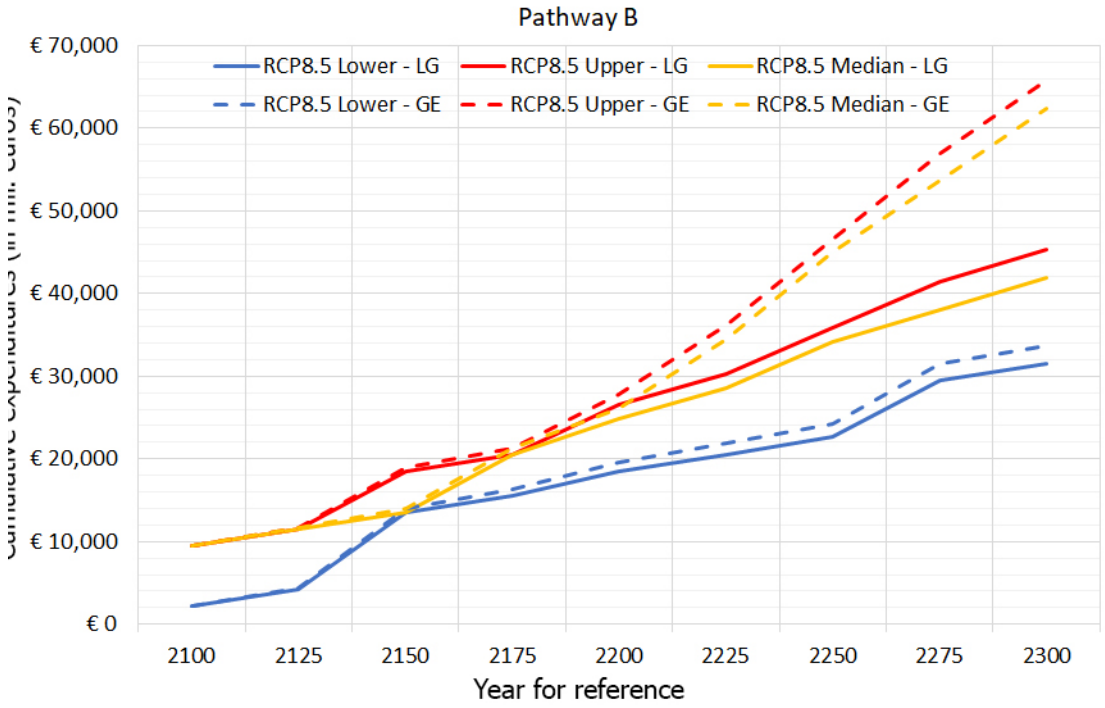

Figure C.7: Cumulative cost graph for all three RCP8.5 scenarios for Pathway B.

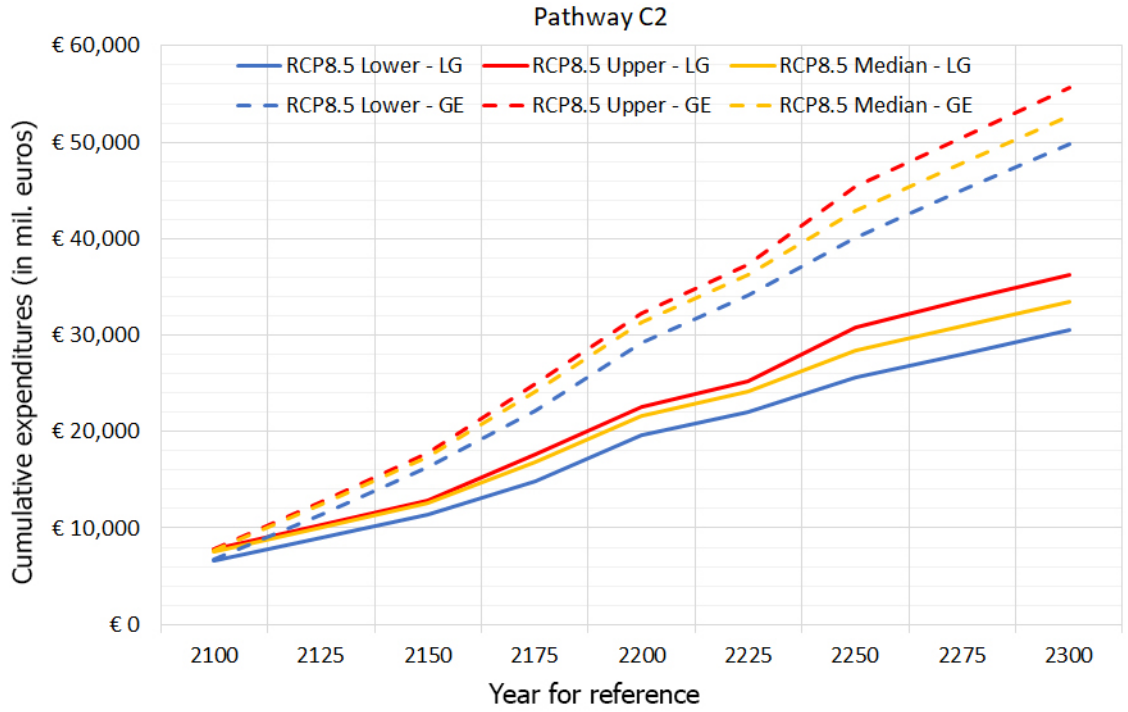

Figure C.8: Cumulative cost graph for all three RCP8.5 scenarios for Pathway C2.

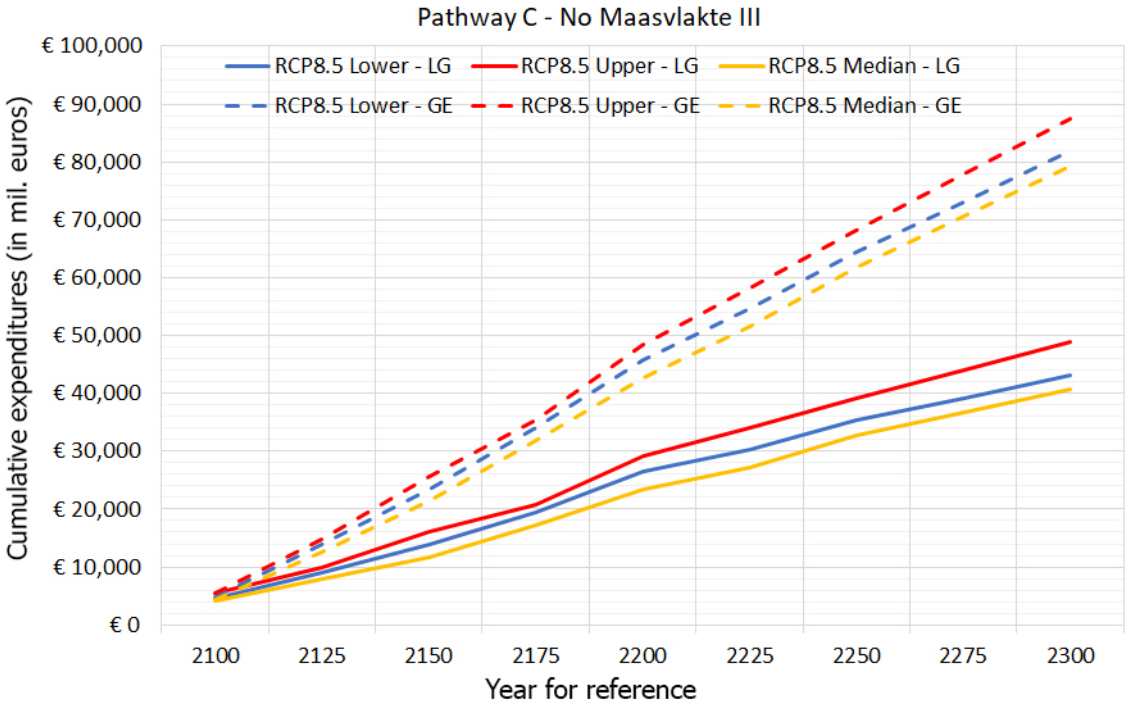

Figure C.9: Cumulative cost graph for all three RCP8.5 scenarios for Pathway C.

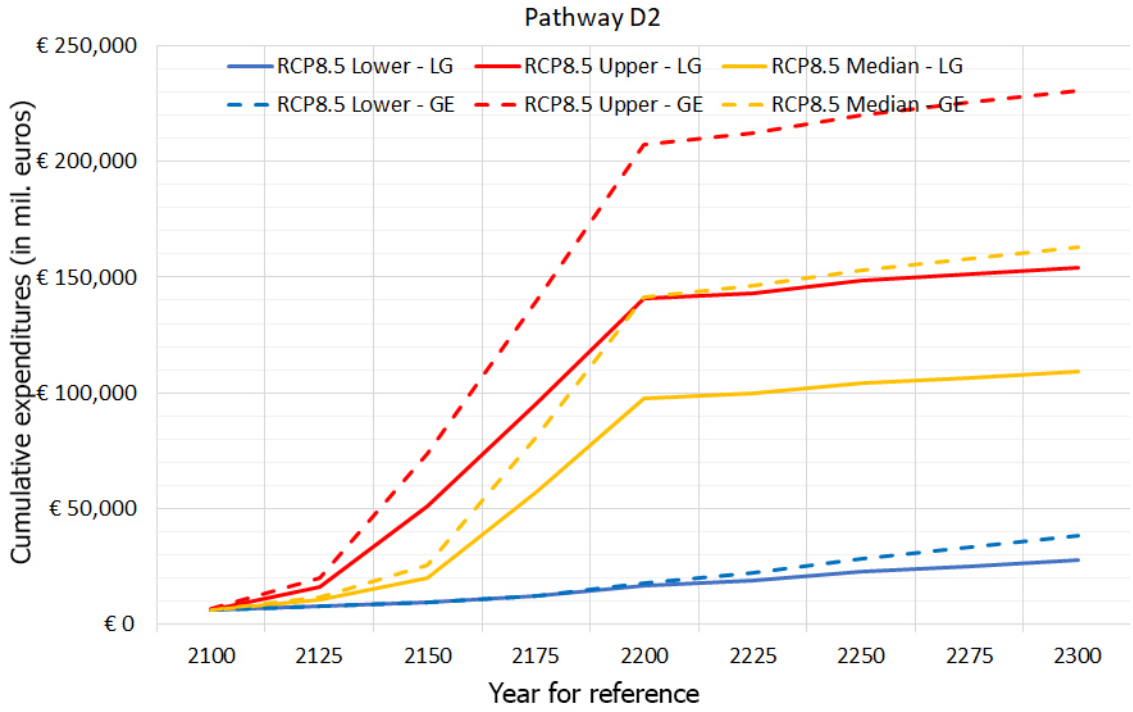

Figure C.10: Cumulative cost graph for all three RCP8.5 scenarios for Pathway D2.

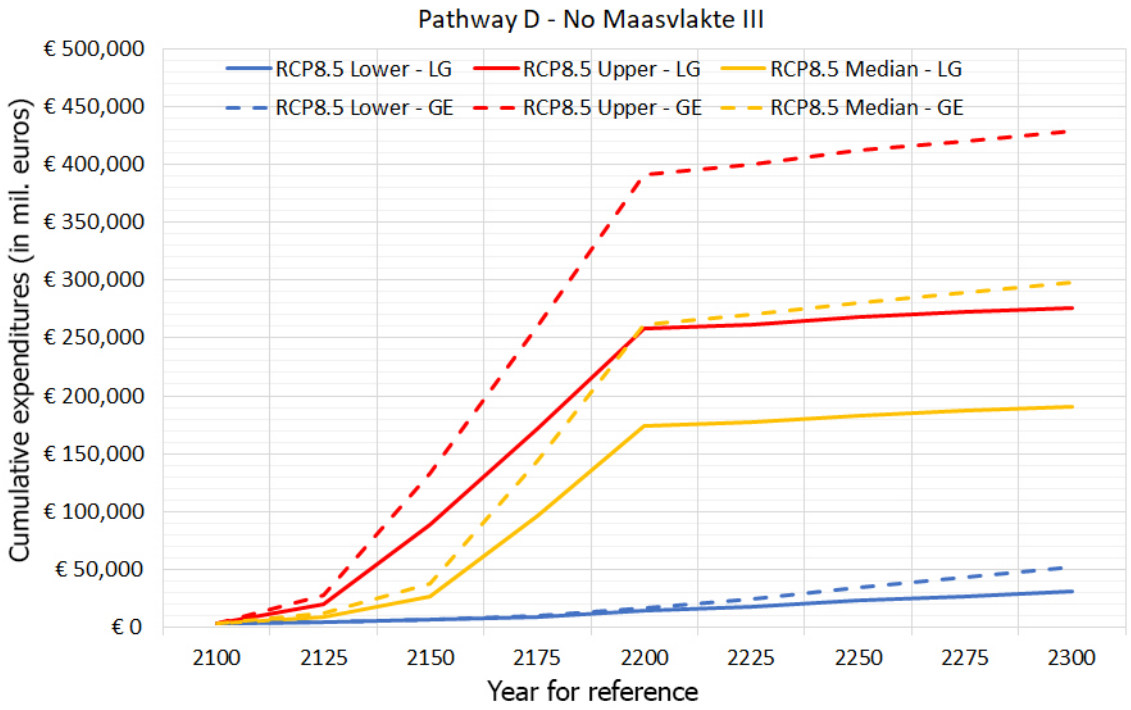

Figure C.11: Cumulative cost graph for all three RCP8.5 scenarios for Pathway D.

C.3. COMPUTATION OF COSTS OF THE ADAPTIVE PATHWAYS

In the following subsection a complete overview of the cost computation of each individual adaptive pathway under varying sea level rise scenarios is elaborated.

C.3.1. PATHWAY A

Expenditures:

- MLK+ construction costs: M€1,010 in 2020 price level, from Section 4.2.1 in 2009 price level
- MLK+ maintenance and management costs: approximately 3%, Section 4.2.1 per year equals to M€30 in 2020 price level
- Raising unembanked areas NAP +3.80 m: approximately 14.2 and 3.1 km^2 in Rotterdam and Dordrecht, respectively, by 1 metre equals to M€424.2 in 2020 price level
- Raising unembanked areas NAP +4.55 m: approximately 19.1 and 3.8 km^2 in Rotterdam and Dordrecht, respectively, by additional metre equals to M€529 in 2020 price level
- KWA+ construction costs: combined costs of KWA+ incidental and increase to KWA++, M€48.7 and 54.7 in 2020 price levels, from Section 4.4.6 in 2015 price level
- KWA+ fundamental exploitation costs: equals to 2.2 M€p/y in 2020 price level, as determined in Section 4.4.6
- Sea lock construction costs: M€2,250 as determined in Section 4.3.1
- Sea lock maintenance and management costs: approximately M€11.3 per year, as determined in Section 4.3.1
- Sea lock salinisation damage reduction: added benefit of -M€10 p/y, as determined in Section 4.3.1

Computation of dikes heightening costs, location B as reference:

- 28.1 (Rural) km and 16.65 (Urban) km of dikes in direct contact with the sea, see Table C.14, raising these dikes by 2 metres per 1 metre sea level rise, as determined in Section 4.4.5
- Multiplying amount of km of rural dikes with M€13.0 in 2020 price levels, average of Table 4.3 for the construction costs
- Multiplying amount of km of urban dikes with M€29.2 in 2020 price levels, average of Table 4.3 for the construction costs
- 3.8 (Rural) km and 51.32 (Urban) km of dikes in need for heightening by 1 metre, see Table C.14, regarding Closing regime, see Section 4.2.2, and Raising unembanked areas, see Section 4.2.4, measures
- Multiplying amount of km of rural dikes with M€6.9 in 2020 price levels, lower boundary value of Table 4.3 for the construction costs
- Multiplying amount of km of urban dikes with M€23.9 in 2020 price levels, lower boundary value Table 4.3 for the construction costs

Added damages

- MLK+ closures: 3 closures per year due to Closing regime and Raising unembanked areas measures, economic consequences for shipping is estimated at M€20 and 31 p/y in 2020 price levels, LG and GE respectively, as determined in Section 4.2.1

- Sea lock hindrance: economic consequences for shipping is estimated at M€95 and 320 p/y in 2020 price levels, LG and GE respectively, as determined in Section 4.3.1

- Sea lock Competitive Position (CP): CP is the economic consequences for the Port of Rotterdam due to decrease in Competitive Position of the port, estimated at M€31 p/y in 2020 price levels, as determined in Section 4.3.1

- **Diff** in Table C.1 represents the economic difference between LG plus CP and GE

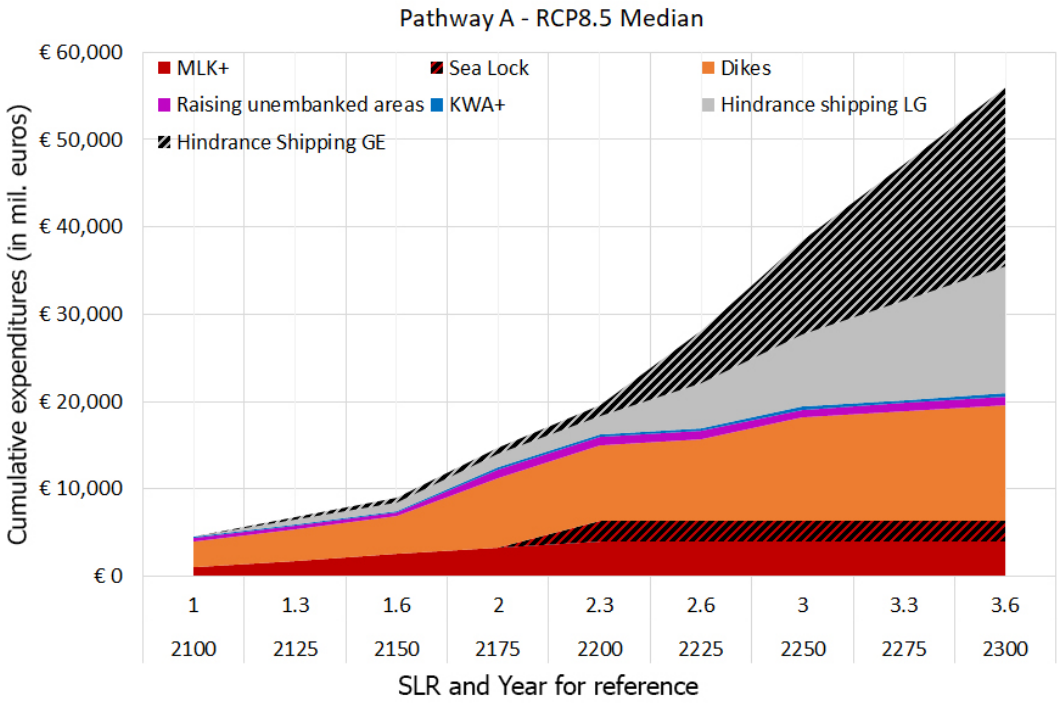

Figure C.12: Cumulative expenditures graph for Pathway A in RCP8.5 Median.

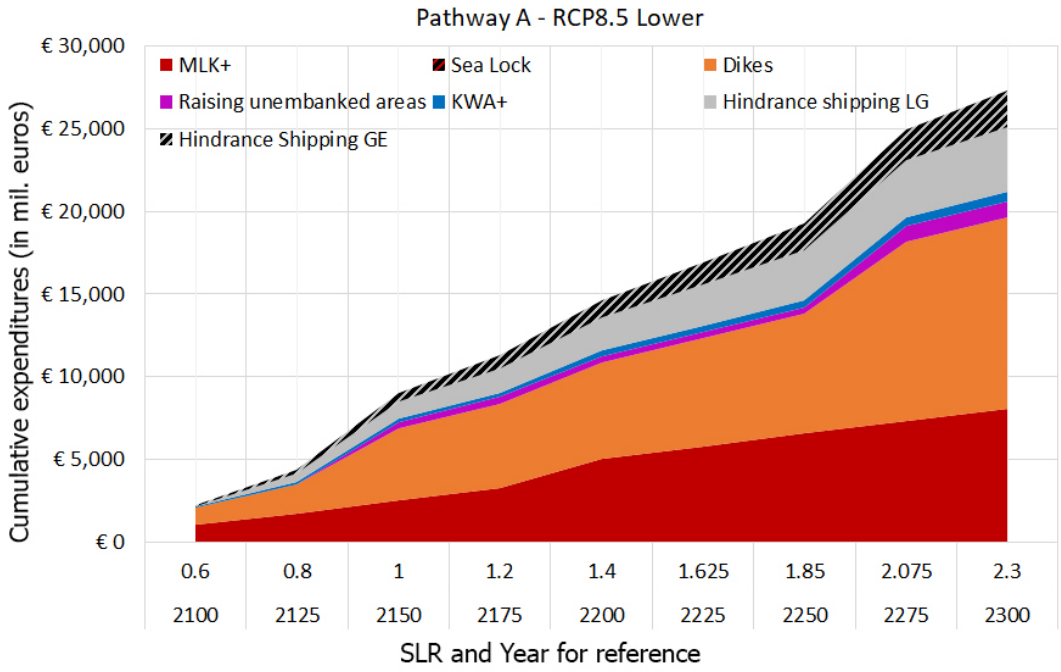

Figure C.13: Cumulative expenditures graph for Pathway A in RCP8.5 Lower.

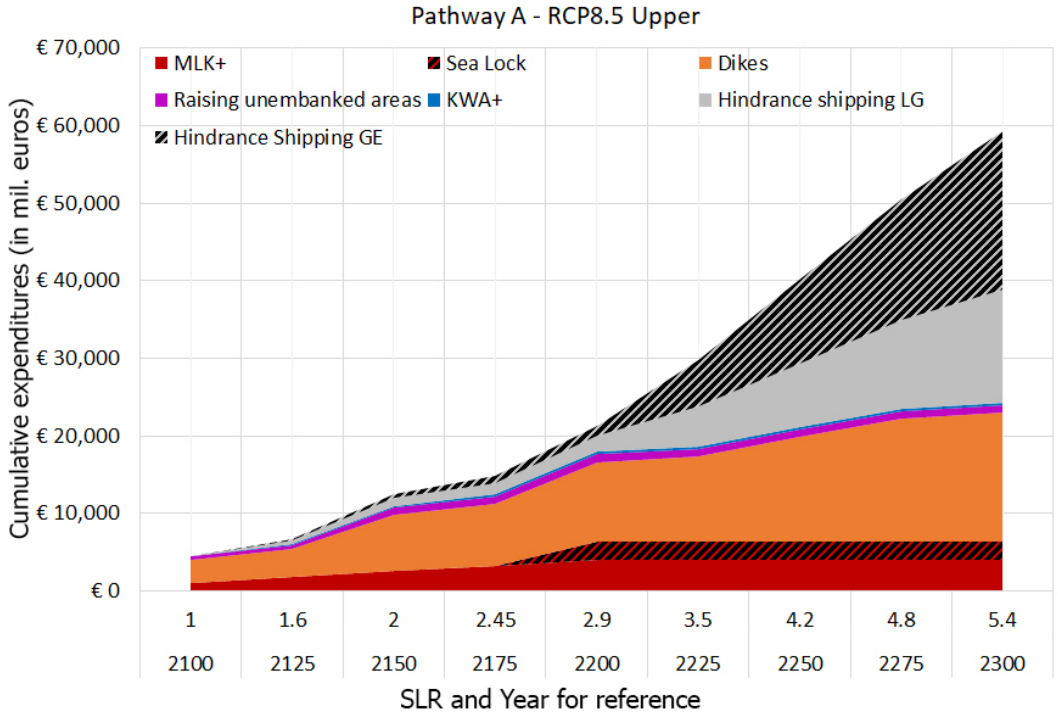

Figure C.14: Cumulative expenditures graph for Pathway A in RCP8.5 Upper.

Table C.1: Cumulative costs calculation for Pathway A in RCP8.5 median sea level rise situation in M€, see Fig. 2.3.

Pathway A1 - Closing Regime and Raising unembanked areas

Expenditures						**Switch to Lock**				
MLK+	Constr.	1,010	1,010	1,010	1,010	1,010	1,010	1,010	1,010	1,010
	p/y	30	757	1,515	2,272	3,030	3,030	3,030	3,030	3,030
	Total	**1,040**	**1,767**	**2,525**	**3,282**	**4,040**	**4,040**	**4,040**	**4,040**	**4,040**
Raising unembanked areas		**424**	**424**	**424**	**953**	**953**	**953**	**953**	**953**	**953**
Dikes	Constr.	2,908	2,908	2,908	5,816	5,816	5,816	7,473	7,473	7,473
	p/y	29	720	1,439	2,159	2,879	3,598	4,318	5,038	5,758
	Total	**2,937**	**3,628**	**4,347**	**7,975**	**8,695**	**9,414**	**11,791**	**12,511**	**13,231**
KWA+	Constr.	103	103	103	103	103	103	103	103	103
	p/y	2	55	109	164	219	219	219	219	219
	Total	**106**	**158**	**213**	**268**	**322**	**322**	**322**	**322**	**322**
Locks	Constr.	0	0	0	0	2,250	2,250	2,250	2,250	2,250
	p/y	0	0	0	0	11	283	565	848	1,130
	Salinisation	0	0	0	0	-10	-250	-500	-750	-1,000
	Total	**0**	**0**	**0**	**0**	**2,251**	**2,283**	**2,315**	**2,348**	**2,380**
Added damage										
Closures	LG	20	495	990	1,485	1,980	1,980	1,980	1,980	1,980
	GE	31	765	1,530	2,295	3,060	3,060	3,060	3,060	3,060
	Diff	**11**	**270**	**540**	**810**	**1,080**	**1,080**	**1,080**	**1,080**	**1,080**
Locks	LG	0	0	0	0	95	2,375	4,750	7,125	9,500
	CP	0	0	0	0	31	775	1,550	2,325	3,100
	LG + CP	0	0	0	0	126	3,150	6,300	9,450	12,600
	GE	0	0	0	0	320	7,993	15,985	23,978	31,970
	Diff	**0**	**0**	**0**	**0**	**194**	**4,843**	**9,685**	**14,528**	**19,370**
Cumulatief	LG + CP	20	495	990	1,485	2,106	5,130	8,280	11,430	14,580
	GE	31	765	1,530	2,295	3,380	11,053	19,045	27,038	35,030
	Diff	**11**	**270**	**540**	**810**	**1,274**	**5,923**	**10,765**	**15,608**	**20,450**
	Total LG	**4,527**	**6,472**	**8,499**	**13,963**	**18,367**	**22,142**	**27,701**	**31,604**	**35,506**
	Total GE	**4,537**	**6,742**	**9,039**	**14,773**	**19,641**	**28,065**	**38,466**	**47,211**	**55,956**
RCP8.5 median	year	2100	2125	2150	2175	2200	2225	2250	2275	2300
	SLR (m)	1	1.3	1.6	2	2.3	2.6	3	3.3	3.6

Table C.2: Cumulative costs calculation for Pathway A in RCP8.5 upper boundary sea level rise situation in M€, see Fig. 2.3.

Pathway A - Closing Regime and Raising unembanked areas

Expenditures						**Switch to Lock**				
MLK+	Constr.	1,010	1,010	1,010	1,010	1,010	1,010	1,010	1,010	1,010
	p/y	30	757	1,515	2,272	3,030	3,030	3,030	3,030	3,030
	Total	**1,040**	**1,767**	**2,525**	**3,282**	**4,040**	**4,040**	**4,040**	**4,040**	**4,040**
Raising unembanked areas		**424**	**424**	**953**	**953**	**953**	**953**	**953**	**953**	**953**
Dikes	Constr.	2,908	2,908	5,816	5,816	7,473	7,473	9,130	10,787	10,787
	p/y	29	720	1,439	2,159	2,879	3,598	4,318	5,038	5,758
	Total	**2,937**	**3,628**	**7,255**	**7,975**	**10,352**	**11,072**	**13,448**	**15,825**	**16,545**
KWA+	Constr.	103	103	103	103	103	103	103	103	103
	p/y	2	55	109	164	219	219	219	219	219
	Total	**106**	**158**	**213**	**268**	**322**	**322**	**322**	**322**	**322**
Locks	Constr.	0	0	0	0	2,250	2,250	2,250	2,250	2,250
	p/y	0	0	0	0	11	283	565	848	1,130
	Salinisation	0	0	0	0	-10	-250	-500	-750	-1,000
	Total	**0**	**0**	**0**	**0**	**2,251**	**2,283**	**2,315**	**2,348**	**2,380**
Added damage										
Closures	LG	20	495	990	1,485	1,980	1,980	1,980	1,980	1,980
	GE	**31**	**765**	**1,530**	**2,295**	**3,060**	**3,060**	**3,060**	**3,060**	**3,060**
	Diff	**11**	**270**	**540**	**810**	**1,080**	**1,080**	**1,080**	**1,080**	**1,080**
Locks	LG	0	0	0	0	95	2,375	4,750	7,125	9,500
	CP	0	0	0	0	31	775	1,550	2,325	3,100
	LG + CP	0	0	0	0	126	3,150	6,300	9,450	12,600
	GE	**0**	**0**	**0**	**0**	**320**	**7,993**	**15,985**	**23,978**	**31,970**
	Diff	**0**	**0**	**0**	**0**	**194**	**4,843**	**9,685**	**14,528**	**19,370**
Cumulative	LG + CP	20	495	990	1,485	2,106	5,130	8,280	11,430	14,580
	GE	**31**	**765**	**1,530**	**2,295**	**3,380**	**11,053**	**19,045**	**27,038**	**35,030**
	Diff	**11**	**270**	**540**	**810**	**1,274**	**5,923**	**10,765**	**15,608**	**20,450**
	Total LG	**4,527**	**6,472**	**11,130**	**14,822**	**21,810**	**26,550**	**31,579**	**35,481**	**41,314**
	Total GE	**4,537**	**6,742**	**11,670**	**15,632**	**23,084**	**32,473**	**42,344**	**51,089**	**61,764**
RCP8.5 Upper bound	year	2100	2125	2150	2175	2200	2225	2250	2275	2300
	SLR (m)	1	1.6	2	2.45	2.9	3.5	4.2	4.8	5.4

Table C.3: Cumulative costs calculation for Pathway A in RCP8.5 lower boundary sea level rise situation in M€, see Fig. 2.3.

Pathway A - Closing Regime and Raising unembanked areas

Expenditures						**Switch to Lock**				
MLK+	Constr.	1009.9	1009.9	1009.9	1009.9	2019.8	2019.8	2019.8	2019.8	2019.8
	p/y	30.3	757.4	1514.8	2272.2	3029.6	3787.1	4544.5	5301.9	6059.3
	Total	**1040.2**	**1767.3**	**2524.7**	**3282.1**	**5049.4**	**5806.8**	**6564.2**	**7321.6**	**8079.1**
Raising unembanked areas		0.0	0.0	424.2	424.2	424.2	424.2	424.2	953.2	953.2
Dikes	Constr.	1013.5	1013.5	2908.0	2908.0	2908.0	2908.0	2908.0	5816.011	5816.011
	p/y	28.8	719.7	1439.4	2159.1	2878.8	3598.5	4318.2	5037.9	5757.6
	Total	**1042.3**	**1733.2**	**4347.4**	**5067.1**	**5786.8**	**6506.5**	**7226.2**	**10853.9**	**11573.6**
KWA+	Constr.	103.4	103.4	103.4	103.4	103.4	103.4	103.4	103.4	103.4
	p/y	2.2	54.7	109.5	164.2	219.0	273.7	328.5	383.2	438.0
	Total	**105.6**	**158.2**	**212.9**	**267.7**	**322.4**	**377.2**	**431.9**	**486.7**	**541.4**
Locks	Constr.	0.0	0.0	0.0	0.0	0	0	0	0	0
	p/y	0	0	0	0	0	0	0	0	0
	Salinisation	0.0	0.0	0.0	0.0	0	0	0	0	0
	Total	0.0	0.0	0.0	0.0	0.0	0.0	0.0	0.0	0.0
Added damage										
Closures	LG	19.8	495.0	990.0	1485.0	1980.0	2475.0	2970.0	3465.0	3960.0
	GE	30.6	765.0	1530.0	2295.0	3060.0	3825.0	4590.0	5355.0	6120.0
	Diff	10.8	270.0	540.0	810.0	1080.0	1350.0	1620.0	1890.0	2160.0
Locks	LG	0	0	0	0	0	0	0	0	0
	CP	0	0	0	0	0	0	0	0	0
	LG + CP	0	0	0	0	0	0	0	0	0
	GE	0	0	0	0	0	0	0	0	0
	Diff	0	0	0	0	0	0	0	0	0
Cumulatief	LG + CP	19.8	495.0	990.0	1485.0	1980.0	2475.0	2970.0	3465.0	3960.0
	GE	30.6	765.0	1530.0	2295.0	3060.0	3825.0	4590.0	5355.0	6120.0
	Diff	10.8	270.0	540.0	810.0	1080.0	1350.0	1620.0	1890.0	2160.0
	Total LG	**€ 2,208**	**€ 4,154**	**€ 8,499**	**€ 10,526**	**€ 13,563**	**€ 15,590**	**€ 17,616**	**€ 23,080**	**€ 25,107**
	Total GE	**€ 2,219**	**€ 4,424**	**€ 9,039**	**€ 11,336**	**€ 14,643**	**€ 16,940**	**€ 19,236**	**€ 24,970**	**€ 27,267**
RCP8.5 Lower bound	year	2100	2125	2150	2175	2200	2225	2250	2275	2300
	SLR (m)	0.6	0.8	1	1.2	1.4	1.625	1.85	2.075	2.3

C.3.2. PATHWAY B

Expenditures:

- MLK+ construction costs: M€1,010 in 2020 price level, from Section 4.2.1 in 2009 price level
- MLK+ maintenance and management costs: approximately 3%, Section 4.2.1 per year equals to M€30 in 2020 price level
- Raising unembanked areas NAP +3.80 m: **Removed**
- Raising unembanked areas NAP +4.55 m: **Removed**
- Managed retreat from areas below NAP +3.80 m: approximately 6,500 and 4,500 residences, Rotterdam and Dordrecht respectively, at M€0.5 per residence in 2020 price level
- Managed retreat from areas below NAP +4.55 m: additional 2,150 and 1,950 residences, Rotterdam and Dordrecht respectively, at M€0.5 per residence in 2020 price level
- KWA+ construction costs: combined costs of KWA+ incidental and increase to KWA++, M€48.7 and 54.7 in 2020 price levels, from Section 4.4.6 in 2015 price level
- KWA+ fundamental exploitation costs: equals to 2.2 M€p/y in 2020 price level, as determined in Section 4.4.6
- Sea lock construction costs: M€2,250 as determined in Section 4.3.1
- Sea lock maintenance and management costs: approximately M€11.3 per year, as determined in Section 4.3.1
- Sea lock salinisation damage reduction: added benefit of -M€10 p/y, as determined in Section 4.3.1

Computation of dikes heightening costs, location B as reference:

- 28.1 (Rural) km and 16.65 (Urban) km of dikes in direct contact with the sea, see Table C.14, raising these dikes by 2 metres per 1 metre sea level rise, as determined in Section 4.4.5
- Multiplying amount of km of rural dikes with M€13.0 in 2020 price levels, average of Table 4.3 for the construction costs
- Multiplying amount of km of urban dikes with M€29.2 in 2020 price levels, average of Table 4.3 for the construction costs
- 3.8 (Rural) km and 51.32 (Urban) km of dikes in need for heightening by 1 metre, see Table C.14, regarding Closing regime, see Section 4.2.2, and Raising unembanked areas, see Section 4.2.4, measures
- Multiplying amount of km of rural dikes with M€6.9 in 2020 price levels, lower boundary value of Table 4.3 for the construction costs
- Multiplying amount of km of urban dikes with M€23.9 in 2020 price levels, lower boundary value Table 4.3 for the construction costs

Added damages

- MLK+ closures: 3 closures per year due to Closing regime and Raising unembanked areas measures, economic consequences for shipping is estimated at M€20 and 31 p/y in 2020 price levels, LG and GE respectively, as determined in Section 4.2.1

- Sea lock hindrance: economic consequences for shipping is estimated at M€95 and 320 p/y in 2020 price levels, LG and GE respectively, as determined in Section 4.3.1

- Sea lock Competitive Position (CP): CP is the economic consequences for the Port of Rotterdam due to decrease in Competitive Position of the port, estimated at M€31 p/y in 2020 price levels, as determined in Section 4.3.1

- **Diff** in Table C.1 represents the economic difference between LG plus CP and GE

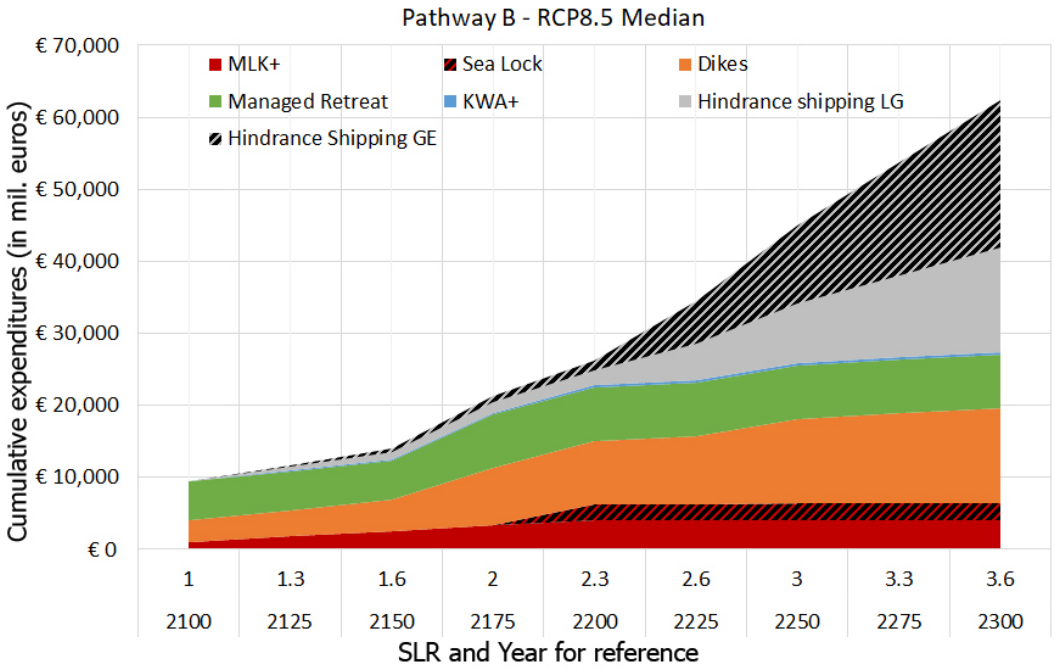

Figure C.15: Cumulative expenditures graph for Pathway B in RCP8.5 Median.

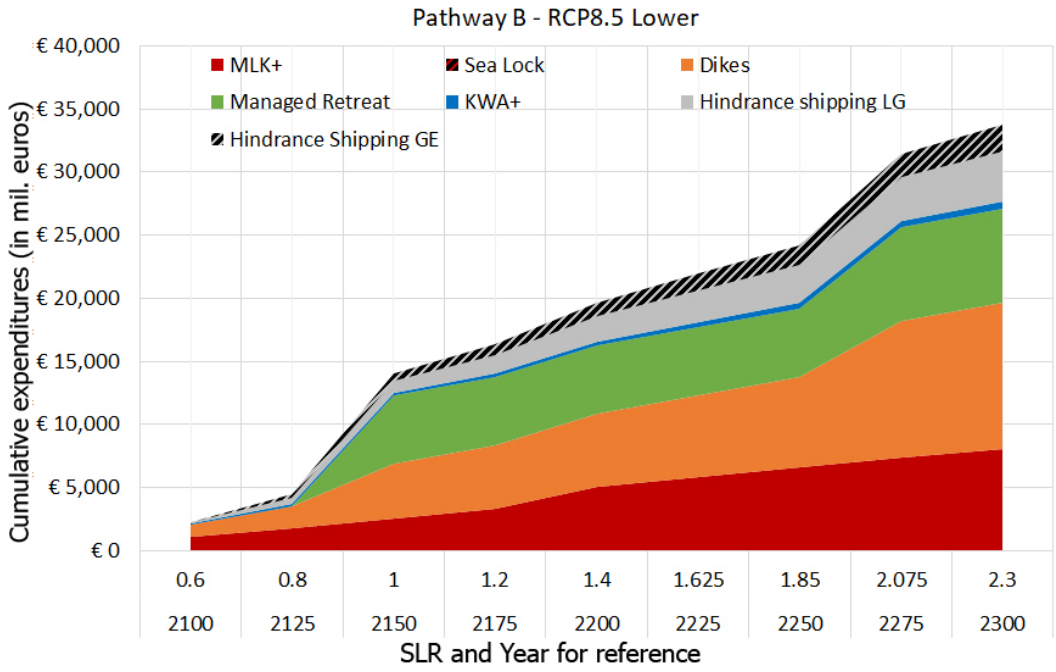

Figure C.16: Cumulative expenditures graph for Pathway B in RCP8.5 Lower.

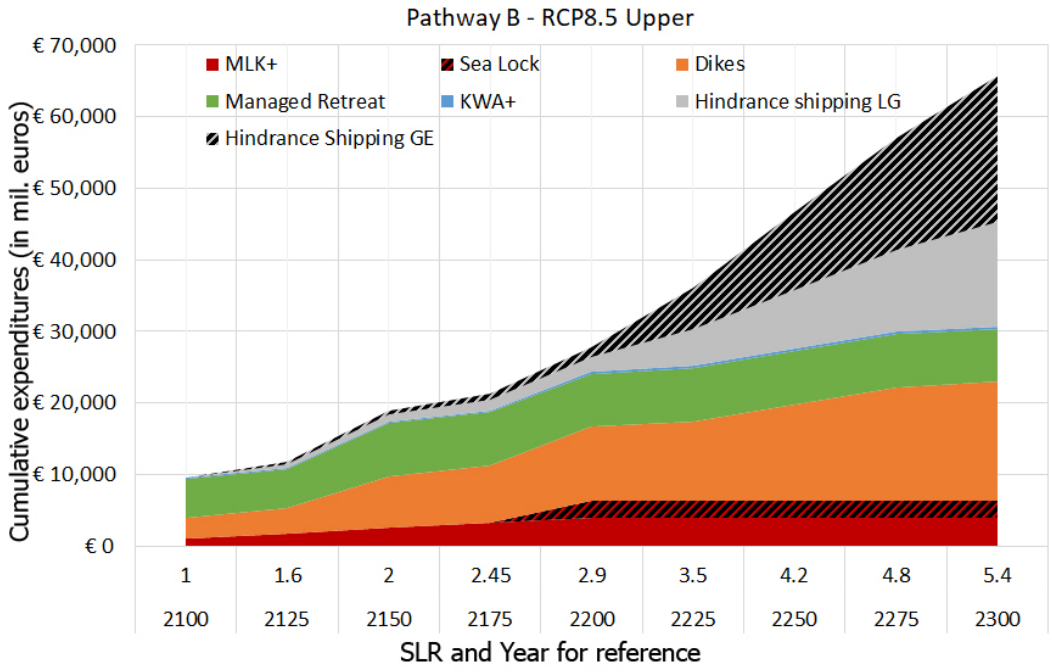

Figure C.17: Cumulative expenditures graph for Pathway B in RCP8.5 Upper.

Table C.4: Cumulative costs calculation for Pathway B in RCP8.5 median sea level rise situation in M€, see Fig. 2.3.

Pathway B - Closing Regime and Managed Retreat										
Expenditures						**Switch to Lock**				
MLK+	Constr.	1,010	1,010	1,010	1,010	1,010	1,010	1,010	1,010	1,010
	p/y	30	757	1,515	2,272	3,030	3,030	3,030	3,030	3,030
	Total	**1,040**	**1,767**	**2,525**	**3,282**	**4,040**	**4,040**	**4,040**	**4,040**	**4,040**
Managed Retreat		5,414	5,414	5,414	7,432	7,432	7,432	7,432	7,432	7,432
Dikes	Constr.	2,908	2,908	2,908	5,816	5,816	5,816	7,473	7,473	7,473
	p/y	29	720	1,439	2,159	2,879	3,598	4,318	5,038	5,758
	Total	**2,937**	**3,628**	**4,347**	**7,975**	**8,695**	**9,414**	**11,791**	**12,511**	**13,231**
KWA+	Constr.	103	103	103	103	103	103	103	103	103
	p/y	2	55	109	164	219	219	219	219	219
	Total	**106**	**158**	**213**	**268**	**322**	**322**	**322**	**322**	**322**
Locks	Constr.	0	0	0	0	2,250	2,250	2,250	2,250	2,250
	p/y	0	0	0	0	11	283	565	848	1,130
	Salinisation	0	0	0	0	-10	-250	-500	-750	-1,000
	Total	**0**	**0**	**0**	**0**	**2,251**	**2,283**	**2,315**	**2,348**	**2,380**
Added damage										
Closures	LG	20	495	990	1,485	1,980	1,980	1,980	1,980	1,980
	GE	31	765	1,530	2,295	3,060	3,060	3,060	3,060	3,060
	Diff	**11**	**270**	**540**	**810**	**1,080**	**1,080**	**1,080**	**1,080**	**1,080**
Locks	LG	0	0	0	0	95	2,375	4,750	7,125	9,500
	CP	0	0	0	0	31	775	1,550	2,325	3,100
	LG + CP	0	0	0	0	126	3,150	6,300	9,450	12,600
	GE	0	0	0	0	320	7,993	15,985	23,978	31,970
	Diff	**0**	**0**	**0**	**0**	**194**	**4,843**	**9,685**	**14,528**	**19,370**
Cumulative	LG + CP	20	495	990	1,485	2,106	5,130	8,280	11,430	14,580
	GE	31	765	1,530	2,295	3,380	11,053	19,045	27,038	35,030
	Diff	**11**	**270**	**540**	**810**	**1,274**	**5,923**	**10,765**	**15,608**	**20,450**
	Total LG	**9,516**	**11,462**	**13,489**	**20,442**	**24,846**	**28,621**	**34,180**	**38,082**	**41,984**
	Total GE	**9,527**	**11,732**	**14,029**	**21,252**	**26,119**	**34,543**	**44,945**	**53,690**	**62,434**
RCP8.5 median	year	2100	2125	2150	2175	2200	2225	2250	2275	2300
	SLR (m)	1	1.3	1.6	2	2.3	2.6	3	3.3	3.6

Table C.5: Cumulative costs calculation for Pathway B in RCP8.5 upper boundary sea level rise situation in M€, see Fig. 2.3.

Pathway B - Closing Regime and Managed Retreat

Expenditures						**Switch to Lock**				
MLK+	Constr.	1,010	1,010	1,010	1,010	1,010	1,010	1,010	1,010	1,010
	p/y	30	757	1,515	2,272	3,030	3,030	3,030	3,030	3,030
	Total	**1,040**	**1,767**	**2,525**	**3,282**	**4,040**	**4,040**	**4,040**	**4,040**	**4,040**
Managed Retreat		5,414	5,414	7,432	7,432	7,432	7,432	7,432	7,432	7,432
Dikes	Constr.	2,908	2,908	5,816	5,816	7,473	7,473	9,130	10,787	10,787
	p/y	29	720	1,439	2,159	2,879	3,598	4,318	5,038	5,758
	Total	**2,937**	**3,628**	**7,255**	**7,975**	**10,352**	**11,072**	**13,448**	**15,825**	**16,545**
KWA+	Constr.	103	103	103	103	103	103	103	103	103
	p/y	2	55	109	164	219	219	219	219	219
	Total	**106**	**158**	**213**	**268**	**322**	**322**	**322**	**322**	**322**
Locks	Constr.	0	0	0	0	2,250	2,250	2,250	2,250	2,250
	p/y	0	0	0	0	11	283	565	848	1,130
	Salinisation	0	0	0	0	-10	-250	-500	-750	-1,000
	Total	**0**	**0**	**0**	**0**	**2,251**	**2,283**	**2,315**	**2,348**	**2,380**
Added damage										
Closures	LG	20	495	990	1,485	1,980	1,980	1,980	1,980	1,980
	GE	31	765	1,530	2,295	3,060	3,060	3,060	3,060	3,060
	Diff	**11**	**270**	**540**	**810**	**1,080**	**1,080**	**1,080**	**1,080**	**1,080**
Locks	LG	0	0	0	0	95	2,375	4,750	7,125	9,500
	CP	0	0	0	0	31	775	1,550	2,325	3,100
	LG + CP	0	0	0	0	126	3,150	6,300	9,450	12,600
	GE	0	0	0	0	320	7,993	15,985	23,978	31,970
	Diff	**0**	**0**	**0**	**0**	**194**	**4,843**	**9,685**	**14,528**	**19,370**
Cumulative	LG + CP	20	495	990	1,485	2,106	5,130	8,280	11,430	14,580
	GE	31	765	1,530	2,295	3,380	11,053	19,045	27,038	35,030
	Diff	**11**	**270**	**540**	**810**	**1,274**	**5,923**	**10,765**	**15,608**	**20,450**
	Total LG	**9,516**	**11,462**	**18,415**	**20,442**	**26,503**	**30,278**	**35,837**	**41,396**	**45,299**
	Total GE	**9,527**	**11,732**	**18,955**	**21,252**	**27,777**	**36,200**	**46,602**	**57,004**	**65,749**
RCP8.5 Upper bound	year	2100	2125	2150	2175	2200	2225	2250	2275	2300
	SLR (m)	1	1.6	2	2.45	2.9	3.5	4.2	4.8	5.4

Table C.6: Cumulative costs calculation for Pathway B in RCP8.5 lower boundary sea level rise situation in M€, see Fig. 2.3.

Pathway B - Closing Regime and Managed Retreat

Expenditures						**Switch to Lock**				
MLK+	Constr.	1,010	1,010	1,010	1,010	2,020	2,020	2,020	2,020	2,020
	p/y	30	757	1,515	2,272	3,030	3,787	4,544	5,302	6,059
	Total	**1,040**	**1,767**	**2,525**	**3,282**	**5,049**	**5,807**	**6,564**	**7,322**	**8,079**
Managed Retreat		0	0	5,414	5,414	5,414	5,414	5,414	7,432	7,432
Dikes	Constr.	1,013	1,013	2,908	2,908	2,908	2,908	2,908	5,816	5,816
	p/y	29	720	1,439	2,159	2,879	3,598	4,318	5,038	5,758
	Total	**1,042**	**1,733**	**4,347**	**5,067**	**5,787**	**6,506**	**7,226**	**10,854**	**11,574**
KWA+	Constr.	103	103	103	103	103	103	103	103	103
	p/y	2	55	109	164	219	274	328	383	438
	Total	**106**	**158**	**213**	**268**	**322**	**377**	**432**	**487**	**541**
Locks	Constr.	0	0	0	0	0	0	0	0	0
	p/y	0	0	0	0	0	0	0	0	0
	Salinisation	0	0	0	0	0	0	0	0	0
	Total	**0**	**0**	**0**	**0**	**0**	**0**	**0**	**0**	**0**
Added damage										
Closures	LG	20	495	990	1,485	1,980	2,475	2,970	3,465	3,960
	GE	31	765	1,530	2,295	3,060	3,825	4,590	5,355	6,120
	Diff	**11**	**270**	**540**	**810**	**1,080**	**1,350**	**1,620**	**1,890**	**2,160**
Locks	LG	0	0	0	0	0	0	0	0	0
	CP	0	0	0	0	0	0	0	0	0
	LG + CP	0	0	0	0	0	0	0	0	0
	GE	0	0	0	0	0	0	0	0	0
	Diff	**0**	**0**	**0**	**0**	**0**	**0**	**0**	**0**	**0**
Cumulative	LG + CP	20	495	990	1,485	1,980	2,475	2,970	3,465	3,960
	GE	31	765	1,530	2,295	3,060	3,825	4,590	5,355	6,120
	Diff	**11**	**270**	**540**	**810**	**1,080**	**1,350**	**1,620**	**1,890**	**2,160**
	Total LG	**2,208**	**4,154**	**13,489**	**15,516**	**18,552**	**20,579**	**22,606**	**29,559**	**31,586**
	Total GE	**2,219**	**4,424**	**14,029**	**16,326**	**19,632**	**21,929**	**24,226**	**31,449**	**33,746**
RCP8.5 Lower bound	year	2100	2125	2150	2175	2200	2225	2250	2275	2300
	SLR (m)	0.6	0.8	1	1.2	1.4	1.625	1.85	2.075	2.3

C.3.3. PATHWAY C2 (MAASVLAKTE III INCORPORATED)

Expenditures:

- Maasvlakte III: Construction costs estimated at M€2,900 in 2020 price level, as determined in Section 4.4.4
- Maasvlakte III Raising area regarding sea level rise: total surface of Waal-, Eem, Petroleum- and Botlek harbour segments (20.7 km^2) per metre sea level rise multiplied with M€30.8 in 2020 price level, as determined in Section 4.2.4
- Sea lock construction costs: M€2,250 as determined in Section 4.3.1
- Sea lock maintenance and management costs: approximately M€11.3 per year, as determined in Section 4.3.1
- Sea lock salinisation damage reduction: added benefit of -M€10 p/y, as determined in Section 4.3.1

Computation of dikes heightening costs, location B as reference:

- 28.1 (Rural) km and 16.65 (Urban) km of dikes in direct contact with the sea, see Table C.14, raising these dikes by 2 metres per 1 metre sea level rise, as determined in Section 4.4.5
- Multiplying amount of km of rural dikes with M€13.0 in 2020 price levels, average of Table 4.3 for the construction costs
- Multiplying amount of km of urban dikes with M€29.2 in 2020 price levels, average of Table 4.3 for the construction costs

Added damages

- Sea lock hindrance: economic consequences for shipping is estimated at M€95 and 320 p/y in 2020 price levels, LG and GE respectively, as determined in Section 4.3.1, and reduced as determined in Appendix C.5
- Sea lock Competitive Position (CP): CP is the economic consequences for the Port of Rotterdam due to decrease in Competitive Position of the port, estimated at M€31 p/y in 2020 price levels, as determined in Section 4.3.1
- **Diff** in Table C.1 represents the economic difference between LG plus CP and GE

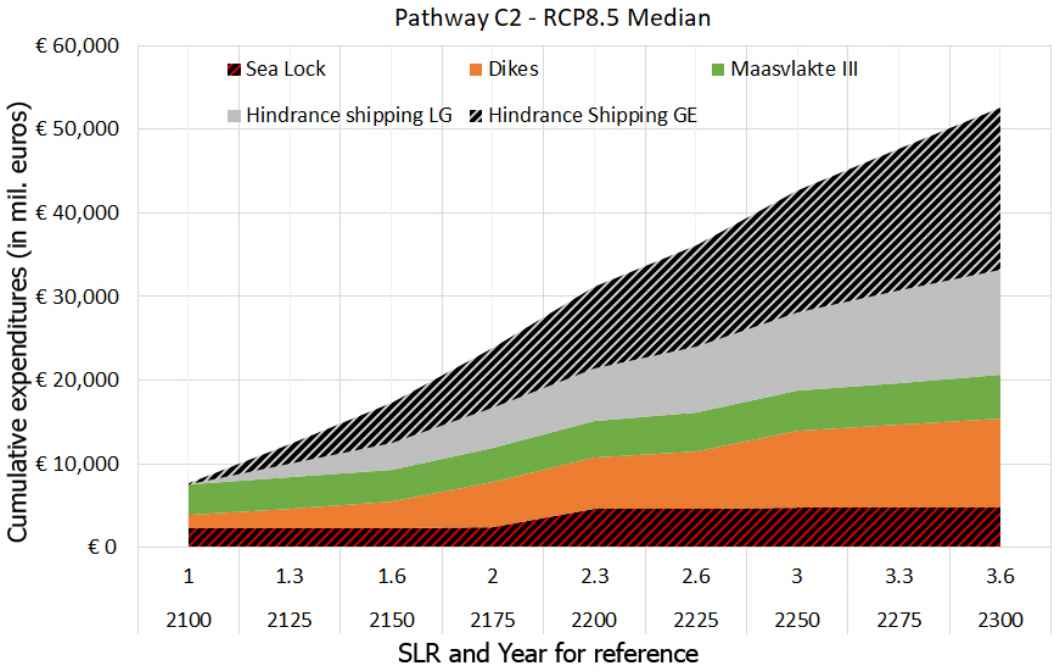

Figure C.18: Cumulative expenditures graph for Pathway C2 in RCP8.5 Median.

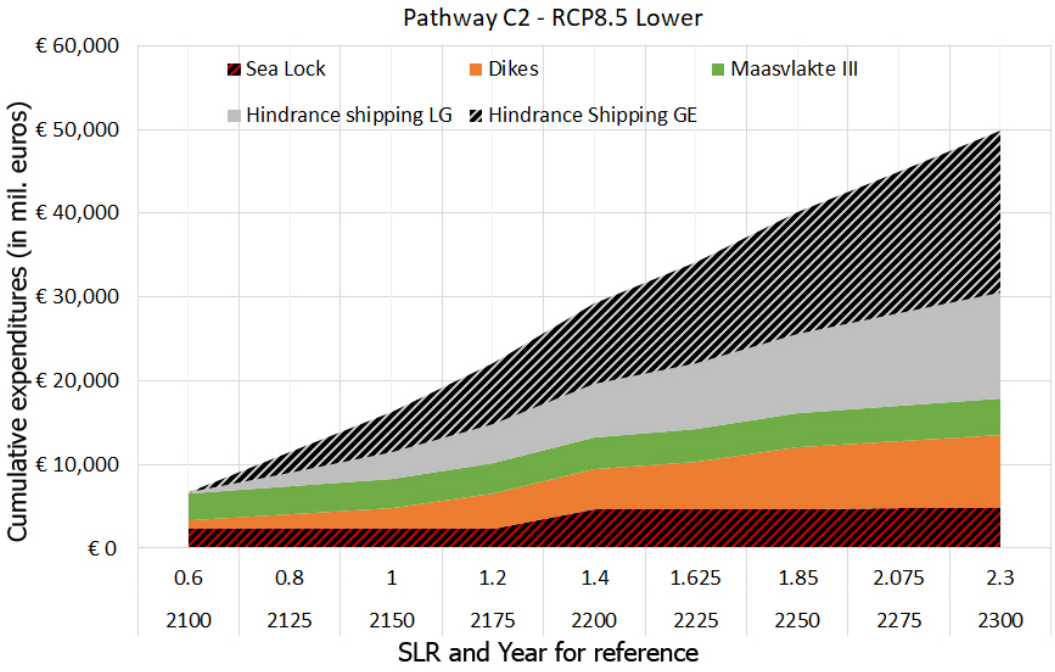

Figure C.19: Cumulative expenditures graph for Pathway C2 in RCP8.5 Lower.

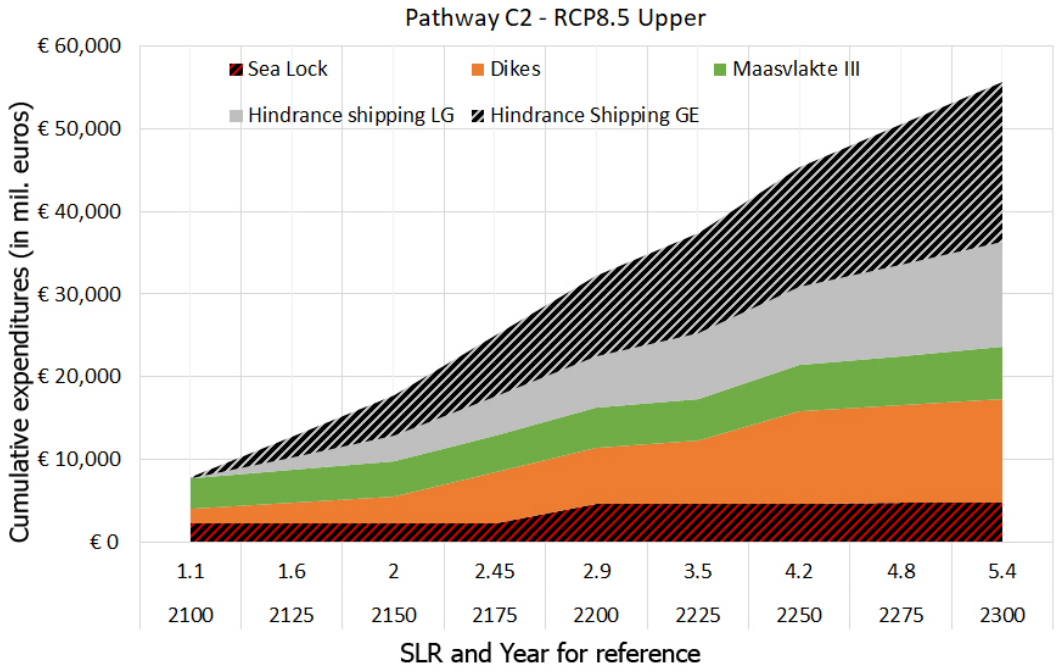

Figure C.20: Cumulative expenditures graph for Pathway C2 in RCP8.5 Upper.

Table C.7: Cumulative costs calculation for Pathway C2 in RCP8.5 median sea level rise situation in M€, see Fig. 2.3.

Pathway C2 - Sea Lock with Maasvlakte III

Expenditures						**Second Lock**				
MLK+	Constr.	0	0	0	0	0	0	0	0	0
	p/y	0	0	0	0	0	0	0	0	0
	Total	**0**	**0**	**0**	**0**	**0**	**0**	**0**	**0**	**0**
Maasvlakte III		3,537	3,729	3,920	4,175	4,366	4,557	4,812	5,003	5,194
Dikes	Constr.	1,657	1,657	1,657	3,266	3,266	3,266	4,875	4,875	4,875
	p/y	29	720	1,439	2,159	2,879	3,598	4,318	5,038	5,758
	Total	**1,686**	**2,377**	**3,096**	**5,425**	**6,145**	**6,865**	**9,193**	**9,913**	**10,633**
KWA+	Constr.	0	0	0	0	0	0	0	0	0
	p/y	0	55	109	164	219	219	219	219	219
	Total	**0**	**55**	**109**	**164**	**219**	**219**	**219**	**219**	**219**
Locks	Constr.	2,250	2,250	2,250	2,250	4,500	4,500	4,500	4,500	4,500
	p/y	11	283	565	848	1,130	1,413	1,695	1,978	2,260
	Salinisation	-10	-250	-500	-750	-1,000	-1,250	-1,500	-1,750	-2,000
	Total	**2,251**	**2,283**	**2,315**	**2,348**	**4,630**	**4,663**	**4,695**	**4,728**	**4,760**
Added damage										
Closures	LG	0	0	0	0	0	0	0	0	0
	GE	0	0	0	0	0	0	0	0	0
	Diff	**0**	**0**	**0**	**0**	**0**	**0**	**0**	**0**	**0**
Locks	LG	48	1,188	2,375	3,563	4,750	5,938	7,125	8,313	9,500
	CP	16	388	775	1,163	1,550	1,938	2,325	2,713	3,100
	LG + CP	63	1,575	3,150	4,725	6,300	7,875	9,450	11,025	12,600
	GE	160	3,996	7,993	11,989	15,985	19,981	23,978	27,974	31,970
	Diff	**97**	**2,421**	**4,843**	**7,264**	**9,685**	**12,106**	**14,528**	**16,949**	**19,370**
Cumulative	LG + CP	63	1,575	3,150	4,725	6,300	7,875	9,450	11,025	12,600
	GE	160	3,996	7,993	11,989	15,985	19,981	23,978	27,974	31,970
	Diff	**97**	**2,421**	**4,843**	**7,264**	**9,685**	**12,106**	**14,528**	**16,949**	**19,370**
	Total LG	**7,538**	**10,018**	**12,591**	**16,837**	**21,660**	**24,178**	**28,369**	**30,888**	**33,406**
	Total GE	**7,634**	**12,439**	**17,433**	**24,100**	**31,345**	**36,284**	**42,897**	**47,837**	**52,776**
RCP8.5 median	year	2100	2125	2150	2175	2200	2225	2250	2275	2300
	SLR (m)	1	1.3	1.6	2	2.3	2.6	3	3.3	3.6

Table C.8: Cumulative costs calculation for Pathway C2 in RCP8.5 upper boundary sea level rise situation in M€, see Fig. 2.3.

Pathway C2 - Sea Lock with Maasvlakte III

Expenditures						**Second Lock**				
MLK+	Constr.	0	0	0	0	0	0	0	0	0
	p/y	0	0	0	0	0	0	0	0	0
	Total	**0**	**0**	**0**	**0**	**0**	**0**	**0**	**0**	**0**
Maasvlakte III		3,601	3,920	4,175	4,461	4,748	5,131	5,577	5,959	6,342
Dikes	Constr.	1,818	1,818	1,818	3,990	3,990	3,990	6,806	6,806	6,806
	p/y	29	720	1,439	2,159	2,879	3,598	4,318	5,038	5,758
	Total	**1,847**	**2,538**	**3,257**	**6,149**	**6,869**	**7,589**	**11,124**	**11,844**	**12,564**
KWA+	Constr.	0	0	0	0	0	0	0	0	0
	p/y	0	0	0	0	0	0	0	0	0
	Total	**0**	**0**	**0**	**0**	**0**	**0**	**0**	**0**	**0**
Locks	Constr.	2,250	2,250	2,250	2,250	4,500	4,500	4,500	4,500	4,500
	p/y	11	283	565	848	1,130	1,413	1,695	1,978	2,260
	Salinisation	-10	-250	-500	-750	-1,000	-1,250	-1,500	-1,750	-2,000
	Total	**2,251**	**2,283**	**2,315**	**2,348**	**4,630**	**4,663**	**4,695**	**4,728**	**4,760**
Added damage										
Closures	LG	0	0	0	0	0	0	0	0	0
	GE	0	0	0	0	0	0	0	0	0
	Diff	**0**	**0**	**0**	**0**	**0**	**0**	**0**	**0**	**0**
Locks	LG	48	1,188	2,375	3,563	4,750	5,938	7,125	8,313	9,500
	CP	16	388	775	1,163	1,550	1,938	2,325	2,713	3,100
	LG + CP	63	1,575	3,150	4,725	6,300	7,875	9,450	11,025	12,600
	GE	160	3,996	7,993	11,989	15,985	19,981	23,978	27,974	31,970
	Diff	**97**	**2,421**	**4,843**	**7,264**	**9,685**	**12,106**	**14,528**	**16,949**	**19,370**
Cumulative	LG + CP	63	1,575	3,150	4,725	6,300	7,875	9,450	11,025	12,600
	GE	160	3,996	7,993	11,989	15,985	19,981	23,978	27,974	31,970
	Diff	**97**	**2,421**	**4,843**	**7,264**	**9,685**	**12,106**	**14,528**	**16,949**	**19,370**
	Total LG	**7,762**	**10,315**	**12,897**	**17,683**	**22,547**	**25,257**	**30,846**	**33,556**	**36,265**
	Total GE	**7,859**	**12,736**	**17,740**	**24,947**	**32,232**	**37,363**	**45,374**	**50,504**	**55,635**
RCP8.5 Upper bound	year	2100	2125	2150	2175	2200	2225	2250	2275	2300
	SLR (m)	1.1	1.6	2	2.45	2.9	3.5	4.2	4.8	5.4

Table C.9: Cumulative costs calculation for Pathway C2 in RCP8.5 lower boundary sea level rise situation in M€, see Fig. 2.3.

Pathway C2 - Sea Lock with Maasvlakte III

Expenditures						**Second Lock**				
MLK+	Constr.	0.0	0.0	0.0	0.0	0.0	0.0	0.0	0.0	0.0
	p/y	0.0	0.0	0.0	0.0	0.0	0.0	0.0	0.0	0.0
	Total	**0.0**	**0.0**	**0.0**	**0.0**	**0.0**	**0.0**	**0.0**	**0.0**	**0.0**
Maasvlakte III		3282.4	3409.9	3537.3	3664.8	3792.3	3935.7	4079.1	4222.5	4365.9
Dikes	Constr.	1013.5	1013.5	1013.5	1978.9	1978.9	1978.9	3024.8	3024.8	3024.8
	p/y	28.8	719.7	1439.4	2159.1	2878.8	3598.5	4318.2	5037.9	5757.6
	Total	**1042.3**	**1733.2**	**2452.9**	**4138.0**	**4857.7**	**5577.4**	**7343.0**	**8062.7**	**8782.4**
KWA+	Constr.	0.0	0.0	0.0	0.0	0.0	0.0	0.0	0.0	0.0
	p/y	0.0	0.0	0.0	0.0	0.0	0.0	0.0	0.0	0.0
	Total	**0.0**	**0.0**	**0.0**	**0.0**	**0.0**	**0.0**	**0.0**	**0.0**	**0.0**
Locks	Constr.	2250.0	2250.0	2250.0	2250.0	4500.0	4500.0	4500.0	4500.0	4500.0
	p/y	11.3	282.5	565	847.5	1130	1412.5	1695	1977.5	2260
	Salinisation	-10.0	-250	-500	-750	-1000	-1250	-1500	-1750	-2000
	Total	**2251.3**	**2282.5**	**2315.0**	**2347.5**	**4630.0**	**4662.5**	**4695.0**	**4727.5**	**4760.0**
Added damage										
Closures	LG	0.0	0.0	0.0	0.0	0.0	0.0	0.0	0.0	0.0
	GE	0.0	0.0	0.0	0.0	0.0	0.0	0.0	0.0	0.0
	Diff	**0.0**	**0.0**	**0.0**	**0.0**	**0.0**	**0.0**	**0.0**	**0.0**	**0.0**
Locks	LG	47.5	1187.5	2375	3562.5	4750	5937.5	7125	8312.5	9500
	CP	15.5	387.5	775	1162.5	1550	1937.5	2325	2712.5	3100
	LG + CP	63	1575	3150	4725	6300	7875	9450	11025	12600
	GE	159.85	3996.25	7992.5	11988.75	15985	19981.25	23977.5	27973.75	31970
	Diff	**96.85**	**2421.25**	**4842.5**	**7263.75**	**9685**	**12106.25**	**14527.5**	**16948.75**	**19370**
Cumulative	LG + CP	63.0	1575.0	3150.0	4725.0	6300.0	7875.0	9450.0	11025.0	12600.0
	GE	159.9	3996.3	7992.5	11988.8	15985.0	19981.3	23977.5	27973.8	31970.0
	Diff	**96.9**	**2421.3**	**4842.5**	**7263.8**	**9685.0**	**12106.3**	**14527.5**	**16948.8**	**19370.0**
	Total LG	**6,639**	**9,001**	**11,455**	**14,875**	**19,580**	**22,051**	**25,567**	**28,038**	**30,508**
	Total GE	**6,736**	**11,422**	**16,298**	**22,139**	**29,265**	**34,157**	**40,095**	**44,986**	**49,878**
RCP8.5 Lower bound	year	2100	2125	2150	2175	2200	2225	2250	2275	2300
	SLR (m)	0.6	0.8	1	1.2	1.4	1.625	1.85	2.075	2.3

C.3.4. PATHWAY D2 (MAASVLAKTE III INCORPORATED)

Expenditures:

- MLK+ construction costs: M€1,010 in 2020 price level, from Section 4.2.1 in 2009 price level
- MLK+ maintenance and management costs: approximately 3%, Section 4.2.1 per year equals to M€30 in 2020 price level
- Maasvlakte III: Construction costs estimated at M€2,900 in 2020 price level, as determined in Section 4.4.4
- Maasvlakte III Raising area regarding sea level rise: total surface of Waal-, Eem, Petroleum- and Botlek harbour segments (20.7 km^2) per metre sea level rise multiplied with M€30.8 in 2020 price level, as determined in Section 4.2.4
- KWA+ construction costs: combined costs of KWA+ incidental and increase to KWA++, M€48.7 and 54.7 in 2020 price levels, from Section 4.4.6 in 2015 price level
- KWA+ fundamental exploitation costs: equals to 2.2 M€p/y in 2020 price level, as determined in Section 4.4.6
- Sea lock construction costs: M€2,250 as determined in Section 4.3.1
- Sea lock maintenance and management costs: approximately M€11.3 per year, as determined in Section 4.3.1
- Sea lock salinisation damage reduction: added benefit of -M€10 p/y, as determined in Section 4.3.1

Computation of dikes heightening costs, location B as reference:

- 28.1 (Rural) km and 16.65 (Urban) km of dikes in direct contact with the sea, see Table C.14, raising these dikes by 2 metres per 1 metre sea level rise, as determined in Section 4.4.5
- Multiplying amount of km of rural dikes with M€13.0 in 2020 price levels, average of Table 4.3 for the construction costs
- Multiplying amount of km of urban dikes with M€29.2 in 2020 price levels, average of Table 4.3 for the construction costs

Added damages

- MLK+ closures: amount of closures increase with increase in sea level rise, economic consequences for shipping is estimated at M€20 and 31 p/y/3 closures in 2020 price levels, LG and GE respectively, as determined in Section 4.2.1 and reduced as determined in Appendix C.5
- Sea lock hindrance: economic consequences for shipping is estimated at M€95 and 320 p/y in 2020 price levels, LG and GE respectively, as determined in Section 4.3.1, and reduced as determined in Appendix C.5
- Sea lock Competitive Position (CP): CP is the economic consequences for the Port of Rotterdam due to decrease in Competitive Position of the port, estimated at M€31 p/y in 2020 price levels, as determined in Section 4.3.1
- **Diff** in Table C.1 represents the economic difference between LG plus CP and GE

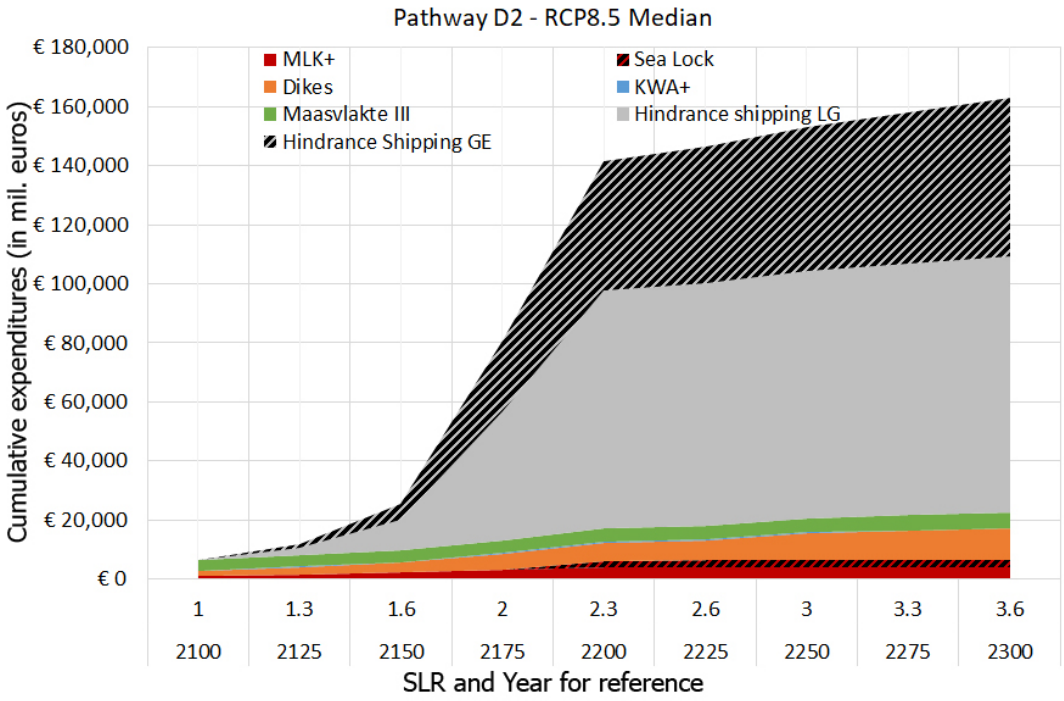

Figure C.21: Cumulative expenditures graph for Pathway D2 in RCP8.5 Median.

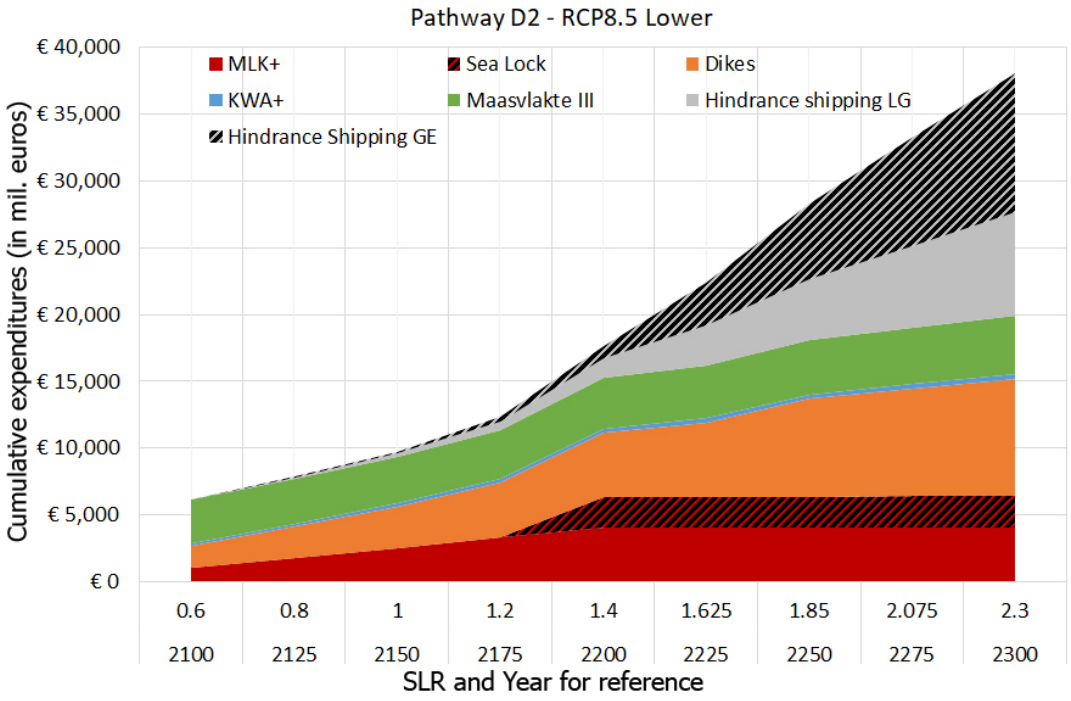

Figure C.22: Cumulative expenditures graph for Pathway D2 in RCP8.5 Lower.

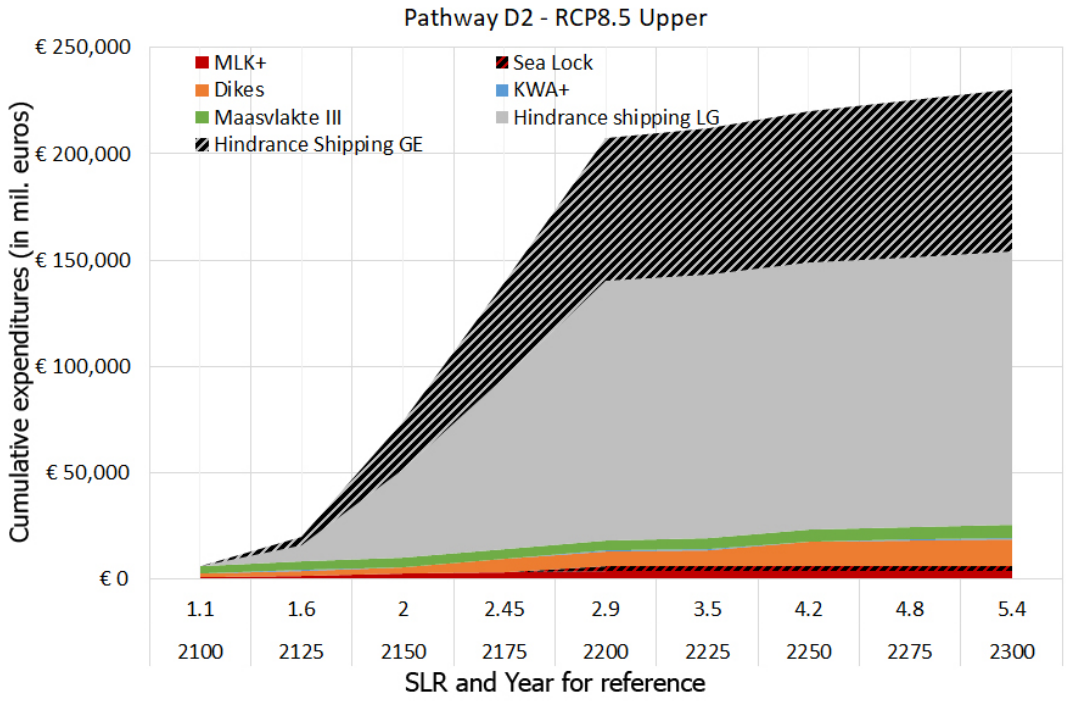

Figure C.23: Cumulative expenditures graph for Pathway D2 in RCP8.5 Upper.

Table C.10: Cumulative costs calculation for Pathway D2 in RCP8.5 median sea level rise situation in M€, see Fig. 2.3.

Pathway D2 - Maintain closing regime and Maasvlakte III

Expenditures						**Switch to Lock**				
MLK+	Constr.	1,010	1,010	1,010	1,010	1,010	1,010	1,010	1,010	1,010
	p/y	30	757	1,515	2,272	3,030	3,030	3,030	3,030	3,030
	Total	**1,040**	**1,767**	**2,525**	**3,282**	**4,040**	**4,040**	**4,040**	**4,040**	**4,040**
Maintain Closing Regime		0	0	0	0	0	0	0	0	0
Maasvlakte III		3,537	3,729	3,920	4,175	4,366	4,557	4,812	5,003	5,194
Dikes	Constr.	1,657	1,657	1,657	3,266	3,266	3,266	4,875	4,875	4,875
	p/y	29	720	1,439	2,159	2,879	3,598	4,318	5,038	5,758
	Total	**1,686**	**2,377**	**3,096**	**5,425**	**6,145**	**6,865**	**9,193**	**9,913**	**10,633**
KWA+	Constr.	103	103	103	103	103	103	103	103	103
	p/y	2	55	109	164	219	219	219	219	219
	Total	**106**	**158**	**213**	**268**	**322**	**322**	**322**	**322**	**322**
Locks	Constr.	0	0	0	0	2,250	2,250	2,250	2,250	2,250
	p/y	0	0	0	0	11	283	565	848	1,130
	Salinisation	0	0	0	0	-10	-250	-500	-750	-1,000
	Total	**0**	**0**	**0**	**0**	**2,251**	**2,283**	**2,315**	**2,348**	**2,380**
Added damage										
Closures	LG	10	2,558	10,230	43,810	80,382	80,382	80,382	80,382	80,382
	GE	16	3,953	15,810	67,706	124,227	124,227	124,227	124,227	124,227
	Diff	**6**	**1,395**	**5,580**	**23,896**	**43,845**	**43,845**	**43,845**	**43,845**	**43,845**
Locks	LG	0	0	0	0	48	1,188	2,375	3,563	4,750
	CP	0	0	0	0	16	388	775	1,163	1,550
	LG + CP	0	0	0	0	63	1,575	3,150	4,725	6,300
	GE	0	0	0	0	160	3,996	7,993	11,989	15,985
	Diff	**0**	**0**	**0**	**0**	**97**	**2,421**	**4,843**	**7,264**	**9,685**
Cumulative	LG + CP	10	2,558	10,230	43,810	80,445	81,957	83,532	85,107	86,682
	GE	16	3,953	15,810	67,706	124,387	128,223	132,220	136,216	140,212
	Diff	**6**	**1,395**	**5,580**	**23,896**	**43,942**	**46,266**	**48,687**	**51,109**	**53,530**
	Total LG	**6,379**	**10,588**	**19,984**	**56,960**	**97,569**	**100,023**	**104,215**	**106,733**	**109,251**
	Total GE	**6,385**	**11,983**	**25,564**	**80,856**	**141,511**	**146,289**	**152,902**	**157,842**	**162,781**
RCP8.5 Median	year	2100	2125	2150	2175	2200	2225	2250	2275	2300
	SLR (m)	1	1.3	1.6	2	2.3	2.6	3	3.3	3.6
	Closures MLK+ p/y	3.1	10	30	131.3	143	158	160.7	160.7	160.7

Table C.11: Cumulative costs calculation for Pathway D2 in RCP8.5 upper boundary sea level rise situation in M€, see Fig. 2.3.

Pathway D2 - Maintain closing regime and Maasvlakte III

Expenditures		**Switch to Lock**								
MLK+	Constr.	1,010	1,010	1,010	1,010	1,010	1,010	1,010	1,010	1,010
	p/y	30	757	1,515	2,272	3,030	3,030	3,030	3,030	3,030
	Total	**1,040**	**1,767**	**2,525**	**3,282**	**4,040**	**4,040**	**4,040**	**4,040**	**4,040**
Maintain Closing Regime		0	0	0	0	0	0	0	0	0
Maasvlakte III		3,601	3,920	4,175	4,461	4,748	5,131	5,577	5,959	6,342
Dikes	Constr.	1,657	1,657	1,657	3,990	3,990	3,990	6,806	6,806	6,806
	p/y	29	720	1,439	2,159	2,879	3,598	4,318	5,038	5,758
	Total	**1,686**	**2,377**	**3,096**	**6,149**	**6,869**	**7,589**	**11,124**	**11,844**	**12,564**
KWA+	Constr.	103	103	103	103	103	103	103	103	103
	p/y	2	55	109	164	219	219	219	219	219
	Total	**106**	**158**	**213**	**268**	**322**	**322**	**322**	**322**	**322**
Locks	Constr.	0	0	0	0	2,250	2,250	2,250	2,250	2,250
	p/y	0	0	0	0	11	283	565	848	1,130
	Salinisation	0	0	0	0	-10	-250	-500	-750	-1,000
	Total	**0**	**0**	**0**	**0**	**2,251**	**2,283**	**2,315**	**2,348**	**2,380**
Added damage										
MLK+ Closures	LG	10	7,673	41,252	81,149	122,249	122,249	122,249	122,249	122,249
	GE	16	11,858	63,754	125,413	188,930	188,930	188,930	188,930	188,930
	Diff	**6**	**4,185**	**22,501**	**44,263**	**66,681**	**66,681**	**66,681**	**66,681**	**66,681**
Locks	LG	0	0	0	0	48	1,188	2,375	3,563	4,750
	CP	0	0	0	0	16	388	775	1,163	1,550
	LG + CP	0	0	0	0	63	1,575	3,150	4,725	6,300
	GE	0	0	0	0	160	3,996	7,993	11,989	**15,985**
	Diff	**0**	**0**	**0**	**0**	**97**	**2,421**	**4,843**	**7,264**	**9,685**
Cumulative	LG + CP	10	7,673	41,252	81,149	122,312	123,824	125,399	126,974	128,549
	GE	16	11,858	63,754	125,413	189,089	192,926	196,922	200,918	204,915
	Diff	**6**	**4,185**	**22,501**	**44,263**	**66,778**	**69,102**	**71,524**	**73,945**	**76,366**
	Total LG	**6,443**	**15,894**	**51,261**	**95,310**	**140,542**	**143,187**	**148,777**	**151,486**	**154,196**
	Total GE	**6,449**	**20,079**	**73,763**	**139,573**	**207,320**	**212,290**	**220,300**	**225,431**	**230,562**
RCP8.5 Upper bound	year	2100	2125	2150	2175	2200	2225	2250	2275	2300
	SLR (m)	1.1	1.6	2	2.45	2.9	3.5	4.2	4.8	5.4
	Closures MLK+ p/y	3.1	30	131.3	156	160.7	160.7	160.7	160.7	160.7

Table C.12: Cumulative costs calculation for Pathway D2 in RCP8.5 lower boundary sea level rise situation in M€, see Fig. 2.3.

Pathway D2 - Maintain closing regime and Maasvlakte III

Expenditures						**Switch to Lock**				
MLK+	Constr.	1,010	1,010	1,010	1,010	1,010	1,010	1,010	1,010	1,010
	p/y	30	757	1,515	2,272	3,030	3,030	3,030	3,030	3,030
	Total	**1,040**	**1,767**	**2,525**	**3,282**	**4,040**	**4,040**	**4,040**	**4,040**	**4,040**
Maintain Closing Regime		0	0	0	0	0	0	0	0	0
Maasvlakte III		3,282	3,410	3,537	3,665	3,792	3,936	4,079	4,222	4,366
Dikes	Constr.	1,657	1,657	1,657	1,979	1,979	1,979	3,025	3,025	3,025
	p/y	29	720	1,439	2,159	2,879	3,598	4,318	5,038	5,758
	Total	**1,686**	**2,377**	**3,096**	**4,138**	**4,858**	**5,577**	**7,343**	**8,063**	**8,782**
KWA+	Constr.	103	103	103	103	103	103	103	103	103
	p/y	2	55	109	164	219	219	219	219	219
	Total	**106**	**158**	**213**	**268**	**322**	**322**	**322**	**322**	**322**
Locks	Constr.	0	0	0	0	2,250	2,250	2,250	2,250	2,250
	p/y	0	0	0	0	11	283	565	848	1,130
	Salinisation	0	0	0	0	-10	-250	-500	-750	-1,000
	Total	**0**	**0**	**0**	**0**	**2,251**	**2,283**	**2,315**	**2,348**	**2,380**
Added damage										
MLK+ Closures	LG	2	89	243	639	1,431	1,431	1,431	1,431	1,431
	GE	3	138	375	987	2,211	2,211	2,211	2,211	2,211
	Diff	**1**	**49**	**132**	**348**	**780**	**780**	**780**	**780**	**780**
Locks	LG	0	0	0	0	48	1,188	2,375	3,563	4,750
	CP	0	0	0	0	16	388	775	1,163	1,550
	LG + CP	0	0	0	0	63	1,575	3,150	4,725	6,300
	GE	0	0	0	0	160	3,996	7,993	11,989	15,985
	Diff	**0**	**0**	**0**	**0**	**97**	**2,421**	**4,843**	**7,264**	**9,685**
Cumulative	LG + CP	2	89	243	639	1,494	3,006	4,581	6,156	7,731
	GE	3	138	375	987	2,371	6,207	10,203	14,200	18,196
	Diff	**1**	**49**	**132**	**348**	**877**	**3,202**	**5,623**	**8,044**	**10,465**
	Total LG	**6,116**	**7,801**	**9,614**	**11,991**	**16,757**	**19,163**	**22,680**	**25,150**	**27,621**
	Total GE	**6,117**	**7,850**	**9,746**	**12,339**	**17,634**	**22,365**	**28,302**	**33,194**	**38,086**
RCP8.5 Lower bound	year	2100	2125	2150	2175	2200	2225	2250	2275	2300
	SLR (m)	0.6	0.8	1	1.2	1.4	1.625	1.85	2.075	2.3
	Closures MLK+ p/y	0.6	1.8	3.1	8	16	30	80	131.3	143

C.4. INFLUENCE OF ALTERNATIVE LOCATIONS

The four locations opted for in this thesis research predominantly influence the amount of dikes in direct contact with the sea and the amount of shipping prone to hindrance due to a potential closure of MLK+ or waiting time for the implementation of a sea lock. In this section the economical differences between these locations are computed based on the values retrieved in Chapter 4.

First, the amount of kilometres of rural and urban dikes for each respective dike stretch, see Fig. 3.4, are identified, see Table C.13, as these differ in costs per meter of dike heightening. These are then coupled to the four locations as stated in Fig. 6.1 with the current Maeslant barrier as reference location. Whereafter the construction, heightening and maintenance costs of any of the dike stretches, mentioned in Table C.13, in respect to the different locations are coupled to produce economic values, Table C.14. The differences in anticipated costs of dike heightening, regarding sea level rise and varying locations, evidently shows that how further a new replacing structure for the current Maeslant barrier is placed the higher the costs are in terms of dike heightening.

Table C.13: Amount of kilometres attributed to the dike type (rural or urban) for the respective dike stretches as measured in GIS-software based on data provided by Rijkswaterstaat (2020).

Dike stretch	Rural (km)	Urban (km)
14-2	N.A	20.88
14-3	7.78	6.90
14-4	4.50	N.A
17-2	N.A	14.57
17-3	N.A	1.59
18-1	N.A.	5.23
19-1	N.A.	3.95
20-1	3.82	N.A.
20-2	19.60	N.A.
208	N.A	6.2
209	N.A.	10.45

The same procedure is undertaken to derive deviations in hindrance for shipping in economic values. The costs for MLK+ and the respective locations are derived with the aforementioned costs in Section 4.2.1 in which the current Maeslant barrier is the reference situation. The costs regarding the implementation of a sea lock is computed with the baseline stated in Section 4.3.1 in which location C is the reference locations as proposed in Plan Sluizen. The amount of vessels passing the respective locations is derived from Ecorys and Deltares (2012), these are then divided by the reference location to retrieve a multiplication factor for both sea and inland going vessels, leading to an average of the two, see Table C.15. The averaged factor is then multiplied with the reference situation to retrieve estimated economic consequences of the locations, see Table C.16.

The differences for the dikes and hindrance of shipping are then combined for each locations and are represented in Fig. C.24. Concluding, on the left side of Fig. C.24 location A2, in which the MLK+ option is able to completely seal of the estuary, and thus Maasvlakte I and II and the Europoort harbour, seems like the most cost efficient. However, it is possible that the economic consequences for hindrance of shipping at this location is underestimated, as throughout a closure no ships are able to enter and leave the estuary. For the application of a sea lock, this would be the case at location D, right side of Fig. C.24. Needless to say, this location provides no protection for the areas in front of the primary dike-stretches, visible as zone A and B in Fig. 3.2, which is probable to result to hefty flooding damages and resistance of the inhabitants.

Table C.14: Amount of kilometres of dikes changing in respect to the reference situation and amount of costs attributed to the respective locations, in 2020 price levels.

	MLK as reference				**Computed amount of kilometres for costs**			Costs dike heightening		Exploitation costs (MEUR p/y)	
	New dikes (km)		Reduction (km)	Increase (km)	Total dike-sea (km)	With reduction (km)	Total dike-river (km)	(MEUR p/m SLR)		Sea dike	River dike
Location A	Rural	6.5	0	0	34.6	34.6	8.3	Rural	984.2	21.3	5.1
Open Caland canal	Urban	0	4.5	0	16.65	12.15	51.32	Urban	708.9	7.5	31.6
								TOT	**1693.1**	**28.8**	**36.7**
Closed Caland canal	Rural	1	29.6	0	29.1	-0.5	8.3	Rural	-0.1	-0.3	5.1
	Urban	0	14.95	0	16.65	1.7	51.32	Urban	99.2	1.0	31.6
								TOT	**99.1**	**0.7**	**36.7**
Location B	Rural	0	4.5	4.5	32.6	28.1	3.8	Rural	731.1	17.3	2.3
	Urban	0	0	0	16.65	16.65	51.32	Urban	971.4	10.3	31.6
								TOT	**1702.5**	**27.6**	**33.9**
Location C	Rural	0	0	8.3	36.4	36.4	0	Rural	947.0	22.4	0.0
	Urban	0	0	12.2	28.85	28.85	39.12	Urban	1683.3	17.8	24.1
								TOT	**2630.3**	**40.2**	**24.1**
Location D	Rural	0	0	8.3	36.4	36.4	0	Rural	947.0	22.4	0.0
	Urban	0	0	51.32	67.97	67.97	0	Urban	3965.7	41.9	0.0
								TOT	**4912.7**	**64.3**	**0.0**

Table C.15: Amount of vessels prone for hindrance regarding the different locations.

	Sea going vessels passages			Inland vessels passages				
Location A	Amount	**Factor**		Amount	**Factor**		**Average**	
Open Caland canal	57,504	1.7	x	76,691	1.0	x	1.3	Locks
		1.0	x		1.0	x	1.0	MLK+
Closed Caland canal	83,529	2.4	x	76,691	1.0	x	1.7	Locks
		1.5	x		1.0	x	1.2	MLK+
Location B	57,504	1.7	x	76,691	1.0	x	1.3	Locks
Reference MLK+		1.0	x		1.0	x	1.0	MLK+
Location C	34,533	1.0	x	76,691	1.0	x	1.0	Locks
Reference Plan Sluizen		0.6	x		1.0	x	0.8	MLK+
Location D	N.A.	0.0	x	111,621	1.5	x	0.7	Locks
		0.0	x		1.5	x	0.7	MLK+

Table C.16: Economic consequences for shipping for each of the locations in both open/closed and closed strategies, in 2020 price levels. Costs elaborated in Section 4.2.1 and Section 4.3.1, respectively, and derived with the factors in Table C.15.

	Economic consequences for shipping				
Location	**Scenario**		**GE**		**LG**
A1	Lock	426.0	MEUR p/y	126.6	MEUR p/y
A1	MLK+	30.6	MEUR p/3x/y	19.8	MEUR p/3x/y
A2	Lock	546.5	MEUR p/y	162.4	MEUR p/y
A2	MLK+	37.5	MEUR p/3x/y	24.3	MEUR p/3x/y
B	Lock	426.0	MEUR p/y	126.6	MEUR p/y
B	MLK+	30.6	MEUR p/3x/y	19.8	MEUR p/3x/y
C	Lock	319.7	MEUR p/y	95.0	MEUR p/y
C	MLK+	24.5	MEUR p/3x/y	15.8	MEUR p/3x/y
D	Lock	232.7	MEUR p/y	69.1	MEUR p/y
D	MLK+	22.3	MEUR p/3x/y	14.4	MEUR p/3x/y

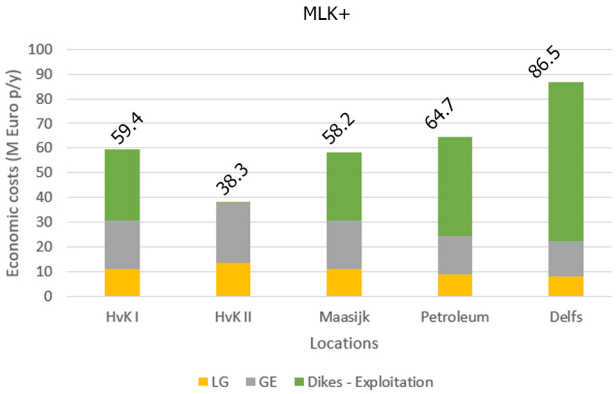

Figure C.24: Yearly economic costs and exploitation costs due to hindrance for shipping and maintenance of the dikes regarding the different locations and open/closed strategies, in 2020 price levels. The costs for MLK+ are based on three closures per year.

From Fig. C.24 it is evident that on the basis of shipping the introduction or continuation of the current open/closable strategy provides the highest economic prospect.

C.5. INFLUENCE OF MAASVLAKTE III

The reduction to hindrance in economic terms for shipping in case of a closure of MLK+ or a lock is determined by utilising Table C.15. For the cumulative expenditures of the main pathways location B is taken as reference, in which a new hydraulic structure would be constructed in the New Waterway. To simplify the reduction of passing vessels that want to reach the port segments behind the barrier or lock, two general assumption are made: all sea going vessels at location B, as determined in Table C.15, utilise the third Maasvlakte instead of the current port segments of Waal-, Eem-, Petroleum- and Botlek ports, equalling to 57,504 and that the current number of passing inland vessels would still want to reach the third Maasvlakte for cargo handling, equalling to 76,691. Both type of vessels and their respective contribution are considered as equal, therefore the reduction implemented is 0.5 times the original consequences as determined in Section 4.2.1 and Section 4.3.1. The fact that these are quite broad assumption is accepted for the time being as further research on the impact of a third Maasvlakte is currently unavailable.

Comparing the total expenditures for Pathways C/C2 and D/D2 in Fig. C.25, under the stated assumptions, visualise the effect of a third Maasvlakte in these pathways. The outcome is logical, as the greatest contributor in the cumulative expenditures graphs are mostly attributed to hindrance for shipping in case of a sea lock and increasing amount of closures per year for MLK+ in these pathways.

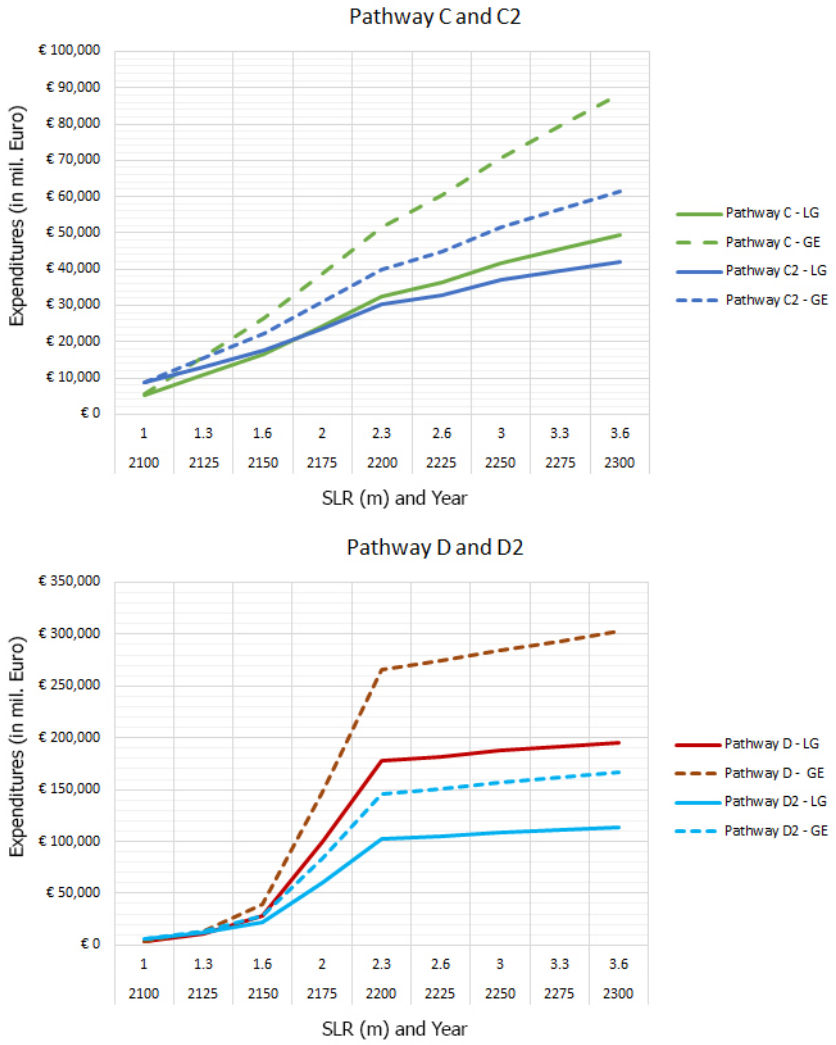

Figure C.25: Comparison of the application of a third Maasvlakte in Pathway C and D in the Deltascenario (low SLR) and in two economic prospects (LG is low growth and GE is high growth scenario).

D | Boundary conditions for the barrier

In this appendix chapter the boundary conditions concerning the natural, artificial and legal boundaries are stated.

D.1. NATURAL

The natural boundary conditions are subdivided into hydraulic, meteorological, geo-technical and geological conditions. The hydraulic conditions include the manner of sea level rise and how this is incorporated into the design of the barrier plus the governing water levels and significant wave heights. In Fig. D.4 the governing water levels are visualised in regard to NAP.

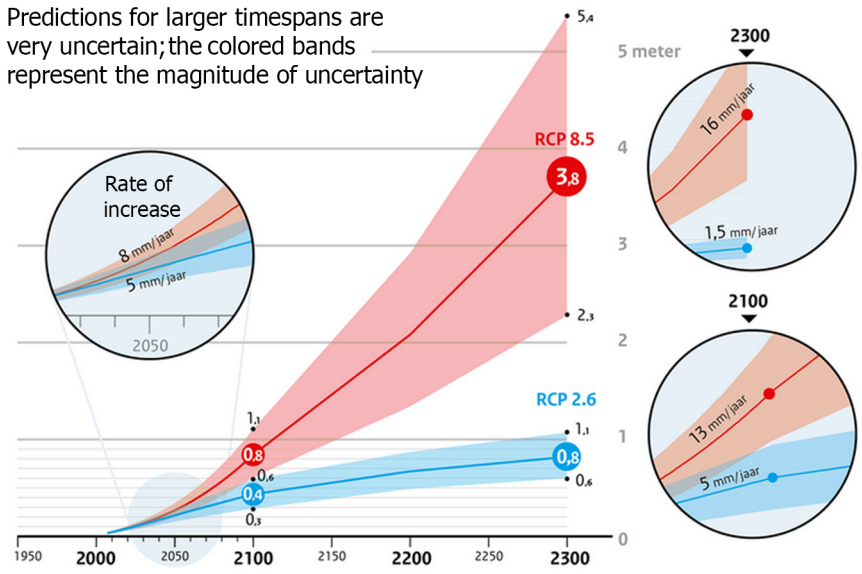

Figure D.1: Predicted sea level rise up to 2300 and rate of sea level increase per year for 2050, 2100 and 2300 according to le Bars (2019). It has to be noted that these estimates are very uncertain due to the large timescale. Retrieved and modified from le Bars (2019).

The current Maeslant barrier is designed to withstand 1:10,000 return storm surge levels which equals to roughly NAP +5 metres, in accordance with Fig. D.2.

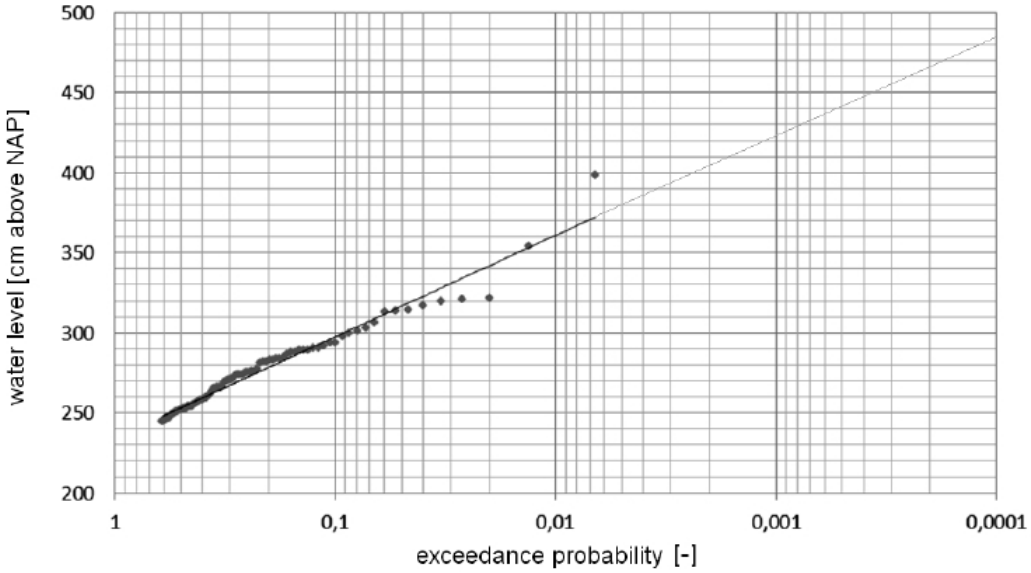

Figure D.2: "Water level exceedance line at Hoek van Holland from measurements of high water levels (> NAP + 2.25 m) between 1863 and 2013, assuming an exponential distribution (Verhagen, 2014), extrapolation by the author of this dissertation." (Voorendt, 2017, p. 258)

And, as has been applied in Huijsman (2021), adding sea level rise predictions to these exceedance probability leads to Fig. D.3.

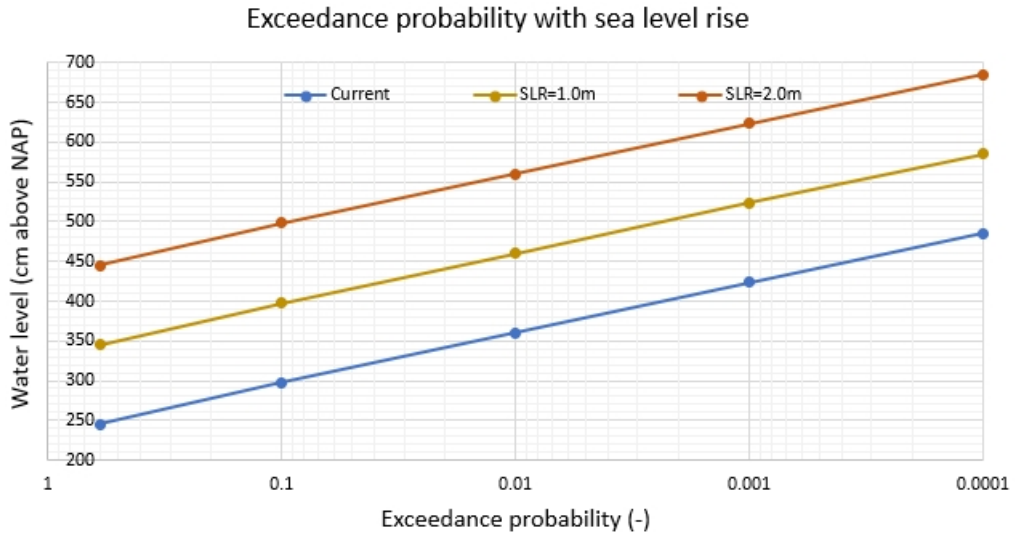

Figure D.3: Water level exceedance lines extrapolated from Fig. D.2 and summed with sea level rise.

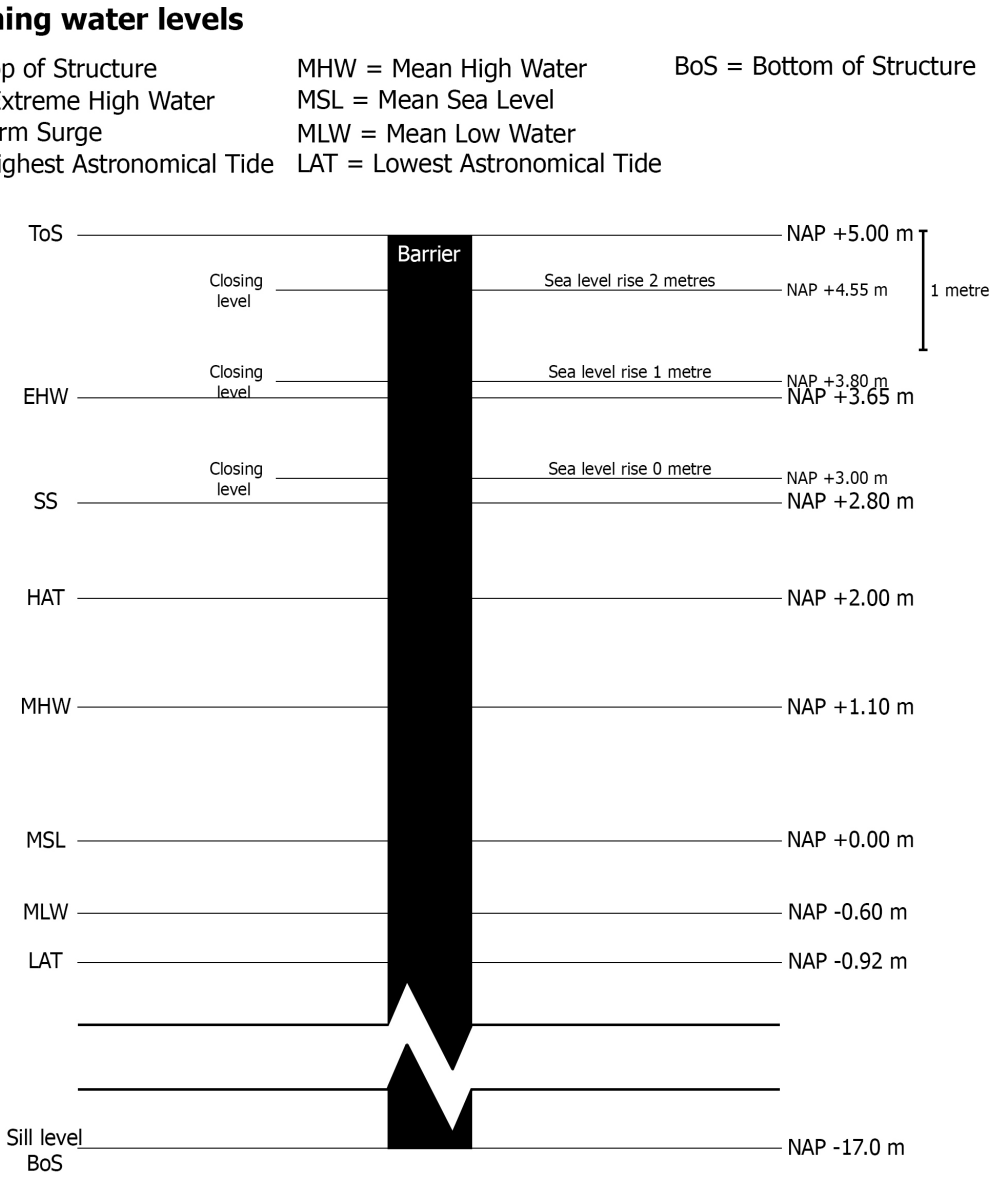

Figure D.4: Hydraulic boundary conditions attributed to the barrier.

The meteorological conditions are retrieved from Port of Rotterdam (2012) near Rozenburg, a village situated in the vicinity of the current Maeslant barrier, which presents the velocity, directions and distributions of the wind components, Fig. D.5. Moreover, the geo-technical properties are retrieved from a CPT test taken at the current Maeslant barrier and visualised in Fig. D.6. The soil properties which can be attributed to the different layers of soil are stated in Fig. D.7. Lastly, the geological conditions, i.e. earthquakes, are presented in Fig. D.8.

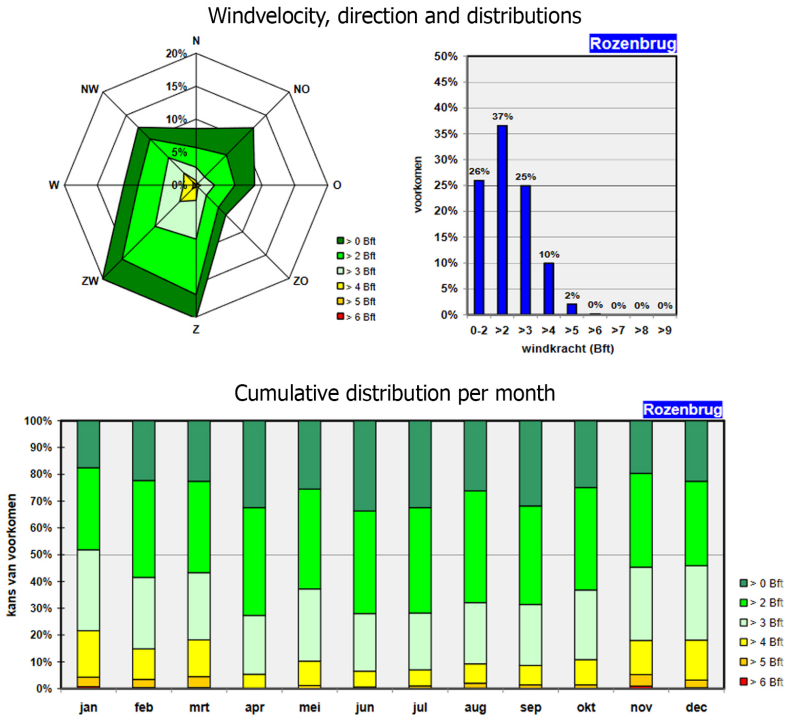

Figure D.5: Meteorological conditions at Rozenburg. Retrieved from Port of Rotterdam (2012, p.87).

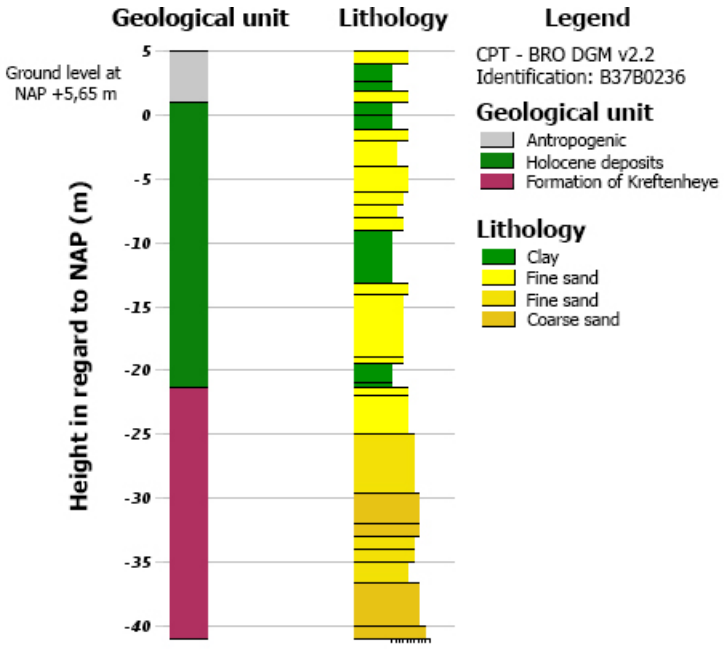

Figure D.6: Soil layers at the current Maeslant barrier. Retrieved and modified from DINOloket (nd).

Soil type			Representative value [a] of the soil property											
Main type	mix	consis-tency [b]	γ [c] kN/m³	γ_{sat} kN/m³	q_c [d,e] Mpa	C'_p -	C'_s -	$C_c/(1+e_0)$ [f]	C_α [f] -	$C_{\alpha v}/(1+e_0)$ [f] -	E_{100} [g,h] Mpa	φ' [g] °	c' kPa	c_u ($= f_{cu;k}$) kPa
gravel	slightly silty	loose	17	19	15	500	∞	0,0046	0	0,0015	45	32,5	0	-
		moderate	18	20	25	1000	∞	0,0023	0	0,0008	75	35	0	-
		solid	19 20	21 22	30	1200 1400	∞	0,0019 0,0016	0	0,0006 0,0005	90	37,5 40	0	-
	greatly silty	loose	18	20	10	400	∞	0,0058	0	0,0019	30	30	0	-
		moderate	19	21	15	600	∞	0,0038	0	0,0013	45	32,5	0	-
		solid	20 21	22 22.5	25	1000 1500	∞	0,0023 0,0015	0	0,0008 0,0005	75 110	35 40	0	-
sand	clean	loose	17	19	5	200	∞	0,0115	0	0,0038	15	30	0	-
		moderate	18	20	15	600	∞	0,0038	0	0,0013	45	32,5	0	-
		solid	19 20	21 22	25	1000 1500	∞	0,0023 0,0015	0	0,0008 0,0005	75 110	35 40	0	-
	slightly silty clayey		18 19	20 21	12	450 650	∞	0,0051 0,0035	0	0,0017 0,0012	35 50	27 32,5	0	-
	greatly silty clayey		18 19	20 21	8	200 400	∞	0,0115 0,0058	0	0,0038 0,0019	15 30	25 30	0	-
loam [f]	slightly sandy	weak	19	19	1	25	650	0,0920	0,0037	0,0307	2	27,5 30	0	50
		moderate	20	20	2	45	1300	0,0511	0,0020	0,0170	3	27,5 32,5	1	100
		solid	21 22	21 22	3	70 100	1900 2500	0,0329 0,0230	0,0013 0,0009	0,0110 0,0077	5 7	27,5 35	2,5 3,8	200 300
	greatly sandy	-	19 20	19 20	2	45 70	1300 2000	0,0511 0,0329	0,0020 0,0013	0,0170 0,0110	3 5	27,5 35	0 1	50 100
clay	clean	weak	14	14	0.5	7	80	0,3286	0,0131	0,1095	1	17,5	0	25
		moderate	17	17	1	15	160	0,1533	0,0061	0,0511	2	17,5	5	50
		solid	19 20	19 20	2	25 30	320 500	0,0920 0,0767	0,0037 0,0031	0,0307 0,0256	4 10	17,5 25	13 15	100 200
	slightly sandy	weak	15	15	0.7	10	110	0,2300	0,0092	0,0767	1,5	22,5	0	40
		moderate	18	18	1.5	20	240	0,1150	0,0046	0,0383	3	22,5	5	80
		solid	20 21	20 21	2.5	30 50	400 600	0,0767 0,0460	0,0031 0,0018	0,0256 0,0153	5 10	22,5 27,5	13 15	120 170
	greatly sandy		18 20	18 20	1	25 50	320 1680	0,0920 0,0164	0,0037 0,0007	0,0307 0,0055	2 5	27,5 32,5	0 1	0 10
	organic	weak	13	13	0.2	7.5	30	0,3067	0,0153	0,1022	0,5	15	0 1	10
		moderate	15 16	15 16	0.5	10 15	40 60	0,2300 0,1533	0,0115 0,0077	0,0767 0,0511	1 2	15	0 1	25 30
peat	not preloaded	weak	10 12	10 12	0.1	5 7.5	20 30	0,4600 0,3067	0,0230 0,0153	0,1533 0,1022	0,2 0,5	15	1 2,5	10 20
	moderately preloaded	moderate	12 13	12 13	0.2	7.5 10	30 40	0,3067 0,2300	0,0153 0,0115	0,1022 0,0767	0,5 1,0	15	2,5 5	20 30
variation coefficient			0,05		-	0,25						0,10	0,20	

[a] The table gives the low and the high characteristic value of the average of the soil type concerned. If an increase of the characteristic value of a soil property would lead to a situation that is more unfavourable than the given low value for that property, the value on the right should be used. If there is no value mentioned on the right side of a cell, then the value just below it should be used. This is, for example, the case for negative friction on a pile where a higher value for φ', c' and c_u also results in a high value of the negative friction. The table gives the high characteristic average values for $C_c/(1+e_0)$, C_α and $C_{\alpha v}/(1+e_0)$.
[b] Loose: $0 < R_s < 0{,}33$; moderate: $0{,}33 < R_s < 0{,}67$; solid: $0{,}67 < R_s < 1{,}00$.
[c] The γ-values are applicable to a natural moisture content.
[d] The values for q_c (cone resistance) given in this table should be considered as entry values for use of the table and should not be used in calculations.
[e] The values concern saturated loam.
[f] The C_α-values are valid for a trajectory of stress increase of at least 100%.
[g] For gravel, sand and to a lesser extent also for loam and sandy clay, q_c, E_{100}, φ' and the compressibility coefficients C'_p, $C_c/(1+e_0)$ and $C_{\alpha v}/(1+e_0)$ are normalised for an effective soil stress σ'_v of 100 kPa. In that sense the equation $q_{c;table} = q_{c;measured} \cdot C_{qc}$ should be used, where $C_{qc} = (100/\sigma'_v)^{0,67}$. For an angle of internal friction φ' and cohesion c' it applies that these are dependent on the consistency of the soil. This implies that this conversion is also needed for φ' and c'. If $q_{c;100}$ would become larger than the value given in the table, the value given in the lowest row of the concerning soil type should be used.
[h] The Youngs' modulus in case of recurrent stress can be considered to be three times the given value.

Example: In clean sand at a depth of 5 m below water it is measured that: $q_{c;field} = 9$ MPa and $\sigma'_v = 50$ kPa. C_{qc} then is $2^{0,67} = 1{,}6$ and $q_{c;table} = 9 \cdot 1{,}6 = 14.4$ MPa. This means that $E = 45$ MPa, $\varphi' = 32{,}5°$, $C'_p = 600$, $C_c/(1+e_0) = 0{,}0038$ and $C_{\alpha v}/(1+e_0) = 0{,}0013$.

Figure D.7: Indicative soil properties according to Eurocode 7 NEN-EN9997 (to be verified by on-site soil investigation). Retrieved from Molenaar and Voorendt (2019, p. 184).

Intensity	Acceleration m/s^2
VIII	2
VII	1
VI	0,5
V	0,2
IV	0,1
III	0,05
II	0,02
I	0,01

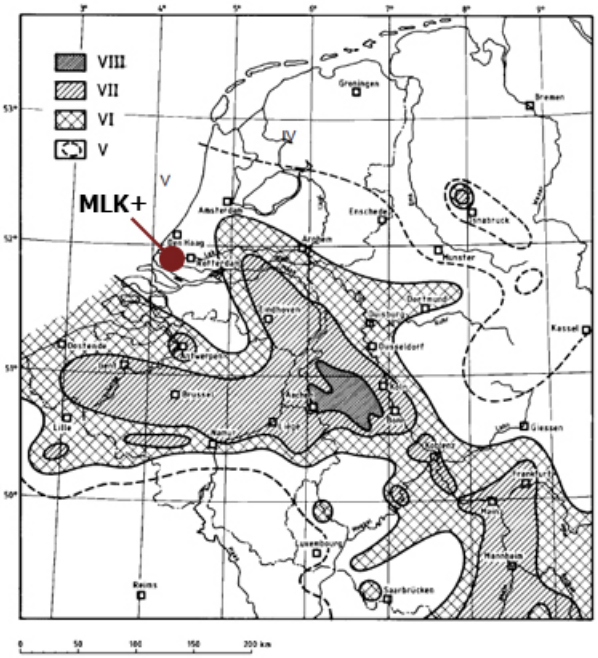

Figure D.8: Intensity regions for earthquakes in the Netherlands (Modified Mercalli Scale). The red dot represents the location of MLK+, which is situated in intensity region V (0.2 m^2/s). Retrieved and modified from Peters (2020, p. 160).

D.2. ARTIFICIAL

The nautical conditions play a dominant role. The intensity and vessels classes utilising the New Waterway are defined in Section 3.5. Some normative values from this section are stated:

- Intensity in 2010: 57,504 vessels
- Intensity in 2050: high growth 87,802 and low growth 60,076 vessels
- Largest class: Class 4, length > 300 m and draught < 14.3 m

D.3. LEGAL

The legal boundary conditions are kept concise, the structure should adhere to the following standards:

- EN Eurocode (European Commission, nd)
- ROK1.4 (Rijkswaterstaat, 2017)
- Norms in accordance with the bottom figure of Fig. 3.4 and Waterveiligheidsportaal (nd):
  - Signalling norm: 1:100,000
  - Lower limit threshold norm: 1:30,000
- High Water Levels with an exceedance probability of 1:10,000, Fig. D.2 and Fig. D.3

E | Elaboration of MCA scores barrier types

In this appendix chapter an elaboration of the multi criteria analysis for each barrier type and criteria is supplied in Appendix E.1 to Appendix E.7

E.1. ROLLING GATES

- Maintenance: the rolling gates can be maintained without interference in the docks constructed on the embankments, however, the guidance rails on the bottom of the river bed need to be maintained underwater resulting in a score of 3 out of 4.
- Hindrance: Little interference to vessels utilising the New Waterway during construction, with the exception of the installation of the needed guidance rails and the required amount of space for the storage docks. Resulting in a score of 2 out of 4.
- Experience and knowledge: Rolling gates are a proven design, applied in various other projects. One of the largest similar projects is the sealock IJmuiden in IJmuiden. Resulting in a score of 4 out of 4.
- Force distribution: The large hydrostatic forces will lead to immense transverse and bending forces on this type of gate, requiring an over-dimensioned design. Resulting in a score of 1 out of 4.
- Reliability: The gates themselves and the rolling mechanisms might be quite reliable, as is the probable case with the sealock IJmuiden, as the chance of blockade, due to sediment, on the guidance system is when used often is low. However, if the gates are opened for quite some time, more sediment is able to accumulate. Resulting in a score of 2 out of 4.
- Dynamic robustness: As the gates are over-dimensioned little room is left to upgrade the barrier over time, with exception of the gate height and bed protection. However, due to the necessity to over-dimension the barrier this might prove to be expensive. Resulting in a score of 2 out of 4.

E.2. FLOATING BARGE GATE

- Maintenance: The gate itself is insensitive to silting and sediment as no guidance system is needed due to the use of buoyancy to displace the barrier. Moreover, the moving parts are located above water. Resulting in a score of 3 out of 4.
- Hindrance:
- Experience and knowledge: Similar to the rolling gates, however, a gate of this size has not been constructed before. Results in a score of 3 out of 4.
- Force distribution: The design loads are difficult to define as these are heavily influences by the closing procedure. Moreover, due to the horizontal nature of the barrier, as is the case with the rolling gates, a over-dimensioned gate is likely to be required.

- Reliability: The reliability is likely to be higher than that of the rolling gates due to the abduction of the guidance system. However, it has to be bared in mind, that if the single hinge of the barrier fails, it is unable to close of the waterway. Moreover, the control of the barrier during the closing procedure is likely to be a difficult one. Resulting in a score of 2 out of 4.
- Dynamic robustness: As the gates are over-dimensioned little room is left to upgrade the barrier over time, with exception of the gate height and bed protection. However, due to the necessity to over-dimension the barrier this might prove to be expensive. Resulting in a score of 2 out of 4.

E.3. FLOATING SECTOR GATES

- Maintenance: The gates rest in a dry dock on the side of the embankment providing easy access for required maintenance. The gate itself is insensitive to silting and sediment as no guidance system is needed due to the use of buoyancy to displace the barrier. Moreover, the moving parts are located above water. Resulting in a score of 4 out of 4.
- Hindrance: Obstruction to vessels utilising the New Waterway is expected to be minimal as construction is done on the dry docks on the sides of the embankments. Resulting in a score of 3 out of 4.
- Experience and knowledge: Being similar to the current Maeslant barrier and many lessons learned, especially from the operating BOS/BES system, should prove that experience and knowledge is readily available. Resulting in a score of 4 out of 4.
- Force distribution: Due to the radial design of the gates the horizontal hydraulic forces concentrate into a single point, reducing bending forces. Although all horizontal forces rely on the ball hinge connection of the barrier. Resulting in a score of 3 out of 4.
- Reliability: The current Maeslant barrier is estimated to have a closing failure probability of 1 out of 100. Making it reliable if the number of closures is low, as stated in Section 4.2.2 the amount of closures increase to 3 times per year, calling for the necessity to increase the overall closing failure probability. Resulting in a score of 3 out of 4.
- Dynamic robustness: Compared to the previously mentioned barrier types, this type is relatively efficient regarding the distribution of forces. The gate height, foundation and steel trusses connecting the gates with the ball hinge, as an example, could be strengthened over time. The ball hinge, however, is likely to be constructed quite conservative. Resulting in a score of 3 out of 4.

E.4. DRIVEN SECTOR GATES

- Maintenance: The gates rest in a wet dock on the side of the embankment making maintenance more difficult. The gate itself is sensitive to silting and sediment as a guidance system is needed to displace the barrier. Resulting in a score of 2 out of 4.
- Hindrance: Obstruction to vessels utilising the New Waterway is expected to be higher when compared to the floating sector, as construction is done in the wet docks on the sides of the embankments. Resulting in a score of 2 out of 4.
- Experience and knowledge: Being similar to the current Maeslant barrier and many lessons learned, especially from the operating BOS/BES system, should prove that experience and knowledge is readily available. Resulting in a score of 4 out of 4.
- Force distribution: Similar to the floating sector. Resulting in a score of 3 out of 4.

- Reliability: Similar to the floating sector, with the addition that the required guidance system on the bed of the river could be blocked by sediment. Resulting in a score of 2 out of 4.
- Dynamic robustness: Similar to the floating sector. Resulting in a score of 3 out of 4.

E.5. PNEUMATIC TUMBLE GATES

- Maintenance: The entirety of the barrier is located on the bottom of the riverbed. Making it more difficult to properly inspect the numerous tumble gates. However, the gates themselves are raised by buoyancy and not a guiding or rising mechanism. Resulting in a score of 2 out of 4.
- Hindrance: Obstruction to vessels utilising the New Waterway is expected to be quite high during installation and construction of the barrier. Moreover, maintenance is performed in the pathway of the New Waterway. Resulting in a score of 2 out of 4.
- Experience and knowledge: Being similar to the MOSE barrier in Venice recent experience and knowledge of this barrier type exists. Resulting in a score of 3 out of 4.
- Force distribution: The barrier balances between the high and low water level by utilising buoyancy. However, the barrier is quite sensitive to negative head. Resulting in a score of 3 out of 4.
- Reliability: Due to the parallel system, as the gate exists out of multiple gate segments (approx. 25), failure of the entire barrier is unlikely. Sediment and silting might prove to form an issue over time. Resulting in a score of 4 out of 4.
- Dynamic robustness: Strengthening or upgrading components requires an conservative spacious design of the sill in which the gates rests if, as an example, the gates are heightened. The number of components that can be adapted are limited. Resulting in a score of 2 out of 4.

E.6. HYDRAULIC TUMBLE GATES

- Maintenance: Similar to the pneumatic tumble gate with the addition of a moving hydraulic system that operates the barrier. Resulting in a score of 1 out of 4.
- Hindrance: Similar to the pneumatic tumble gate. Resulting in a score of 2 out of 4.
- Experience and knowledge: Similar to the pneumatic tumble gate. Resulting in a score of 2 out of 4.
- Force distribution: The resulting hydraulic forces are likely to rest on 2 points, connection with the sill and the gate and on the attachment of the hydraulic arm. Compared to the pneumatic tumble gates, due to the hydraulic arm attachment it is less sensitive to negative head. Resulting in a score of 2 out of 4.
- Reliability: Similar to the pneumatic tumble gate. Resulting in a score of 4 out of 4.
- Dynamic robustness: Similar to the pneumatic tumble gates, with the addition that it likely that the hydraulic arms have to be designed conservative. Resulting in a score of 2 out of 4.

E.7. INFLATABLE RUBBER BARRIER

- Maintenance: Although the rubber membrane is situated entirely underwater, it is presumable easy to replace and minimal maintenance is required. However, it has to be determined whether that is also the cases with the required width of the membrane. Resulting in a score of 3 out of 4.

- Hindrance: Similar to the pneumatic and hydraulic tumble gate. Resulting in a score of 2 out of 4.
- Experience and knowledge: The rubber membrane is relatively new, the Rampsol barrier near Zwolle is one of the applications of the barrier, albeit of a considerate smaller size. Resulting in a score of 2 out of 4.
- Force distribution: The rubber membrane balances between high and low water levels with buoyancy. According to Riteco (2017) peak pressures could form in the folds of the rubber membrane. Resulting in a score of 2 out of 4.
- Reliability: The reliability of the barrier is high as no complex movable components are required. However, if at one point the barrier is damaged due to debris or collisions the entire barrier is prone to deflate leading to a failure of the barrier. Resulting in a score of 4 out of 4.
- Dynamic robustness: Easily adaptable by replacing entire rubber membrane if necessary. Resulting in a score of 4 out of 4.

F | Verification of the computational model and components

Within the computational model the loading conditions and resistances are coupled and should be verified. In this appendix the relationships between these two are stated and verified. Worthwhile to note, is that the computations that follow in this appendix are also how the computations are integrated into the computational model. Furthermore, some adaptations to the structural components of the barrier are verified within this chapter, as an example, the option to add an extra steel truss in Appendix F.3.1.

F.1. SIGNIFICANT WAVE HEIGHT

The significant wave height (H_s) impacts the barrier, when closed, from both the sea and river side. As a first estimate the significant wave height is determined by utilising the improved equation by Young and Verhagen (1996) and Breugem and Holthuijsen (2006):

$$\tilde{H} = \tilde{H}_{\infty} \left\{ \tanh\left(0,343\tilde{d}^{114}\right) \cdot \tanh\left(\frac{4,41 \cdot 10^{-4} \tilde{F}^{0,79}}{\tanh\left(0,343\tilde{d}^{1,14}\right)} \right) \right\}^{0.572} \tag{F.1.1}$$

$$\tilde{T} = \tilde{T}_{\infty} \left\{ \tanh\left(0,10\tilde{d}^{2,01}\right) \cdot \tanh\left(\frac{2,77 \cdot 10^{-7} \tilde{F}^{1,45}}{\tanh\left(0,10\tilde{d}^{2,01}\right)} \right) \right\}^{0,187} \tag{F.1.2}$$

Where:

- $\tilde{H} = \frac{g \cdot H_{m0}}{U_{10}^2}$
- $\tilde{T} = \frac{g \cdot T_p}{U_{10}}$
- $\tilde{F} = \frac{g \cdot F}{U_{10}^2}$
- $\tilde{d} = \frac{g \cdot d}{U_{10}}$
- F the distance travelled by wind across open water (fetch)
- d is the average water depth = 22 metres during storm surge
- U_{10} is the wind velocity at 10 metres altitude
- T_p is the peak period
- "$\tilde{H}_{\infty}$ is the dimensionless wave height at deep water = 0.24" (Molenaar and Voorendt, 2019, p. 99)
- "$\tilde{T}_{\infty}$ is the dimensionless wave height at deep water = 7.69" (Molenaar and Voorendt, 2019, p. 99)
- H_{m0} is the significant wave height

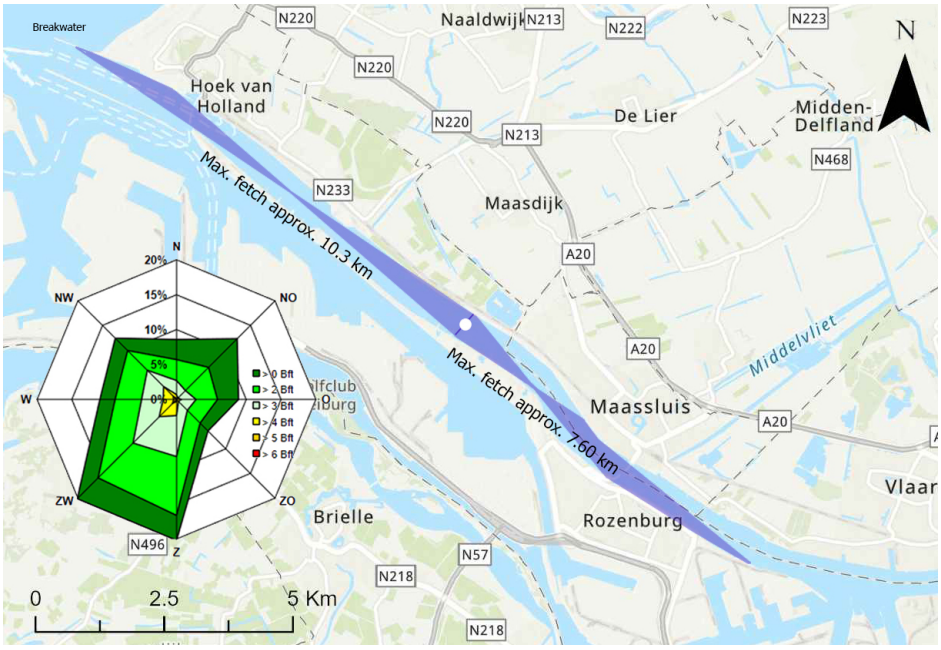

Figure F.1: Approximate maximum fetch for the wind induced waves impacting the barrier on both sides. With the wind speeds on the Beaufort scale measured at Rozenburg.

The approximate fetch of the wind induced waves are measured in GIS and visualised in Fig. F.1. However, in accordance with Saville (1954), the max. fetch in canals can not exceed five times the width (≈ 2.0 km). With a wind velocity of Bft 6 (≈ 14.0 m/s) at the sea side results in a design wave height of 0.97 metres. Comparing this estimation with a computed estimation of the significant wave height with a SWAN-model at the sea lock of IJmuiden, Fig. F.2, it is safe to say that the design wave heights are relatively in the same order of magnitude and are assumed valid.

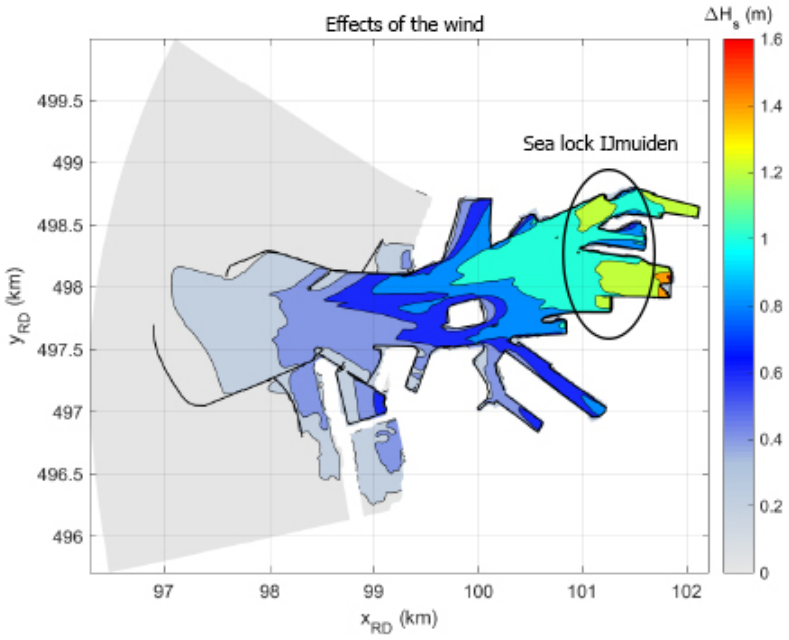

Figure F.2: Difference on the significant wave heights due to wind induced waves with U_{10} is 25 m/s. Retrieved from Aktis Hydraulics (2018, p. 16).

F.2. HYDRAULIC LOADS

In this section the manner of determining the positive and negative hydrostatic loads acting on the barrier are shown, Appendix F.2.1 and Appendix F.2.2, respectively, along a hydraulic boundary condition. The reason these loads are not determined for the normative conditions, is due to the fact that with an uncertain sea level in the future, it is unknown what the normative boundary conditions are. The reliability model eventually determines what dimensions the barrier should adhere to and thus, the manner shown in this section is integrated into the model. The static loads are followed by the loads due to wave impacts on the barrier in Appendix F.2.3.

F.2.1. POSITIVE HYDROSTATIC LOADS

Positive hydrostatic loads are defined as the horizontal loads due to the water pressure in which the water level at the sea side (A) of the barrier is higher than the water level at the back side (B) of the barrier. Initially, a storm surge of NAP +5.0 metres is assumed with a water level of NAP +3.0 metres on the back side of the barrier. The sill is located at NAP -17.0 metres, as is shown in Fig. F.3.

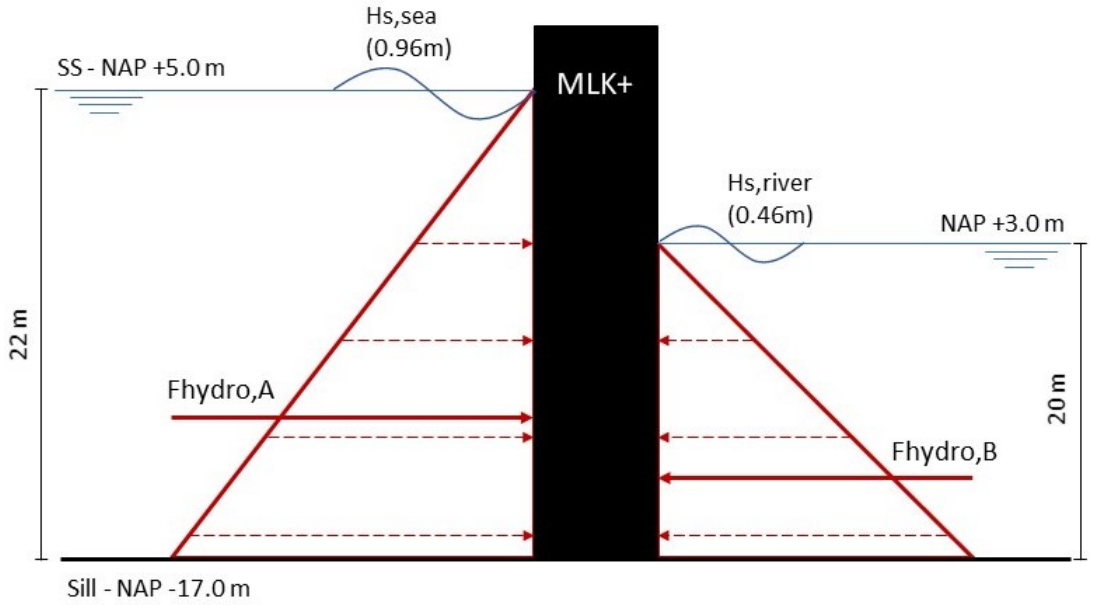

Figure F.3: The hydrostatic pressures and forces on the barrier. Not to scale.

With the following properties:

- $\rho_{saltwater} = 1025$ kg/m^3
- $\rho_{freshwater} = 1000$ kg/m^3

The hydrostatic pressures become:

$$p_{hydro,A} = \rho_{saltwater} \cdot g \cdot \Delta H_A = 1025 \cdot 9.81 \cdot 22 = 221 \text{ kpa per metre width} \quad \text{(F.2.1)}$$

$$p_{hydro,B} = \rho_{saltwater} \cdot g \cdot \Delta H_B = 1025 \cdot 9.81 \cdot 20 = 201 \text{ kpa per metre width} \quad \text{(F.2.2)}$$

And the resulting hydrostatic forces:

$$F_{hydro,A} = 0.5 \cdot p_{hydro,A} \cdot \Delta H_A = 0.5 \cdot 221 \cdot 22 = 2433 \ kN \text{ per meter width} \quad \text{(F.2.3)}$$

$$F_{hydro,B} = 0.5 \cdot p_{hydro,A} \cdot \Delta H_B = 0.5 \cdot 201 \cdot 20 = 2011 \ kN \text{ per meter width} \quad \text{(F.2.4)}$$

Subtracting $F_{hydro,B}$ from $F_{hydro,A}$ results in:

$$F_{hydro,Res} = F_{hydro,A} - F_{hydro,B} = 422.3\ kN \text{ per meter width} \tag{F.2.5}$$

The eccentricity of the resulting hydrostatic forces leads to a bending moment, referenced at the bottom of the barrier:

$$M_{z,Res} = F_{hydro,A} \cdot \frac{1}{3} \cdot \Delta H_A - F_{hydro,B} \cdot \frac{1}{3} \cdot \Delta H_B = 4437.6\ kNm \text{ per meter width} \tag{F.2.6}$$

If sea level rise and the changes to the closing regime are added to the hydrostatic calculations, the forces in Fig. F.4 are derived. In the computation the amount of sea level rise is added to the Storm Surge (SS) water level, and at two instances the water level of the river side (B) are increased: 1 metre SLR leads to a water level of NAP +3.80 m and 2 metres SLR leads to a water level of NAP +4.55 m. With Fig. F.4 it can be deducted that the altercations in the closing regime heavily influence the increase of the hydrostatic forces.

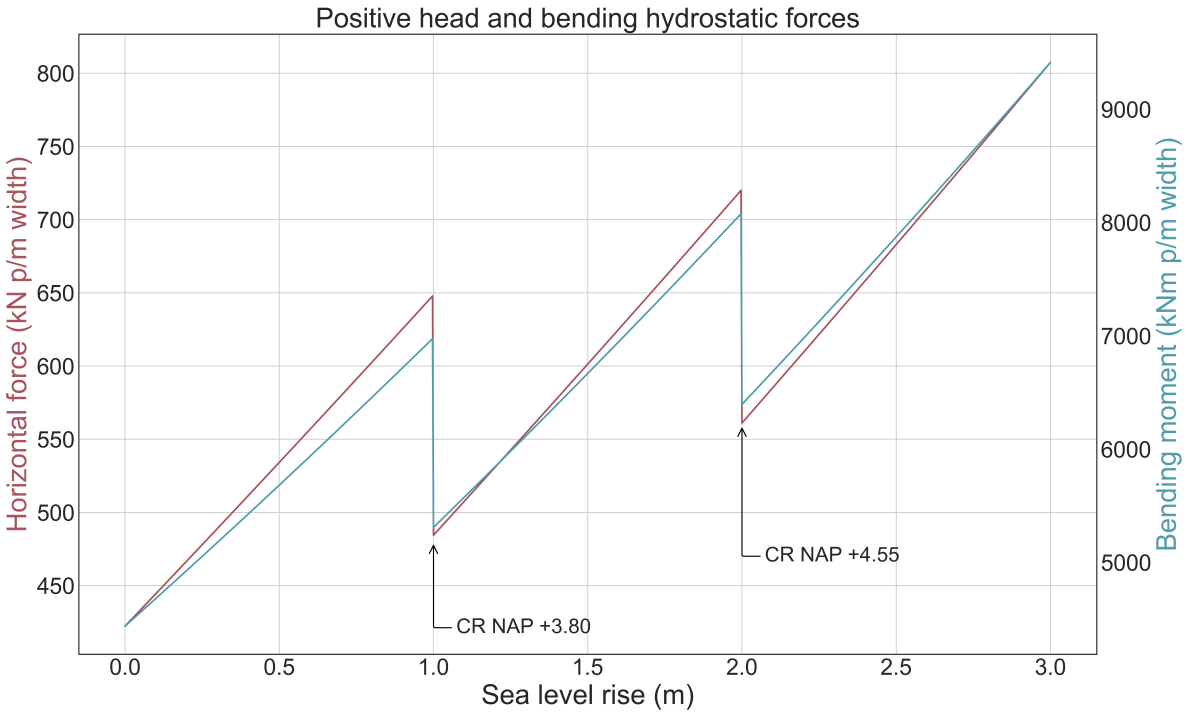

Figure F.4: The positive hydrostatic loads under the influence of the closing regime (CR) and sea level rise.

F.2.2. NEGATIVE HYDROSTATIC LOADS

The calculated forces above are repeated in a situation where the water level at B surpasses that of A. This is the case when the water at the sea side of the barrier retreats due to the passing of the storm and/or low water tide (ebb). In the most severe situation a Lowest Astronomical Tide of NAP -0.92 m could be reached. Thus the resulting hydrostatic forces for this situation are calculated:

$$p_{hydro,A} = \rho_{saltwater} \cdot g \cdot \Delta H_A = 1025 \cdot 9.81 \cdot 16.08 = 162\ kpa \tag{F.2.7}$$

$$p_{hydro,B} = \rho_{saltwater} \cdot g \cdot \Delta H_B = 1025 \cdot 9.81 \cdot 20 = 201\ kpa \tag{F.2.8}$$

And the resulting hydrostatic forces:

$$F_{hydro,A} = 0.5 \cdot p_{hydro,A} \cdot \Delta H_A = 0.5 \cdot 162 \cdot 16.08 = 1300\ kN \text{ per meter width} \tag{F.2.9}$$

$$F_{hydro,B} = 0.5 \cdot p_{hydro,A} \cdot \Delta H_B = 0.5 \cdot 201 \cdot 20 = 2011\ kN \text{ per meter width} \tag{F.2.10}$$

Subtracting $F_{hydro,B}$ from $F_{hydro,A}$ results in:

$$F_{hydro,Res} = F_{hydro,A} - F_{hydro,B} = -711.1\ kN \text{ per meter width} \tag{F.2.11}$$

If sea level rise and the changes to the closing regime are added to the hydrostatic calculations, the forces in Fig. F.5 are derived. In the computation the amount of sea level rise is added to the Lowest Astronomical Tide (LAT) water level, and at two instances the water level of the river side (B) are increased: 1 metre SLR leads to a water level of NAP +3.80 m and 2 metres SLR leads to a water level of NAP +4.55 m. From Fig. F.5 it can be deducted that the negative head increases when the closing regime is altered, compared to the positive head which decreases after altercations. Of course, the value of 700 MN of negative head seems a bit extreme, the occurrence of negative head mostly depends on various factors, e.g. functional aspect, when and how does the barrier open again and the water level during ebb. It should therefore be noted that this is the most extreme negative head that can occur.

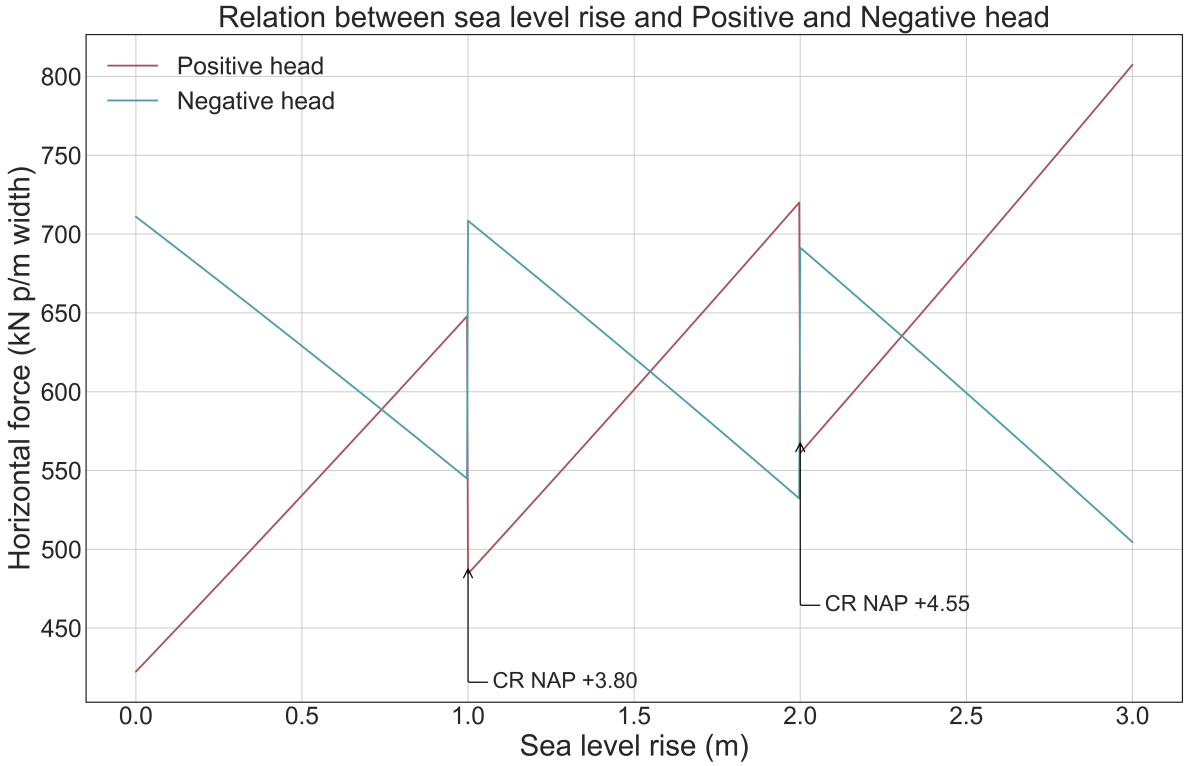

Figure F.5: The positive and negative hydrostatic loads under the influence of the closing regime and sea level rise. CR is instigates the altercations to the closing regime of the barrier influencing the water level on the riverside of the barrier.

F.2.3. WAVE IMPACT

The horizontal wave impact is determined with Sainflou. Sainflou is a simple approximation to determine the total force on a wall for non-breaking waves. The distribution of forces, due to a wave, are divided in three segments: top triangle (above water level), bottom triangle (below water

level) and the rectangular distribution (below water level), as visualised in Fig. F.6.

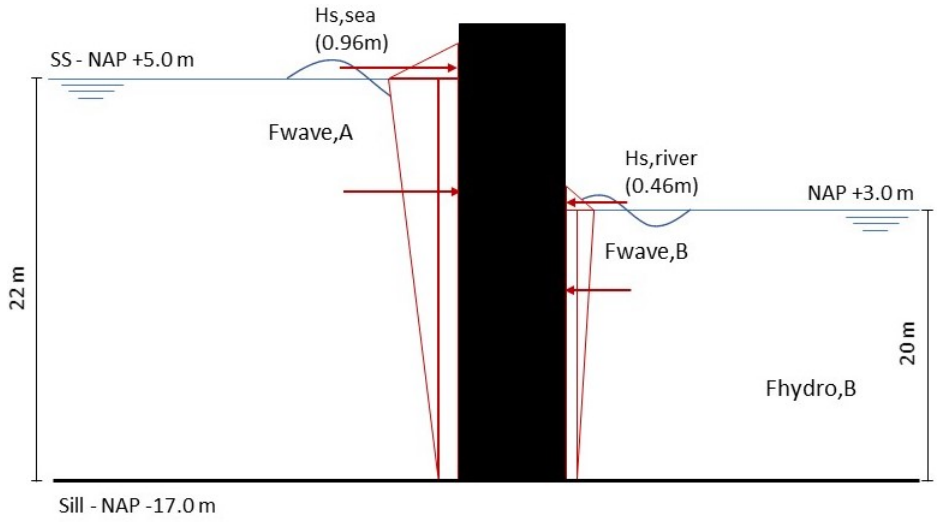

Figure F.6: The wave loads on the barrier. Not to scale.

With a significant wave of 0.96 m at the sea side the impact force can be determined. For the top triangle:

$$p_{max,A} = 2 \cdot \rho_{saltwater} \cdot g \cdot H_s = 19.3\ kN/m^2$$
$$F_{top,A} = \frac{1}{2} \cdot p_{max,A} \cdot H_s = 9.3\ kN \text{ per metre width}$$

And the bottom triangle plus rectangle:

$$d_1 = \Delta H_A - \frac{1}{2} \cdot H_s = 21.52\ m$$
$$k = 0.32, \text{ see Appendix F.5.1}$$
$$p_{bottom,A} = \frac{p_{max,A}}{cosh(k \cdot d1} = 0.0394\ kN/m^2$$
$$F_{bottom,A} = (p_{bottom,A} + \frac{p_{max,A}}{2}) \cdot \Delta H_A = 213.2\ kN \text{ per metre width}$$

This results in a cumulative horizontal force for $F_{waves,A}$ = 222.5 kN per metre width. At this stage the influence of sea level rise on the impact of the wave is unclear and undetermined.

F.3. STEEL TRUSSES

In this section the adaptation of the steel trusses, by adding an additional truss, is discussed in Appendix F.3.1. Followed by the verification of the steel trusses (Appendix F.3.2) for the preferred design from Chapter 10.

F.3.1. STEEL TRUSSES ADAPTATION

The addition of an extra steel truss in the middle of the sector gate is verified in this subsection, see Fig. F.7. The aim of the extra truss is to reduce the compressive force acting on the other two steel trusses. However, it is also possible that the addition of this truss interferes with the flow of forces in the arch of the sector gate. Sector gates, and thus the arched shaped gate, naturally do not develop bending moment forces due to the shape of the gate (Welleman, 2020), making it quite efficient in diverting hydrostatic forces.

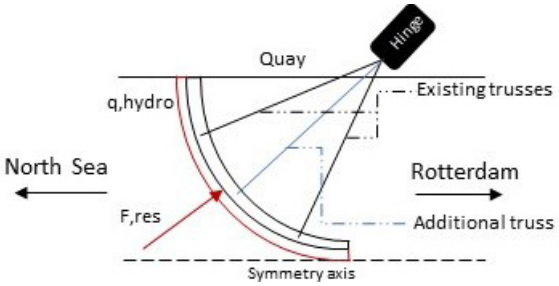

Figure F.7: Schematised overview of the structure with an additional truss.

In Fig. F.8 a single sector gate is modelled in MatrixFrame where the placement of the three trusses is evenly spaced along the arch (≈ 50 metres). An equally distributed force of 425 kN/m, see Fig. F.5 at 0 m sea level rise, representing the hydraulic loading on the sector gates during closure, is placed perpendicular on and along the arch.

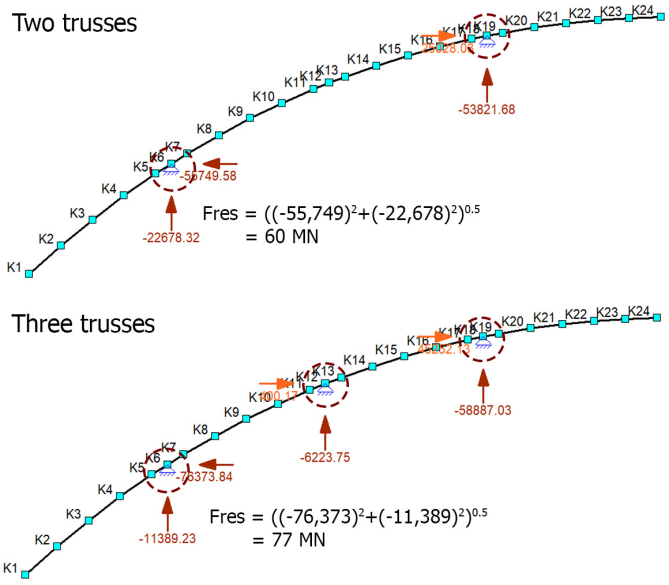

Figure F.8: MatrixFrame model with three steel trusses supporting the sector gate.

Now the differences in forces acting on the trusses are computed and compared between two and three trusses (Fig. F.9). From the computation it becomes clear that adding an additional truss increased the resulting forces acting on the two original trusses. This is due to the formation of bending moments in the arched gate and thus this adaptation is counter-productive.

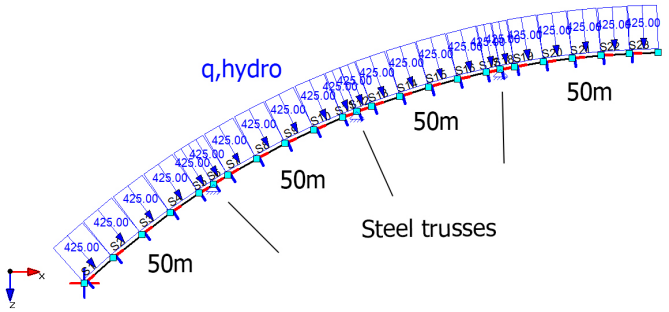

Figure F.9: MatrixFrame computations with two (left) and three (right) trusses supporting the sector gate. The encircled supports visualise the simplified attachment of the steel trusses to the sector gate.

F.3.2. VERIFICATION STEEL TRUSSES

Considering the compressive force the static design strategy should adhere to (141 MN), the profiles of the main beams (see Fig. F.10) are dimensioned as follows:

$$F_{Ed,beam} = \frac{F_{Comp,max}}{N_{trusses} \cdot N_{main,beams}} = 23.5\ MN$$

Where:

- $N_{trusses}$ is the number of steel trusses supporting the gates: 2
- $N_{main,beams}$ is the number of main beams: 3

The compressive capacity of the main beams is computed as follows:

$$N_{c,Rd} = \frac{A \cdot f_y}{\gamma_{m0}} \text{ for class 1, 2 and 3 cross-sections}$$

Where:

- A is the surface of the main beam
- f_y the steel quality (S355)
- γ_{m0} the safety factor (1.0)

Using the equation results in a required steel surface of 66,200 mm^2. This is fulfilled by a hollow section: CHS762/30 Eurocode Applied (nd) with the properties stated in Fig. F.10. Now that the

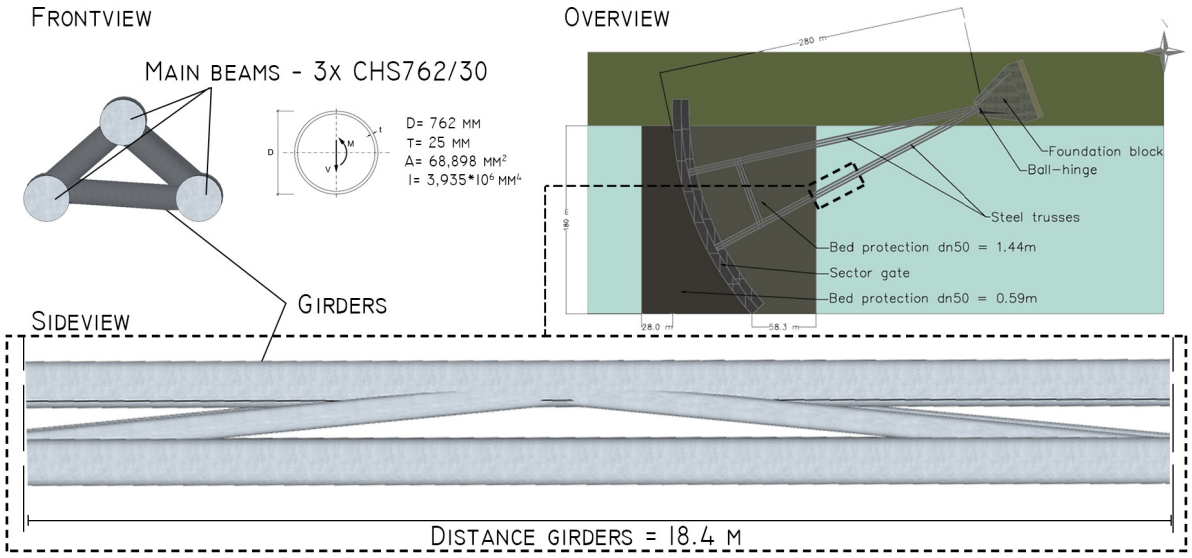

Figure F.10: Design and dimension of the steel trusses. Not to scale.

main beams are determined a simplistic approach, based on the buckling length of the main beams (SLS), is applied to determine the length between the girders. To derive the maximum allowable length between the girders, the buckling force for global instability is determined and along with it the amplification factor (α_{cr}). (Molenaar and Voorendt, 2019). If an elastic analysis is assumed the maximum allowable amplification factor can be computed by dividing the compressive capacity by

the compressive force:

$$\alpha_{cr} = \frac{F_{Rd}}{F_{Ed}} = \frac{23.5\,MN}{24.0MN} = 1.021$$

This then results in the maximum allowable elastic buckling force of ≈ 24.0 MN. Then with the characteristics of the hollow section from Fig. F.10 the distance between the girders (L) is computed:

$$F_{cr} = \frac{\pi^2 \cdot EI}{L^2}$$

$$L = \sqrt{\frac{\pi^2 \cdot EI}{F_{cr}}} = \sqrt{\frac{\pi^2 \cdot 8.26E^14}{24E^6}} = 18.4 \text{ metres}$$

Compared to the current Maeslant barrier (≈ 19.80 metres), this is a decrease of 1.4 metres but quite similar and thus considered as valid.

F.4. SECTOR GATES

In this section the computations for the height of the gate (Appendix F.4.1), buoyancy (Appendix F.4.2) and strength of the gates (Appendix F.4.3) are stated.

F.4.1. HEIGHT OF THE GATES

Waves or water overtopping the gates results in a influx of water into the basin behind the barrier and oscillations of the gates. To determine whether the water retention height of the gates is sufficient a limit of 0.2 $m^3/s/m$ (200 l/s/m) discharge over the gates is introduced. This assumption is based on the Ultimate Limit State (ULS) mean discharge attributed to embankment sea walls and sea dikes (van der Meer et al., 2018). However, one has to consider that the aforementioned ULS might lead to a very conservative design as the limit applicable to sea walls and dikes can not be considered similar to the application of gates of a barrier. Nonetheless, due to the lack of research about the ULS of sector gates, the discharge limit is applied in the sections that follow.

Overtopping or overflow can be classified as positive, zero and negative freeboard. These types are visualised in Fig. F.11. These classifications depend on several factors: the retention height, significant wave height and water level height.

Positive and zero freeboard

To quantify the amount of overtopping in case of a positive freeboard it has to be determined whether this is in impulsive or non-impulsive conditions. These boundaries are retrieved from van der Meer et al. (2018):

Impulsive conditions:

$$0,03 < h_* \frac{R_c}{H_{m0}} < 1,0 \; or \; h_* < 0.2 \qquad \text{(F.4.1)}$$

Non-impulsive conditions:

$$0,1 < \frac{R_c}{H_{m0}} < 3.5 \; or \; h_* > 0.3 \qquad \text{(F.4.2)}$$

In which h_* is equal to:

$$h_* = 1.35 \frac{h_s}{H_{m0}} \cdot \frac{2 \cdot \pi \cdot h_s}{g \cdot T^2_{m-1.0}} \qquad \text{(F.4.3)}$$

The overtopping volumes are then calculated with the following formulas for (non-)impulsive conditions:

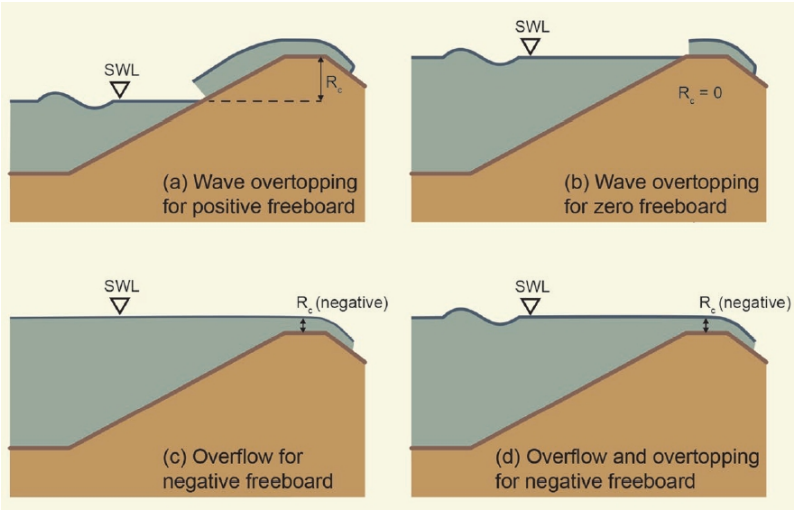

Figure F.11: Classification of overtopping mechanisms. Retrieved from van der Meer et al. (2018, p.122).

Impulsive conditions:

$$\frac{q}{h_*^2\sqrt{g\cdot h_s^3}} = 2.8\cdot 10^{-4}(h_*\frac{R_c}{H_{m0}})^{-3.1} \tag{F.4.4}$$

Non-impulsive conditions:

$$\frac{q}{\sqrt{g\cdot H_{m0}^3}} = 0.04\cdot e^{-1.8\frac{R_c}{H_{m0}}} \tag{F.4.5}$$

In which the various parameters are identified:

- R_c is the freeboard, dependent on the height of the structure and water level
- h_s is the water depth in front of the barrier
- H_{m0} is the estimate of the significant wave height
- $T_{m-0.0}$ is the average wave period

In most events the overtopping takes place in non-impulsive conditions. This is largely due to the relatively small computed significant wave height (H_s) of approximately 1.0 metre, Appendix F.1. If a zero freeboard is assumed the specific discharge over the barrier becomes:

$$\frac{q}{\sqrt{9.81\cdot 1.0^3}} = 0.04\cdot e^0 = 0.12\ m^3/s/m \tag{F.4.6}$$

From this it is concluded that the ULS of 0.2 m^3/s/m is not reached in case of positive and zero freeboard.

Negative freeboard

The overflow discharge with a negative freeboard is calculated in accordance with the European Overtopping Manual (van der Meer et al., 2018):

$$q_{overflow} = 0.54\cdot\sqrt{g\cdot[-R_c^3]} \tag{F.4.7}$$

With Eq. (F.4.7) the maximum allowable negative freeboard, and eventually the required height of the gates, is determined in Eq. (F.4.8).

$$0.2 = 0.54 \cdot \sqrt{9.81 \cdot [-R_c^3]};\ R_c = -0.241\ m \tag{F.4.8}$$

In Fig. F.12 the overflow and/or overtopping discharges for varying gate heights, under increasing sea level, are quantified. In this figure the gate height is an absolute value, ranging from the bottom of the structure (NAP -17.0 m) to the top of the structure.

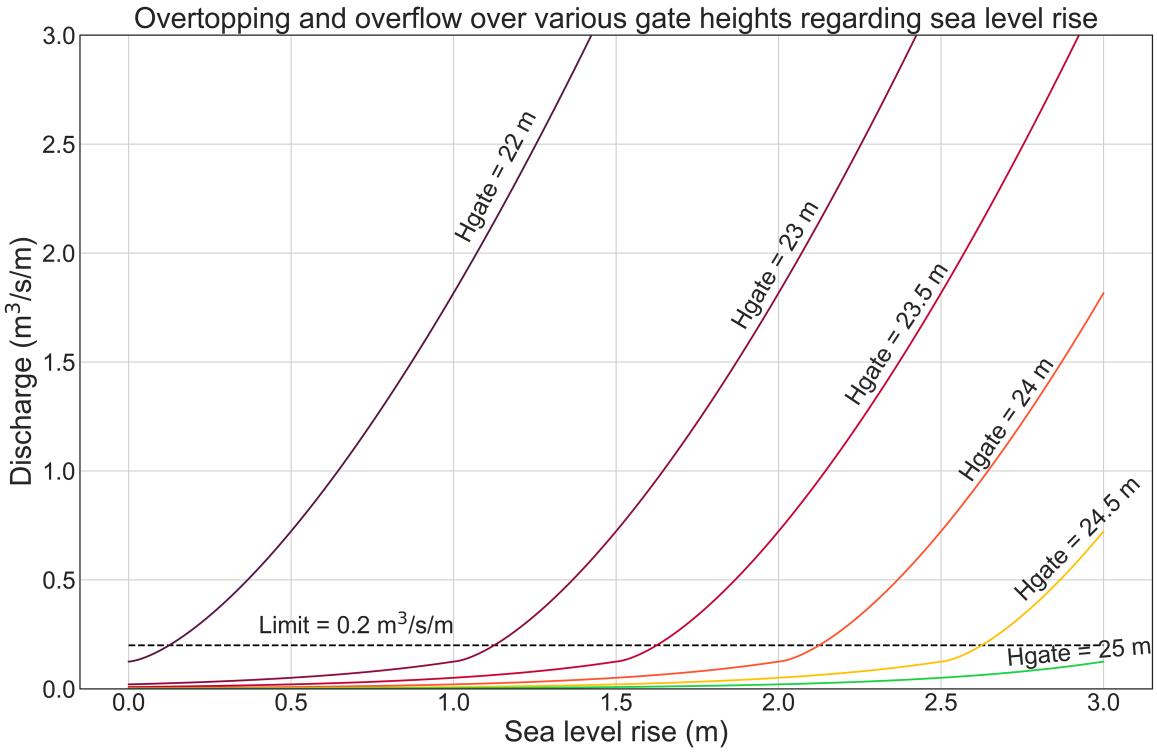

Figure F.12: Computation of the overflow and/or overtopping quantities for varying gate heights regarding sea level rise.

F.4.2. BUOYANCY

The barrier is sunken to the bottom of the waterway by gravitational forces: buoyancy. The water in the waterway results in an upward force and the mass of the barrier in a downward one. Due to changes in the closing regime and sea level rise, the buoyancy of the barrier is checked. The upward forces are defined into two segments, one for the sea -and riverside:

$$F_{b,sea} = \rho_{saltwater} \cdot g \cdot h_{sea} \cdot \frac{A_{barrier}}{2}$$

$$F_{b,river} = \rho_{saltwater} \cdot g \cdot h_{river} \cdot \frac{A_{barrier}}{2}$$

The depth of the seaside is computed with a storm surge height with a probability of 1:10,000 p/y (NAP +5.0 m) plus depth to the sill and magnitude of sea level rise. The depth at the riverside is computed with the respective sea level rise, which leads to the altercations of the closing regime plus the depth to the sill.

The downward force is a combination of the selfweight of the steel barrier, the water on top of the cantilevering segment of the barrier and the voids in the barrier that can be filled with water. Thus, the equation reads:

$$F_{down} = F_{sw} + F_{w,CR} + F_{w,fill} \tag{F.4.9}$$

The filling areas and the dimensions thereof are viewable in Fig. F.13 and provide the required buoyancy to sink and lift the gate. Filling in the parameters yield the results of figure Fig. F.14 and the

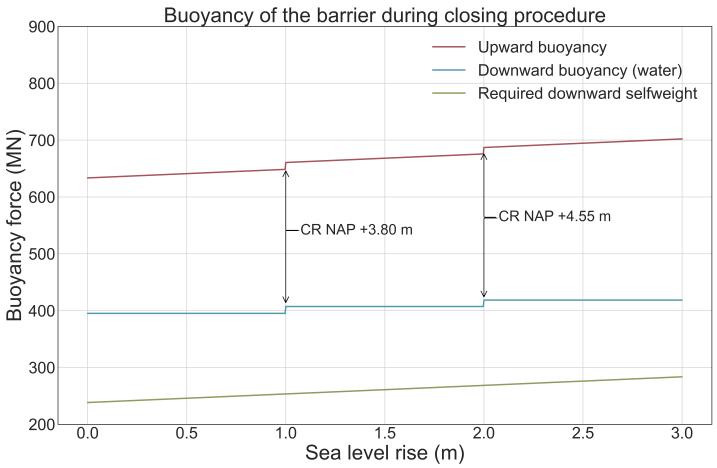

Figure F.13: Cross-sectional view of a sector gate with the filling areas numbered A1, A2 and A3.

required selfweight of the steel gates. From the figure it can be deducted that over the course of sea level rise an increase in selfweight of the barrier is required to adequately sink the barrier. The gates of the current Maeslant barrier weigh approximately 15,000 tons (≈ 150 MN), with this figure an estimate for the steel trusses can be deducted at zero sea level rise: 238 MN minus 150 MN results in 88 MN for both steel trusses (44 MN for a single truss).

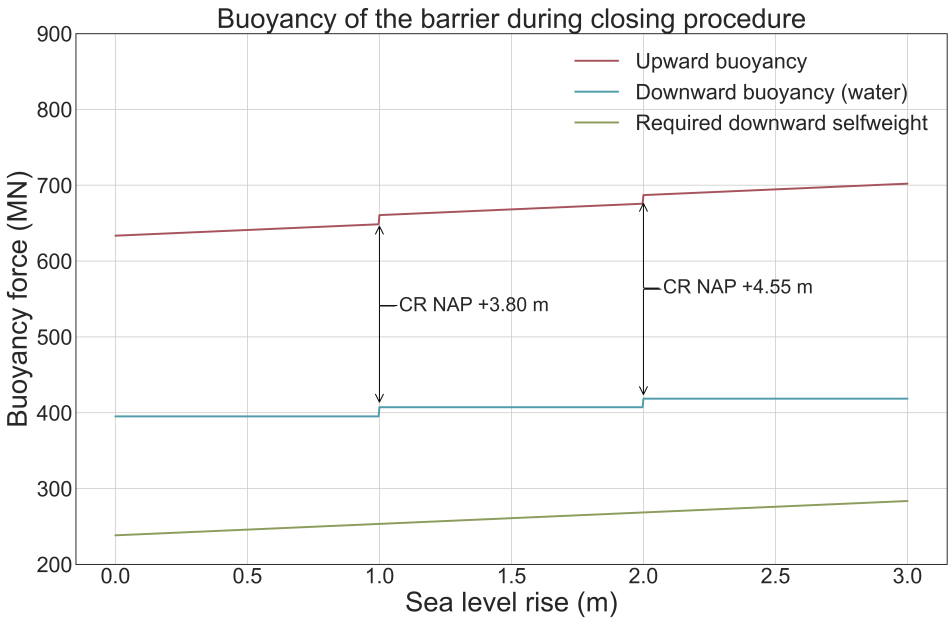

Figure F.14: Influence of sea level rise on the buoyancy and required selfweight of the gates.

F.4.3. STRENGTH OF THE GATES

The hydraulic forces are uniformly distributed along the sector gate as visualised in Fig. F.15. The considered distributed load from Appendix F.2.1 is applied and one has to consider that the load increases with sea level rise as shown in Fig. F.4. The distributed hydrostatic load is computed with the following conditions and are elaborated further on:

- h_{top} = NAP +5.0 m, top of the barrier, see Fig. F.3
- h_{bottom} = NAP -17.0 m, bottom of the barrier (excluding sill), see Fig. F.3
- Storm surge height = NAP +5.0 m

Within the computational model only the segment of the gate where the highest loads convert, see Fig. F.15, is checked by comparing the bending resistance of the skin plate and deflection of the skin plate at this location. The skin plate is the outer steel layer, which is commonly supported by vertical and/or horizontal girders and is elaborated further on.

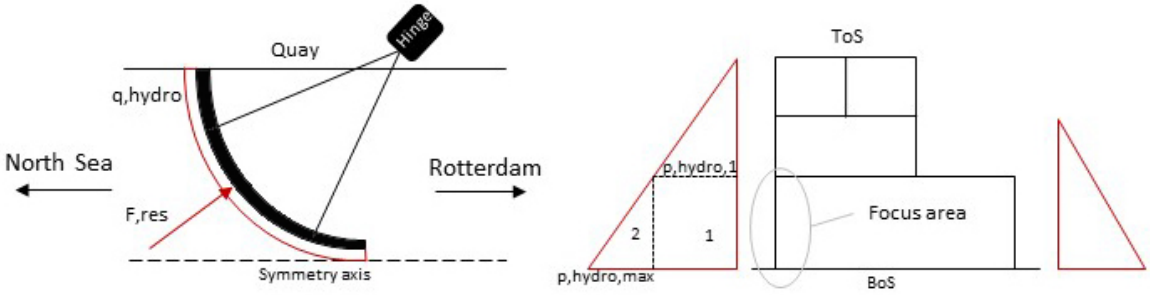

Figure F.15: Simplified sketch of the direction of the resultant water pressure on the sector gates (left) and water pressure on the cross-section of the gate (right).

The bending resistance of the skin plate is determined with Eq. (F.4.10) and the deflection with Eq. (F.4.11):

$$M_{rd} = \frac{W_{el} \cdot f_y}{\gamma_{steel}} \qquad \text{(F.4.10)}$$

$$f = \frac{\alpha \cdot p \cdot a^4}{E \cdot t^3} \qquad \text{(F.4.11)}$$

Where:

- $W_{el} = \frac{1}{6} \cdot width \cdot thickness^2$
- $f_y = 355$ N/mm^2
- $\gamma_{steel} = 1$

Where:

- $\alpha = 0.0138$ (Molenaar, 2019, p. 60)
- p is the pressure
- a is the distance between girders
- $E_{steel} = 210{,}000$ N/mm^2

The hydraulic loads follow from the hydraulic pressure acting on the gates and the way the gate is dimensioned, i.e. the positioning of the horizontal and vertical girders. In addition, the loads are multiplied by a safety factor of 1.5 and with a factor following from the Consequence Class of the barrier (CC3 = 1.1). The hydraulic pressures, denoted as p,hydro,max and p,hydro,1, see Fig. F.15, are computed as follows:

$$p_{hydro,1} = Factor_{safety} \cdot \frac{\rho_{saltwater} \cdot g \cdot (h_{top} - h_1)}{1000}$$

$$p_{hydro,max} = Factor_{safety} \cdot \frac{\rho_{saltwater} \cdot g \cdot h_{top}}{1000}$$

In case of a gate height of up to NAP +5.0 m and an acting storm surge of up to NAP +5.0 m with the

bottom of the structure at NAP -17.0 m, this would result in:

$$p_{hydro,1} = 1.5 \cdot 1.1 \cdot \frac{1025 \cdot 9.81 \cdot (22.0 - 7)}{1000} = 249 \text{ kpa}$$
$$p_{hydro,max} = 1.5 \cdot 1.1 \cdot \frac{1025 \cdot 9.81 \cdot 22.0}{1000} = 365 \text{ kpa}$$

Bending resistance of the skin plate
Let us consider the segment where the highest force occur: bottom segment of the barrier. Initially, the bending moment without girders on the skinplate is computed. This then would result in the following bending moments acting on the focus area as designated in Fig. F.15 and Fig. F.16:

$$M_{ed,1} = \frac{1}{8} \cdot p_{hydro,1} \cdot h^2 = \frac{1}{8} \cdot 249 \cdot 7^2 = 1525 \text{ kNm p/m}$$
$$x_{max,2} = \frac{h}{\sqrt{3}} = 4.04 \text{ m}$$
$$M_{ed,2} = \frac{x_{max,2} \cdot h \cdot (p_{hydro,max} - p_{hydro,1})}{6} \cdot (1 - \frac{x_{max,2}^2}{h^2})$$
$$= \frac{4.04 \cdot 7 \cdot (365 - 249}{6} \cdot (1 - \frac{4.04^2}{7^2}) = 365 \text{ kNm p/m}$$

Then the max bending moment in the cross-section is approximated by summing the two as these are within half a metre of each other, results in $M_{max} = 1890$ kNm per metre width. After computing the bending resistance it is concluded that both horizontal and vertical girders are needed to provide sufficient resistance without over dimensioning the thickness of the skin plate. Therefore, girders are added in both directions with a spacing of (L girder) 2.5 metres, see Fig. F.16. The acting moment can then be computed by applying the basic mechanics as in Fig. F.17.

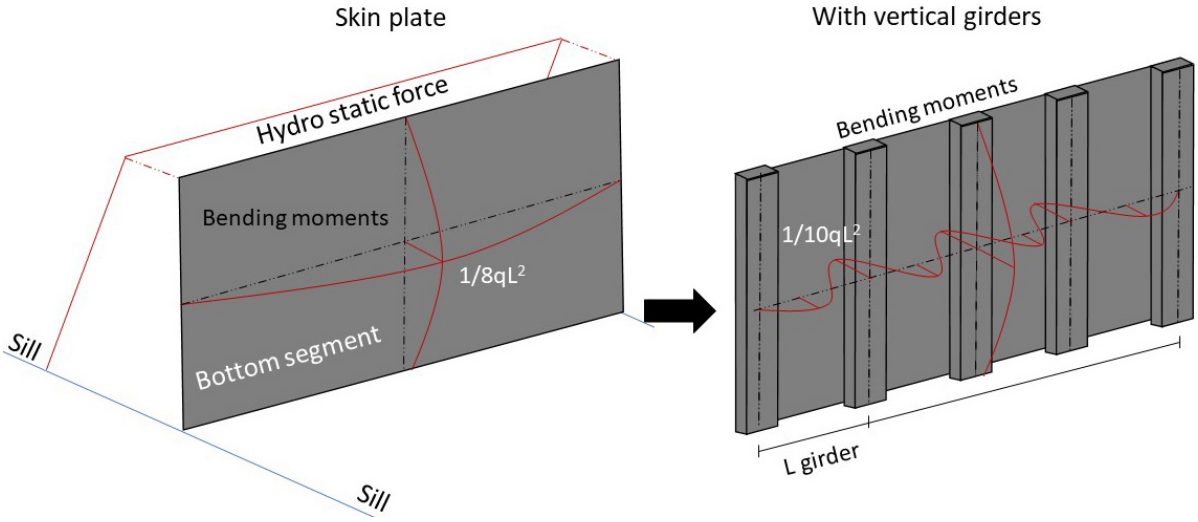

Figure F.16: Bending moments on the skin plate with(out) vertical girders, horizontal girders can be applied similarly but are left out for the sake of readability. The moment distribution in horizontal direction with girders follows the distribution over a multi-support span, see Fig. F.17.

By applying the hydraulic pressure at the height of the maximum bending moment, approximately at the centre of $p_{hydro,1}$, results in a combined hydraulic pressure of:

$$p_{approx,max} = p_{hydro,1} + (p_{hydro,max} - p_{hydro,1})/2 = 307 \text{ kpa}$$

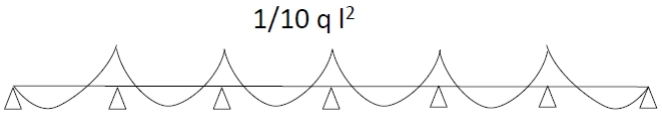

Figure F.17: Bending moment over a multi-supported span. Retrieved from Molenaar (2019, p. 54).

This then results in a bending moment of:

$$M_{Ed} = \frac{1}{10} \cdot p_{approx,max} \cdot Spacing^2 = 192 \text{ kNm p/m}$$

The resistance, M_{Rd}, with a skin plate thickness of 30 mm is:

$$M_{Rd} = \frac{1}{6} \cdot Spacing \cdot t_{steel}^2 \cdot f_y = \frac{1}{6} \cdot 2{,}500\,[mm] \cdot 30^2\,[mm] \cdot 355\,[N/mm^2] = 133 \text{ kNm}$$

This is lower than the acting bending moment, either the thickness of the skin plate is increased of the spacing between the girders is decreased. If the latter is decreased to 2.0 metres, the acting bending moment and bending resistance become:

$$M_{Rd} = \frac{1}{6} \cdot 2{,}000\,[mm] \cdot 30^2\,[mm] \cdot 355\,[N/mm^2] = 107 \text{ kNm}$$
$$M_{Ed} = \frac{1}{10} \cdot 307 \cdot 2^2 = 123 \text{ kNm p/m}$$

Now by increasing the thickness of the skin plate by 5 mm, the resistance of the gate is sufficient:

$$M_{Rd} = \frac{1}{6} \cdot 2{,}000\,[mm] \cdot 35^2\,[mm] \cdot 355\,[N/mm^2] = 145 \text{ kNm} > 123 \text{ kNm p/m}$$

Sea level rise, logically, has an influence on the hydraulic pressures. In Fig. F.18 the relation between the acting bending moment and sea level rise, and the resistance of the skin plate with the stated dimensions are visualised.

Deflection of the skin plate

The deflection on a single skin plate constrained between the horizontal and vertical girders should adhere to a limit of the deflection. The maximum pressure is found in the middle of the skin plate, located at the bottom of the barrier, and is approximated by applying $p_{hydro,max}$ which is equal to 365 kpa. The deflection then is computed with Eq. (F.4.11):

$$f = \frac{0.0138 \cdot 365/1000 \cdot 2{,}000^4}{210{,}000 \cdot 35^3} = 8.95 \text{ mm} \tag{F.4.12}$$

To determine whether the deflection is acceptable a limit for the deflection, equal to 1/200 times the spacing between girders, of 12.5 mm is introduced and the progression of the deflection under sea level rise is computed. In Fig. F.19 the progression of the deflection due to an increase of sea level rise in comparison with the acceptable deflection is visualised. At a certain point of sea level rise, it is anticipated that with the assumed horizontal and vertical girders and thickness of the skin plate, the deflection will surpass the instated limit.

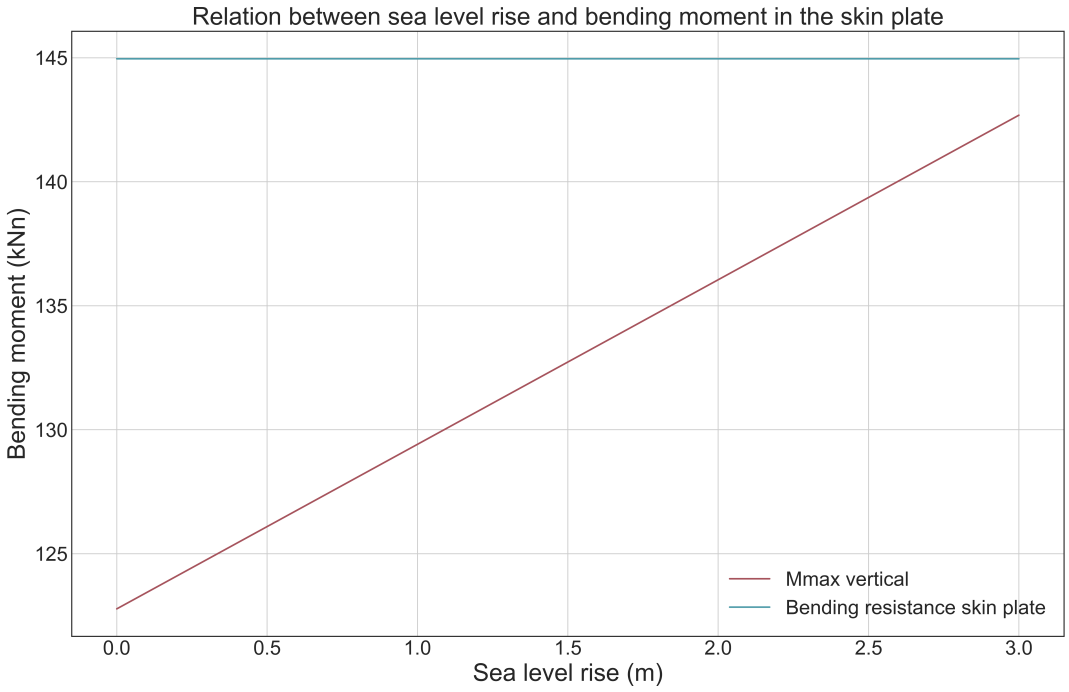

Figure F.18: Influence of sea level rise on the acting bending moment of the skin plate and bending resistance of the skin plate.

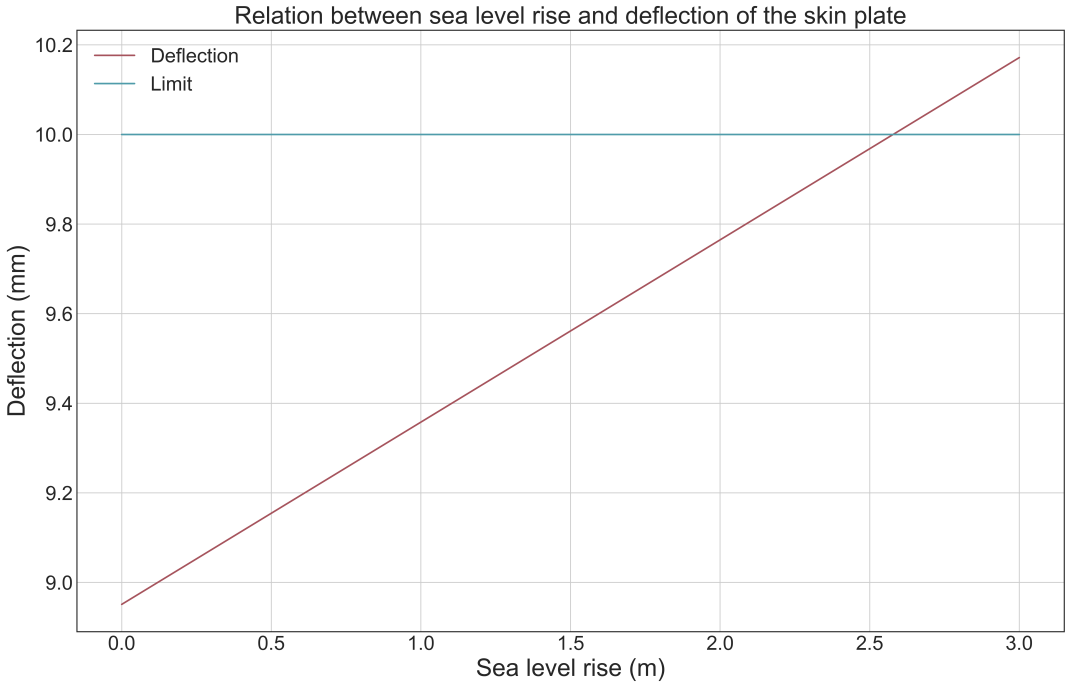

Figure F.19: Influence of sea level rise on deflection of the skin plate.

F.5. BED PROTECTION

The bed protection input module and functions is described with the flow chart in Fig. F.20. The bed protection is determined by varying factors. These factors include erosion due to waves occurring at both the sea and river side, resulting in a scour hole at the toe of the gate when closed and if left unprotected, this emphasises the need to determine the required bed protection length. Additionally, flow velocities effect erosion of the bed. These flows occur in the open state of the barrier, due to tidal current and river discharge, but as well during the closing and opening procedures of the barrier. These aspects are attributed to the flow erosion component. Furthermore, erosion could occur due to a plunging jet from waves overtopping the barrier, however, this is quite unlikely due to the relative large depth of the New Waterway. Nevertheless, this mechanism is included in the bed protection module.

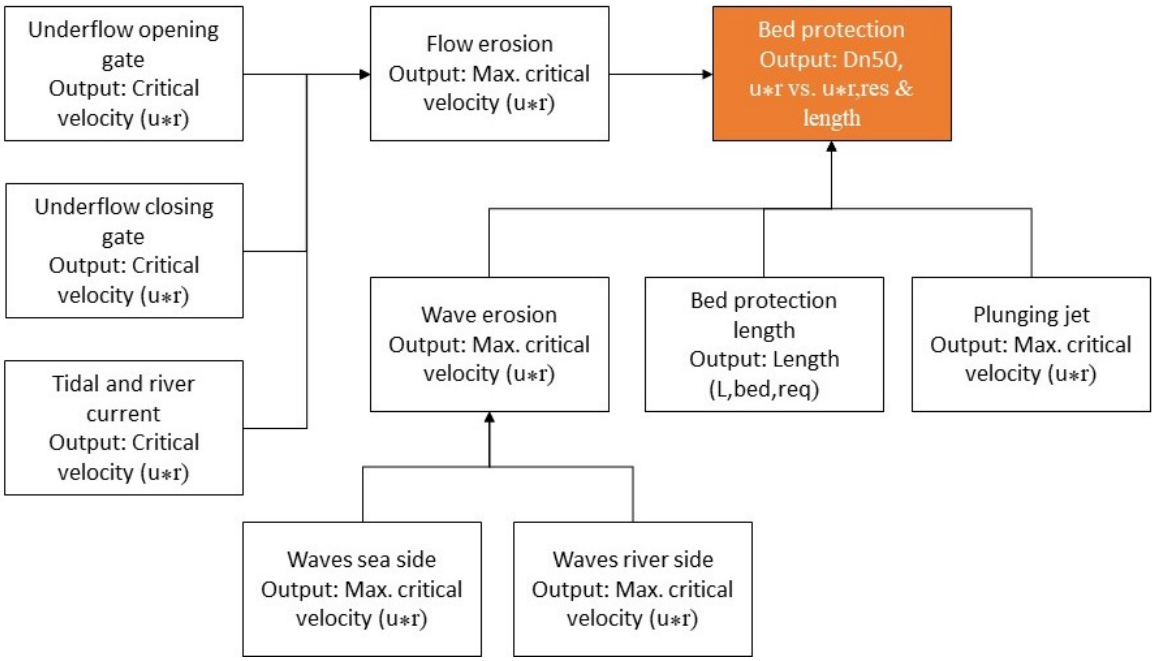

Figure F.20: Flow chart of the python script that envelopes the bed protection module (orange) used in the computations.

F.5.1. EROSION DUE TO WAVES

Erosion due to waves occurs on both sides of the barrier. To determine the critical velocity (u_{*r}), on which the bed protection is designed, the characteristics of the waves are determined. The peak period of the waves (T_p) is dependent on the significant wave height (H_s). For an initial estimation an significant wave height of 0.97 metres, computed in Appendix F.1, is applied. According to Schiereck and Verhagen (2019, p. 180) the peak period can be computed with Eq. (F.5.1).

$$T_p = 3.6 \cdot \sqrt{H_s} = 3.6 \cdot \sqrt{0.97} = 3.55 \text{ sec} \tag{F.5.1}$$

Then with Fig. F.21 the appropriate 'Relative depth characteristics' is determined. Through iteratively solving the equations for the wave lengths with the shallow, transitional and deep water boundary conditions, the correct wave length of the wave is yielded. As an initial assumption a storm surge of NAP +5.0 metres is assumed and a sill depth of the barrier of NAP -17.0 metres. This eventually results in the following wave length in transitional water depth:

$H_{sill} = 17.0$ m

$SS = 5.0$ m, storm surge height for 1:10,000 p/y recurring storms (Appendix D)

$h = H_{sill}(NAP - 17.0m) + SS(NAP + 5.0m) = 22$

$$L = \frac{g \cdot T_p^2}{2\pi} \cdot \tanh k \cdot h = 19.63 \text{ m}$$

$$k = \frac{2 \cdot \pi}{L} = 0.32, \text{ the wave number}$$

$$\omega = \frac{2 \cdot \pi}{T_p} = 1.77 \text{ rad/s, the angular frequency}$$

'h' represents the total amount of metres of hydrostatic contact from the sill (NAP -17.0 m) to the height of the storm surge (NAP +5.0 m) on the barrier, see Fig. D.4 and for the applied storm surge see Appendix D.1.

Relative depth Characteristics	Shallow Water $\frac{h}{L} < \frac{1}{20}$	Transitional water depth $\frac{1}{20} < \frac{h}{L} < \frac{1}{2}$	Deep Water $\frac{h}{L} > \frac{1}{2}$
Wave Celerity	$c = \frac{L}{T} = \sqrt{gh}$	$c = \frac{L}{T} = \frac{gT}{2\pi}\tanh kh$	$c = c_0 = \frac{L}{T} = \frac{gT}{2\pi}$
Wave Length	$L = T\sqrt{gh}$	$L = \frac{gT^2}{2\pi}\tanh kh$	$L = L_0 = \frac{gT^2}{2\pi}$
Group Velocity	$c_g = c = \sqrt{gh}$	$c_g = nc = \frac{1}{2}\left[1 + \frac{2kh}{\sinh 2kh}\right] \cdot c$	$c_g = \frac{1}{2}c_0 = \frac{gT}{4\pi}$
Energy Flux (per m width)	$F = Ec_g = \frac{1}{2}\rho g a^2 \sqrt{gh}$	$F = Ec_g = \frac{1}{2}\rho g a^2 nc$	$F = \frac{T}{8\pi}\rho g^2 a^2$
Particle velocity			
Horizontal	$u = a\sqrt{\frac{g}{h}}\sin\theta$	$u = \omega a \frac{\cosh k(h+z)}{\sinh kh}\sin\theta$	$u = \omega a e^{kz}\sin\theta$
Vertical	$w = \omega a\left(1 + \frac{z}{h}\right)\cos\theta$	$w = \omega a \frac{\sinh k(h+z)}{\sinh kh}\cos\theta$	$w = \omega a e^{kz}\sin\theta$
Particle displacement			
Horizontal	$\xi = -\frac{a}{\omega}\sqrt{\frac{g}{h}}\cos\theta$	$\xi = -a\frac{\cosh k(h+z)}{\sinh kh}\cos\theta$	$\xi = -ae^{kz}\cos\theta$
Vertical		$\zeta = a\frac{\sinh k(h+z)}{\sinh kh}\sin\theta$	$\zeta = ae^{kz}\sin\theta$
Subsurface pressure	$p = -\rho g z + \rho g a \sin\theta$	$p = -\rho g z + \rho g a \frac{\cosh k(h+z)}{\cosh kh}\sin\theta$	$p = -\rho g z + \rho g a e^{kz}\sin\theta$
$a = \frac{H}{2}$ $\omega = \frac{2\pi}{T}$ $k = \frac{2\pi}{L}$ $\theta = \omega t - kx$			

Figure F.21: Summary of wave characteristics. Retrieved from Schiereck and Verhagen (2019, p. 175).

Furthermore, the wave amplitude at sea level and bottom are computed in accordance with Schiereck and Verhagen (2019, p. 154):

$$a = \frac{H_s}{2} = \frac{0.97}{2} = 0.485\ [m], \text{ amplitude sea level}$$

$$a_b = \frac{H_s}{2 \cdot \sinh(k \cdot \text{depth})} = \frac{0.97}{2 \cdot \sinh(0.32 \cdot 22)} = 0.0008\ [m], \text{ amplitude at bottom}$$

Which result in the orbital velocity of the waves at the bottom:

$$\hat{u}_b = \omega \cdot a_b = 1.77 \cdot 0.0008 = 0.00142\ [m/s]$$

Assuming that the angle of attacking waves is perpendicular to the direction of the barrier, i.e. the most severe situation, results in an ϕ (angle between waves and current) of:

$$\phi = \frac{90 + \alpha}{180} \cdot \pi = 1.571\ [rad]$$

Subsequently, the friction velocity on the bed protection, with the defined wave characteristics and an initial median nominal diameter (d_n50), is computed. In this computation a design approach is applied. A set of varying diameter sizes from Schiereck and Verhagen (2019, p. 362) is taken and the resulting critical flow velocities are checked against the resistance of the stones.

The roughness of the bottom (k_r) is computed by multiplying the median nominal diameter with two, as this is *"a practical choice when a statically stable protection needs to be designed."* (Schiereck and Verhagen, 2019, p. 59). The roughness of the bottom should adhere to a certain boundary condition: the wave amplitude at the bottom (a_b) should exceed the value of $0.636 \cdot k_r$. The friction coefficient (c_f) is computed in accordance with Swart. (Schiereck and Verhagen, 2019, p. 154) The maximum friction coefficient is set at 0.3.

$$k_r = 2 \cdot d_{n50}\ \text{m}$$
$$c_f = 0.237 \cdot (\frac{a_b}{k_r})^{-0.52}, \text{ for } a_b > 0.636 \cdot k_r$$
$$\text{else } c_{f,max} \text{ is } 0.3$$

Following from the bed roughness, the Chézy coefficient is computed. The Chézy coefficient influences the bed friction and velocity.

$C = 18 \cdot \log(\frac{12 \cdot R}{k_r})\ [m^{1/2}/s]$, where:

$R \approx h = 22\ [m]$, when the width is significantly larger than the depth (Molenaar and Voorendt, 2019, p. 66)

This results in Table F.1:

Table F.1: Stone classes and their respective characteristics based on computed parameters.

Parameter	**LMa 60-300**	**HMa 300-1000**	**HMa 1000-3000**	**Unit**
d_{n50}	0.38	0.59	0.90	m
k_r	0.76	1.18	1.80	m
$a_b > 0.636 \cdot k_r$	False	False	False	-
$c_{f,max}$	0.30	0.30	0.30	-
C	45.73	42.29	38.99	$m^{1/2}/s$

Finally the resulting friction velocities over the bed can be calculated. In which the initial tidal cur-

rent (u_c) is set at 2.9 m/s. Shear velocity due to current:

$$u_{*c} = \frac{\sqrt{g}}{C} \cdot u_c \tag{F.5.2}$$

Shear velocity due to waves:

$$u_{*b} = \sqrt{\frac{c_f}{2}} \cdot \hat{u}_b \cdot \sin(\omega \cdot t) \tag{F.5.3}$$

Resulting shear velocity due to waves and current with given angle of waves:

$$u_{*r} = \sqrt{u_{*c}^2 + u_{*b}^2 + 2 \cdot u_{*c} \cdot u_{*b} \cdot \sin(\phi)} \tag{F.5.4}$$

Rewriting the formula:

$$u_{*r} = \sqrt{\frac{g}{C^2 \cdot u_c^2} + \frac{c_f}{2} \cdot \hat{u}_b^2 + \frac{2 \cdot \sqrt{g}}{C} \cdot u_c \cdot \sqrt{\frac{c_f}{2}} \cdot \hat{u}_b \cdot \sin(\phi)} \tag{F.5.5}$$

Results in Table F.2, in which the friction velocities for the respective stone classes are stated.

Table F.2: Resulting shear velocity for the stone classes.

Parameter	**LMa 60-300**	**HMa 300-1000**	**HMa 1000-3000**	**Unit**
u_{*c}	0.199	0.215	0.233	m/s
u_{*b}	5.5e−4	5.5e−4	5.5e−4	m/s
u_{*r}	0.199	0.215	0.233	m/s

Subsequently, the resistances of the various stones classes are determined by applying the Shields equation with a fixed value for ψ_c of 0.03. Shields is applied due to the characterisation of the waterway as deep water, and therefore has preferences over Izbash. The velocity resistance of the stones is determined with Eq. (F.5.6).

$$u_{*r,Res} = \sqrt{\psi_c \cdot \Delta \cdot g \cdot d_{n50}} \tag{F.5.6}$$

Where:

- $\Delta = \frac{\rho_s - \rho_w}{\rho_w} = \frac{2650-1025}{1025} = 1.585$
- $\psi_c = 0.03$

In addition, the upper boundary value, until where Shields may safely be applied Schiereck and Verhagen (2019, p. 57), is checked according to the following formula:

$$\text{Shields' upper boundary: } \frac{h}{d_{n50}} < 100 \tag{F.5.7}$$

Table F.3: Resulting and capacity friction velocity for the respective stone classes.

Parameter	LMa 60-300	HMa 300-1000	HMa 1000-3000	Unit
u_{*r}	0.199	0.215	0.233	m/s
$u_{*r\ Res.}$	0.421	0.525	0.648	m/s
Unity Check	0.47	0.41	0.36	-
Shields' upper limit	57.9	37.3	24.4	-

From the unity check, presented in Table F.3, it is evident that the initially opted stone classes are over-dimensioned in preventing erosion due to waves on the barrier.

F.5.2. EROSION DUE TO UNDERFLOW

Besides erosion of the bed due to waves and natural occurring flows due to the tide and river discharge, erosion will occur due to the closing procedure of the barrier. Throughout the closing procedure, the gap through water is able to flow decreases, which in turn increases the overall flow velocity over the bed. The flow velocity due to free and submerged underflow is checked during both the closing and opening procedure of the barrier.

Free underflow

$$Q = m_{fuf} \cdot b \cdot a \cdot \sqrt{2 \cdot g \cdot (h_1 - a)} \tag{F.5.8}$$

Where:

- m_{fuf} is the discharge coefficient and equal to 0.611 for a sharp edged gate finish (Boiten, 1992)
- b is the width of the structure and equal to 360 metres
- a is the gap opening and is checked over a range of 0.01 (fully closed) to 20 (fully opened) in steps of 0.25 metres.
- h_1 is the high water level depth

Occurs when $\frac{h_3}{a} \leq 1.42 \cdot \sqrt{\frac{h_1}{a}} - 0.3$ is valid.

Submerged underflow

Occurs when the boundary condition of free underflow is not valid.

$$Q = m_{suf} \cdot b \cdot a \cdot \sqrt{2 \cdot g \cdot (h_1 - h_3)} \tag{F.5.9}$$

Where:

- m_{suf} is the discharge coefficient and equal to 0.8 (Molenaar and Voorendt, 2019)
- b is the width of the structure and equal to 360 metres
- a is the gap opening and is checked over a range of 0.01 (fully closed) to 20 (fully opened) in steps of 0.25 metres.
- h_1 is the high water level depth
- h_3 is the low water level depth

The underflow during the closing procedure is initially assumed with a high water level depth (h_1) is 17, which is the difference between mean sea level and the sill of the barrier, plus 5 metres of

storm surge and a low water level depth (h_3) is 17 plus 3 metres, the latter is the closing water level of the unembanked areas. In Fig. F.22 the flow velocities and relative discharge due to underflow are presented. However, it is worthwhile to mention that it is highly unlikely that at the moment of the closure the water level on the sea side is much higher than on the river side as it is an open system.

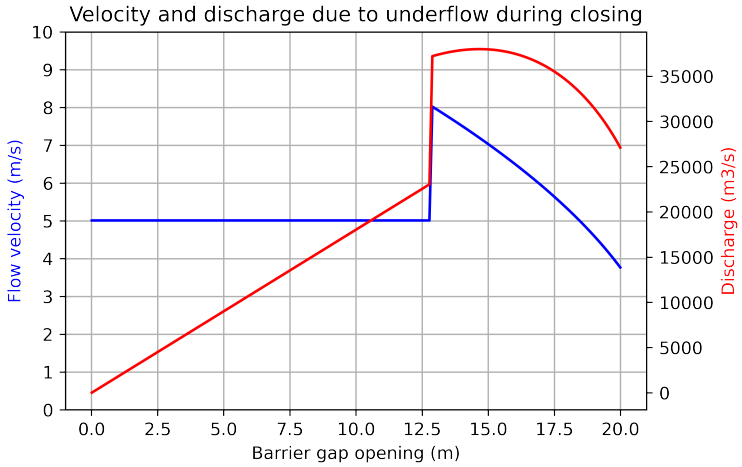

Figure F.22: Flow velocities and relative discharge due to underflow in the closing procedure.

The same can be performed during the opening procedure. Assume a worst case scenario, LAT (NAP -0.92 m) at the sea side of the barrier and h1 is equal to NAP +3.00 m during the start of the opening procedure. Results in Fig. F.23.

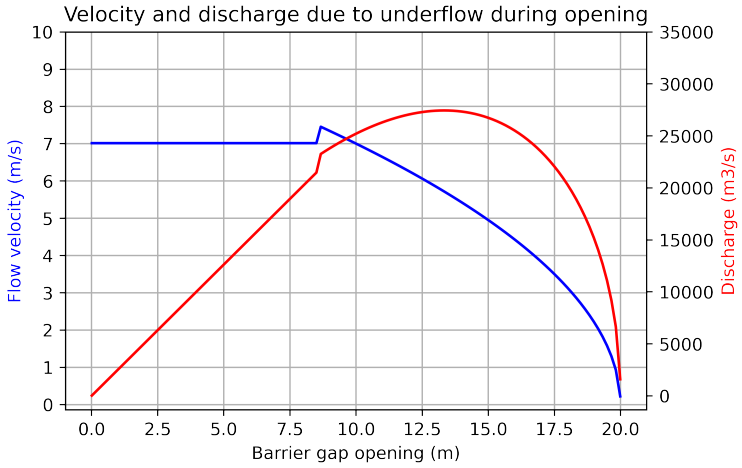

Figure F.23: Flow velocities and relative discharge due to underflow in the opening procedure.

The flow velocity can now be translated into the shear velocity as has been done by applying Eq. (F.5.2) in Appendix F.5.1. Normally, to determine the resulting shear velocity due to a combination of waves and the current, formula Eq. (F.5.5) is applied, however, as the significant wave is relatively low and barely impacts the shear velocity, as is shown with the shear velocity due to waves (u_{*b}) in Table F.2, the shear velocity due to current (u_{*c}) is set as the resulting shear velocity (u_{*r}). Thus the shear velocity is:

$$u_{*c} = \frac{\sqrt{g}}{C} \cdot u_c = u_{*r} \tag{F.5.10}$$

With Chézy according to the stone classes:

$$C = 18 \cdot \log \frac{12 \cdot R}{k_r} \tag{F.5.11}$$

With a maximum flow velocity of 7.4 m/s (u_c), results in Table F.4.

Table F.4: Stone classes and their respective characteristics based on computed parameters and calculated values for Chézy and shear velocities.

Parameter	**LMa 60-300**	**HMa 300-1000**	**HMa 1000-3000**	**Unit**
d_{n50}	0.38	0.59	0.90	m
k_r	0.76	1.18	1.80	m
$a_b > 0.636 \cdot k_r$	False	False	False	-
$c_{f,max}$	0.30	0.30	0.30	-
C	45.73	42.29	38.99	$m^{1/2}/s$
u_{*c}	0.507	0.548	0.594	m/s
$u_{*r,Res}$	0.421	0.525	0.648	m/s
Unity Check	1.20	1.04	0.92	-

Now that the deterministic calculations for a bed protection are shown the uncertainty due to sea level rise could be added. Fig. F.24 visualises what the effects of sea level rise are on the flow velocity regarding underflow. Bare in mind that the calculations of the flow velocities include altercations of the system as a whole, i.e. the closing regime changes in coalescence with sea level rise, which influences the water level on the river side:

- 0 metre sea level rise - closing water level NAP +3.00 metre
- 1 metre sea level rise - closing water level NAP +3.80 metre
- 2 metres sea level rise - closing water level NAP +4.55 metre

And, of course, the respective sea level rise is added to the Lowest Astronomical Tide (LAT): NAP -0.92 m + SLR. These factor influence how the underflow develops, both of free and submerged underflow. In the Python script, sea level rise is included ranging from 0 metres to 3 metres in steps of 0.03 metres and the gate opening procedure ranging from 0 (fully closed) to 20 metres (fully open) in steps of 0.25 metres. If a closer look is taken at Fig. F.24 it is evident that the maximum flow velocity (yellow) during the opening procedure of the barrier decreases with an increase of sea level rise, this is due to the fact that the occurring sea level rise is summed to the LAT, thus decreasing the difference in energy between the sea and river side of the barrier. Peaks in flow velocity can be seen at 1 and 2 metre sea level rise, this is due to the altercation in the closing regime, which increases the water level on the river side of the barrier and increases the difference in energy between the two sides. The dashed lines represent the resistance of the different stone classes, if these lines are beneath their partner shear velocity it means that the resistance is insufficient and a higher stone class has to be applied, see Fig. F.25. Logically, as the resistances of the bed protection are constant (the dashed lines in Fig. F.24), the Unity Check follows the patterns of the resulting shear velocity.

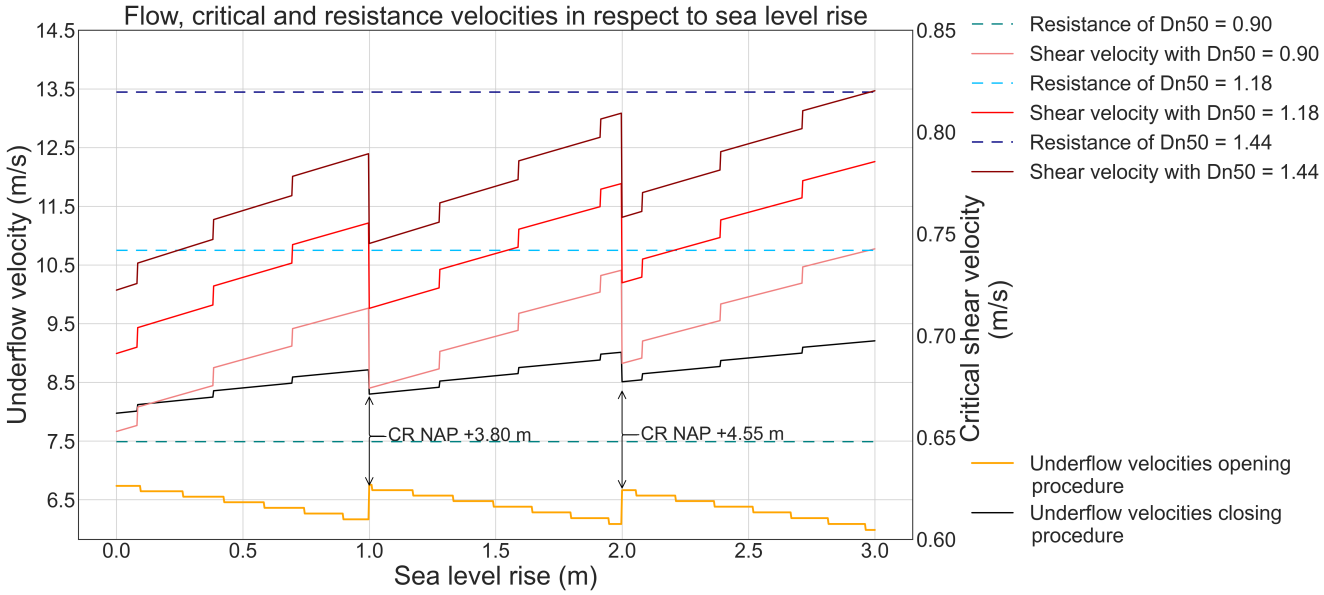

Figure F.24: Computation of the maximum flow velocities due to underflow during the opening procedure, translated into shear velocity over the bed protection and the resistance of the bed protection regarding sea level rise. CR is the altercation in the closing regime closing water level.

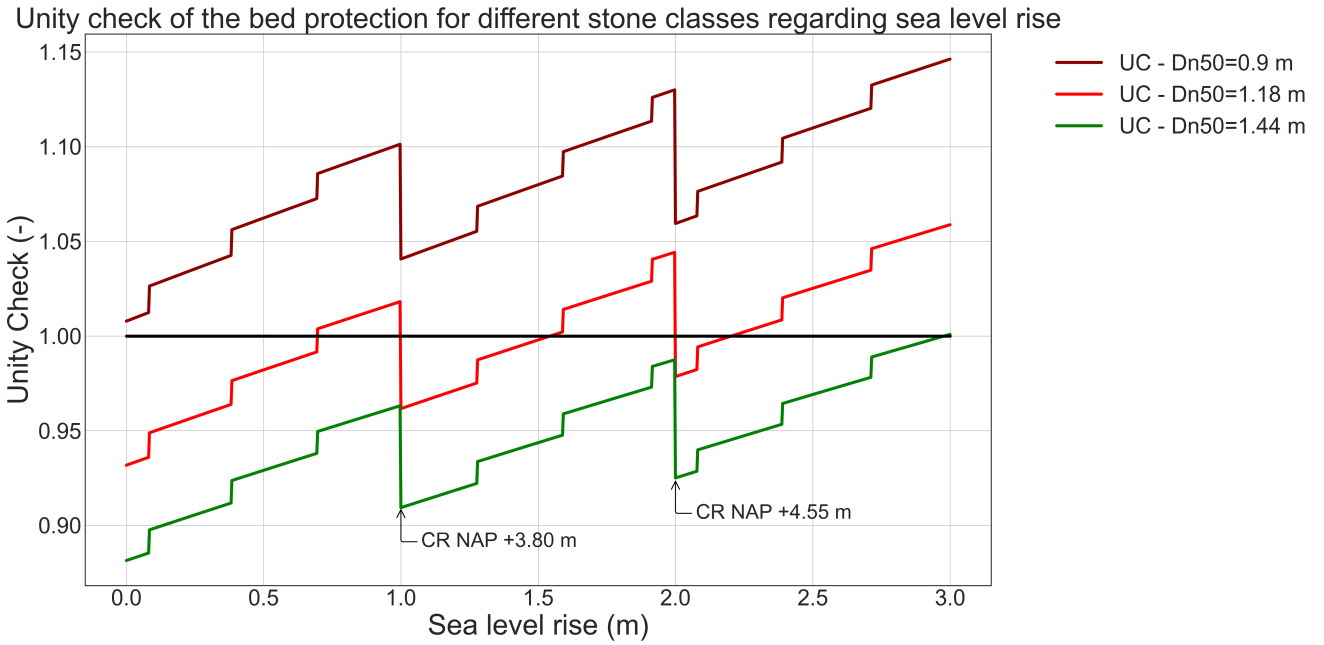

Figure F.25: Unity Check (UC) for the different stone classes. CR is the altercation in the closing regime closing water level.

F.5.3. EROSION DUE TO PLUNGING JET

Although quite unlikely, and mostly dependent on the height of the barrier, occurring storm surge, overtopping waves and water depth, erosion due to a plunging jet could occur. This is verified with the maximum scour depth equation from Molenaar and Voorendt (2019, p. 282):

$$h_{max} = 0.4 \cdot q^{0.6} \cdot \Delta h^{0.4} \cdot D_{50}^{-0.3} - 0.5 \cdot h_0 \tag{F.5.12}$$

Where:

- h_{max} is the max. scour depth
- q is the specific discharge per meter width
- Δh water level difference
- h_0 is the water depth at the plunging jet
- D_{50} is the median nominal diameter, for sand = 1 mm

If a specific discharge of 1 $m^3/s/m$ (1000 l/s/m) is assumed, similar to Huijsman (2021), to check whether plunging jet can cause erosion on the sandy unprotected bed, a water level difference of 17.57 metres is required to form a minimal scour hole in the sandy bed. This phenomena is therefore highly unlikely under the stated conditions.

F.6. BED PROTECTION LENGTH

Erosion can lead to scour holes at the base of the structure, which can cause foundation instabilities. To prevent these instabilities at the base of the structure, a bed protection with a certain length has to be applied. The bed protection displaces the location of the scour hole. The scour hole itself can not be prevented and will always form under the right conditions. The depth of the scour hole is calculated with Eq. (F.6.1):

$$h_s(t) = \frac{(\alpha \cdot \bar{u} - \bar{u}_c)^{1.7} \cdot h_0^{0.2}}{10 \cdot \Delta^{0.7}} \cdot t^{0.4} \tag{F.6.1}$$

Where:

- t is the amount of time elapsed in hours
- $\Delta = 1.585$
- $h_0 = 17$ m
- $\bar{u}$ is the vertically averaged velocity
- $\bar{u}_c$ is the vertically averaged velocity in the base filter
- α factor accounting for turbulence

α is determined by $\alpha = 1.5 + 5 \cdot r_0 \cdot f_c$ with a mini. of 2. (Schiereck and Verhagen, 2019, p. 95) Where:

$$r_0 = \frac{1.2 \cdot \sqrt{g}}{C}$$

$$f_0 = \frac{C}{40}, \text{ with a min. value of 1}$$

The scour hole is checked for various time scales. The different flow velocities occur in different situations:

- Barrier is open: Natural tide ($u_c = 2.9$) with a timescale of 100 years
- During closure: Waves and flow velocity with an average closure time of 8 hours
- During opening and closure of the barrier: Underflow with a timescale of 2 hours and 3 closures per year (6 hours), according to van Oorschot (2016)

The erosion due to natural tide is not checked, for the time being it is assumed that a dynamic equilibrium situation exists. Moreover, some assumptions regarding the operational aspects of the barrier have to be made: the flow velocity during the opening and closing of the barrier is maximum throughout the entire procedure which in reality, as calculated in Fig. F.22 and Fig. F.23, is not the case.

The required length of the bed protection is based on the depth of the scour hole which would occur in the initial base layer of the bed which in this case is sand with a D_{n50} = 1.035 mm. (Verruijt, 2005, p. 12) Initially the required bed length is calculation in the present where sea level rise is equal to 0 metres. For 1 opening procedure of the barrier, with t=2 hours and $u_{c,max}$ = 7.4 m/s, this would result in:

$$d_{n50} = \frac{0.063 + 2}{2} = 1.035mm$$

The characteristics for sand:

$$d_{n50} = 1.035mm$$
$$k_r = 0.1 - 0.5\ m\text{ , assume 0.5 m (unfavourable), height of the ripples (Molenaar and Voorendt, 2019, p. 281)}$$
$$c_f = 0.237 \cdot \frac{a_b}{k_r}^{-0.52} = 0.121$$
$$C_{sand} = 18 \cdot log\frac{12 \cdot R}{k_r} \approx 49\ m^{1/2}/s$$
$$r_{0\,sand} = \frac{1.2 \cdot \sqrt{g}}{C_{sand}} = 0.08$$
$$f_{c\,sand} = \frac{C_{sand}}{40} = 1.225$$
$$\alpha = \max(1.5 + 5 \cdot 0.08 \cdot 1.225\ ;\ 2) = 2$$
$$\psi_c = 0.055$$

ψ_c is the shields parameters, ψ_c = 0.055 is opted for as ψ_c = 0.03 is considered as a conservative choice as it signifies "occasional movement at some locations" of the sand particles (Schiereck and Verhagen, 2019). Therefore, ψ_c = 0.055 is chosen, in which "frequent movement at many locations" transport stage is present.

The shear velocities:

$$u_{*c\,sand} = \frac{\sqrt{g}}{C_{sand}} \cdot u_c = 0.493\ m/s$$
$$u_{*b\,sand} = \sqrt{\frac{c_f}{2}} \cdot \hat{u}_b = 3.49E^{-4}\ m/s$$
$$\bar{u} = u_{*r\,sand} = \sqrt{(u^2_{*c,sand} + u^2_{*b,sand} + 2 \cdot u_{*b,sand} \cdot u_{*c,sand} \cdot \sin(\phi))} = 0.193\ m/s$$
$$\bar{u}_c = u_{c\,sand} = \sqrt{(\psi_c \cdot \Delta \cdot g \cdot d_{n50}} = 0.0297\ m/s$$

Combined the aforementioned values in Eq. (F.6.1) results in scour hole during 1 opening procedure, see Eq. (F.6.2):

$$h_s = \frac{(2 \cdot 0.493 - 0.0297)^{1.7} \cdot 17^{0.2}}{10 \cdot \Delta^{1.7}} \cdot (2 \cdot 3 \cdot 100) = 22.35m \tag{F.6.2}$$

Subsequently, the required length for 1 procedure is calculated for densely packed sand (Schiereck and Verhagen, 2019, p. 100), with the help of the slope angle (β) and ratio in accordance with Schiereck and Verhagen (2019, p. 99):

$$\beta = \arcsin|\,3E^{-04} \cdot \frac{u_0^2}{\Delta \cdot g \cdot d_{n50}} + (0.11 + 0.75 \cdot r_0) f_c\,| \tag{F.6.3}$$

$$\beta = \arcsin|\,3E^{-04} \cdot \frac{2^2}{1.585 \cdot 9.81 \cdot \frac{1.035}{1000}} + (0.11 + 0.75 \cdot 0.08) \cdot 1.175\,| = 0.278$$

Slope ratio:

$$\beta_{ratio} = \frac{1}{\tan\beta} = \frac{1}{\tan 0.278} = 3.51 \tag{F.6.4}$$

Then the required bed length follows from subtracting the previous mentioned ratio from the average slide ratio of densely packed sand of 1:6 Schiereck and Verhagen (2019, p. 100):

$$L_{bed\ protection} = (6 - \beta_{ratio}) \cdot h_s = (6 - 3.51) \cdot 22.35 \approx\ [m] \tag{F.6.5}$$

If this procedure is undertaken for both the required bed length at the sea -and riverside of the barrier, under the influence of sea level rise, the results in Fig. F.26 can be yielded. The progression of the required bed length follows the pattern of the flow velocities regarding the required stone diameter (Fig. F.25).

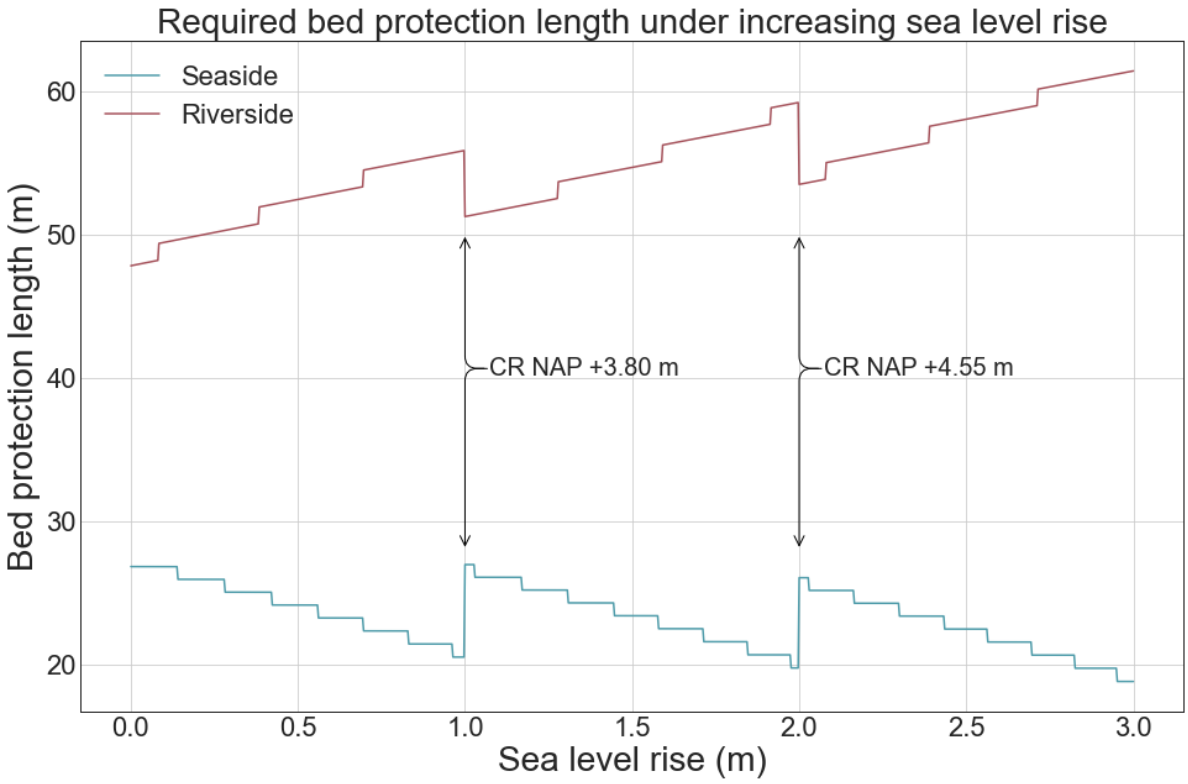

Figure F.26: The required bed length protection of both the sea -and riverside under the influence of sea level rise. The annotations represent the altercations to the closing regime of the barrier (CR = Closing Regime).

F.7. FOUNDATION

The shallow foundation block provides the horizontal, vertical and rotational stability of the barrier. With the attribution of some initial dimensions to the foundation block the influence of sea level rise on these three stability parameters can be evaluated: Appendix F.7.1, Appendix F.7.2 and Appendix F.7.3. The foundation block is shaped as a trapezium installed on a rectangular body, the dimensions of the block (equal to dynamic robust +1.0m design from Table 9.1) are supplied in Fig. F.27. The height of the block in contact with the soil is set at 4 metres.

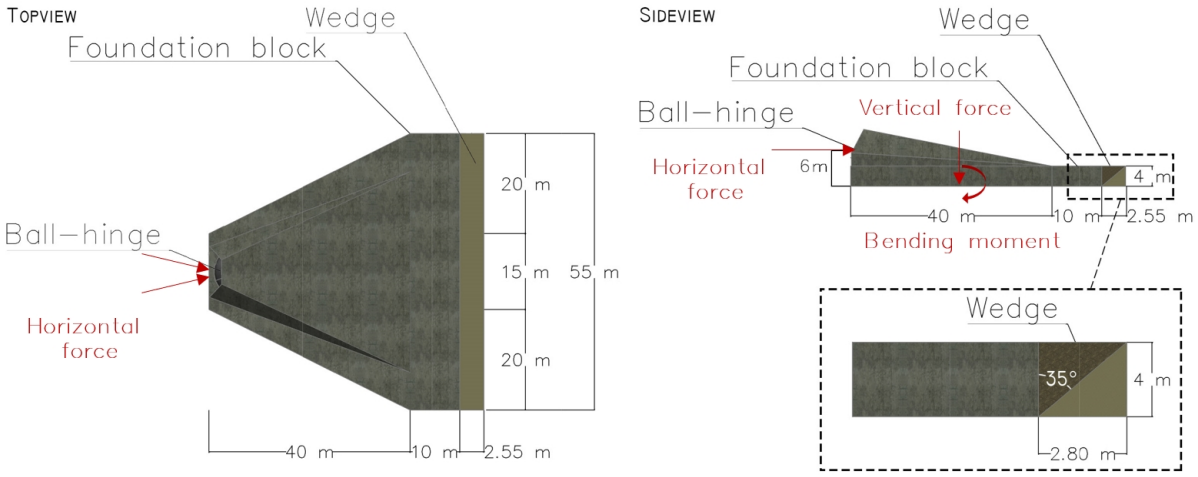

Figure F.27: Top -and side view of the foundation block with direction of forces.

F.7.1. HORIZONTAL STABILITY

To determine whether the foundation is sufficient in horizontal stability the friction force and passive soil pressure are combined and checked versus the acting horizontal force. The friction force is calculated by the vertical acting force on the foundation block in three slip planes:

$$\sum H = f \cdot \sum V \tag{F.7.1}$$

Where:

- Slip plane 1: $f1 = \tan(\delta)$, $\delta = 0.5$ for cast concrete on clean fine to medium sand (Molenaar and Voorendt, 2019)
- Slip plane 2: $f2 = \tan(\phi)$, $\phi = 32.5$ angle of internal friction of sand (Fig. D.7)
- Slip plane 3: $f3 = \tan(\Phi)$, $\Phi = 32.5$ angle of internal friction of sand (Fig. D.7)

The first slip plane yields the lowest resistance and thus the horizontal friction force resistance is calculated with the limit of the first slip plane:

$$H_{friction,Res} = 0.5 \cdot V_{volume,block} \cdot 2{,}500 \cdot 9.81 \text{ kg/m}^3\text{, for reinforced concrete} \tag{F.7.2}$$

What follows is the horizontal resistance due to the passive soil pressure acting on the foundation block. The passive pressure is the soil pressure when a structure pushes against the soil in horizontal direction, visualised in Fig. F.28. Surpassing the bearing capacity of the soil leads to a collapse of the subsoil and results in horizontal settlements of the foundation block.

To determine the maximum allowable horizontal force acting on the soil the method of Coulomb is applied. In Vardon (2020, p.20) an equation is yielded that represents the limit state functions between the horizontal force and the bearing capacity of the soil wedge:

$$Q = \frac{1}{2} \cdot \gamma_{sand} \cdot h^2 + \frac{\frac{1}{2} \cdot \gamma_{sand} \cdot h^2 \cdot \sin\phi_{sand} + c \cdot h \cdot \cos\phi_{sand}}{\cos\theta \cdot \sin(\theta - \phi_{sand})} \tag{F.7.3}$$

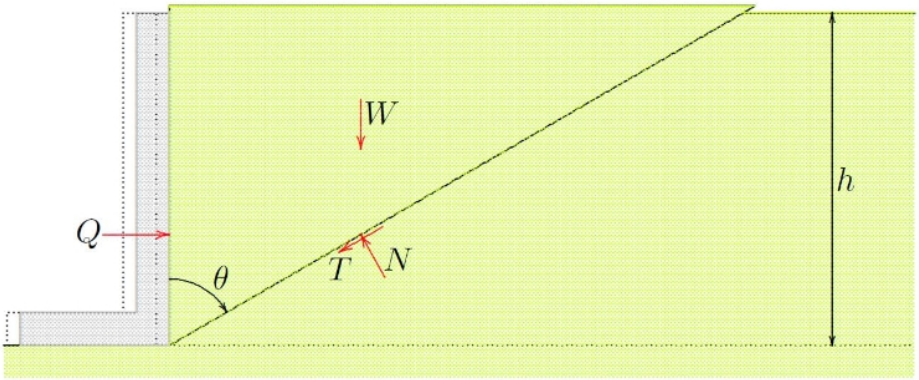

Figure F.28: Passive soil pressure. In which Q is the horizontal force, W is the weight of the soil wedge, T is max. shear force, N the normal force on the wedge, h the height and θ is the angle of the wedge.

Where:

- γ_{sand} = 18 kN/m^2, moderate dense sand Fig. D.7
- ϕ_{sand} = 32.5 degrees, moderate dense sand Fig. D.7
- c = 0, moderate dense sand Fig. D.7
- θ = 45 degrees (Vardon, 2020, p. 20)
- h is the height of the structure in contact with the soil

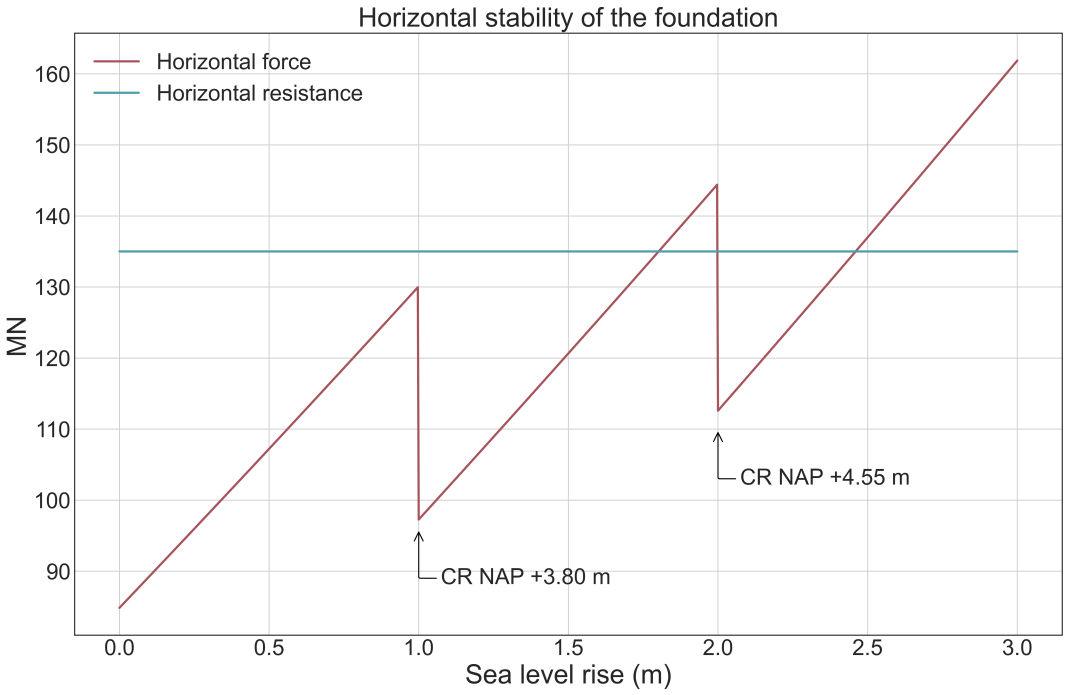

Figure F.29: Horizontal stability of the barrier in regard to the sea level rise. 'CR' are the altercations to the Closing Regime of the barrier.

Combining the equations leads to the following horizontal resistance equation:

$$H_{Res} = f1 \cdot \sum V + Q \tag{F.7.4}$$

By applying the horizontal load influenced by sea level rise and integrating the resistance (Eq. (F.7.4)), the results of Fig. F.29 are yielded. The horizontal force, influencing the horizontal stability, follows

the pattern of the hydraulic loading in Appendix F.2. At a certain value, under the designed dimensions, the horizontal force surpasses the ability of the foundation block to resist these forces.

F.7.2. VERTICAL STABILITY

The vertical stability of a shallow foundation is determined by the comparing the bearing capacity of the subsoil with the acting vertical force and settlement that occur over the lifespan. However, as stated in the scope (Section 1.6), considerations of land subsidence, i.e. settlements, are withheld from the scope of this thesis due to the lack of estimations beyond 2050.

In Molenaar and Voorendt (2019, p. 276) a function that compares the acting forces versus the bearing capacity of the soil is stated. This function, Eq. (F.7.5), is from here on interpreted as the limit state function for the vertical stability.

$$\sigma_{k,max} < p'_{max} \tag{F.7.5}$$

In which the acting load ($\sigma_{k,max}$) is calculated as follows:

$$\sigma_{k,max} = \frac{F}{A_{Foundation}} + \frac{M}{\frac{1}{6} \cdot B \cdot L^2} \tag{F.7.6}$$

The bearing capacity of the subsoil can be determined by applying the Brinch Hansen method. However, according to CUR (2010), as a rule of thumb for densely packed sand, the bearing capacity can be assumed to be equal to 400 N/mm^2.

By applying the horizontal load influenced by sea level rise and the respective selfweight of the foundation block, the results of Fig. F.30 are yielded. The horizontal force, and subsequent bending moment due to the eccentricity of the steel trusses reaching the bottom of the foundation block, follows the pattern of the hydraulic loading in Appendix F.2. As can be deducted form Fig. F.30, with the dimensions of the foundation block, the foundation block is stable over the course of sea level rise.

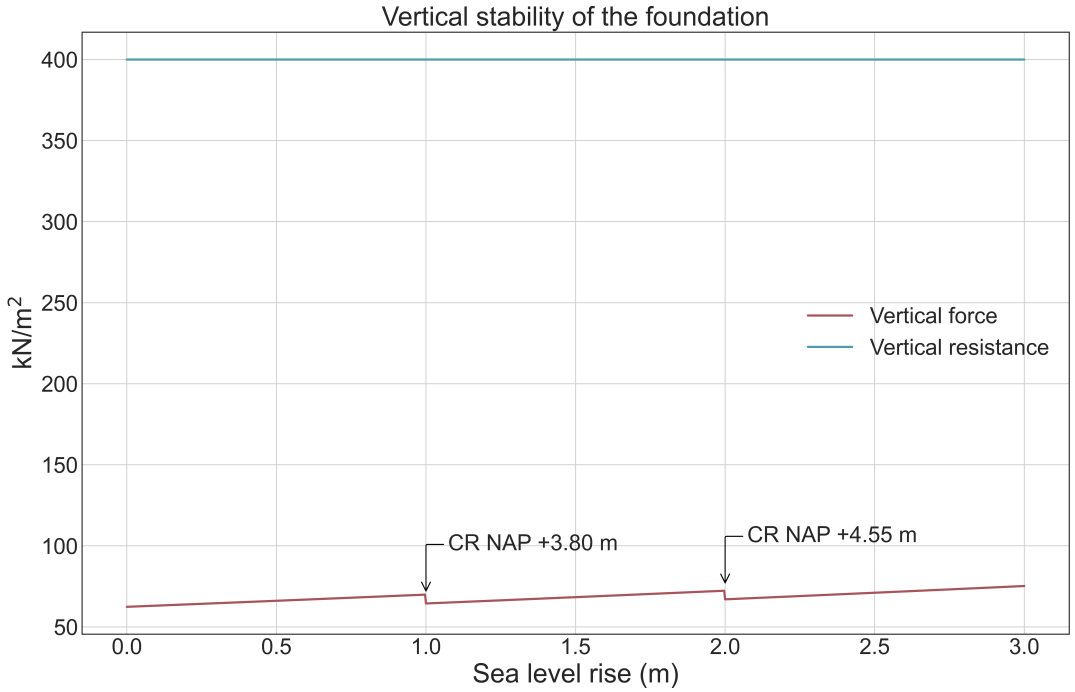

Figure F.30: Vertical stability of the barrier in regard to the sea level rise. 'CR' are the altercations to the Closing Regime of the barrier.

F.7.3. ROTATIONAL STABILITY

The rotational stability of the foundation block is defined by eccentricity of the resulting forces. Due to the poor properties in adhesion and cohesion of soil, no tensile stresses are allowed to develop. This is the case when the resulting force (M divided by V) intersects the core of the foundation block (Molenaar and Voorendt, 2019). Thus, the limit state function (Eq. (F.7.8)) to determine the rotational stability of the foundation block is rewritten from the equation that defines the eccentricity of the resulting force in relation to the width of the core, see Eq. (F.7.7).

$$e_R = \frac{\sum M}{\sum V} \leq \frac{1}{6} \cdot L \qquad \text{(F.7.7)}$$

$$Z = \frac{1}{6} \cdot L - \frac{\sum M}{\sum V} \qquad \text{(F.7.8)}$$

The vertical downward force follows from the combined selfweight of the foundation block and the ball-hinge. The bending moment follows from the compressive force in the steel trusses, which transfer the loading to the ball-hinge and foundation block, multiplied with the arm, from point of ball-hinge attachment to bottom of the block. As an example the selfweight of the block, with the dimensions provided in Fig. F.27, and bending moment at +1.0 metre sea level rise (130 MN, see Fig. F.29) is computed:

$$\sum V_{Ed} = A_{block} \cdot h_{block} \cdot \rho_{concrete} \cdot g + V_{ball-hinge} = 2{,}050 \cdot 4 \cdot 2{,}500 \cdot 9.81 = 208\ MN + 6.8\ MN$$
$$\sum M_{Ed} = F_{steel\ trusses} \cdot h_{Arm} = 130{,}000 \cdot 6 = 780\ MN$$

Integrating the forces over a range of sea level rise, yields the results in Fig. F.31 and shows that instability due to rotational instability is highly unlikely.

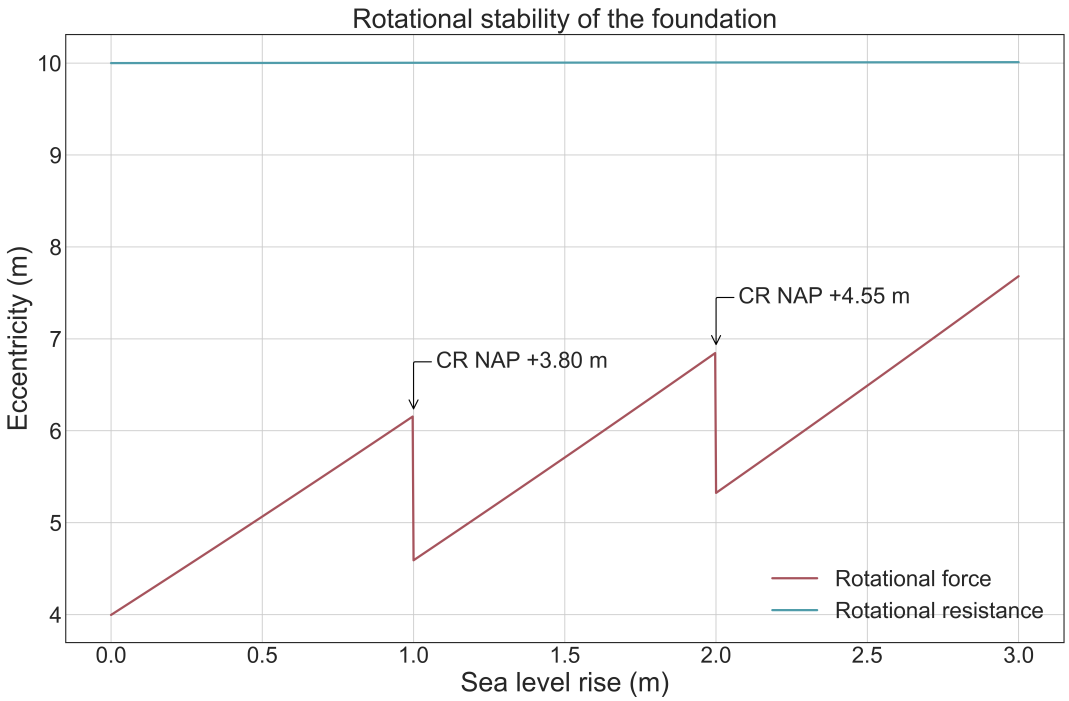

Figure F.31: Rotational stability of the barrier in regard to the sea level rise. 'CR' are the altercations to the Closing Regime of the barrier.

F.7.4. HORIZONTAL STABILITY AND WEDGE SOIL IMPROVEMENT ADAPTATION

If the horizontal forces surpass that of the resistance an soil improvement of the wedge, see Fig. F.27 and Fig. F.28, could be applied. The improvement increases the resistance in passive soil pressure. By replacing the sand in the wedge by a heavier material, i.e. gravel, the passive soil pressure is increased (Eq. (F.7.3)):

$$Q = \frac{1}{2} \cdot \gamma_{sand} \cdot h^2 + \frac{\frac{1}{2} \cdot \gamma_{sand} \cdot h^2 \cdot \sin\phi_{sand} + c \cdot h \cdot \cos\phi_{sand}}{\cos\theta \cdot \sin(\theta - \phi_{sand})}$$

Where:

- γ_{sand} = 18 kN/m^2, moderate dense sand Fig. D.7
- γ_{gravel} = 21 kN/m^2, solid gravel Fig. D.7
- ϕ_{sand} = 32.5 degrees, moderate dense sand Fig. D.7
- ϕ_{gravel} = 35 degrees, solid gravel Fig. D.7
- c = 0, for both sand and gravel Fig. D.7
- θ = 45 degrees (Vardon, 2020, p. 20)
- h is the height of the structure in contact with the soil

Where the dimensions of the preferable design, in Chapter 10, are taken (50x55x4 - LxBxh). Would result in the passive soil pressure over the entire width:

$$Q_{sand} = 29.5\ MN$$
$$Q_{gravel} = 43.0\ MN$$

These values are then added to the Comparing this over a range of sea level rise results in Fig. F.32 and shows the increase in horizontal stability with the adaptation.

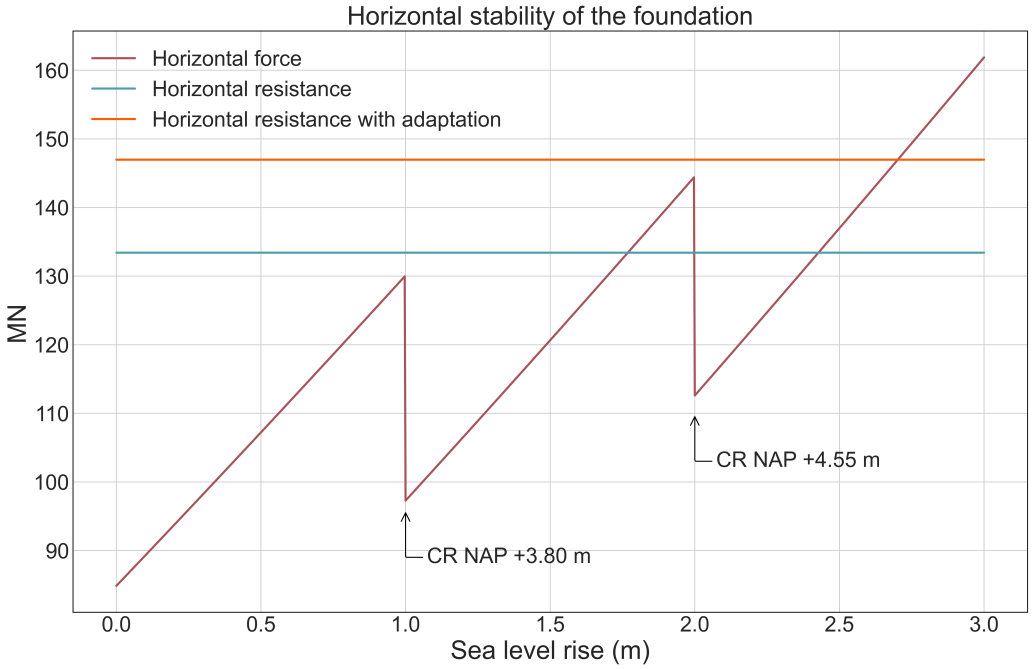

Figure F.32: Horizontal stability of the barrier in regard to the sea level rise with(out) wedge soil improvement adaptation. 'CR' are the altercations to the Closing Regime of the barrier.

G | Integration of sea level rise distributions

In this appendix chapter the computation and integration of a sea level rise scenario is elaborated. In Appendix G.1 the saturation of the sea level rise (growth) scenarios into the reliability model is discussed. Followed by the Python model used to generate these scenarios in Appendix G.2.

G.1. Saturation of the scenarios in the reliability model

The sea level rise scenario RCP8.5 from the Fifth Assessment Report in IPCC (2014a) is inserted into the model with an Excel sheet defining the 5th, 50th and 95th percentiles of the prediction of each specific RCP scenario. These values are then inserted into the Sea level rise Python module, see Fig. G.3. In this module the relative percentiles are transformed into Probability Density Functions (PDF's), see Fig. G.1. The Python module is supplied in Appendix G.2.

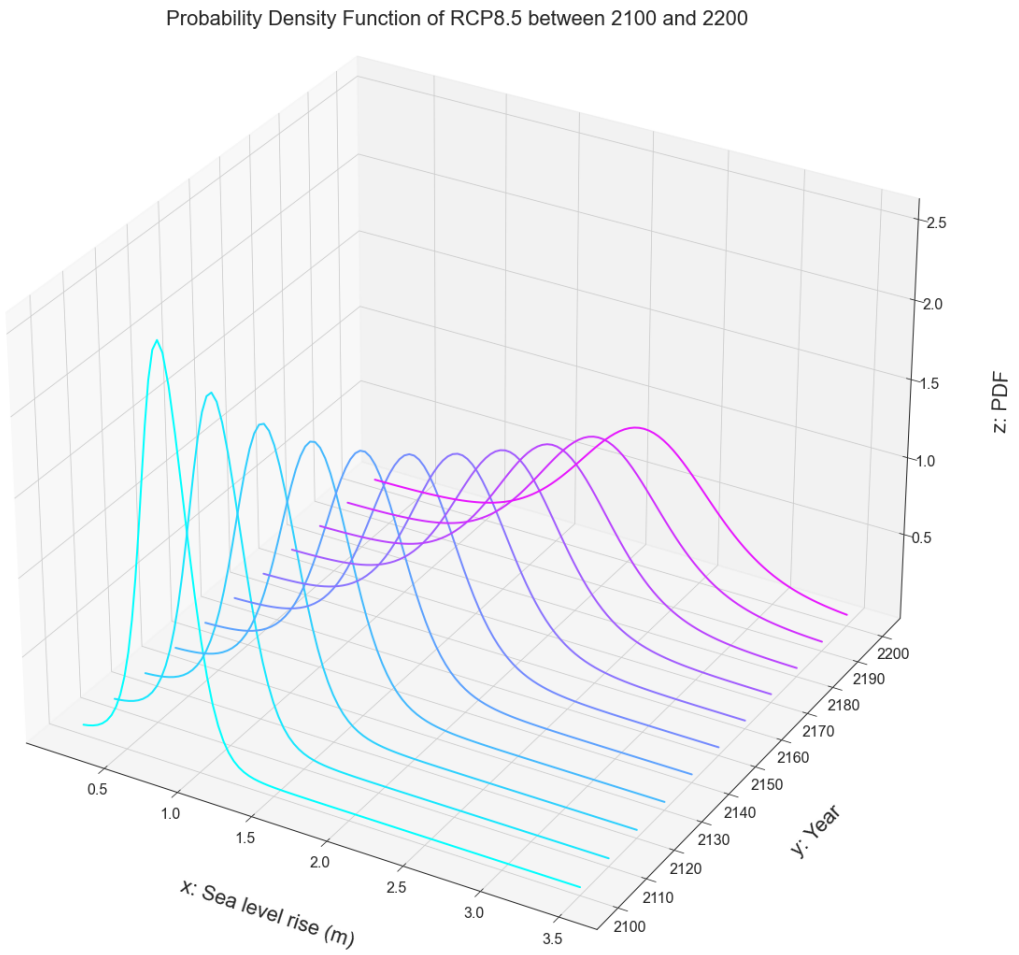

Figure G.1: Probability Density Functions over time for sea level rise scenario RCP8.5.

From these PDF's N random values are drawn over the entire time frame. The time frame utilised in the reliability model is a simple array ranging from 2100 to the year 2200 with time steps of 10 years, so 11 steps in total. The N scenarios drawn from the PDF's and over the time frame are defined as 'growth scenarios' as for each N scenario drawn in time step i, a new value in time step i+1 is drawn, see Fig. G.2.

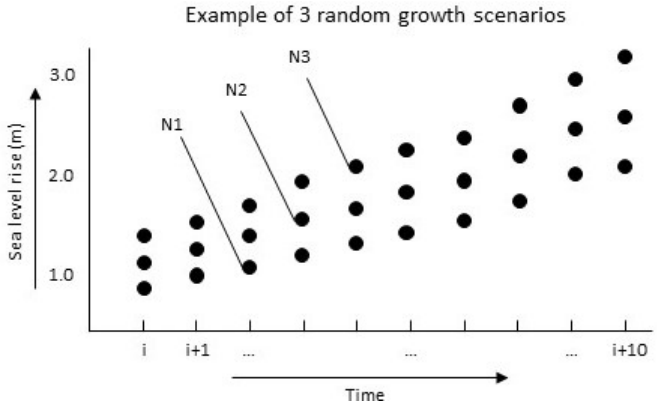

Figure G.2: Example generation sea level rise growth scenarios.

The height of the scenario in the next time step is bounded between a certain range of increase, for RCP8.5 the increase in sea level rise is between 0.1 and 0.3 metres. These random scenarios are then defined as 'growth scenarios'. Eventually this leads to the results of Fig. G.3 and these growth scenarios are inserted into the reliability model to define the loading conditions and in turn the exceedance probabilities.

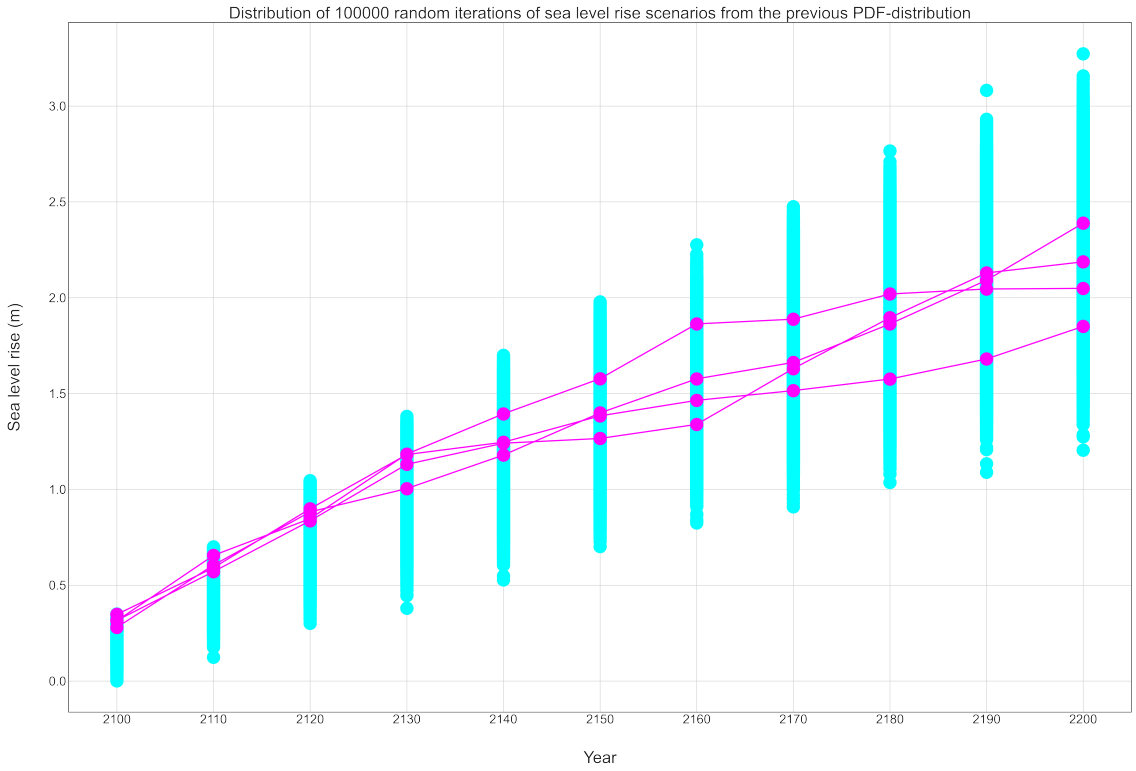

Figure G.3: Visualisation of N random growth scenarios from sea level rise scenario RCP8.5 which is utilised for the reliability model. The purple scenarios represent four individual growth scenarios.

However, due to the setup of the model, the generated scenarios deviates from the original PDF's (Fig. G.1). In Fig. G.4 a comparison between the original distribution and the generated distribution for the year 2200 is made.

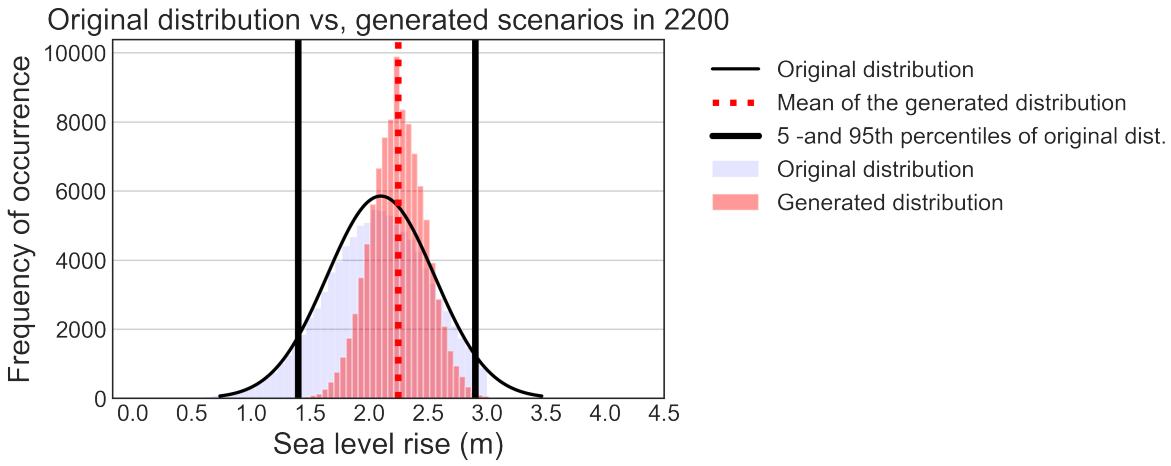

Figure G.4: Comparison between the distribution of the original and generated sea level rise scenarios in 2200.

From the figure it can be concluded that the generated distribution deviates from the original one. More scenarios lie around the median and the median has shifted a bit to the right. Additionally, the spread of the distribution has become less. The reason behind this deviation is due to a set of rules implemented in order to generate the sea level rise scenarios over time:

- The relative sea level rise in year 'i+1' must be higher than in year 'i'
- The relative sea level rise between year 'i' and 'i+1' must be lower than 0.35 metres

These rules were implemented so that sea level rise between intervals could not suddenly be lower than the previous year and to limit the amount of possible increase between two intervals.

G.2. SEA LEVEL RISE PYTHON MODULE

```
def Sea_level_rise(Sealevelrise, N, x, H_MLK):

    RCP85_Lower = Sealevelrise.iloc[0,:]
    RCP85_Median = Sealevelrise.iloc[1,:]
    RCP85_Upper = Sealevelrise.iloc[2,:]
    RCP85_Extreme = Sealevelrise.iloc[3,:]

    x = np.linspace(2100,2200,11)

    SLR_lower = np.array(RCP85_Lower)
    SLR_median = np.array(RCP85_Median)
    SLR_upper = np.array(RCP85_Upper)
    sigma = np.zeros(11)

    for i in range(11):
        year = np.linspace(2100,2200,11)
        a = SLR_lower[i]
        b = SLR_median[i]
        d = SLR_upper[i]
        sigma_05 = (b - a)/1.65
        sigma_95 = -(b - d)/1.65
        sigma_true = (sigma_05 + sigma_95)/2
        xvalue_05_SLR = norm.ppf(0.05, loc = SLR_median[i], scale = sigma_true)
        xvalue_50_SLR = norm.ppf(0.50, loc = SLR_median[i], scale = sigma_true)
        xvalue_95_SLR = norm.ppf(0.95, loc = SLR_median[i], scale = sigma_true)
        sigma[i] = sigma_true

    #print('5th percentile SLR of the year', year[i] , round(xvalue_05_SLR, 2), 'in metre NAP+')
    #print('50th percentile SLR of the year', year[i] , round(xvalue_50_SLR, 2), 'in metre NAP+')
    #print('95th percentile SLR of the year', year[i] , round(xvalue_95_SLR, 2), 'in metre NAP+')
    sigma2200 = sigma[10]

    DWL = np.zeros((N,len(x))) #Empty matrix for design water level
    SLR_matrix = []             #Empty matrix for SLR scenarios in 'j'
    DWL_matrix = []             #Empty matrix for design water level in 'i'
    H_MLK_matrix = np.full((N, 1), H_MLK, dtype=int) #Matrix full of initial design height of the gates for in the loop

    for i in range(N):
        SLR = np.zeros(len(x))                                      #Empty array for SLR scenario for every 'N' loop
        for j in range(len(x)):
            SLR[j] = rng.normal(SLR_median[j], sigma[j], 1)         #Draws random value out of the PDF per year cycle along 'j'
            while SLR[j] <= SLR[j-1] or SLR[j] - SLR[j-1] >= 0.35:   #If the value in 't+1' is smaller than
                                                                      #->in 't' neglect that string
                SLR[j] = rng.normal(SLR_median[j], sigma[j], 1)
            if j == len(x)-1:
                SLR_matrix.append(SLR)
                #print('These are the', N,'SLR matrices:', SLR_matrix)
        if i == N-1:                                                #Looping the SLR_matrix, with SLR scenario 1 step,
                                                                    #->N times and storing in matrix
            DWL_matrix.append(SLR_matrix)
            DWL = round(pd.DataFrame(data=SLR_matrix, columns=['2100', '2110', '2120', '2130', '2140', '2150', '2160', '2170',
                                                               '2180', '2190', '2200']),2) #replace columns by 'x' if float
            #print(DWL)
            DWL.insert(0, "Scenario", np.linspace(1,N,N), True)     #Inserting columns into the matrix
            H_MLK_matrix = np.full((N, 1), H_MLK, dtype=int)        #Inserting columns into the matrix
            DWL.insert(1, "Height MLK", H_MLK_matrix, True)         #Inserting columns into the matrix
            #print(DWL)
            DWL_plot = np.transpose(np.squeeze(DWL_matrix))
            SLR = DWL_plot
    return DWL_plot, SLR
```

Figure G.5: Python script that generates the N sea level rise growth scenarios.

```
from mpl_toolkits.mplot3d import Axes3D
from matplotlib.collections import PolyCollection
from matplotlib import colors as mcolors

import matplotlib as mpl
import seaborn as sns
import warnings; warnings.filterwarnings(action='once')

large = 22; med = 16; small = 12
params = {'axes.titlesize': large,
          'legend.fontsize': med,
          'figure.figsize': (16, 10),
          'axes.labelsize': large,
          'axes.titlesize': large,
          'xtick.labelsize': med,
          'ytick.labelsize': med,
          'figure.titlesize': large}
plt.rcParams.update(params)
plt.style.use('seaborn-whitegrid')
sns.set_style("white")


fig = plt.figure(figsize=(30,20))
irange = np.linspace(0,N,N+1)
cmap = matplotlib.cm.get_cmap('cool')
cmap_list = (irange)/(len(irange)-1)
list_colours = cmap(cmap_list)



plt.plot(x, DWL_plot, marker='o', linestyle=' ', c=list_colours[8], markersize=20) #keep
plt.plot(x, DWL_plot[:,0:4], marker='o', markersize=20) #keep

plt.xlabel('Year', labelpad=40)
plt.ylabel('Sea level rise (m)', labelpad=40)
plt.xticks(np.arange(2100, 2210, 10))
plt.title('Distribution of '+str(N)+ ' random iterations of sea level rise scenarios from the previous PDF-distribution')
plt.grid()
plt.show()
```

Figure G.6: Python script that generates the growth scenarios from Fig. G.3.

H | Cost derivations of the design strategies and adaptations

When considering the varying design strategies the overall construction costs of the strategy is not included. Instead, where the costs of the components where adaptations are possible are compared. In Appendix H.1 the cost of the static robust (conservative) and the three dynamic robust designs are derived. This is followed by the derivation of costs for the necessary adaptations in Appendix H.2. In Appendix H.3 the applied investment and inflation rate is elaborated. To compare the varying design strategies the overall

H.1. Derivation of cost differences of the design strategies

The costs of the components that can be adapted are stated for each individual design strategy. In addition, the savings on the initial investment is stated, this amount is able to compound over time until an adaption has to be applied.

H.1.1. Foundation

To derive the differences in costs between the four design strategies, the volume of the foundation blocks are multiplied with the costs of concrete (€152.00 p/m^3) and amount of reinforcement needed (€2.20 p/kg), this would result in a cost of €172.70 p/m^3 of concrete, if an reinforcement ratio of 1% is assumed. (Cobouw, nd) Subtracting the initial investments of the dynamic strategies from the static strategy results in initial savings that are able to compound over time and results in Table H.1.

Table H.1: Comparative costs of the foundation blocks of the four design strategies.

Foundation block	**Static**	**Dynamic+1.0**	**Dynamic+1.5**	**Dynamic+2.0**
Width (m)	59	53	55	56
Volume single (m^3)	8,680	7,960	8,200	8,320
Two foundation blocks	17,360	15,920	16,400	16,640
Concrete costs (€p/m^3)	152.00	152.00	152.00	152.00
Reinforcement (€p/m^3) ≈ 1% reinforcement ratio	172.70	172.70	172.70	172.70
Total (M€)	**5.64**	**5.17**	**5.33**	**5.40**
Savings (€)	-	**470,000**	**310,000**	**240,000**

H.1.2. Bed protection

To derive the differences in costs between the four design strategies, the required tonnage per square metre of the armour layer is multiplied with the total width (360 m) and length of the bed protection. The transporation and 'production' of the stones to the designated location of the barrier is retrieved with the help of H&B grondstoffen (2021) and Sweco Nederland Bv (2021) , €33.18 p/ton and €30.18 p/ton for d_{n50} 1.44 m and 1.18 m respectively. Subtracting the initial investments of the dynamic strategies from the static strategy results in initial savings that are able to compound over time and results in Table H.2. When considering the savings between different lengths of the bed protection are equal to the additional length adaptation in Table H.6. Differences in installation times for the

bed protection, leading to hindrance to shipping utilising the New Waterway is not included in the costs as it is assumed that these for all four design strategies is somewhat similar. The costs of the hindrance when installing the adaptation, however, is included as installation of a bed protection has to be conducted for a second time.

Table H.2: Comparative costs of the bed protection of the four design strategies.

Bed protection - Armour layer	**Static**	**Dynamic+1.0**	**Dynamic+1.5**	**Dynamic+2.0**
d_{n50} (m)	1.44	1.18	1.18	1.18
Required thickness ($1.5d_{n50}$)	2.16	1.77	1.77	1.77
Ton per m^2	3.25	2.70	2.70	2.70
Length (m)	58.3	55.0	56.0	57.0
Costs stone (€p/ton)	37.37	33.99	33.99	33.99
Placement (€p/ton)	34.30	34.30	34.30	34.30
Total (M€)	**4.89**	**3.65**	**3.72**	**3.78**
Savings (M€)	-	**1.24**	**1.17**	**1.11**

H.1.3. SECTOR GATES

In Huijsman (2021) an approximation of various costs for gate segments of locks to ratio of their dimensions is established. In this thesis a similar approach is applied. However, as of yet, no costs for only the gate segments of sector gate barrier are retrieved. Therefor, a reference gate segment, its dimensions and costs from Huijsman (2021) is scaled to the dimensions of the sector gate applied in this thesis. The ratio is determined as in Eq. (H.1.1).

$$\text{Ratio} = \frac{T_1 \cdot W_1 \cdot H_1}{L_2 \cdot W_2 \cdot H_2} \tag{H.1.1}$$

Where:

- T is the thickness of the gate
- W is the width of the gate
- H is the height of the gate

The reference roller gate in Huijsman (2021, p. 179) is computed at M€8.0 with 7.5x38x19.8. The ratio is separated into two segments, one for the top and one for the bottom, as the barrier is L-shaped. The ratios for the static robust design then are:

$$\text{Ratio}_{bottom} = \frac{15 \cdot 200 \cdot 7}{7.5 \cdot 38 \cdot 19.8} = 3.72$$

$$\text{Ratio}_{top} = \frac{7 \cdot 200 \cdot 17.7}{7.5 \cdot 38 \cdot 19.8} = 4.39$$

To compute the total costs of two sector gates the monetary values for the bottom and top segments are multiplied with two (two sector gates) and a factor of 1.5 due to the complexity of the sector gates in comparison to the roller gate, which could be considered as a relatively simpler design. The same process is repeated for the derivation of the gate extension cost in Appendix H.2.3.

H.2. DERIVATION OF COSTS OF THE ADAPTATIONS

In this section the costs of the various adaptations are derived.

H.2.1. FOUNDATION

By replacing the soil that provides a part of the horizontal support to the foundation block it is aimed to increase this support in case the horizontal loads increase. As stated in Appendix F.7.1, the soil behind the barrier has a horizontal bearing capacity before settlements occur. This bearing capacity

Table H.3: Comparative costs of the sector gates of the four design strategies.

Sector gates	**Static**	**Dynamic+1.0**	**Dynamic+1.5**	**Dynamic+2.0**
Sector gate height (m)	24.3	22.8	23.2	23.5
Sector gate length (m)		200		
Reference roller gate (TxWxH)		7.5x38x19.8		
Reference roller gate (M€)		8.0		
Sector gate bottom (TxWxH)		15x200x7		
Sector gate bottom (M€)		29.8		
Sector gate top (TxWxH)	7x200x17.7	7x200x15.8	7x200x16.2	7x200x16.5
Sector gate top (M€)	35.1	31.4	32.2	32.8
Total two sector gates (M€)	**194.7**	**183.6**	**186.0**	**187.8**
Savings (M€)	-	**11.1**	**8.7**	**6.9**

is determined by the height of the foundation block in contact with the soil and the soil properties. The most dominant soil properties that influence this capacity are the angle of internal friction and selfweight of the soil. Initially it is assumed that the foundation block is supported by moderately dense clean sand with a selfweight of 18 kN/m^3 and angle of internal friction ϕ = 32.5. If necessary the soil is replaced by gravel which has a higher selfweight value of 21 kN/m^3 and an angle of internal friction of ϕ = 35 if it is assumed that it is silty and the consistency is solid. To determine the amount of backfill behind the foundation blocks it is assumed that a cube is excavated behind the barrier and filled by gravel. The amount of cubic metres necessary to be excavated and filled is determined as follows:

$$L_{wedge} = H_{block} \cdot \tan\phi \cdot \alpha = 4.20\ m$$
$$A_{surface} = (B_{block} + \beta) \cdot L_{wedge}$$
$$V_{volume} = A_{surface} \cdot H_{block}$$

Where the factor α is introduced so that the length of the backfill properly surpasses that of the maximum length of the wedge and β to ensure the backfill is properly in contact with the foundation blocks, 1.5 (-) and 10 (m) respectively. These dimensions are then multiplied with derived costs from Cobouw (nd) and Grondverzet (nd), which are stated in the list below. The costs are divided into two categories, costs per square metre and per cubic metre. In Table H.4 the derived costs of the adaptation for the three dynamic strategies are stated.

- Excavation and transport: €35.00 p/m^3 Grondverzet (nd)
- Flatten subsoil: €7.54 p/m^2 Cobouw (nd)
- Supply and transport gravel: €61.53 p/m^3 Cobouw (nd)
- Densification: €42.50 p/m^2 Cobouw (nd)
- Finishing:€7.50 p/m^2 Cobouw (nd)
- Total costs p/m^2: €57.54
- Total costs p/m^3: €96.53

H.2.2. BED PROTECTION

The adaptations of the bed protection is sub-divided into two segments: the armour layer and length of the bed protection at the riverside of the barrier. The costs of these adaptations are elaborated:

Table H.4: Costs of the adaptation of the foundation for the dynamic design strategies.

Foundation	**Dynamic+1.0**	**Dynamic+1.5**	**Dynamic+2.0**
Width (m)	53	55	56
Height (m)		4	
Wedge length (m)		≈ 4.20	
Surface area double backfill (m^2)	530	546	554
Surface costs (€)	€30,500	€31,400	€31,900
Volume double backfill (m^3)	2,120	2,184	2,216
Volume costs (€)	€205,000	€211,000	€214,000
Total (€)	**€235,500**	**€242,400**	**€245,900**

Armour layer

Within this thesis two adaptation option for the armour layer of the bed protection are considered: replacing the current armour layer and instate a larger stone dimensions (from d_{n50} = 1.18 to 1.44 m) or penetrate the armour layer with colloidal concrete to increase the 'adhesiveness' of the armour layer and prevent the movement of the stones. Costs of the removal of the armour layer and penetration with colloidal concrete are retrieved from Cobouw (nd). Costs concerning the placement of d_{n50} as the armour layer has, similarly as in Appendix H.1.2, been retrieved from H&B grondstoffen (2021). From Table H.5 it is evident that applying colloidal concrete has the economical advantage by large margin, therefore, the option of replacing the armour layer with a larger stone dimension is abolished.

Table H.5: Costs of the adaptation of the armour layer of the bed protection for the dynamic design strategies.

Action	**Unit indicator**	**Dynamic+1.0**	**Dynamic+1.5**	**Dynamic+2.0**	**Cost per unit**
Removal (d_{n50} = 1.18 m)	Tonnage	53,460	54,432	55,404	€4.41
Placement (d_{n50} = 1.44 m)	Tonnage	64,350	65,520	66,690	€71.67
Combined Replacement	€	-	-	-	-
Colloïdal concrete	Tonnage	17,820	18,114	18,468	€119.00

Action	**Unit indicator**	**Dynamic+1.0**	**Dynamic+1.5**	**Dynamic+2.0**
Removal (d_{n50} = 1.18 m)	€	€236,000	€240,000	€244,000
Placement (d_{n50} = 1.44 m)	€	€4,610,000	€4,700,000	€4,780,000
Combined Replacement	€	€4,726,000	€4,810,000	€4,894,000
Colloïdal concrete	€	€2,120,000	€2,160,000	€2,200,000

Bed length increase

Due to the formation of scour holes at the toe of the bed protection instabilities of the structure could occur over the duration of the structures lifetime. As is verified in Appendix F.6 the required bed protection length increases with sea level rise and although the margin between the static and dynamic design strategies are very slim, the variance in costs between these are approximated in Table H.6. When considering the hindrance to shipping utilising the New Waterway in economical terms an estimate of the duration of the works is determined. According to Cobouw (nd) it takes roughly 0,009 hours per ton for projects around 1,000 tons. A full day of hindrance is estimated to inflict around M€2.2 and M€3.4 of damages (Section 4.2.1). It is assumed that during the installation of the adaptation some passage is still possible therefore the lower boundary value is taken and divided by three. These damages are considered to be inflicted over a full day (24 hours).

Table H.6: Costs of the adaptation of the length of the bed protection for the dynamic design strategies.

Action	**Length+3.0**	**Length+2.0**	**Dynamic+1.0**
Additional protection length (m)	+3.0	+2.0	+1.0
Costs d_{n50} = 1.44 m	€131,169	€87,446	€43,723
Costs d_{n50} = 1.18 m	€99,115	€66,077	€33,038
Tonnage (d_{n50} = 1.18 m)	2,916	1,944	972
≈ Hours	26.2	17.5	8.8
Costs hindrance shipping	€400,000	€267,000	€134,000
Total costs d_{n50} = 1.18 m	**€531,000**	**€354,000**	**€178,000**

H.2.3. SECTOR GATES

Considering the same method applied in Table H.3 an indicative cost can be retrieved for the gate extension. However, due to the increased complexity of the installation an extra amount of work needed to install these extensions, the costs are multiplied with a factor of 2.5. Sector gates with an extension of 0.5 and 1.0 metres are considered in Table H.7.

Table H.7: Costs of the adaptation of the sector gates for the dynamic design strategies.

Action	**Extension +0.5m**	**Extension +1.0m**
Reference roller gate (TxWxH)	7.5x38x19.8	
Reference roller gate (M€)	8.0	
Sector gate (TxWxH)	7x200x0.5	7x200x1.0
Sector gate extension (M€)	M€2.48	M€4.96
Total (two) extension costs (M€)	**M€4.96**	**M€9.92**

H.3. APPLIED RATES ON SAVINGS AND COSTS OVER TIME

The economic savings, determined in the previous sections, are available to be invested elsewhere. As long as no additional investment is needed, the value is able to gain compounded interest. In this thesis the interest rate is equalised to the discount rate of 4% used for the determination of the costs of the varying adaptive pathways. The equation to determine the economic savings in a specific year is given in Eq. (H.3.1), where $S_{t=0}$ is the initial save of the design strategy and $S_{t=X}$ value of the compounded savings in year X.

$$S_{t=X} = S_{t=0} \cdot (100 + 4\%)^X \tag{H.3.1}$$

Although the savings increase over time, so do the costs of the adaptation through inflation. The European Union aims to, on average, have an inflation rate of 2%. (European Central Bank, nd) Therefor, the costs of the adaptation are compounded with this inflation rate. The equation to determine the costs of the adaptation in a specific year is given in Eq. (H.3.2), where $C_{t=0}$ is the initial costs of the adaptation and $C_{t=X}$ the costs in year X.

$$C_{t=X} = C_{t=0} \cdot (100 + 2\%)^X \tag{H.3.2}$$

At a certain point in time the compounded savings equals the compounded costs, if the adaptation could be delayed even further this would result in positive economic effect of the adaptation and the design strategy. This principle is shown with an example. Let us assume an initial save of €1000 and the costs of strengthening this fictive component of €2000. This results in the progression over time as shown in Fig. H.1, after 36 years, the adaptation becomes efficient.

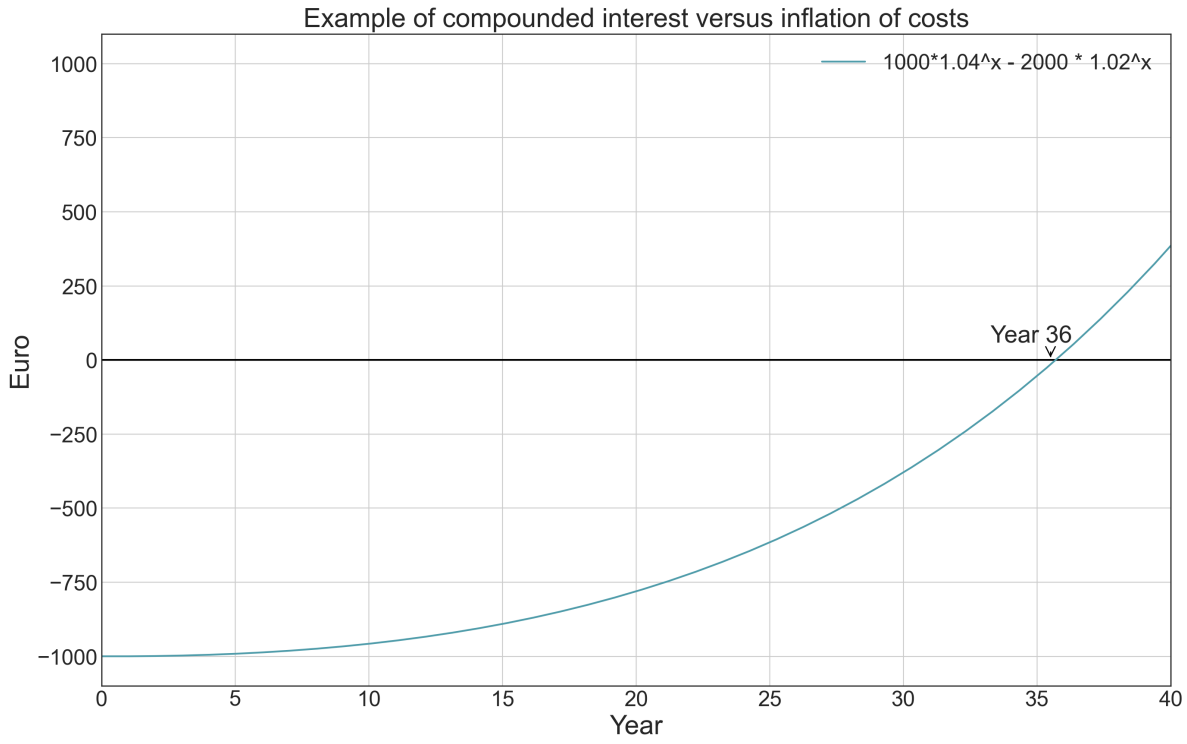

Figure H.1: Example of progression of compounded savings versus inflation of costs.

H.4. DETERMINATION PERFORMANCE ADAPTATION

To elaborate on the manner of determining whether an adaptation is considered as cost-effective an example is supplied in Fig. H.2. In Fig. H.2 three different scenarios of the same component with the same adaptation is visualised. Hypothetically, the moment when a component has to be adapted depends on the input from the sea level rise distribution and thus can vary for different scenarios, this in turn leads to varying moments in time when this adaptation is necessary: alphabetical letter A to D in Fig. H.2. If a closer look is taken at Scenario 3 (green) and location A, it can be concluded that the adaptation is resulting in a negative monetary effect. This is due to hypothetical equation that determines the economic value Eq. (H.4.1) and one could deduct that the adaptation was required too soon in order to net a beneficial economic value, thus the adaptation is considered as in-effective in this scenario.

$$€\text{Savings}_{t=0} \cdot 10^6 \cdot 1.04^X - €\text{Costs Adaptation}_{t=0} \cdot 10^6 \cdot 1.02^X \tag{H.4.1}$$

Where:

- $€\text{Savings}_{t=0}$ = M€12.5
- $€\text{Costs Adaptation}_{t=0}$ = M€15.0

Now consider Scenario 2 (red), it can be seen that the first adaptation (first dip near C) is delayed enough to net a positive economic value. However, whilst progressing in time towards B, when a second adaptation of the component is necessary the effectiveness of the adaptation becomes negative, one could argue that the years between the first and second adaptation provided to be insufficient to net a positive economic value. Lastly, consider Scenario 1 (blue) and locations C and D in time, from this scenario it can easily be conducted that both adaptations net a very beneficial economic value. In this hypothetical example, it can be concluded that the first adaptation is cost-

effective in 2 out of 3 scenarios and the second adaptation is effective in 1 out of 3 scenarios.

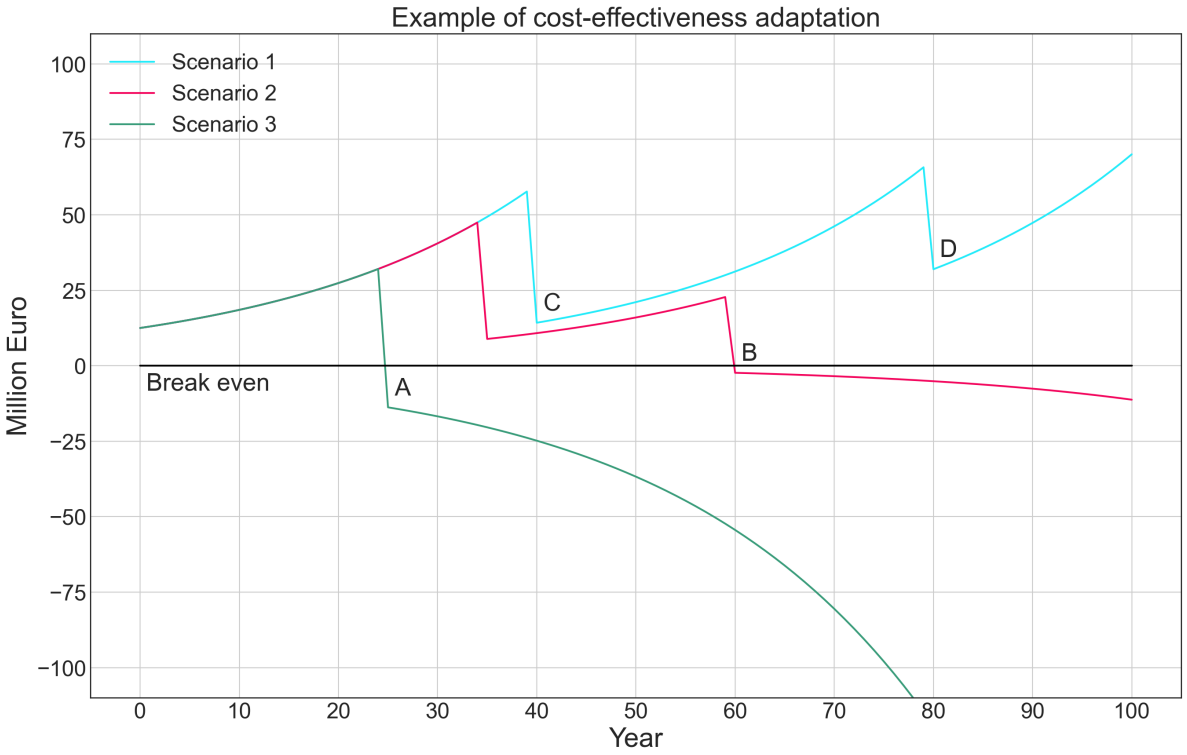

Figure H.2: Example of three different cost-effectiveness results of the same adaptation strategy.

I | Reliability model analysis of design strategies

In this chapter the various design strategies considered are stated. In Appendix I.1 a conservative and the required dimensions of the components is stated. Followed by the dynamic robust strategies that are opted for in Appendix I.2.

I.1. CONSERVATIVE DESIGN

In the list below the additional dimensions of the foundation block are stated, other dimensions are viewable in Table I.1. With these components a structural failure of the barrier is kept below 1:10,000 p/y over its lifetime. Each of the components are designed based on an equal individual exceedance threshold of 1:80,000 p/y, setting the threshold at this values ensures the structural failure probability limit. The growth of the failure probabilities of the individual components is visualised in Fig. I.2 and is integrated with the sea level rise distribution from Appendix G.1. In Fig. I.1 the total structural failure probability with the main components is supplied.

Foundation block

- Width = 59 metres
- Length = 50 metres
- Height = 4 metres
- Effective surface = 3,000 m^2
- Vertical contact with soil at max. width = 4 metres
- Selfweight ball-hinge = 6,800 kN
- Selfweight foundation block = 470,880 kN

The exceedance of the lower threshold limit (1:80,000 p/y) for all four components in Fig. I.2 are deemed acceptable.

Table I.1: Global overview of the dimensions for the main components for each individual design strategy.

Component	Parameter	Static	Dynamic+1.0	Dynamic+1.5	Dynamic+2.0
Foundation block	LxBxH	50x59x4	50x53x4	50x55x4	50x56x4
Bed protection	$d_{n50,river}$	1.44 m	1.18 m	1.18 m	1.18 m
	L_{river}	58.5 m	55.0 m	56.0 m	57.0 m
	$d_{n50,sea}$	0.59 m	0.59 m	0.59 m	0.59 m
	L_{sea}	28.0 m	28.0 m	28.0 m	28.0 m
Steel trusses/Ball-hinge	N_{Rd}	141 MN	130 MN	130 MN	135 MN
Gate height	H_{gate}	24.3 m	22.8 m	23.2 m	23.5 m

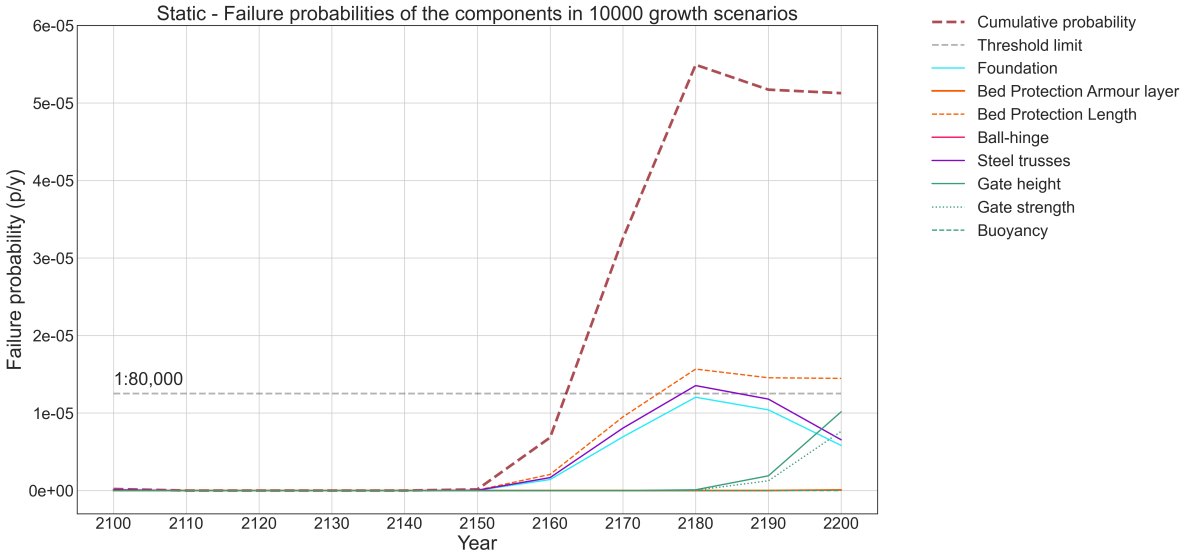

Figure I.1: Failure probabilities of the main components in 10,000 sea level rise growth scenarios.

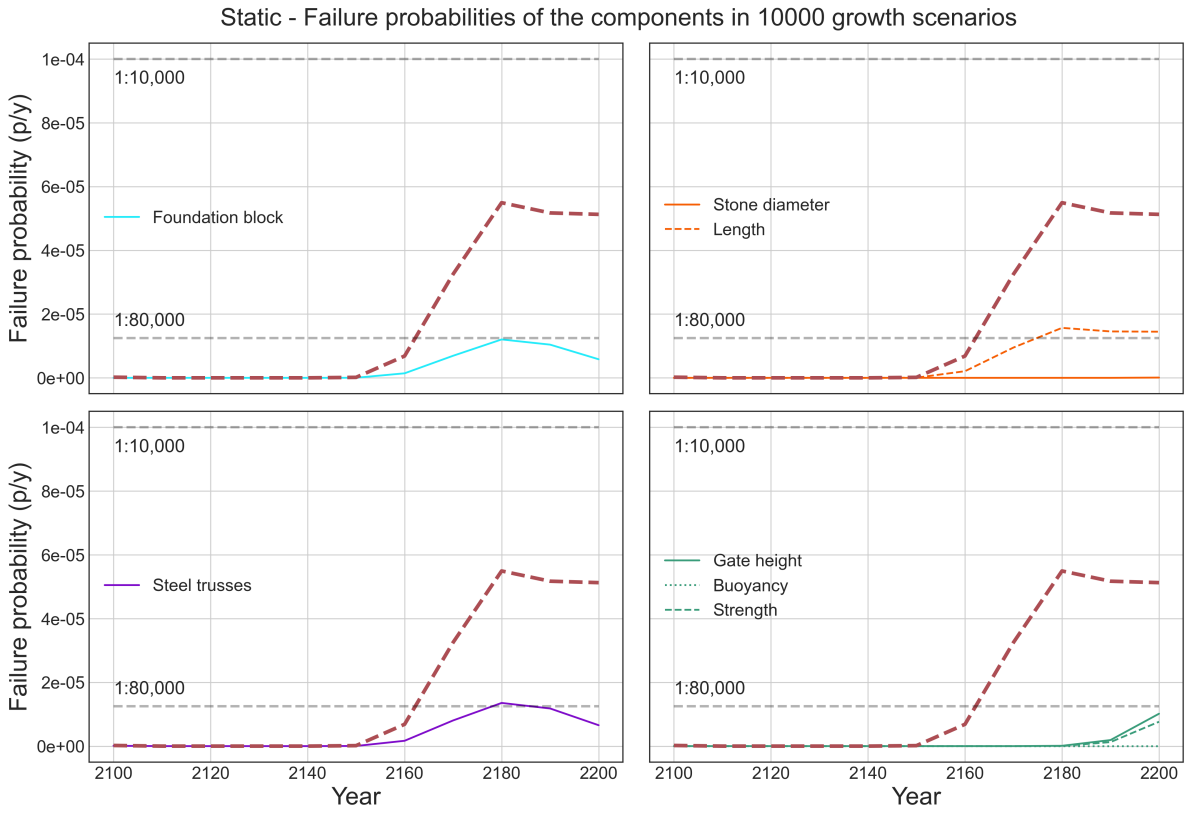

Figure I.2: Individual failure probabilities of the main components, that are identified as potentially adaptable, in 10,000 sea level rise growth scenarios.

I.2. DYNAMIC ROBUST DESIGNS

In this section all three dynamic robust design strategies are elaborated along their individual progression of failure probabilities performance. When considering the individual failure probabilities of the components, only the components that have available options to be adapted are included.

These adaptations and the components followed from the third filter in Table 9.2 and contain the foundation block, bed protection armour layer and length and the sector gate height.

I.2.1. DYNAMIC+1.0 METRE SEA LEVEL RISE

With the characteristics of the components stated in Table I.1 the failure probabilities are computed. Each of the components are designed based on an equal individual failure probability threshold of 1:80,000 p/y, setting the threshold at this values ensures the structural failure probability of 1:10,000 p/y. The growth of the failure probabilities of the individual components is visualised in Fig. I.3 and is integrated with the sea level rise distribution from Appendix G.1. In Fig. I.3 the total structural failure probability with the main components is supplied and applied adaptations, the latter as determined in Table 9.2 (foundation), Table I.2 (bed protection length) and Table I.3 (gates). The exceedance of the lower threshold limit (1:80,000 p/y) in all four components in Fig. I.4 are deemed acceptable. The integrated adaptations are:

- Wedge soil improvement
- Bed protection length increase +3.0 metres
- Gate height extension +1.0 metre

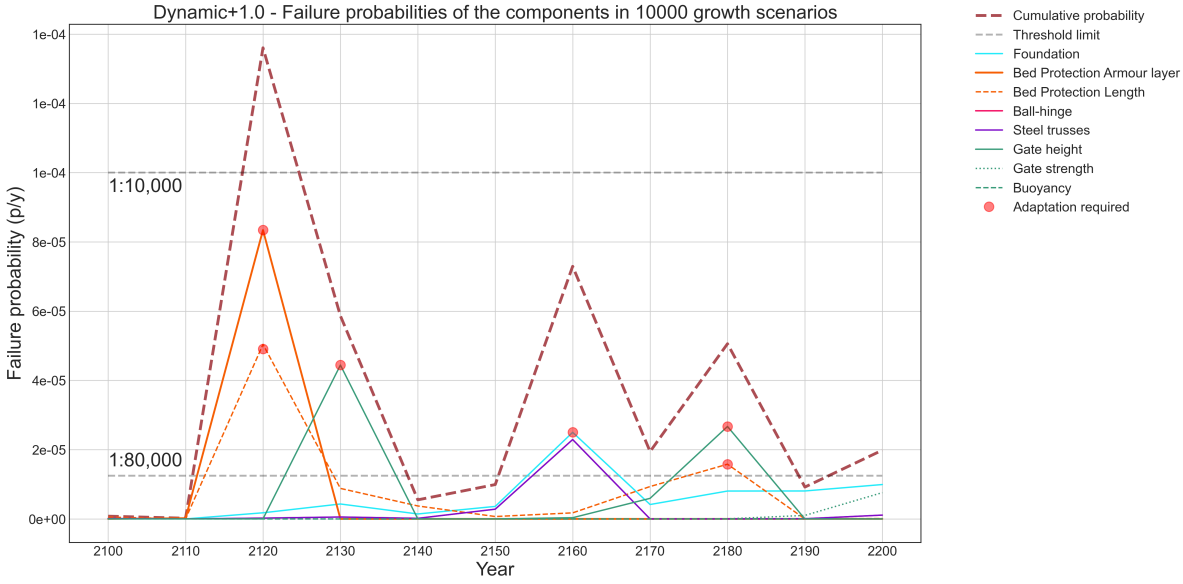

Figure I.3: Failure probabilities and probable adaptation moments of the main components in 10,000 sea level rise growth scenarios.

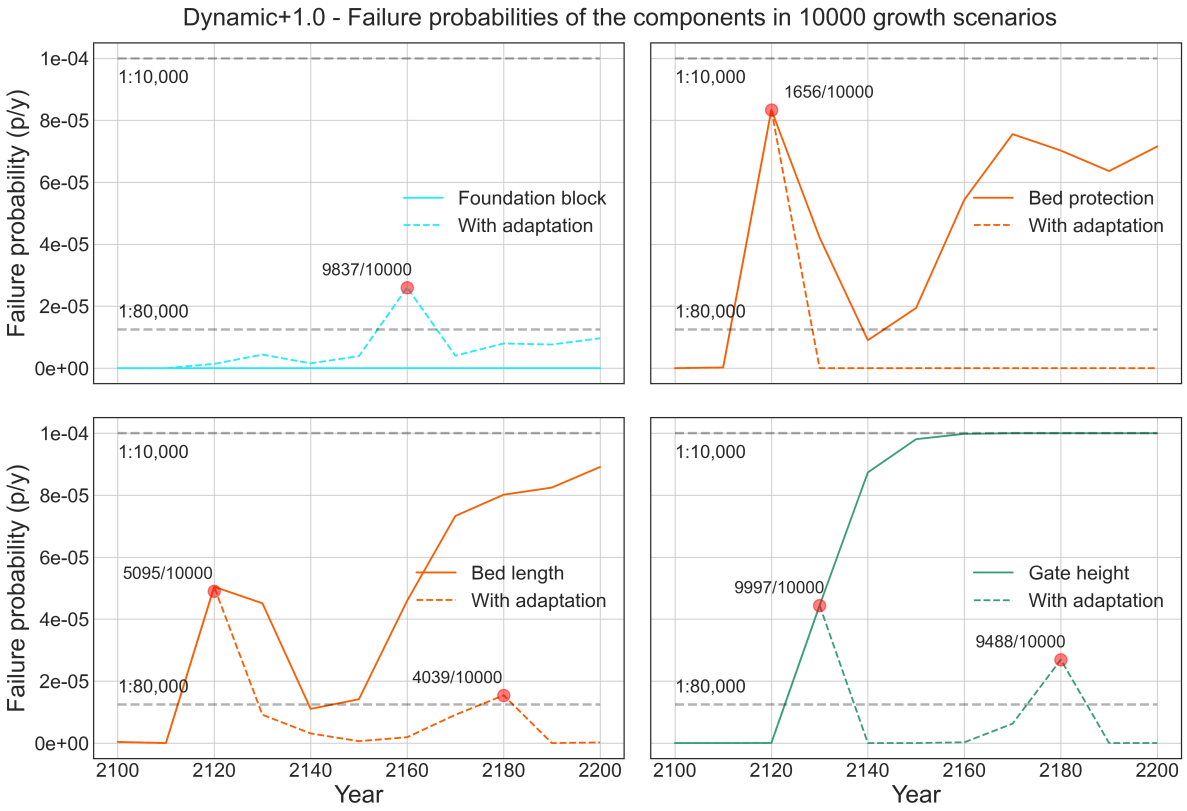

Figure I.4: Individual failure probabilities of the main components in 10,000 sea level rise growth scenarios and cost-effectivity ratios of the adaptations.

I.2.2. DYNAMIC+1.5 METRE SEA LEVEL RISE

The growth of the failure probabilities of the individual components is visualised in Fig. I.6 and is integrated with the sea level rise distribution from Appendix G.1. In Fig. I.5 the total structural failure probability with the main components is supplied and applied adaptations, the latter as determined in Table 9.2 (foundation), Table I.2 (bed protection length) and Table I.3 (gates). The exceedance of the lower threshold limit (1:80,000 p/y) in all four components in Fig. I.6 are deemed acceptable. The integrated adaptations are:

- Wedge soil improvement
- Bed protection length increase +3.0 metres
- Gate height extension +1.5 metre

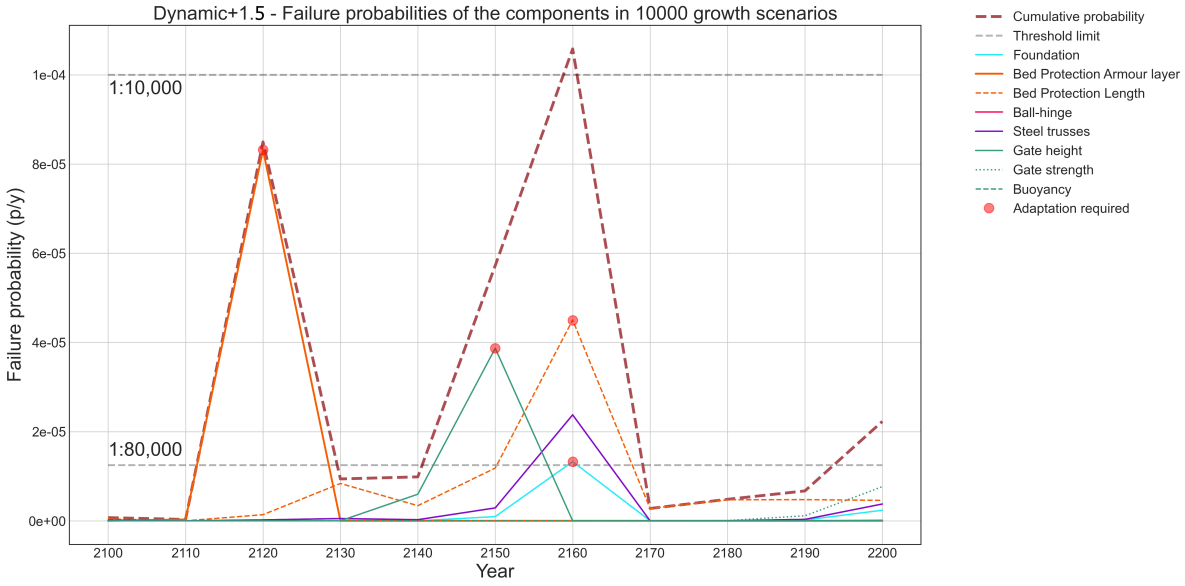

Figure I.5: Failure probabilities and probable adaptation moments of the main components in 10,000 sea level rise growth scenarios.

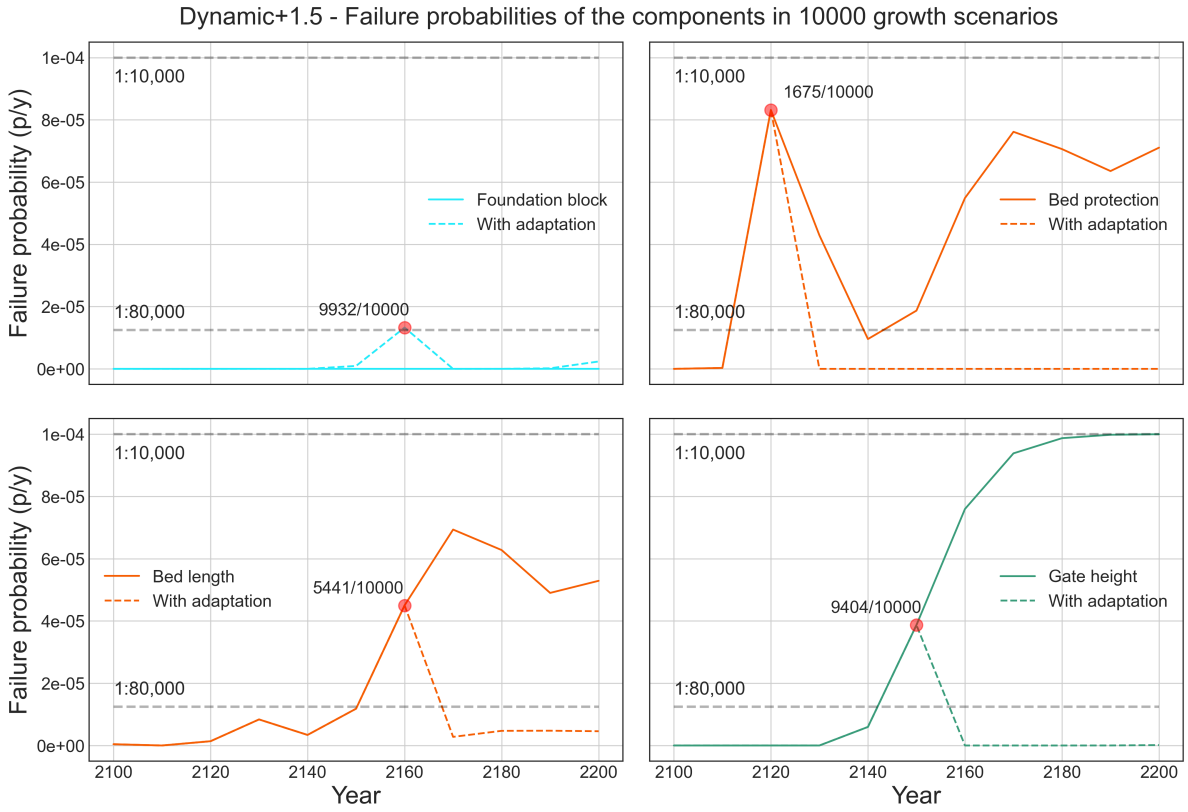

Figure I.6: Individual failure probabilities of the main components in 10,000 sea level rise growth scenarios and cost-effectivity ratios of the adaptations.

I.2.3. DYNAMIC+2.0 METRE SEA LEVEL RISE

The growth of the failure probabilities of the individual components is visualised in Fig. I.8 and is integrated with the sea level rise distribution from Appendix G.1. In Fig. I.7 the total structural failure

probability with the main components is supplied and applied adaptations, the latter as determined in Table 9.2 (foundation), Table I.2 (bed protection length) and Table I.3 (gates). The exceedance of the lower threshold limit (1:80,000 p/y) in all four components in Fig. I.8 are deemed acceptable. The integrated adaptations are:

- Wedge soil improvement
- Bed protection length increase +1.0 metres
- Gate height extension +1.0 metre

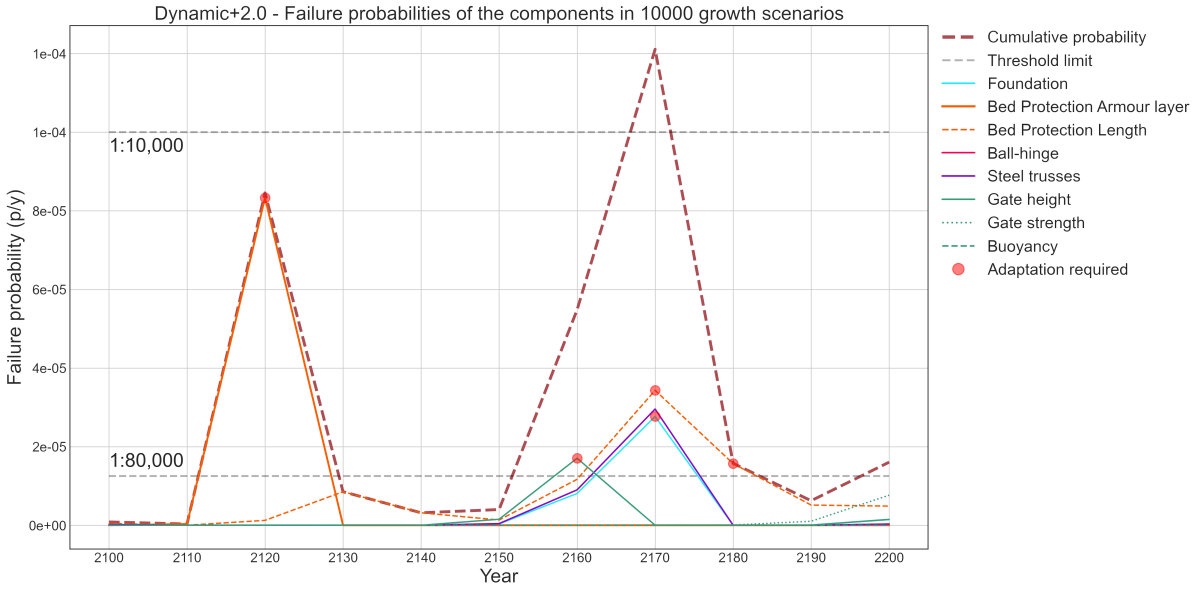

Figure I.7: Failure probabilities and probable adaptation moments of the main components in 10,000 sea level rise growth scenarios.

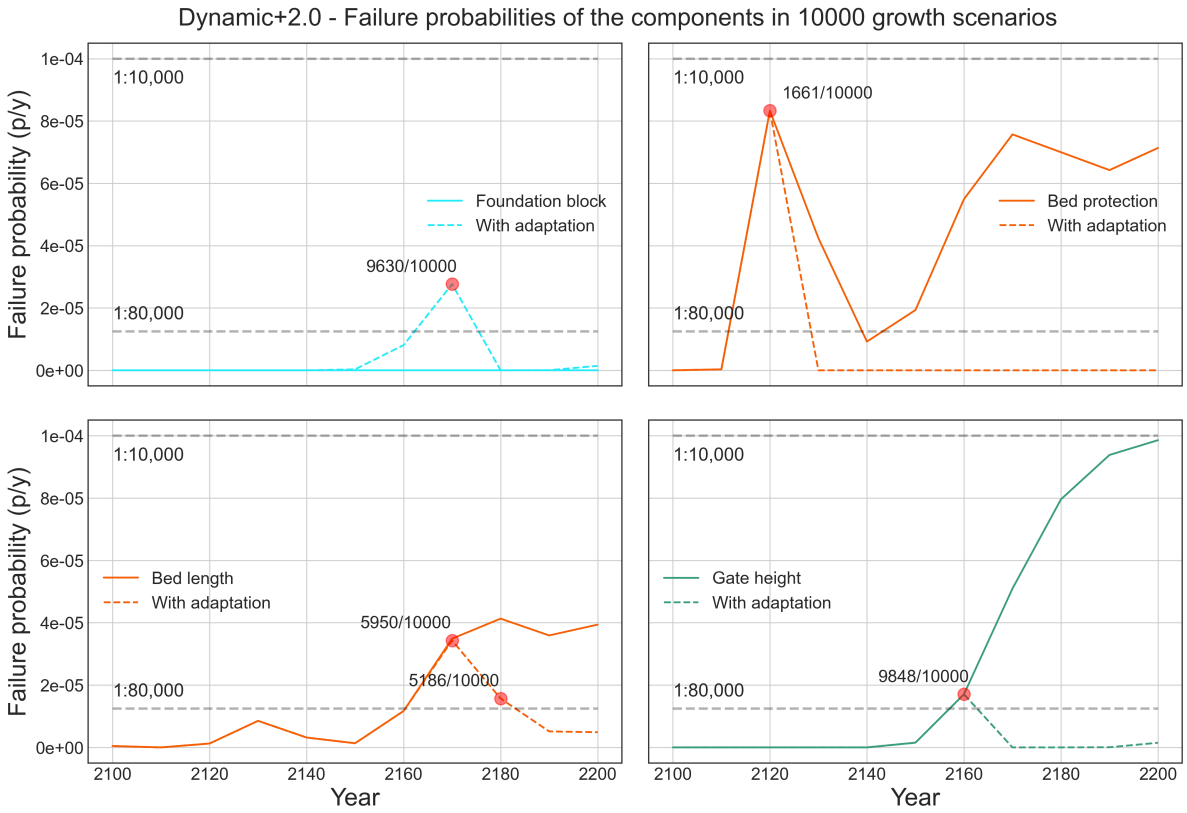

Figure I.8: Individual failure probabilities of the main components in 10,000 sea level rise growth scenarios and cost-effectivity ratios of the adaptations.

I.3. IN-DEPTH BENEFIT EFFECTIVENESS ANALYSIS OF THE FILTERED ADAPTATION OPTIONS

With the computational model the number of required adaptations to a individual components is computed. According to the computations the bed protection length and gate heights are prone to be adapted twice of the respective adaption is small. In Appendix I.3.1 and Appendix I.3.2 these two adaptations are reviewed more thoroughly.

I.3.1. BED PROTECTION LENGTH INCREASE

Let us consider the adaptation *Bed protection length increase*. In Table H.6 the costs for an additional length of +1, +2 and +3 metres have been considered. Now if dynamic robust +1.0 (DD+1.0) with the option of a length increase of +3 metres is considered, it is clear that the adaptation is needed twice, see Fig. I.9 (orange), this leads to a decrease in cost-effectiveness of the adaptations, from 520/1000 to 398/1000. If the additional length of the adaptation is increased to, as an example, +4 and +5 metres, this would lead to the necessity to apply the adaptation only once with an increase in cost of the adaptation. However, the cost-effectivity around the first implementation stays the same, which might be more favourable. From Fig. I.9 it can be deducted that an length increase of +5 metres is unnecessary and would only lead to an increase of costs.

The same procedure is repeated for the dynamic +1.5 and +2.0 design strategies. Lets us consider the dynamic +1.0 strategy. In Fig. I.10 two variances in additional bed protection lengths are considered, +2.0 (orange) and +3.0 metres (purple). As can be seen in the figure, the bed protections length needs to be increased twice if an adaptation with +2.0 metres is considered but only once when an adaptation with +3.0 metres is considered. When comparing the two variances it becomes clear that

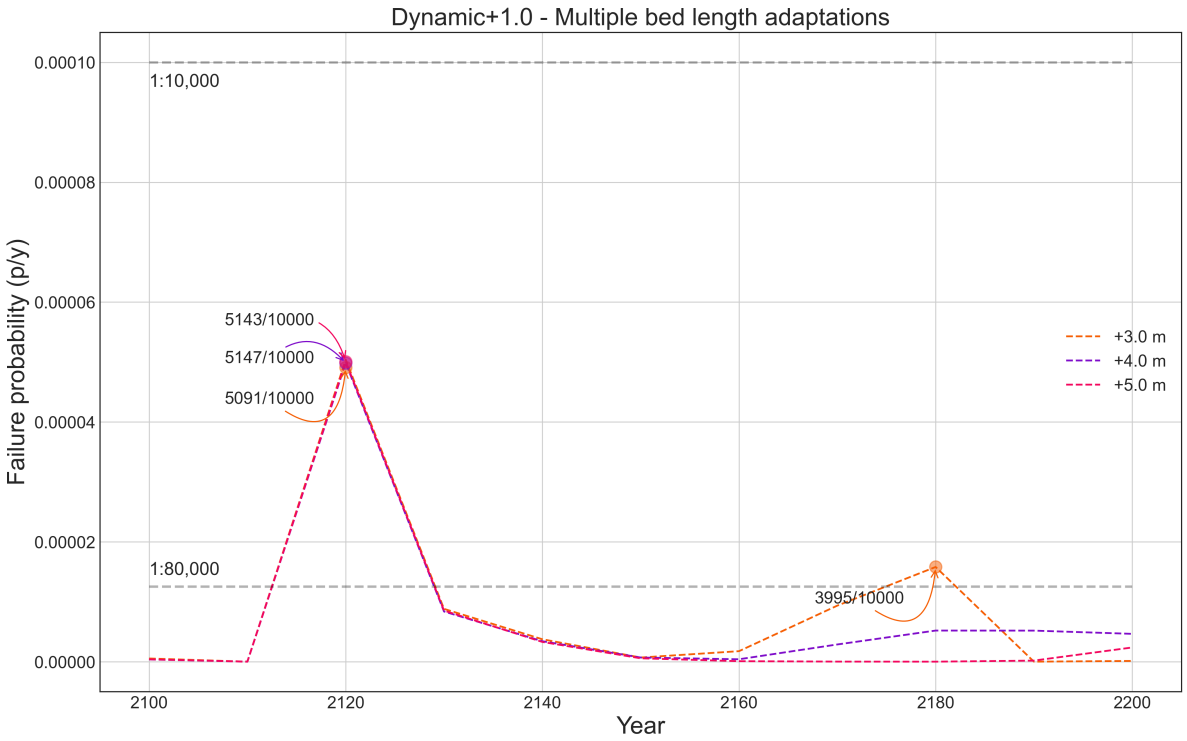

Figure I.9: Performance of the adaptation of the bed protection length with varying lengths. The numerical fraction X/1000 represents the cost-effectiveness in the total number of scenarios.

initially, at the first adaptation moment, the cost-effectiveness can be considered to be equal. However, continuing along the timeline, it becomes clear that the cost-effectiveness of the +2.0 metres adaptation decreases by quite a bit, but is supported by a greater reduction in exceedance probability of the component.

Lastly, the procedure is repeated for the dynamic +2.0 strategy. In Fig. I.11 two variances in additional bed protection lengths are considered, +1.0 (orange) and +2.0 metres (purple). As can be seen in the figure, the bed protections length needs to be increased twice if an adaptation with +1.0 metres is considered but only once when an adaptation with +2.0 metres is considered. When comparing the two variances it becomes clear that initially, at the first adaptation moment, the cost-effectiveness can be considered to be equal. However, continuing along the timeline, it becomes clear that the cost-effectiveness of the +1.0 metres adaptation decreases by quite a bit, additionally it is not supported by a greater reduction in exceedance probability of the component.

Besides the effectiveness ratio of the adaptations, the bandwidth and mean of the economical returns are taken into consideration. This yields a general prediction of monetary value of the adaptation. In Fig. I.12 the three dynamic robust design with the respective adaptations to the bed protection length are visualised. From the figure it is evidently clear that the bandwidth decreases when the initial dimensions of the design strategy increases. Furthermore, it can be seen that the bed protection length adaptation for the dynamic +1.0 (DD+1.0) is prone to net a negative economic return (top figure of Fig. I.12), whilst the adaptations for dynamic +1.5 (DD+1.5) and dynamic +2.0 (DD+2.0) are prone to net either a very positive or negative economic return (middle and bottom figure of Fig. I.12).

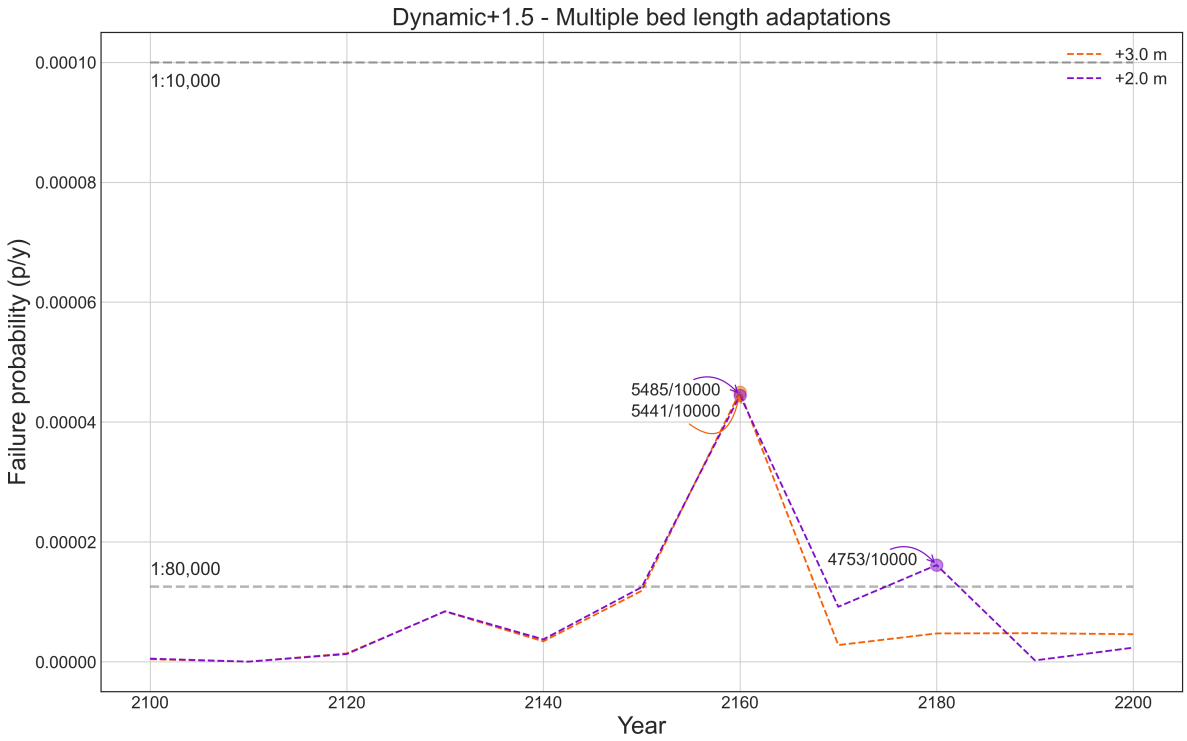

Figure I.10: Performance of the adaptation of the bed protection length with varying lengths. The numerical fraction X/1000 represents the cost-effectiveness in the total number of scenarios.

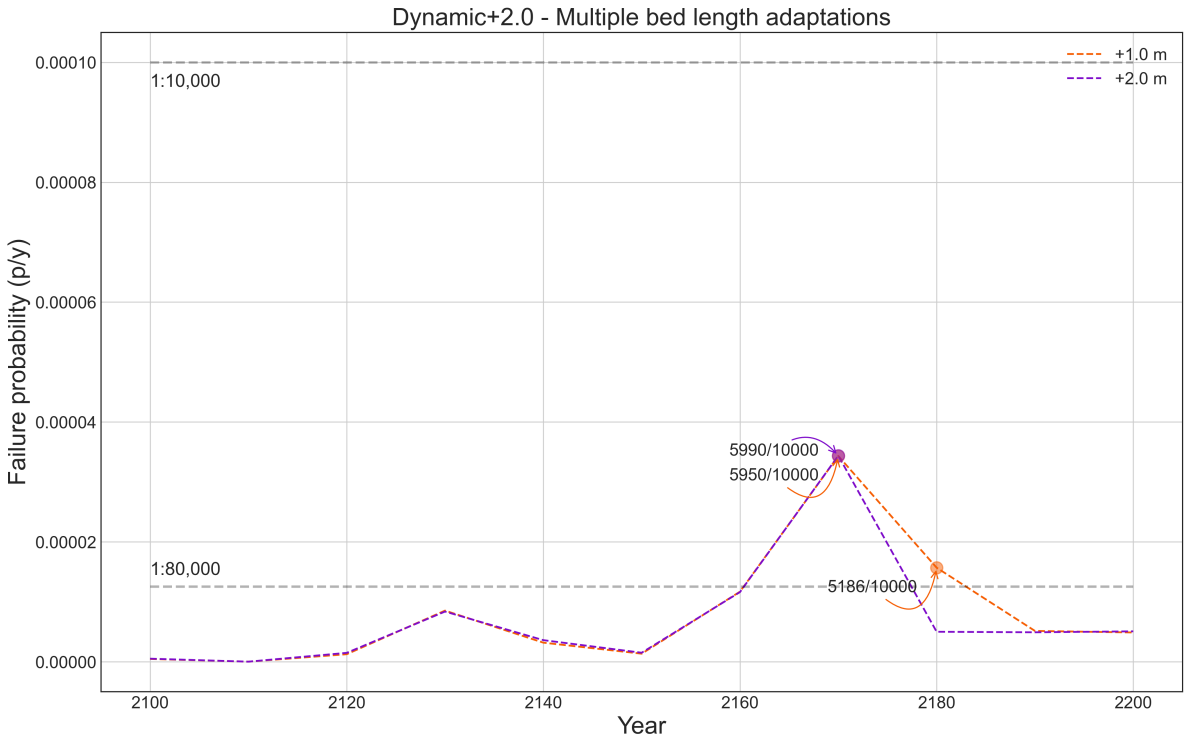

Figure I.11: Performance of the adaptation of the bed protection length with varying lengths. The numerical fraction X/1000 represents the cost-effectiveness in the total number of scenarios.

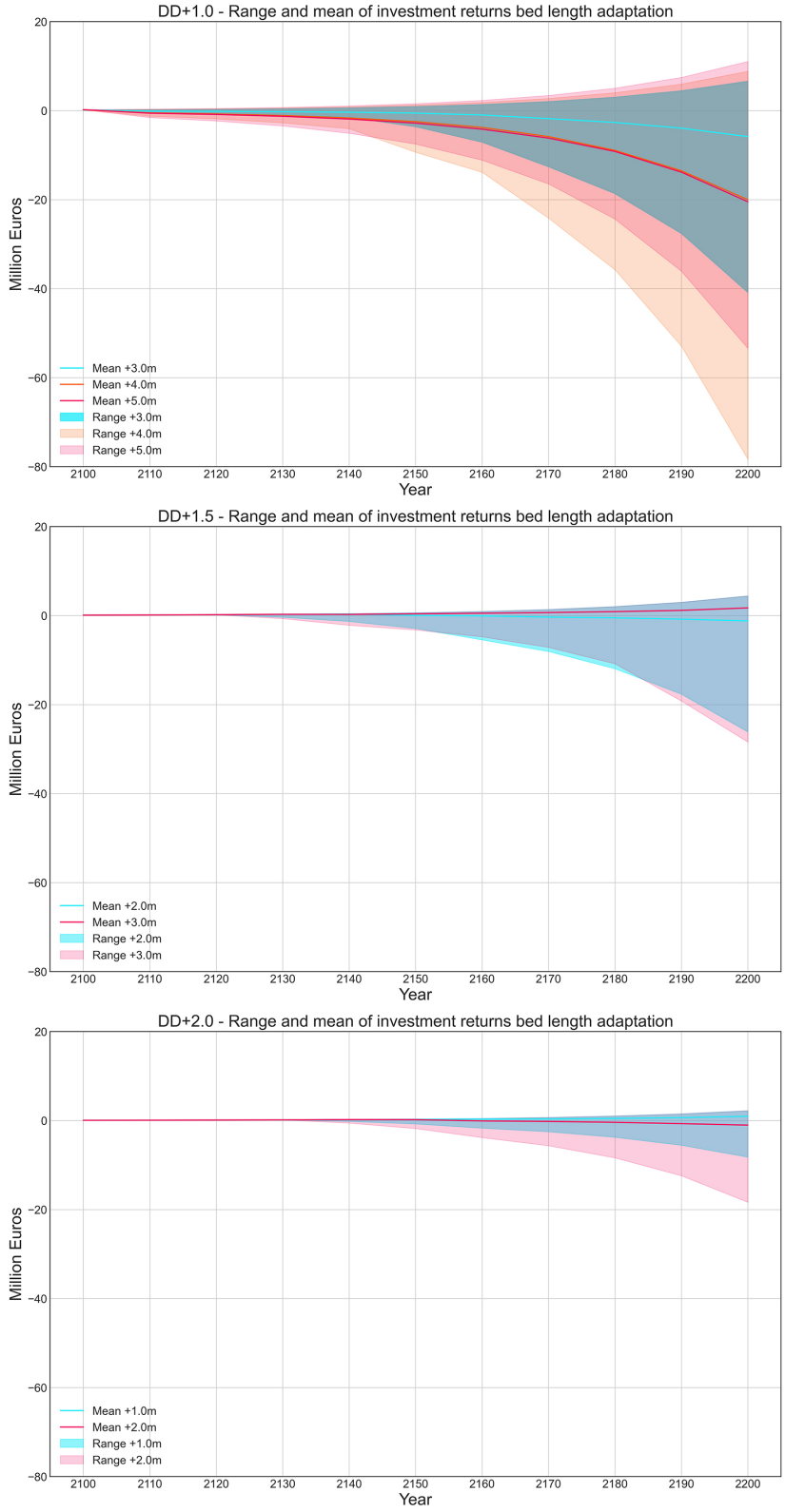

Figure I.12: Performance of the adaptation *bed length increase* with varying lengths in three dynamic designs.

Thus, the likelihood of netting a positive economic return with the bed protection length adaptation is slim. However, if adaptability is preferred, the adaption with the highest mean net economic

return is advised and these are summarised in Table I.2. The construction costs are computed and extrapolated to the appropriate length as in Table H.6.

Table I.2: Summary of the advised length of the adaptation for the bed protection length for the three dynamic design strategies, including the estimated costs.

Bed protection length	**Dynamic+1.0**	**Dynamic+1.5**	**Dynamic+2.0**
Advised dimension increase	+3.0	+3.0	+1.0
Estimated costs in 2021 price levels	€531,000	€531,000	€178,000

I.3.2. GATE EXTENSION

Let us consider the adaptation *Gate extension*. In Table H.7 the costs for an additional gate height of +0.5 and +1.0 metres have been considered. Now if dynamic robust +1.0 (DD+1.0) with the option of an gate extension of +1.0 metres is considered, it is clear that the adaptation is needed twice, see Fig. I.13 (green), this leads to a decrease in cost-effectiveness of the adaptations, from 1000/1000 to 961/1000. If the extension of the adaptation is increased to, as an example, +1.5 (purple) and +2 metres (pink), this would lead to the necessity to apply the adaptation only once with an increase in cost of the adaptation. However, the cost-effectivity around the first implementation stays the same, which might be more favourable. From Fig. I.13 it can be deducted that an gate extension +2.0 metres is unnecessary and would only lead to an increase of costs.

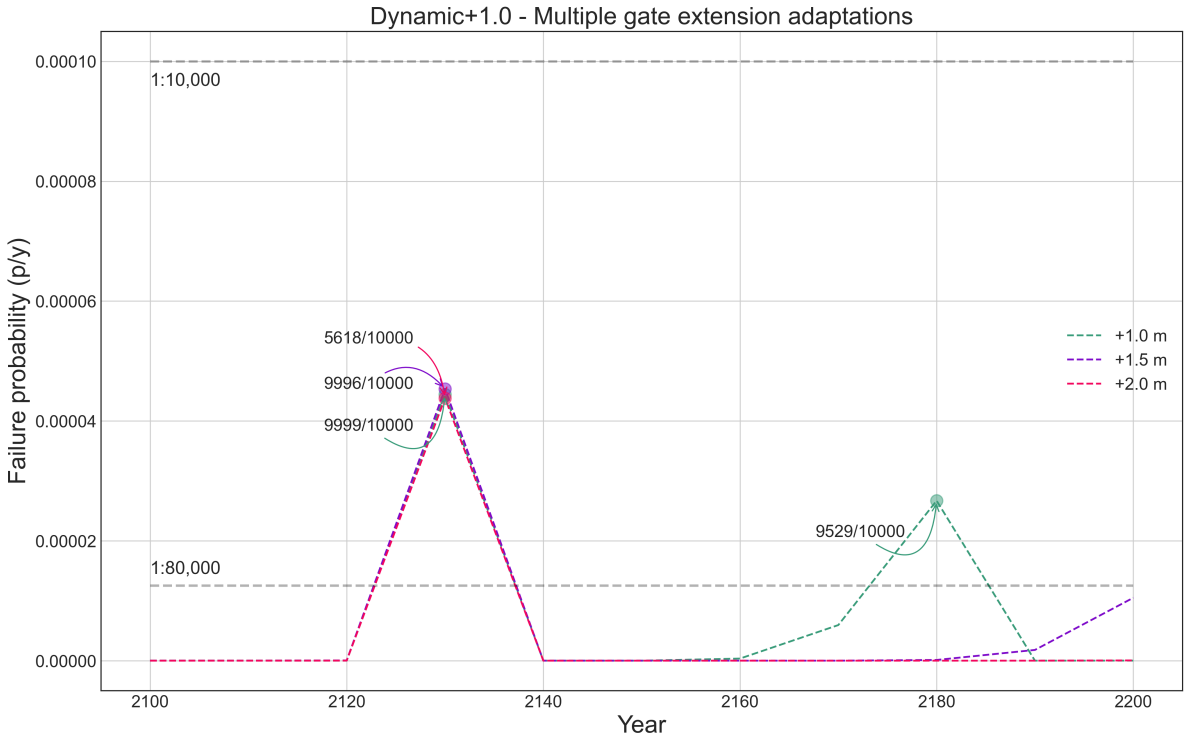

Figure I.13: Performance of the adaptation of gate extension with varying extension height. The numerical fraction X/1000 represents the cost-effectiveness in the total number of scenarios.

The same procedure is repeated for the dynamic +1.5 and +2.0 design strategies. Lets us consider the dynamic +1.0 strategy. In Fig. I.14 two variances for the gate extensions are considered, +1.0 (green) and +1.5 metres (purple). As can be seen in the figure, the gates needs to be extended twice

if an adaptation with +1.0 metres is considered but only once when an adaptation with +1.5 metres is considered. When comparing the two variances it becomes clear that initially, at the first adaptation moment, the cost-effectiveness can be considered to be equal. However, continuing along the timeline, it is computed that the average benefit in monetary terms of an extension of +1.0 m is higher due to reduced costs when compared to the extension of +1.5 m. Although this comes at the result the gate might have to be heightened near the end of its lifetime. Concluding, both variances provide sufficient reduction in the exceeding probability and in cost-effectiveness, although the adaptation with an extension of +1.0 m is prone to yield higher benefits.

Lastly, the procedure is repeated for the dynamic +2.0 strategy. In Fig. I.14 two variances for the gate extensions are considered, +0.5 (green) and +1.0 metres (purple). As can be seen in the figure, the gates needs to be extended twice if an adaptation with +0.5 metres is considered but only once when an adaptation with +1.0 metres is considered. When comparing the two variances it becomes clear that initially, at the first adaptation moment, the cost-effectiveness can be considered to be equal and very cost-effective. And, continuing along the timeline, the extension by +0.5 m seems to yield a near guarantee to net a positive monetary benefit. The average benefit in monetary terms of both extension variances are near equal to each other.

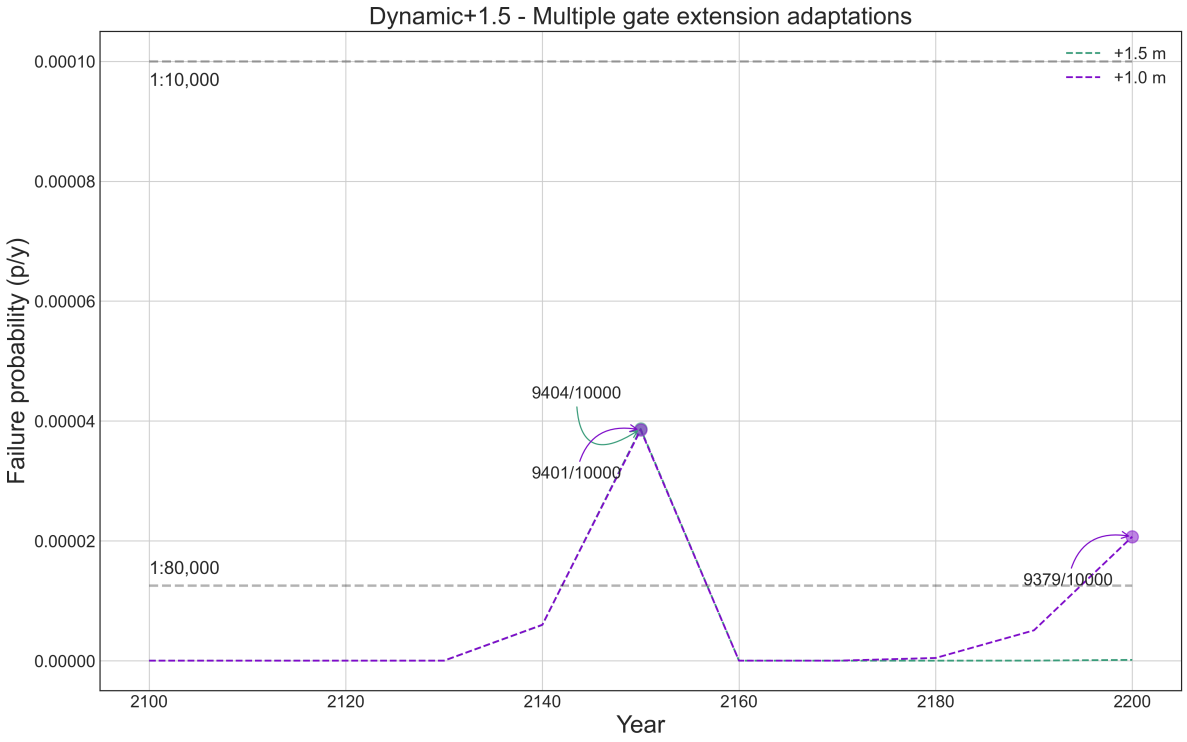

Figure I.14: Performance of the adaptation of gate extension with varying extension height. The numerical fraction X/1000 represents the cost-effectiveness in the total number of scenarios.

Besides the effectiveness ratio of the adaptations, the range and mean of the economical returns are taken into consideration. This yields a general prediction of monetary value of the adaptation. In Fig. I.16 the three dynamic robust design with the respective adaptations to the bed protection length are visualised. If one looks closely over all three figures, it can be deducted that applying the same adaptation, e.g. +1.0 m gate extension, the range of the economical return decreases and becomes more confident and thus the range decreases when initial dimensions of the gate increases. All three design strategies, with their respective extension of the gate, are prone to net a positive economical return if one follows the mean of the adaptation. However, it can not be excluded that

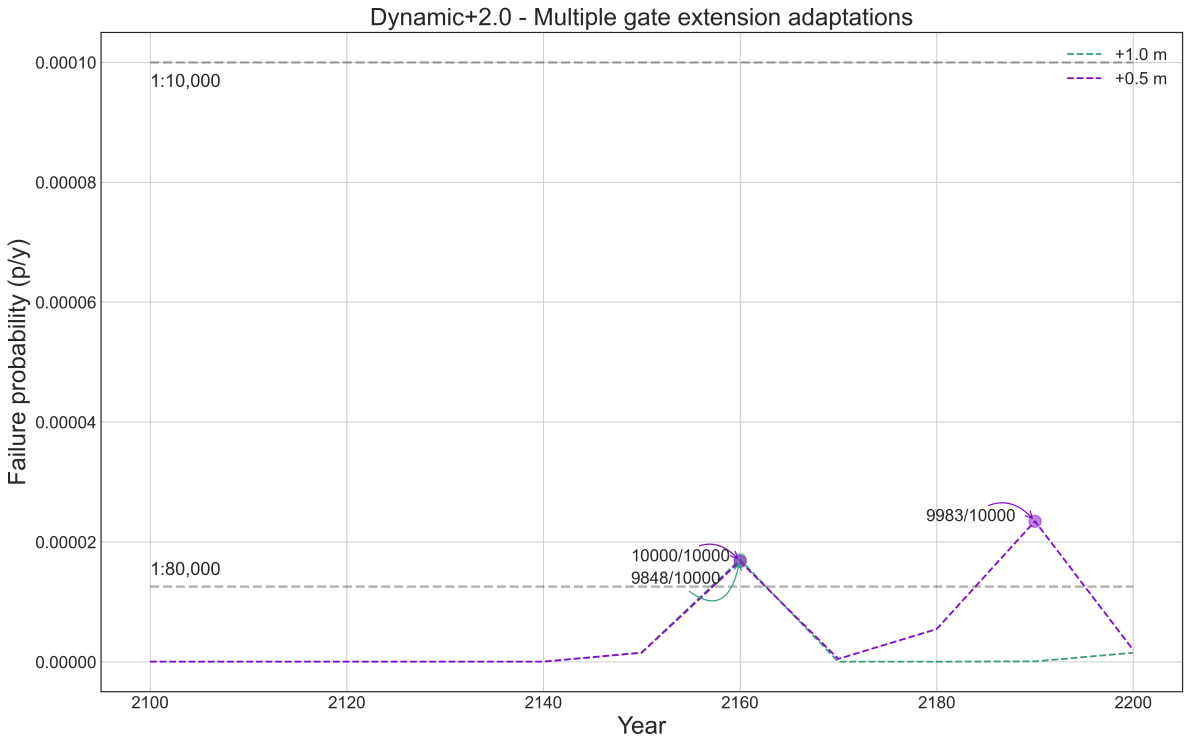

Figure I.15: Performance of the adaptation of gate extension with varying extension height. The numerical fraction X/1000 represents the cost-effectiveness in the total number of scenarios.

negative economical returns are to occur.

Thus the likelihood of netting a positive economic return with the *gate extension* adaptation is substantial. When considering the three dynamic designs the following dimensions of the adaptations are advised:

- D+1.0: +1.0, likely to be applied twice, mean economical benefit higher than +1.5m/+2.0m but range is larger
- D+1.5: +1.5 m, likely to be applied once, mean economical benefits (2x) +1.0m/ (1x) +1.5m relatively similar, range is smaller
- D+2.0: +1.0 m, likely to be applied once, mean economical benefits (2x) +0.5m/ (1x) +1.0m relatively similar but range is larger

Table I.3 is supplied to summarise the advised adaptations to the gate height for the three dynamic robust design strategies. The construction costs are computed and extrapolated to the appropriated extension as in Table H.7.

Table I.3: Summary of the advised height of the adaptation gate extension for the three dynamic design strategies, including the estimated costs.

Gate extension	**Dynamic+1.0**	**Dynamic+1.5**	**Dynamic+2.0**
Advised height increase	+1.0 (2x)	+1.5	+1.0
Estimated costs in 2021 price levels	M€9.92	M€14.88	M€9.92

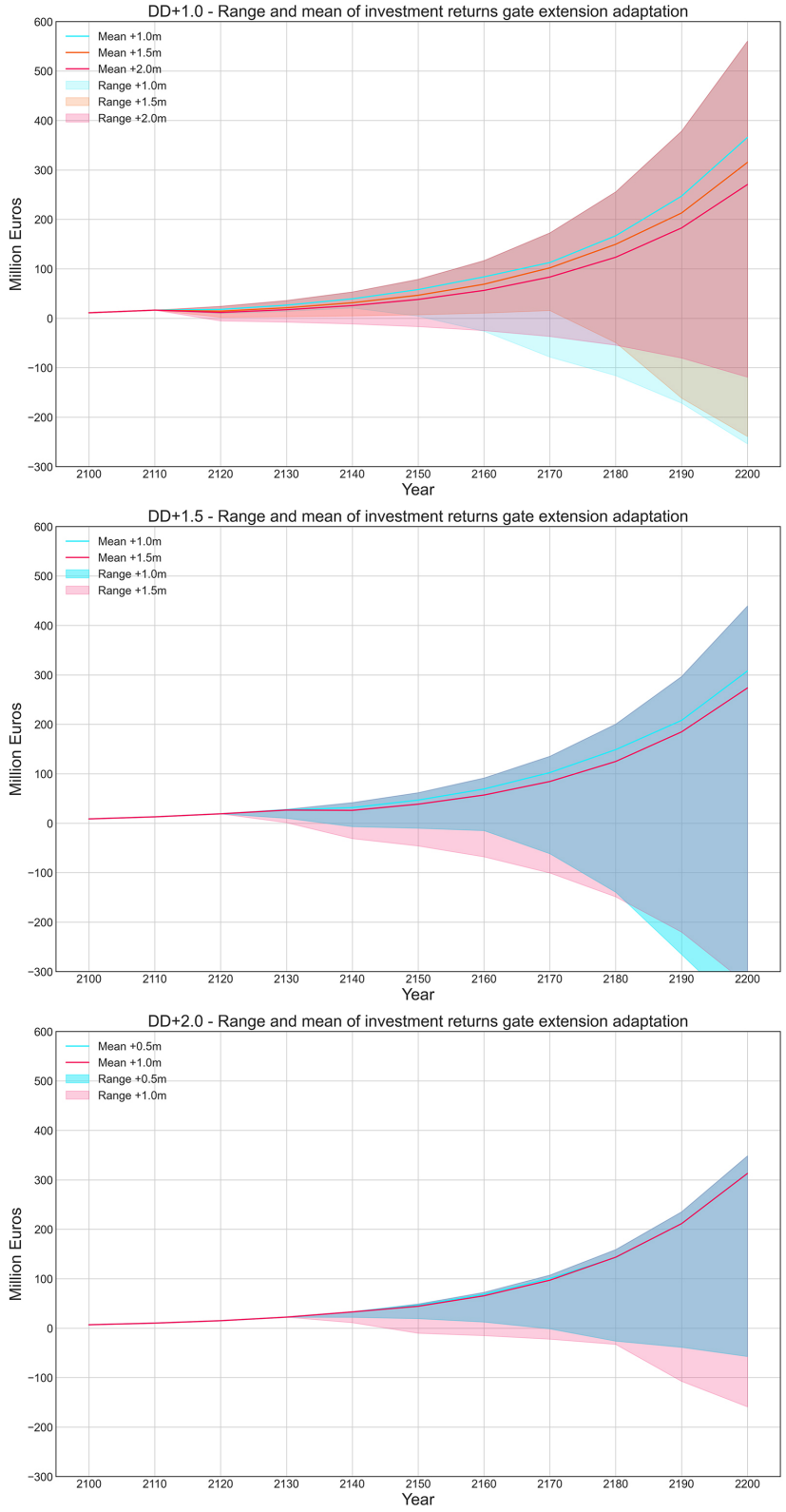

Figure I.16: Performance of the adaptation *gate extension* with varying heights in three dynamic designs. The 'Range +1.5m' is labelled as orange, however, as blue and orange overlap the colour turns green.

I.4. IN-DEPTH ANALYSIS OF THE DYNAMIC ROBUST DESIGNS

An in depth analysis of the individual dynamic strategies follows the advised adaptations per component from Appendix I.3. In Appendix I.2 the progression of the exceedance probabilities of these strategies are stated and all adhere to the instated threshold limits. Therefor, this section limits itself to the analysis of the cost-effectiveness of the strategies. The three dynamic design strategies are compared per component (Appendix I.4.1, Appendix I.4.2 and Appendix I.4.3) and, as last, over the global designs (Appendix I.4.4).

I.4.1. FOUNDATION

Comparing the full range of investment returns of the three dynamic designs (Fig. I.17) it is for the foundation adaptation it is clear that, although the mean return are above the break-even point, can lead to negative benefit when compared to the static robust design. However, the full range of probable returns might supply a twisted view of the more probable return. Therefor, in Fig. I.18, the range is decreases to visualise the 5th -and 95th-percentiles of the benefits. With the help of this figure a more positive benefit is expected when compared to the previous figure.

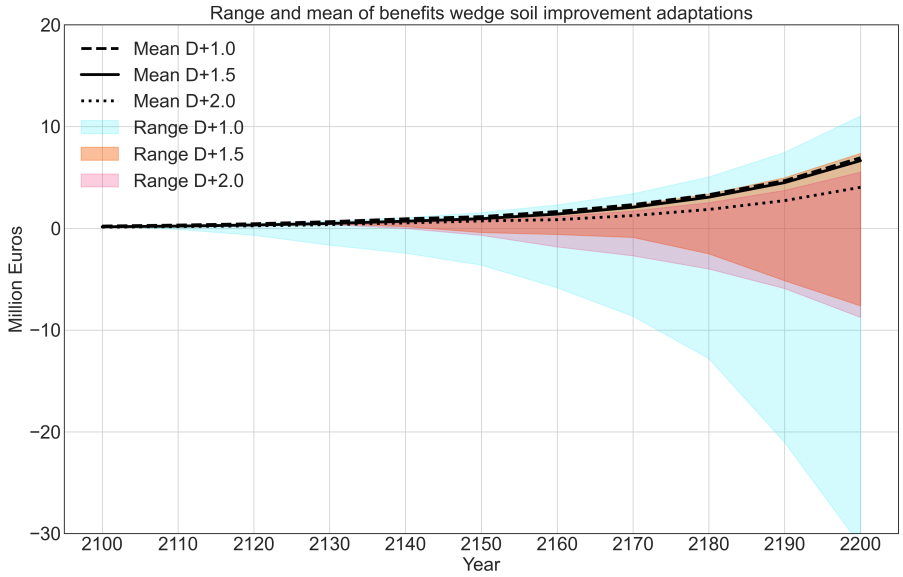

Figure I.17: Full range of investment returns of the soil improvement adaptation for all three dynamic design strategies.

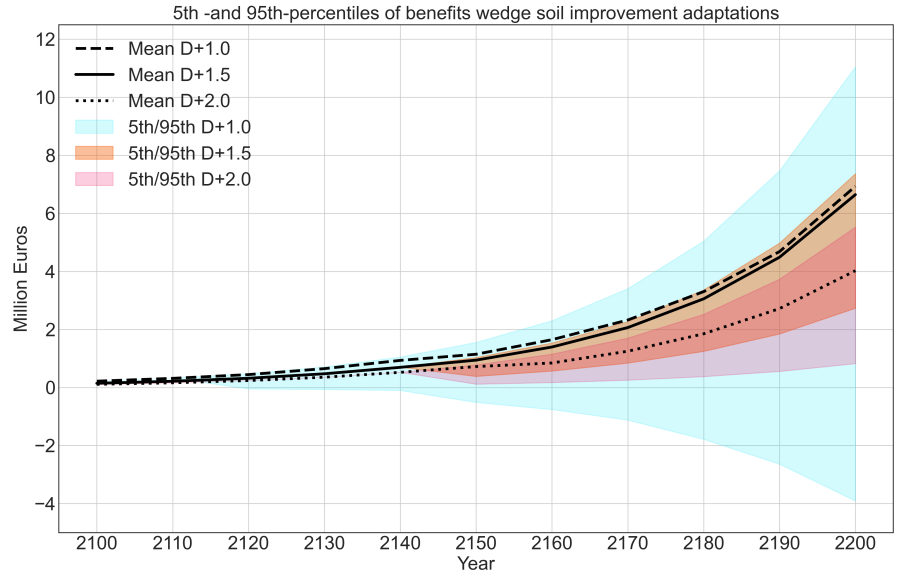

Figure I.18: 5th -and 95th-percentiles of investment returns of the soil improvement adaptation for all three dynamic design strategies.

I.4.2. BED PROTECTION LENGTH

As expected from Appendix I.3.1 it is unlikely that the adaptation of the bed protection length will lead to positive benefits and this is show in Fig. I.19 and Fig. I.20. Furthermore, deducted from the

figure displaying the 5th -and 95th-percentiles (Fig. I.20), the range of likely returns is of a considerable size and therefore quite uncertain. To conclude, the likelihood of netting a positive benefit for all three dynamic designs is too slim and it is therefore advised to apply the bed protection length as dimensioned for the static design.

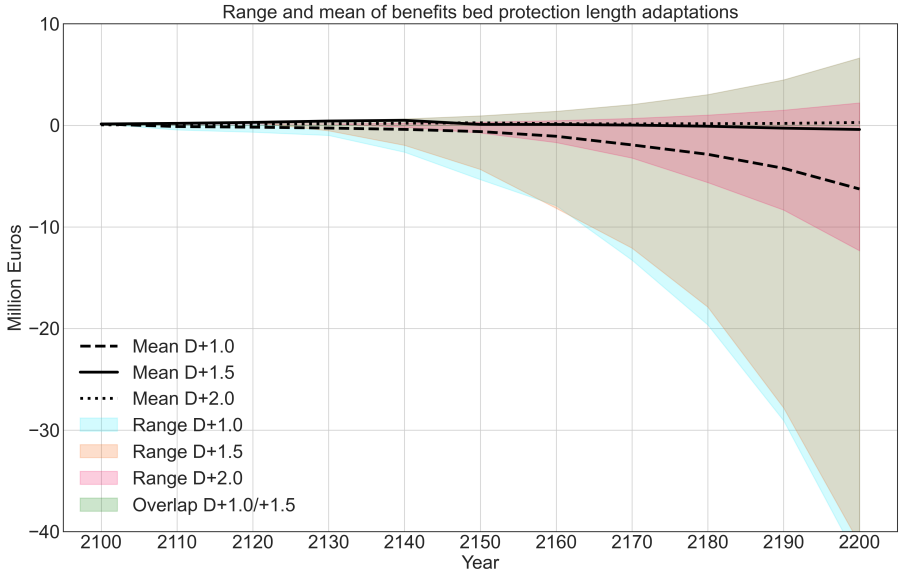

Figure I.19: Performance of the bed protection length adaptation for all three dynamic design strategies.

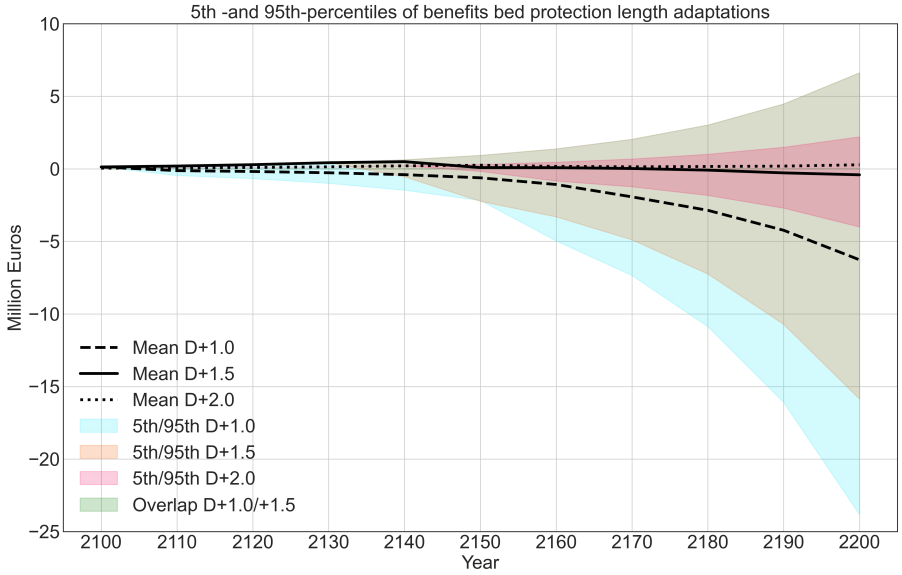

Figure I.20: 5th -and 95th-percentiles of investment returns of the bed protection length adaptation for all three dynamic design strategies.

I.4.3. SECTOR GATES

As analysed in Appendix I.3.2 it is highly likely that most of the adaptations for the three dynamic design strategies are cost-effective. However, it can not be completely ruled out that in some sea level rise scenarios a negative benefit is yielded. In Fig. I.21 the full spread, or range, and in Fig. I.22 the 5th -and 95th-percentiles of the investment returns are visualised. Fig. I.21 indicates a high

spread in economical returns for all three designs, whilst the mean of these designs indicate that a positive benefit is more likely. The 5th -and 95th-percentiles perhaps supply a better indication of these benefits, and as seen in Fig. I.22, it is more likely that the adaptations result in a positive benefit. Additionally, it can be deducted that with the progression in the designs (from D+1.0 to D+2.0) the spread decreases, which is logical as adaptations are delayed in time with progressing designs. However, this decrease is accompanied by a decrease in the mean returns as well and thus this follows the low risk low reward and high risk high reward principle.

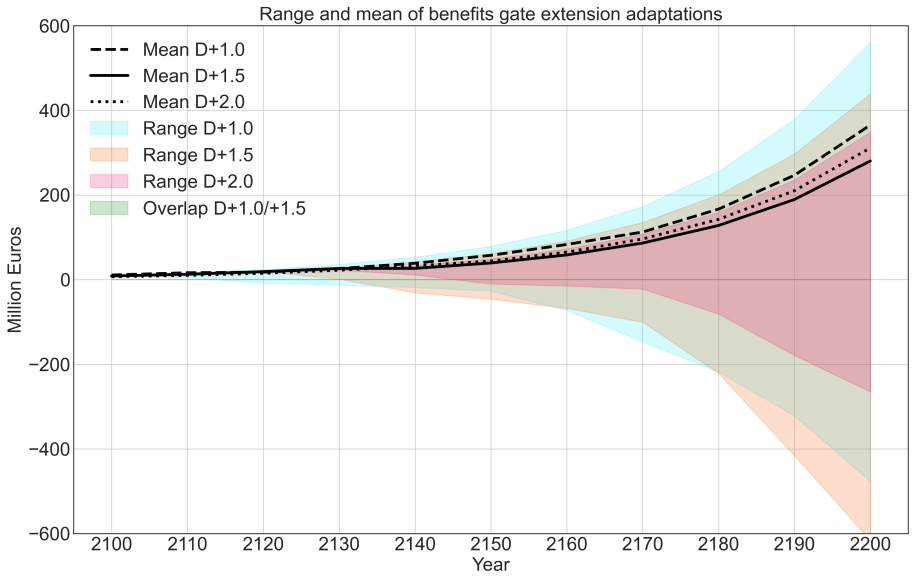

Figure I.21: Performance of the gate extension adaptation for all three dynamic design strategies.

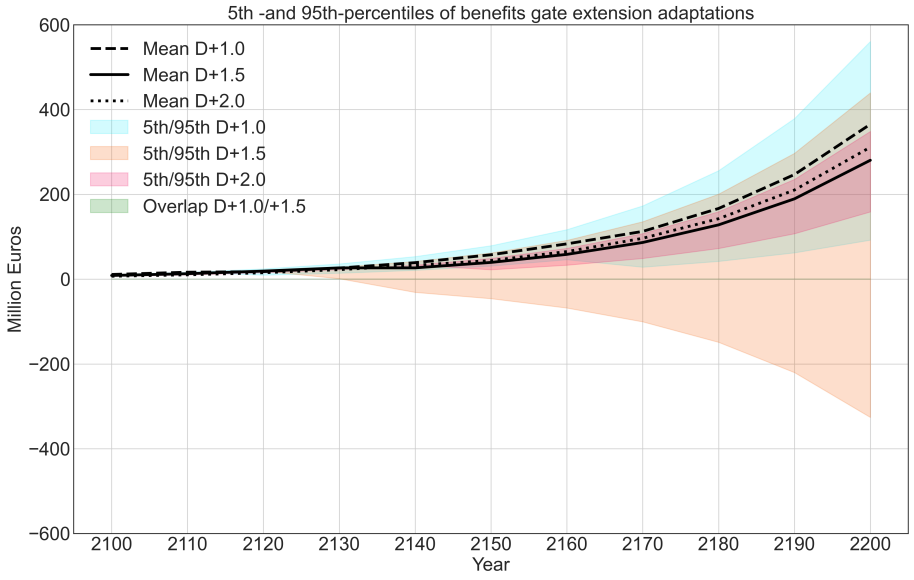

Figure I.22: 5th -and 95th-percentiles of investment returns of the gate extension adaptation for the design strategies.

I.4.4. GLOBAL

Now the three remaining adaptations, i.e. soil improvement, bed protection length increase and gate extension, are combined for each individual designs and the results can be viewed in Fig. I.23

and Fig. I.24. First thing to notice is that the pattern and value of the spread follow the results supplied in Appendix I.4.3 where the benefits of the gate extension are stated. Thus the benefits (positive or negative) dwarfs the possible gains or losses from the other two adaptations and thus no adequate analysis can be made by viewing the global design strategies.

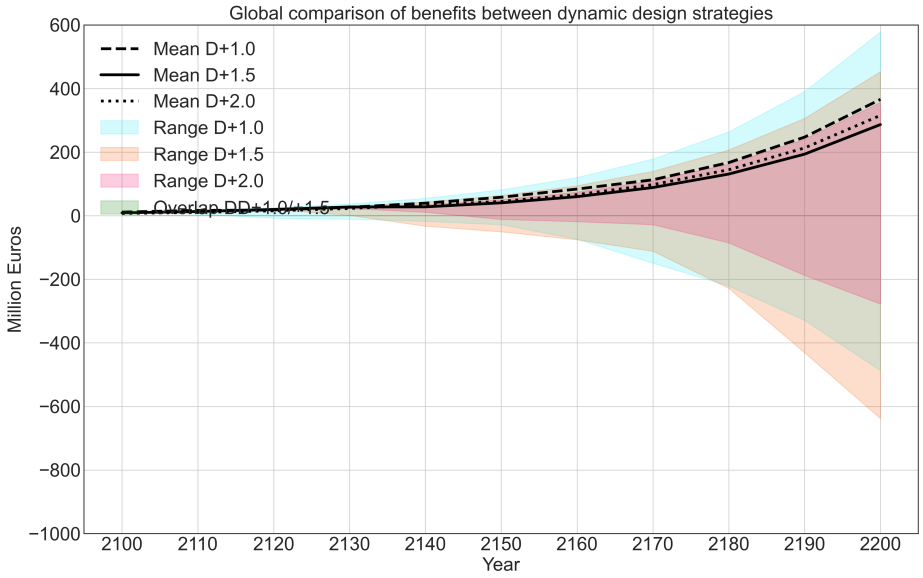

Figure I.23: Performance of all three dynamic design strategies with their respective advised adaptations.

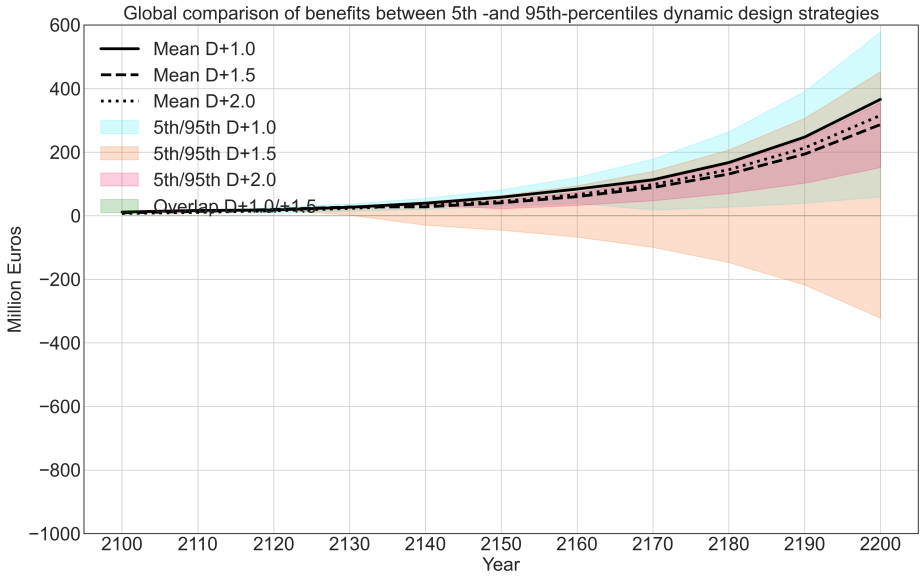

Figure I.24: 5th -and 95th-percentiles of all three dynamic design strategies with their respective advised adaptations.

J | Environmental Cost Index computation

In this appendix chapter an example of ECI-value computation for the foundation block is provided.

J.1. QUANTITIES CONCRETE MATERIALS

In this section the composure and required materials per cubic metre of concrete are stated and the volume of these materials for the Static and Dynamic+1.0 foundation block designs is provided.

Table J.1: Necessary amount of materials for the foundation blocks of the Static and Dynamic+1.0 designs.

	Required material kg	**Static (m3)**	**Dynamic+1.0 (m3)**
Ingredient	**kg per cubic metre of concrete**	8,680 m3 concrete	7,960 m3 concrete
CEM I	125	1,085,000	995,000
CEM III	350	3,038,000	2,786,000
Super plasticizer	3	26,040	23,880
Sand 0/4 mm	684	5,937,120	5,444,640
Gravel 4/8 mm	1177	10,216,360	9,368,920
Well water	160	1,388,800	1,273,600

J.2. LIFE CYCLE INVENTORY DATA

The Life Cycle Inventory data is of 11 environmental impact categories is provided in Table J.2. The ECI-values of the materials are multiplied with these values to yield the environmental costs.

Table J.2: "To calculate the total environmental cost of a product in Euro, the individual category equivalent amounts (kgs or tkms) must be multiplied first by the specific category shadow cost value (forth row, value in Euro). Subsequently, the sum of all specific impact category values are summed to yield the total ECI value (Environmental Cost Indicator value) of that specific material, element, or process. Only the 11 'basic' impact categories are included in the ECI value calculation according to 'Bouwbesluit 2012', additional ones can be listed separate." (Jonker, 2019, p. 47).

	Abiotic Depletion	**Abiotic Depletion**	**Global Warming Potential**
Product	non fuel (ADnf)	fuel (ADf)	(GWP)
Unit/Equivalent	kg Sb eq	kg Sb eq	kg CO2 eq
Shadow costs €/unit	**0.16**	**0.16**	**0.05**
	Ozone Layer Depletion	**Photochemical Oxidation Potential**	**Acidification Potential**
Product	(ODP)	(POCP)	(AP)
Unit/Equivalent	kg CFC-11 eq	kg C2H4 eq	kg SO2 eq
Shadow costs €/unit	**30**	**2**	**4**
	Eutrophication Potential	**Human Toxicity Potential**	**Ecotoxicity Potential, Fresh water**
Product	(EP)	(HT)	(FAETP)
Unit/Equivalent	kg PO42- eq	kg 1,4-DB eq	kg 1,4-DB eq
Shadow costs €/unit	**9**	**0.09**	**0.03**
	Ecotoxcity Potential, Marine water	**Ecotoxicity Potential, Terrestrial Environment**	
Product	(MAETP)	(TETP)	
Unit/Equivalent	kg 1,4-DB eq	kg 1,4-DB eq	
Shadow costs €/unit	**0.0001**	**0.06**	

J.3. ECI-VALUES

In this section the required amount of materials from Table J.1 are multiplied with the ECI-values and result in the monetary values of Table J.4 and Table J.5. Additionally, the ECI-value of the wedge soil improvement is provided in Table J.3. ECI-values computed based on Jonker (2019).

Table J.3: ECI-values and monetisation of the wedge soil improvement for the Dynamic+1.0 design strategy.

Ingredient		**ADnf**	**ADf**	**GW**	**ODP**	**POCP**	**AP**
Gravel, river >4 mm NL							
2,120 m3	€	4.07E-08	2.41E-03	1.17E-01	1.08E-05	1.53E-03	1.19E-02
Ingredient		**EP**	**HT**	**FAETP**	**MAETP**	**TETP**	**Total**
Gravel, river >4 mm NL							
2,120 m3	€	4.39E-03	3.05E-02	5.34E-04	1.10E-02	8.90E-05	€1.79E-01

Table J.4: ECI-values and monetisation of the foundation block for the Static design strategy.

Ingredient	**ADnf**	**ADf**	**GW**	**ODP**	**POCP**	**AP**
CEM I NL	1.16E-01	9.90E+01	4.45E+04	1.69E-01	4.56E+02	1.17E+04
CEM IIIA NL	3.26E-01	3.74E+02	6.68E+04	4.92E-01	7.29E+02	1.82E+04
Super plasticizer	0.00E+00	3.37E+01	9.37E+02	7.50E-02	7.29E+01	1.01E+03
Sand, river 0-4 mm NL	1.23E-03	1.90E+01	8.61E+02	5.52E-02	2.73E+01	4.27E+02
Gravel, river >4 mm NL	1.96E-04	1.16E+01	5.62E+02	5.21E-02	7.36E+00	5.72E+01
Surface / well water	0.00E+00	0.00E+00	0.00E+00	0.00E+00	0.00E+00	0.00E+00
Monetary value (€)	4.43E-01	5.38E+02	1.14E+05	8.44E-01	1.29E+03	3.14E+04

Ingredient	**EP**	**HT**	**FAETP**	**MAETP**	**TETP**	
CEM I NL	3.52E+03	4.88E+03	2.25E+01	5.53E+02	4.43E+01	
CEM IIIA NL	4.65E+03	9.02E+03	4.01E+01	2.22E+03	8.20E+01	
Super plasticizer	1.08E+02	1.92E+02	2.34E+01	2.37E+01	5.62E-01	
Sand, river 0-4 mm NL	2.24E+02	1.02E+03	5.52E+00	1.19E+02	3.92E+00	
Gravel, river >4 mm NL	2.11E+01	1.47E+02	2.57E+00	5.31E+01	4.29E-01	
Surface / well water	0.00E+00	0.00E+00	0.00E+00	0.00E+00	0.00E+00	**Total [€]**
Monetary value (€)	8.52E+03	1.53E+04	9.41E+01	2.97E+03	1.31E+02	€173,922.30

Table J.5: ECI-values and monetisation of the foundation block for the Dynamic+1.0 design strategy.

Ingredient	**ADnf**	**ADf**	**GW**	**ODP**	**POCP**	**AP**
CEM I NL	1.07E-01	9.07E+01	4.08E+04	1.55E-01	4.18E+02	1.07E+04
CEM IIIA NL	2.99E-01	3.43E+02	6.13E+04	4.51E-01	6.69E+02	1.67E+04
Super plasticizer	0.00E+00	3.09E+01	8.60E+02	6.88E-02	6.69E+01	9.27E+02
Sand, river 0-4 mm NL	1.13E-03	1.74E+01	7.89E+02	5.06E-02	2.50E+01	3.92E+02
Gravel, river >4 mm NL	1.80E-04	1.06E+01	5.15E+02	4.78E-02	6.75E+00	5.25E+01
Surface / well water	0.00E+00	0.00E+00	0.00E+00	0.00E+00	0.00E+00	0.00E+00
Monetary value (€)	4.07E-01	4.93E+02	1.04E+05	7.74E-01	1.19E+03	2.88E+04

Ingredient	**EP**	**HT**	**FAETP**	**MAETP**	**TETP**	
CEM I NL	3.22E+03	4.48E+03	2.06E+01	5.07E+02	4.06E+01	
CEM IIIA NL	4.26E+03	8.27E+03	3.68E+01	2.03E+03	7.52E+01	
Super plasticizer	9.89E+01	1.76E+02	2.15E+01	2.17E+01	5.16E-01	
Sand, river 0-4 mm NL	2.06E+02	9.31E+02	5.06E+00	1.09E+02	3.59E+00	
Gravel, river >4 mm NL	1.94E+01	1.35E+02	2.36E+00	4.87E+01	3.93E-01	
Surface / well water	0.00E+00	0.00E+00	0.00E+00	0.00E+00	0.00E+00	**Total [€]**
Monetary value (€)	7.81E+03	1.40E+04	8.63E+01	2.72E+03	1.20E+02	€159,495

J.4. ECI-VALUE COMPARISON

The difference between the ECI-values of the Static and Dynamic+1.0, of the foundation block, is roughly €15,000,-, which is not a massive sum. The ECI costs of the wedge soil adaptation is negligible. Albeit, that the costs savings in ECI-values are generally small, it does bolster the idea of applying adaptive designs.

K | Python modules of the reliability model

The calculations performed in Appendix F are transformed into Python modules to form the reliability model. The modules are functions automatically calculating the desired output with varying or many input parameters. These modules are linked so that a change of output in one module can lead to a change in output in another module.

K.1. ENVELOPING STATIC MODULE - RELIABILITY MODEL

The main function of the model for the static robust design computations.

```
def MAIN_Exceedance_probability(F_horizontal_positive, F_horizontal_negative, N, Fsw_gate, A1, A2,
        A3, B_gate, H_GateBottom, A_foundation, B_foundation, L_foundation,
        H_foundation, H_arm_foundation, F_selfweight, h_soil, H_DWL, slr_matrix, SS, Hs, B_MLK,
        H_sill, h_gateAB, delta_H, Hs_river, LAT, u_c1, u_c2, dn50_A, dn50_B, L_Bed_A, L_Bed_B,
        b_girder, t_steel):

    H_gate = delta_H
    count_Pos_head = np.zeros(len(slr_matrix))
    count_Neg_head = np.zeros(len(slr_matrix))

    count_Foundation_Hor = np.zeros(len(slr_matrix))
    count_Foundation_Vert = np.zeros(len(slr_matrix))
    count_Foundation_Mom = np.zeros(len(slr_matrix))
    count_Foundation = np.zeros(len(slr_matrix))

    count_Bedprotection_River = np.zeros(len(slr_matrix))
    count_Bedprotection_Sea = np.zeros(len(slr_matrix))
    count_Bedlength_A = np.zeros(len(slr_matrix))
    count_Bedlength_B = np.zeros(len(slr_matrix))

    count_GatesHeight = np.zeros(len(slr_matrix))
    count_GatesBuoyancy = np.zeros(len(slr_matrix))
    count_GatesBending = np.zeros(len(slr_matrix))
    count_GatesDeflection = np.zeros(len(slr_matrix))

    #Trusses
    Fhydro_static_pos = np.zeros(N)
    Fhydro_static_neg = np.zeros(N)
    F_hor_total_B_pos = np.zeros(N)
    F_hor_total_B_neg = np.zeros(N)

    #Foundation
    H_cap_soil = np.zeros(N)

    V_cap_soil = np.zeros(N)
    V_force_soil = np.zeros(N)

    M_cap_soil = np.zeros(N)
    M_force = np.zeros(N)
    M_eccentricity = np.zeros(N)

    #Bed protection
    u_star_r = np.zeros(N)

    Opening_MaxU = np.zeros(N)
    Closing_MaxU = np.zeros(N)

    u_star_r_sea = np.zeros(N)
    u_star_r_res_sea = np.zeros(N)

    u_star_r_river = np.zeros(N)
    u_star_r_res_river = np.zeros(N)

    u_flow_velocity = np.zeros(N)
    Closing_MaxU = np.zeros(N)
    Opening_MaxU = np.zeros(N)

    L_bed_req_A = np.zeros(N)
    L_bed_req_B = np.zeros(N)

    #Gates
    q_overflow = np.zeros(N)
    Fb_tot = np.zeros(N)
    Fdown = np.zeros(N)
    Fw_cr = np.zeros(N)
    Fsw_req = np.zeros(N)
    Fsw = np.zeros(N)

    M_maxHG_vert = np.zeros(N)
    p_triangle = np.zeros(N)
    f_deflect = np.zeros(N)

    z = np.linspace(2100,2200,11)
    for i, slr_year in enumerate(slr_matrix):
        for j, SLR in enumerate(slr_year):
    #Positive Head
```

Figure K.1: Python module computing the failure probabilities for the static design strategies (Part 1 out of 3).

```
#Positive Head
        Fhydro_static_pos[j], Mz_static_res_B, F_waves_hor_sea, F_waves_hor_river,
    F_hor_total_B_pos[j], Mz_waves_res_B, Mz_total_B = Horizontal_Force_Positive(H_DWL,
            SLR, SS, Hs, B_MLK, H_sill, h_gateAB, delta_H, Hs_river)

        if F_hor_total_B_pos[j]*B_MLK >= F_horizontal_positive:
            count_Pos_head[i] += 1

#Negative Head
        Fhydro_static_neg[j], Mz_static_res_B, F_waves_hor_sea, F_waves_hor_river,
    F_hor_total_B_neg[j], Mz_waves_res_B, Mz_total_B = Horizontal_Force_Positive(H_DWL,
            SLR, LAT, Hs, B_MLK, H_sill, h_gateAB, delta_H, Hs_river)

        if abs(F_hor_total_B_neg[j]*B_MLK) >= F_horizontal_negative:
            count_Neg_head[i] += 1

#Foundation stability
        H_cap_soil[j], V_cap_soil[j], M_cap_soil[j] = Res_foundation_shallow(B_foundation,
            L_foundation, H_foundation, A_foundation, F_selfweight,
            F_hor_total_B_pos[j]*B_MLK, h_soil)

    #Vertical
        V_force_soil[j] = Vertical_soil_pressure(B_foundation, L_foundation, H_foundation,
            A_foundation, H_arm_foundation, F_selfweight, Fhydro_static_pos[j], M_cap_soil)

        V_cap_soil[j] = 400
        if V_force_soil[j] >= V_cap_soil[j]:
            count_Foundation_Vert[i] += 1

    #Horizontal
        if 1000*F_hor_total_B_pos[j]*B_MLK >= H_cap_soil[j]:   #kN
            count_Foundation_Hor[i] += 1

    #Rotational
        M_eccentricity[j] = (1000*F_hor_total_B_pos[j]*B_MLK * H_arm_foundation)/F_selfweight
        if M_eccentricity[j] > 1/6*L_foundation:
            count_Foundation_Mom[i] += 1

        count_Foundation[i] = (1 - (1-count_Foundation_Vert[i])*(1-count_Foundation_Hor[i])*
                                                    (1- count_Foundation_Mom[i]))

#Bed Protection - Seaside stones
        u_c, Opening_MaxU, Closing_MaxU = Current_velocities(H_sill, B_MLK, u_c1, u_c2, SLR,
            SS, LAT)
        u_star_r_sea[j], u_star_r_river[j] = Shear_velocity_bed(H_sill, delta_H, Hs, Hs_river,
            SS, SLR, Opening_MaxU, Closing_MaxU, dn50_A)

        u_star_r_res_sea[j] = Resistance_bedprotection(H_sill, SS, SLR, dn50_A)

        if u_star_r_sea[j] >= u_star_r_res_sea[j]:
            count_Bedprotection_Sea[i] += 1

#Bed Protection - Riverside stones
        u_star_r_sea[j], u_star_r_river[j] = Shear_velocity_bed(H_sill, delta_H, Hs, Hs_river,
            SS, SLR, Opening_MaxU, Closing_MaxU, dn50_B)
        u_star_r_res_river[j] = Resistance_bedprotection(H_sill, SS, SLR, dn50_B)

        if u_star_r_river[j] >= u_star_r_res_river[j]:
            count_Bedprotection_River[i] += 1

#Bed Protection - Length at seaside
        u_c = Opening_MaxU
        hmax, hs, L_bed_req_A[j] = Scour_bedlength_depth(H_sill, Hs, SS, SLR, u_c, delta_H)
        if L_bed_req_A[j] >= L_Bed_A:
            count_Bedlength_A[i] += 1

#Bed Protection - Length at riverside
        u_c = Closing_MaxU
        hmax, hs, L_bed_req_B[j] = Scour_bedlength_depth(H_sill, Hs, SS, SLR, u_c, delta_H)
        if L_bed_req_B[j] >= L_Bed_B:
            count_Bedlength_B[i] += 1

#Gates - Retention height
        q_limit = 0.2 #l/s/m
        q_overflow[j] = Overtopping(H_gate, H_sill, Hs, SLR, SS)
        if q_limit <= q_overflow[j]:
```

Figure K.2: Python module computing the failure probabilities for the static design strategies (Part 2 out of 3).

```
    #Gates - Retention height
            q_limit = 0.2 #l/s/m
            q_overflow[j] = Overtopping(H_gate, H_sill, Hs, SLR, SS)
            if q_limit <= q_overflow[j]:
                count_GatesHeight[i] += 1

     #Gates - Buoyancy
            Fb_tot[j] = Buoyancy_upward(B_gate, B_MLK, H_sill, SS, SLR)
            Fdown[j], Fw_cr[j] = Buoyance_downward(A1, A2, A3, B_gate, H_GateBottom, B_MLK, H_sill,
                SS, SLR)

            Fsw_req[j] = Fb_tot[j] - Fdown[j]
            if Fsw_gate <= Fsw_req[j]:
                count_GatesBuoyancy[i] += 1

     #Gates - Strength
            f_limit = 10 #mm
            Mrd_gate = Gates_Strength(b_girder, t_steel)
            M_max_vert, M_maxHG_vert[j], p_triangle[j] = Gates_BendingMoment(SLR, SS, H_gate, H_sill,
                b_girder)

            f_deflect[j] = Gates_Deflection(b_girder, t_steel, p_triangle[j])
            if Mrd_gate <= M_maxHG_vert[j]:
                count_GatesBending[i] += 1
            if f_limit <= f_deflect[j]:
                count_GatesDeflection[i] += 1


        print(round((i+1)/len(z)*100,0),'%')
    return count_GatesBending, count_GatesDeflection, count_GatesBuoyancy, count_Foundation_Vert,
count_Foundation_Hor, count_Foundation_Mom, count_GatesHeight, count_Pos_head, count_Neg_head,
count_Bedlength_A, count_Bedlength_B, count_Foundation, count_Bedprotection_Sea,
count_Bedprotection_River
```

Figure K.3: Python module computing the failure probabilities for the static design strategies (Part 3 out of 3).

K.2. ENVELOPING DYNAMIC MODULE - RELIABILITY MODEL

The main function of the model for the dynamic robust computations. The static module is incorporated in this module.

```
def Dynamic_Exceedance_probability(F_horizontal_positive, F_horizontal_negative, N, Components, Adapt_comp,
        Saving_Costs, Costs_comp, Fsw_gate, A1, A2, A3, B_gate, H_GateBottom, A_foundation, B_foundation,
        L_foundation, H_foundation, H_arm_foundation, F_selfweight, h_soil, H_DWL, slr_matrix, SS, Hs, B_MLK,
        H_sill, h_gateAB, delta_H, Hs_river, LAT, u_c1, u_c2, dn50_A, dn50_B, L_Bed_A, L_Bed_B):

    #Dynamic Robustness parameters
    Failure = np.zeros(len(Components))
    Fail_prop = [[]]
    R = 0.04
    Pf_StormSurge = 1/10000
    Pf_component = 1/80000
    Pf_Pos_Head = np.zeros(len(slr_matrix))
    Pf_Bedprotection_River = np.zeros(len(slr_matrix))
    Pf_Bedlength_B = np.zeros(len(slr_matrix))
    Pf_Gateheight = np.zeros(len(slr_matrix))
    Pf_Foundation_Hor = np.zeros(len(slr_matrix))

    #Benefit_comp = np.zeros(len(Components))
    Benefit_SteelTruss = np.zeros((N, len(slr_matrix)))
    Benefit_dn50_B = np.zeros((N, len(slr_matrix)))
    Benefit_BedLength = np.zeros((N, len(slr_matrix)))
    Benefit_GateHeight = np.zeros((N, len(slr_matrix)))
    Benefit_FoundationGrout =np.zeros((N, len(slr_matrix)))

    Number_adapt = np.zeros(len(Components))

    #Probability matrices
    count_Pos_head = np.zeros(len(slr_matrix))
    count_Neg_head = np.zeros(len(slr_matrix))

    count_Foundation_Hor = np.zeros(len(slr_matrix))
    count_Foundation_Vert = np.zeros(len(slr_matrix))
    count_Foundation_Mom = np.zeros(len(slr_matrix))
    count_Foundation = np.zeros(len(slr_matrix))

    count_Bedprotection_River = np.zeros(len(slr_matrix))
    count_Bedprotection_Sea = np.zeros(len(slr_matrix))
    count_Bedlength_A = np.zeros(len(slr_matrix))
    count_Bedlength_B = np.zeros(len(slr_matrix))

    count_GatesHeight = np.zeros(len(slr_matrix))
    count_GatesBuoyancy = np.zeros(len(slr_matrix))

    #Trusses
    Fhydro_static_pos = np.zeros(N)
    Fhydro_static_neg = np.zeros(N)
    F_hor_total_B_pos = np.zeros(N)
    F_hor_total_B_neg = np.zeros(N)

    #Foundation
    H_cap_soil = np.zeros(N)

    V_cap_soil = np.zeros(N)
    V_force_soil = np.zeros(N)

    M_cap_soil = np.zeros(N)
    M_force = np.zeros(N)
    M_eccentricity = np.zeros(N)

    #Bed protection
    u_star_r = np.zeros(N)
    #u_star_r_res = np.zeros(N)

    Opening_MaxU = np.zeros(N)
    Closing_MaxU = np.zeros(N)

    u_star_r_sea = np.zeros(N)
    u_star_r_res_sea = np.zeros(N)

    u_star_r_river = np.zeros(N)
    u_star_r_res_river = np.zeros(N)

    u_flow_velocity = np.zeros(N)
    Closing_MaxU = np.zeros(N)
    Opening_MaxU = np.zeros(N)
```

Figure K.4: Python module computing the failure probabilities and benefits for the dynamic design strategies (Part 1 out of 4).

```
    u_flow_velocity = np.zeros(N)
    Closing_MaxU = np.zeros(N)
    Opening_MaxU = np.zeros(N)

    L_bed_req_A = np.zeros(N)
    L_bed_req_B = np.zeros(N)

    #Gates
    q_overflow = np.zeros(N)
    Fb_tot = np.zeros(N)
    Fdown = np.zeros(N)
    Fw_cr = np.zeros(N)
    Fsw_req = np.zeros(N)
    Fsw = np.zeros(N)

    for i, slr_year in enumerate(slr_matrix):
        for j, SLR in enumerate(slr_year):
            H_DWL = Components[3][0]
            delta_H = H_DWL
    #Positive Head
            Fhydro_static_pos[j], Mz_static_res_B, F_waves_hor_sea, F_waves_hor_river, F_hor_total_B_pos[j],
        Mz_waves_res_B, Mz_total_B = Horizontal_Force_Positive(H_DWL, SLR, SS, Hs, B_MLK, H_sill, h_gateAB,
                                                                                    delta_H, Hs_river)
            if F_hor_total_B_pos[j]*B_MLK >= Components[0][0]:
                count_Pos_head[i] += 1
                Components[0][1] = False
                Components[0][2] = i
                Benefit_SteelTruss[j,i] += Benefit_SteelTruss[j, i-1]*(1+R)**(10) - Costs_comp[0][0]*(1+0.02)
                                                                                                **((i-1)*10)
            else:
                if i == 0:
                    Benefit_SteelTruss[j,0] = Saving_Costs[0]
                else:
                    Benefit_SteelTruss[j,i] += Benefit_SteelTruss[j, i-1]*(1+R)**(10)

    #Foundation stability
            H_cap_soil[j], V_cap_soil[j], M_cap_soil[j] = Res_foundation_shallow_adapt(B_foundation,
        L_foundation, H_foundation, A_foundation, F_selfweight, F_hor_total_B_pos[j]*B_MLK, h_soil,
                                                                                    Components[4][0])
        #Vertical
            V_force_soil[j] = Vertical_soil_pressure(B_foundation, L_foundation, H_foundation, A_foundation,
        H_arm_foundation, F_selfweight, Fhydro_static_pos[j]*B_MLK, M_cap_soil)
            V_cap_soil[j] = 400
            if V_force_soil[j] >= V_cap_soil[j]:
                count_Foundation_Vert[i] += 1

        #Horizontal
            if 1000*F_hor_total_B_pos[j]*B_MLK >= H_cap_soil[j]:   #kN
                count_Foundation_Hor[i] += 1
                Components[4][1] = False
                Components[4][2] = i
                Benefit_FoundationGrout[j,i] += Benefit_FoundationGrout[j, i-1]*(1+R)**(10) -
                                                                    Costs_comp[4][0]*(1+0.02)**((i-1)*10)
            else:
                if i == 0:
                    Benefit_FoundationGrout[j,0] = Saving_Costs[4]
                else:
                    Benefit_FoundationGrout[j,i] += Benefit_FoundationGrout[j, i-1]*(1+R)**(10)
        #Rotational
            M_eccentricity[j] = (1000*F_hor_total_B_pos[j]*B_MLK * H_arm_foundation)/F_selfweight
            M_eccentricity[j] = M_force[j]/F_selfweight
            if M_eccentricity[j] > 1/6*L_foundation:
                count_Foundation_Mom[i] += 1

            count_Foundation[i] = (1 - (1-count_Foundation_Vert[i])*(1-count_Foundation_Hor[i])*
                                                                    (1- count_Foundation_Mom[i]))

    #Bed Protection - Seaside stones
            u_c, Opening_MaxU, Closing_MaxU = Current_velocities(H_sill, B_MLK, u_c1, u_c2, SLR, SS, LAT)

    #Bed Protection - Riverside stones
            u_star_r_sea[j], u_star_r_river[j] = Shear_velocity_bed(H_sill, delta_H, Hs, Hs_river, SS, SLR,
                                                                    Opening_MaxU, Closing_MaxU, dn50_B)
            u_star_r_res_river[j] = Resistance_bedprotection(H_sill, SS, SLR, Components[1][0])
            if u_star_r_river[j] >= u_star_r_res_river[j]:
                count_Bedprotection_River[i] += 1
                Components[1][1] = False
                Components[1][2] = i
                Benefit_dn50_B[j,i] += Benefit_dn50_B[j, i-1]*(1+R)**(10) - Costs_comp[1][0]*(1+0.02)
                                                                                                **((i-1)*10)
```

Figure K.5: Python module computing the failure probabilities and benefits for the dynamic design strategies (Part 2 out of 4).

```
                                                                                                **((i-1)*10)
        else:
            if i == 0:
                Benefit_dn50_B[j,0] = Saving_Costs[1]
            else:
                Benefit_dn50_B[j,i] += Benefit_dn50_B[j, i-1]*(1+R)**(10)

#Bed Protection - Length at riverside
        u_c = Closing_MaxU
        hmax, hs, L_bed_req_B[j] = Scour_bedlength_depth(H_sill, Hs, SS, SLR, u_c, delta_H)
        if L_bed_req_B[j] >= Components[2][0]:
            count_Bedlength_B[i] += 1
            Components[2][1] = False
            Components[2][2] = i
            Benefit_BedLength[j,i] += Benefit_BedLength[j, i-1]*(1+R)**(10) - Costs_comp[2][0]*(1+0.02)
                                                                                                **((i-1)*10)
        else:
            if i == 0:
                Benefit_BedLength[j,0] = Saving_Costs[2]
            else:
                Benefit_BedLength[j,i] += Benefit_BedLength[j, i-1]*(1+R)**(10)
#Gates - Retention height
        q_limit = 0.2 #m3/s/m
        q_overflow[j] = Overtopping(Components[3][0], H_sill, Hs, SLR, SS)
        #Benefit_GateHeight[j,0] = Saving_Costs[3]
        if q_limit <= q_overflow[j]:
            count_GatesHeight[i] += 1
            Components[3][1] = False
            Components[3][2] = i
            Benefit_GateHeight[j,i] += Benefit_GateHeight[j, i-1]*(1+R)**(10) - Costs_comp[3][0]*(1+0.02)
                                                                                                **((i-1)*10)
        else:
            if i == 0:
                Benefit_GateHeight[j,0] = Saving_Costs[3]
            else:
                Benefit_GateHeight[j,i] += Benefit_GateHeight[j, i-1]*(1+R)**(10)

    Benefit_comp = [[Benefit_SteelTruss],[Benefit_dn50_B],[Benefit_BedLength],[Benefit_GateHeight],
                                                                        [Benefit_FoundationGrout]]

#Start determining adaptation moments with lower threshold norm 1:80,000 p/y exceedance probability
    Time = 0
    #Failure probability for component 0 - Steel trusses, and adaptation
    Pf_Pos_Head[i] = count_Pos_head[i]/N*Pf_StormSurge
    if Pf_Pos_Head[i] >= Pf_component:
        Fail_prop.append(Pf_Pos_Head[i])
        Time = i*10
        Failure[0] += 1
        if Components[0][1] == False:
            Components[0][0] += Adapt_comp[0]   #Loop through component adaption in chrono order
            #Benefit_SteelTruss[i-1] += Costs_comp[0][0]*(1+R)**((i-1)*10)
            Components[0][1] = True
    #Failure probability for component 1 - Bed protection stones, and adaptation
    Pf_Bedprotection_River[i] = count_Bedprotection_River[i]/N*Pf_StormSurge
    if Pf_Bedprotection_River[i] >= Pf_component:
        Fail_prop.append(Pf_Bedprotection_River[i])
        Time = i*10
        Failure[1] += 1
        if Components[1][1] == False:
            Components[1][0] = Adapt_comp[1]   #Loop through component adaption in chrono order
            #Benefit_dn50_B[i-1] += Costs_comp[1][0]*(1+R)**((i-1)*10)
            Components[1][1] = True
    #Failure probability for component 2 - Bed protection length, and adaptation
    Pf_Bedlength_B[i] = count_Bedlength_B[i]/N*Pf_StormSurge
    if Pf_Bedlength_B[i] >= Pf_component:
        Fail_prop.append(Pf_Bedlength_B[i])
        Time = i*10
        Failure[2] += 1
        if Components[2][1] == False:
            Components[2][0] += Adapt_comp[2]   #Loop through component adaption in chrono order
            #Benefit_BedLength[i-1] += Costs_comp[2][0]*(1+R)**((i-1)*10)
            Components[2][1] = True
    #Failure probability for component 3 - Gates retention height, and adaptation
```

Figure K.6: Python module computing the failure probabilities and benefits for the dynamic design strategies (Part 3 out of 4).

```
        #Failure probability for component 3 - Gates retention height, and adaptation
        Pf_Gateheight[i] = count_GatesHeight[i]/N*Pf_StormSurge
        if Pf_Gateheight[i] >= Pf_component:
            Fail_prop.append(Pf_Gateheight[i])
            Time = i*10
            Failure[3] += 1
            if Components[3][1] == False:
                Components[3][0] += Adapt_comp[3]   #Loop through component adaption in chrono order
                #Benefit_GateHeight[i-1] += Costs_comp[3][0]*(1+R)**((i-1)*10)
                Components[3][1] = True
        #Failure probability for component 3 - Gates retention height, and adaptation
        Pf_Foundation_Hor[i] = count_Foundation_Hor[i]/N*Pf_StormSurge
        if Pf_Foundation_Hor[i] >= Pf_component:
            Fail_prop.append(Pf_Foundation_Hor[i])
            Time = i*10
            Failure[4] += 1
            if Components[4][1] == False:
                Components[4][0] += Adapt_comp[4]   #Loop through component adaption in chrono order
                #Benefit_FoundationGrout[i-1] += Costs_comp[4][0]*(1+R)**((i-1)*10)
                Components[4][1] = True

        print(round((i+1)/len(slr_matrix)*100,0),'%')
    return Fail_prop, Time, Failure, Benefit_FoundationGrout, Pf_Pos_Head, Pf_Bedprotection_River,
Pf_Bedlength_B, Pf_Gateheight, Pf_Foundation_Hor
```

Figure K.7: Python module computing the failure probabilities and benefits for the dynamic design strategies (Part 4 out of 4).

K.3. BED PROTECTION

```
def Forcingvelocities_Bedprotection(H_sill, delta_H, Hs, Hs_river, SS, SLR, u_c1, u_c2, dn50, B_MLK, LAT):
#Determine the highest (tidal) velocities over the bed protection
    u_c_tide, Opening_MaxU, Closing_MaxU = Current_velocities(H_sill, B_MLK, u_c1, u_c2, SLR, SS, LAT)
    Opening_Max_uc = np.max(Opening_MaxU)
    Closing_Max_uc = np.max(Closing_MaxU)
    u_c = max(u_c_tide, Opening_Max_uc, Closing_Max_uc)

#Shear velocities over the bed protection
    u_star_r_sea, alpha_sea, r0_sea, fc_sea = Waves_Sea_velocities(H_sill, delta_H, Hs, SS, SLR, u_c, dn50)
    u_star_r_river, alpha_river, r0_river, fc_river = Waves_River_velocities(H_sill, delta_H, Hs_river, SS,
                                                                             SLR, u_c, dn50)

    u_star_r = max(u_star_r_sea, u_star_r_river) #[m/s]
    return u_star_r, u_c
```

Figure K.8: Python module computing the shear velocity on the bed protection

```
def Resistance_bedprotection(H_sill, SS, SLR, dn50):
    g = 9.81
    Delta = 1.585
    shields = 0.03

    h = H_sill + SS + SLR
    if h/dn50 > 5: #Shields is most applicable when valid
        #print(round(h/dn50,1), '> 5')
#Check for upper boundary value of appliance of Shields - Schiereck [p.57]
        if h/dn50 < 100:
            u_star_r_res = np.sqrt(shields * Delta * g * dn50)
            #print('Conditions met')
        else:
            print('apply different method (Izbash)')
    return u_star_r_res
```

Figure K.9: Python module computing the resistance of the stones applied.

```
def Scour_bedlength_depth(H_sill, Hs, SS, SLR, u_c, delta_H):
    g = 9.81
    #Induced by waves
    h0 = H_sill + SS + SLR                    #Original water depth under the worst conditions
    hmax = 0.7 * h0                           #Max. Scouring depth in front of structure

    #Determine wave length for hmax
    Lwave, kwave, c_wave, u_hat_b, ab = Wave_character_sea(Hs, delta_H)
    hmax = 0.4 * Hs * (sinh(2*np.pi*h0/Lwave))**(-1.35) #Based on experiments

    #Sand characteristics
    dn50 = 1.035/1000 #[m] for sand
    kr = 0.5 #Voorendt [p.275]
    R = h0
    #Check validity of Chezy formula
    if ab >= 0.636*kr:
        cf = min(0.237*(ab/kr)**(-0.52),0.3)
        C_sand = 18*np.log10(12*R/kr)       #[m0.5/s]
    else:
        cf = 0.3
        C_sand = 18*np.log10(12*R/kr)       #[m0.5/s]
        #print('Conditions not met')

    r0_sand = 1.2*np.sqrt(g)/C_sand         #Schiereck [p.95]
    fc_sand = max(C_sand/40,1)              #Schiereck [p.95]
    alpha = max(1.5+ 5*r0_sand*fc_sand,2)   #Schiereck [p.95]
    psi_c = 0.055                           #Value at which particles are moving, 0.03 deemed too safe
    Delta = 1.585                           #Relative density

    #Shear velocities
    angle = 0                               #Angle of attack
    phi = (90 + angle)*np.pi/180            #Radian of attack

    u_c                                     #Tidal velocity - http://www.vetwetwet.nl/stroomatlas/
    u_hat_b                                 #Orbital velocity at bottom
    u_star_c_sand = np.sqrt(g)/C_sand * u_c #Shear velocity due to current
    u_star_b_sand = np.sqrt(cf/2) * u_hat_b #Shear velocity due to waves
    u_star_r_sand = np.sqrt(u_star_c_sand**2 + u_star_b_sand**2 + 2*u_star_b_sand*u_star_c_sand*np.sin(phi))
    u_c_sand = np.sqrt(psi_c*Delta*g*dn50)
    u_stripe = u_star_r_sand
    u_stripe_c = u_c_sand

    #Development scourhole depth over 1 storm
    t_storm_average = 2*3600
    n_closures = 1
    time = t_storm_average * n_closures
    hs = (((alpha * u_stripe - u_stripe_c)**1.7*h0**0.2)/(10*Delta**0.7))*time**0.4

    #Determine required bed length protection
    u0 = u_stripe
    r0 = r0_sand
    Beta = np.arcsin(abs(3*10**(-4) * u0**2/(Delta*g*dn50)+(0.11+0.75*r0)*fc_sand))
    B_ratio = 1/np.tan(Beta)

    Slope_loose_sand = 15                 #Schiereck [p.100]
    L_bed_req = (Slope_loose_sand - B_ratio) * hs  #[m] Length of bed protection required

    return hmax, hs, L_bed_req
```

Figure K.10: Python module computing the scour hole at the toe of the bed protection and required length of the bed protection.

K.3.1. VELOCITIES DUE TO WAVES

```
def Waves_Sea_velocities(H_sill, delta_H, Hs, SS, SLR, u_c, dn50):
    g = 9.81
    #Induced by waves
    h0 = H_sill + SLR                    #Original water depth under the worst conditions

    #Determine wave length for hmax
    Lwave, kwave, c_wave, u_hat_b, ab = Wave_character_sea(Hs, delta_H)

    #Stone characteristics
    kr = 2*dn50 #Practical choice for statically stable protection - Schiereck [p.59]
    R = h0
    #Check validity of Chezy formula
    if ab >= 0.636*kr:
        cf = min(0.237*(ab/kr)**(-0.52),0.3)
        C = 18*np.log10(12*R/kr)        #[m0.5/s]
        #print('Conditions met')
    else:
        cf = 0.3
        C = 18*np.log10(12*R/kr)        #[m0.5/s]
    r0 = 1.2*np.sqrt(g)/C          #Schiereck [p.95]
    fc = C/40
    if fc > 1:                      #Schiereck [p.95]
        fc = 1
    alpha = max(1.5+ 5*r0*fc,2)    #Schiereck [p.95]
    psi_c = 0.055                           #Value at which particles are moving, 0.03 deemed too safe
    Delta = 1.585                           #Relative density

    #Shear velocities
    angle = 0                               #Angle of attack
    phi = (90 + angle)*np.pi/180            #Radian of attack

    #u_c = 2.6                               #Tidal velocity - http://www.wetwetwet.nl/stroomatlas/
    u_hat_b                                 #Orbital velocity at bottom
    u_star_c = np.sqrt(g)/C * u_c #Shear velocity due to current
    u_star_b = np.sqrt(cf/2) * u_hat_b #Shear velocity due to waves

    u_star_r = np.sqrt(u_star_c**2 + u_star_b**2 + 2*u_star_b*u_star_c*np.sin(phi))
    return u_star_r, alpha, r0, fc
```

Figure K.11: Python module computing the shear velocities over the bed protection due to waves on the seaside.

```
def Waves_River_velocities(H_sill, delta_H, Hs_river, SS, SLR, u_c, dn50):
    g = 9.81
    #Induced by waves
    #Closing regime
    if SLR < 1.0:
        hwl_behind = 3.00
    elif 1.0 <= SLR < 2.0:
        hwl_behind = 3.80
    else:
        hwl_behind = 4.55
    h0 = H_sill + hwl_behind                    #Original water depth under the worst conditions

    #Determine wave length for hmax
    Lwave, kwave, c_wave, u_hat_b, ab = Wave_character_river(Hs_river, delta_H)

    #Stone characteristics
    kr = 2*dn50 #Practical choice for statically stable protection - Schiereck [p.59]
    R = h0
    #Check validity of Chezy formula
    if ab >= 0.636*kr:
        cf = min(0.237*(ab/kr)**(-0.52),0.3)
        C = 18*np.log10(12*R/kr)        #[m0.5/s]
        #print('Conditions met')
    else:
        cf = 0.3
        C = 18*np.log10(12*R/kr)        #[m0.5/s]
    r0 = 1.2*np.sqrt(g)/C          #Schiereck [p.95]
    fc = max(C/40,1)               #Schiereck [p.95]
    alpha = max(1.5+ 5*r0*fc,2)    #Schiereck [p.95]
    psi_c = 0.055                           #Value at which particles are moving, 0.03 deemed too safe
    Delta = 1.585                           #Relative density

    #Shear velocities
    angle = 0                               #Angle of attack
    phi = (90 + angle)*np.pi/180            #Radian of attack

    #u_c = 2.6                               #Tidal velocity - http://www.wetwetwet.nl/stroomatlas/
    u_hat_b                                 #Orbital velocity at bottom
    u_star_c = np.sqrt(g)/C * u_c #Shear velocity due to current
    u_star_b = np.sqrt(cf/2) * u_hat_b #Shear velocity due to waves

    u_star_r = np.sqrt(u_star_c**2 + u_star_b**2 + 2*u_star_b*u_star_c*np.sin(phi))
    return u_star_r, alpha, r0, fc
```

Figure K.12: Python module computing the shear velocities over the bed protection due to waves on the riverside.

K.3.2. UNDERFLOW VELOCITIES

```
def Current_velocities(H_sill, B_MLK, u_c1, u_c2, SLR, SS, LAT):
#Velocities due to natural tide
    u_c1                                    #Spring tide
    u_c2                                    #Neap tide
    u_c = max(u_c1, u_c2)

#Velocities due to opening of the gate
    Opening_MaxQ, Opening_Q, Opening_AMaxQ, Opening_MaxU = Underflow_opening(SLR, LAT, H_sill, B_MLK)

#Velocities due to closing of the gate
    Closing_MaxQ, Closing_Q, Closing_AMaxQ, Closing_MaxU = Underflow_closing(SLR, H_sill, B_MLK, u_c, SS)


    return u_c, Opening_MaxU, Closing_MaxU
```

Figure K.13: Python module connecting the modules of Fig. K.14 and Fig. K.15.

```
def Underflow_closing(SLR, H_sill, B_MLK, u_c, SS):
    u_c = 3                                     #The tidal current of the storm surge
    Opening_gate = np.linspace(0.01,19.99,81)    #Opening of the gate in steps
    A = np.linspace(0,3,10)
    MaxQ = np.zeros(len(A))
    AMaxQ = np.zeros(len(A))
    MaxU = np.zeros(len(A))
    #for i, slr in enumerate(SLR):
    if SLR < 1.0:
        h3 = 3.0 + H_sill            #Riverside WL
    if 1.0 <= SLR < 2.0:
        h3 = 3.8 + H_sill
    if SLR >= 2.0:
        h3 = 4.55 + H_sill
    h1 = SS + H_sill + SLR                #Seaside   WL
    mfuf = 0.6
    msuf = 0.8
    Q = np.zeros(len(Opening_gate))
    U = np.zeros(len(Opening_gate))

    for j, a in enumerate(Opening_gate):
        #Free underflow
        #print(h3/a)
        #print((1.42 * np.sqrt(h1/a))-0.3)
        if h3/a <= (1.42 * np.sqrt(h1/a)) - 0.3:
            Q[j] = mfuf * B_MLK * a * np.sqrt(2*9.81*(h1 - a)) #[m3/s]
        #Submerged underflow
        else:
            Q[j] = msuf * B_MLK * a * np.sqrt(2*9.81*abs(h1 - h3+0.0001)) #[m3/s]
        U[j] = Q[j]/B_MLK/a  #Calculate velocities based on discharge Q divided by respective gate opening

    MaxU = np.max(U)
        #print(MaxU)
    MaxQ = np.max(Q)
        #print(MaxQ)
    AMaxQ = Opening_gate[np.argmax(Q)]
        #print(AMaxQ)
    return MaxQ, Q, AMaxQ, MaxU
```

Figure K.14: Python module computing the underflow velocities during the closing procedure of the barrier.

```
def Underflow_opening(SLR, LAT, H_sill, B_MLK):
    Opening_gate = np.linspace(0.01,19.99,81)   #Opening of the gate in steps
    A = np.linspace(0,3,10)
    MaxQ = np.zeros(len(A))
    AMaxQ = np.zeros(len(A))
    MaxU = np.zeros(len(A))
    #for i, slr in enumerate(SLR):
    if SLR < 1.0:
        h1 = 3.0 + H_sill            #Riverside WL
    if 1.0 <= SLR < 2.0:
        h1 = 3.8 + H_sill
    if SLR >= 2.0:
        h1 = 4.55 + H_sill
    h3 = LAT + H_sill + SLR                #Seaside   WL
    mfuf = 0.5
    msuf = 0.8
    Q = np.zeros(len(Opening_gate))
    U = np.zeros(len(Opening_gate))
    for j, a in enumerate(Opening_gate):
    #Free underflow
        if h3/a <= (1.42 * np.sqrt(h1/a)) - 0.3:
            Q[j] = mfuf * B_MLK * a * np.sqrt(2*9.81*(h1 - a)) #[m3/s]
    #Submerged underflow
        else:
            Q[j] = msuf * B_MLK * a * np.sqrt(2*9.81*abs(h1 - h3+0.0001)) #[m3/s]

        U[j] = Q[j]/B_MLK/a  #Calculate velocities based on discharge Q divided by respective gate opening

    MaxU = np.max(U)
    #print(MaxU)
    MaxQ = np.max(Q)
    #print(MaxQ)
    AMaxQ = Opening_gate[np.argmax(Q)]
    #print(AMaxQ)
    return MaxQ, Q, AMaxQ, MaxU
```

Figure K.15: Python module computing the underflow velocities during the opening procedure of the barrier.

K.4. SUB -AND SUPERSTRUCTURE

K.4.1. HEAD DIFFERENCE - HORIZONTAL HYDROSTATIC FORCE

```python
def Fhydro_hor_Negative(H_DWL, SLR, LAT, H_sill):
    g = 9.81
    hwl_behind = 0
    SS = LAT
    rho_saltwater = 1025 #kg/m3
    rho_freshwater = 1000 #kg/m3
    h_stormsurge = SS + SLR
    delta_H = H_sill + min(h_stormsurge, H_DWL)              #The hydraulic loading coupled to SLR

    #Determines water level behind the barrier
    if SLR < 1.0:
        hwl_behind = 3.00
    elif 1.0 <= SLR < 2.0:
        hwl_behind = 3.80
    else:
        hwl_behind = 4.55

    #Determine hydraulic loading - Seaside
    p_hydroA_hor = rho_saltwater * g * delta_H/1000 #kpa
    F_hydroA_hor = 0.5 * p_hydroA_hor * delta_H #kN/m
    F_hydroA_hor_resulting = F_hydroA_hor #* B_MLK #kN

    #Determine hydraulic loading - Riverside
    p_hydroB_hor = rho_saltwater * g * (hwl_behind + H_sill)/1000 #kpa
    F_hydroB_hor = 0.5 * p_hydroB_hor * (hwl_behind + H_sill) #kN/m
    F_hydroB_hor_resulting = F_hydroB_hor #* B_MLK #kN

    F_hydro_hor_total = round((F_hydroA_hor_resulting - F_hydroB_hor_resulting)/1000,1) #MN

    #Determine resulting bending moment from static loading - to bottom of sill
    MzA = F_hydroA_hor_resulting * 1/3 * delta_H #MNm
    MzB = F_hydroB_hor_resulting * 1/3 * (hwl_behind + H_sill) #MNm
    Mz_resulting = MzA - MzB #MNm

    return F_hydro_hor_total, Mz_resulting, F_hydroA_hor_resulting, F_hydroB_hor_resulting
```

Figure K.16: Python module computing horizontal hydrostatic force due to negative head.

```python
def Fhydro_hor_Positive(H_DWL, SLR, SS, H_sill):
    g = 9.81
    #hwl_behind = 0
    rho_saltwater = 1025 #kg/m3
    rho_freshwater = 1000 #kg/m3
    h_stormsurge = SS + SLR

    #Determines water level behind the barrier
    if SLR < 1.0:
        hwl_behind = 3.00
    elif 1.0 <= SLR < 2.0:
        hwl_behind = 3.80
    else:
        hwl_behind = 4.55

    #If the height of the water is equal or lower than the gate height
    if h_stormsurge <= H_DWL:
        delta_H = H_sill + h_stormsurge             #The hydraulic loading coupled to SLR

        #Determine hydraulic loading - Seaside
        p_hydroA_hor = rho_saltwater * g * delta_H/1000 #kpa
        F_hydroA_hor = 0.5 * p_hydroA_hor * delta_H #kN/m
        F_hydroA_hor_resulting = F_hydroA_hor #* B_MLK #kN

        #Determine hydraulic loading - Riverside
        p_hydroB_hor = rho_saltwater * g * (hwl_behind + H_sill)/1000 #kpa
        F_hydroB_hor = 0.5 * p_hydroB_hor * (hwl_behind + H_sill) #kN/m
        F_hydroB_hor_resulting = F_hydroB_hor #* B_MLK #kN

        F_hydro_hor_total = (F_hydroA_hor_resulting - F_hydroB_hor_resulting)/1000 #MN

        #Determine resulting bending moment from static loading - to bottom of sill
        MzA = F_hydroA_hor_resulting * 1/3 * delta_H #MNm
        MzB = F_hydroB_hor_resulting * 1/3 * (hwl_behind + H_sill) #MNm
        Mz_resulting = MzA - MzB #MNm

    #If the height of the water is higher than the gate height
    if h_stormsurge > H_DWL:
        delta_H = H_sill + H_DWL             #The hydraulic loading coupled to SLR

        #Determine hydraulic loading top of gate = block - Seaside
        p_hydroA_minTriangle = rho_saltwater * g * (h_stormsurge - H_DWL)/1000 #kpa
        F_hydroA_block = p_hydroA_minTriangle * delta_H  #kN/m

        #Determine hydraulic loading max = bottom - seaside
        p_hydroA_hor = rho_saltwater * g * delta_H/1000 #kpa
        F_hydroA_max = 0.5 * (p_hydroA_hor - p_hydroA_minTriangle) * delta_H   #kN/m

        F_hydroA_hor_resulting = F_hydroA_max + F_hydroA_block #kN

        #Determine hydraulic loading - Riverside
        p_hydroB_hor = rho_saltwater * g * (hwl_behind + H_sill)/1000 #kpa
        F_hydroB_hor = 0.5 * p_hydroB_hor * (hwl_behind + H_sill) #kN/m
        F_hydroB_hor_resulting = F_hydroB_hor #* B_MLK #kN

        F_hydro_hor_total = (F_hydroA_hor_resulting - F_hydroB_hor_resulting)/1000 #MN

        #Determine resulting bending moment from static loading - to bottom of sill
        MzA = F_hydroA_hor_resulting * 1/3 * delta_H #MNm
        MzB = F_hydroB_hor_resulting * 1/3 * (hwl_behind + H_sill) #MNm
        Mz_resulting = MzA - MzB #MNm

    return F_hydro_hor_total, Mz_resulting, F_hydroA_hor_resulting, F_hydroB_hor_resulting
```

Figure K.17: Python module computing horizontal hydrostatic force due to positive head.

K.4.2. FOUNDATION MODULE

```
def Vertical_soil_pressure(B_foundation, L_foundation, H_foundation, A_foundation,
                           H_arm_foundation, F_selfweight, F_hor_total_B, M_cap_soil):
    B=B_foundation
    L=L_foundation
    h=H_arm_foundation
    A=A_foundation

    H = F_hor_total_B*1000              #kN
    F = F_selfweight                    #kN
    W = 1/6* B * L**2
    M = H*h                             #kNm

    sigma_k_max = (F)/(A) + (M)/(W)     #kN/m2
    V_force_soil = sigma_k_max          #kN/m2
    return V_force_soil
```

Figure K.18: Python module computing acting vertical force on the foundation and soil.

```
def Res_foundation_shallow(B_foundation, L_foundation, H_foundation, A_foundation, F_selfweight,
                           F_hor_total_B, h_soil):
    #Forcing conditions
    H = F_hor_total_B*1000  #kN
    V = F_selfweight        #Vertical force (selfweight)
    B = B_foundation
    L = L_foundation
    A = A_foundation
    Aeff = A
    if h_soil <= H_foundation:
        h = h_soil          #Height of structure in contact with the soil,
                            #cannot be larger than the height of the block
    else:
        h = H_foundation

    #Soil properties - Fine sand - P.191 Voorendt Sand,Clean,Moderate
    c1 = 0
    phi1 = 32.5 * np.pi/180  #Radians
    gamma1 = 18
    Nc = 37
    Nq = 24.6
    Ngamma = 21.9
    phi = 0
    alpha_f = np.pi/4 + phi/2
    sigmaq1 = 1000*9.81*h/1000

#Horizontal stability
    f1 = 0.5                #Concrete on sand P.274 Voorendt
    f2 = np.tan(phi1)       #Friction subsoil sand
    f3 = np.tan(phi1)       #Friction deeper soil layer

    Hf_construction1 = f1 * V
    Hf_construction2 = f2 * V
    Hf_construction3 = f3 * V

    H_friction = min(Hf_construction1,Hf_construction2,Hf_construction3)

    #Bearing capacity of the soil behind the barrier -
    #Passive pressure Lecture 24 - Soil mechanics3
    gamma_sand = gamma1
    H_cap_soil_passive = 0.5*gamma_sand*h**2 + (0.5*gamma_sand*h**2*np.sin(phi1))/
                (np.cos(((45*np.pi)/180*np.pi)/18+phi1/2)*np.sin((45*np.pi)/180-phi1))
    H_cap_soil = H_cap_soil_passive*B + H_friction

#Vertical stability
        #Determine max. length of slip planes
    Dmax = min(B*np.cos(phi)/(2*np.cos(alpha_f)) * np.exp(alpha_f * np.tan(phi)), 3*B)
    Bmax = min(B*np.tan(alpha_f)*np.exp(np.pi/2 * np.tan(phi)), 10*B)

        #Bearing capacity factors
    Nq = (1 + np.sin(phi1))/(1 - np.sin(phi1))*np.exp(np.pi*np.tan(phi1))
    Nc = (Nq - 1)*cot(phi1)
    Ngamma = (Nq - 1)*np.tan(1.32*phi1)

        #Shape factors
    sq = 1 + B/L*sin(phi1)
    sc = (sq * Nq - 1)/(Nq - 1)
    sgamma = 1 - 0.3*B/L

        #Inclination factors - H parallel to L and L/B>2
    iq = 1 - H/(V+Aeff*c1*cot(phi1))
    ic = (iq*Nq-1)/(Nq-1)
    igamma = iq

    pmax_drained = (c1*Nc*sc*ic + sigmaq1*Nq*sq*iq + 0.5*gamma1*B*Ngamma*sgamma*igamma)
    V_cap_soil = pmax_drained     #kN/m2
    Vmax = (pmax_drained * Aeff)  #kN


#Rotational stability
    Q_passive =  0.5*gamma_sand*h**2 + (0.5*gamma_sand*h**2*np.sin(phi1))/
                        (np.cos((45*np.pi)/180+phi1/2)*np.sin((45*np.pi)/180-phi1))
    M_passive = 2/3 * h * Q_passive #*B #kNm
    M_cap_soil = M_passive
    return H_cap_soil, V_cap_soil, M_cap_soil
```

Figure K.19: Python module computing the resistance of the foundation for the static design strategies.

```
def Res_foundation_shallow_adapt(B_foundation, L_foundation, H_foundation, A_foundation,
                                 F_selfweight, F_hor_total_B, h_soil, Adapt_grout):
    #Forcing conditions
    H = F_hor_total_B*1000  #kN
    V = F_selfweight        #Vertical force (selfweight)
    B = B_foundation
    L = L_foundation
    A = A_foundation
    Aeff = A
    if h_soil <= H_foundation:
        h = h_soil          #Height of structure in contact with the soil,
                            #cannot be larger than the height of the block
    else:
        h = H_foundation

    #Soil properties - Fine sand - P.191 Voorendt Sand,Clean,Moderate
    c1 = 0
    phi1 = 32.5 * np.pi/180  #Radians
    gamma1 = 18
    Nc = 37
    Nq = 24.6
    Ngamma = 21.9
    phi = 0
    alpha_f = np.pi/4 + phi/2
    sigmaq1 = 1000*9.81*h/1000

#Horizontal stability
    f1 = 0.5                #Concrete on sand P.274 Voorendt
    f2 = np.tan(phi1)       #Friction subsoil sand
    f3 = np.tan(phi1)       #Friction deeper soil layer

    Hf_construction1 = f1 * V
    Hf_construction2 = f2 * V
    Hf_construction3 = f3 * V

    H_friction = min(Hf_construction1,Hf_construction2,Hf_construction3)

    #Bearing capacity of the soil behind the barrier -
    #Passive pressure Lecture 24 - Soil mechanics3
    gamma_sand = gamma1*Adapt_grout

    H_cap_soil_passive = 0.5*gamma_sand*h**2 + (0.5*gamma_sand*h**2*np.sin(phi1))/
                (np.cos(((45*np.pi)/180*np.pi)/18+phi1/2)*np.sin((45*np.pi)/180-phi1))
    H_cap_soil = H_cap_soil_passive*B + H_friction

#Vertical stability
        #Determine max. length of slip planes
    Dmax = min(B*np.cos(phi)/(2*np.cos(alpha_f)) * np.exp(alpha_f * np.tan(phi)), 3*B)
    Bmax = min(B*np.tan(alpha_f)*np.exp(np.pi/2 * np.tan(phi)), 10*B)

        #Bearing capacity factors
    Nq = (1 + np.sin(phi1))/(1 - np.sin(phi1))*np.exp(np.pi*np.tan(phi1))
    Nc = (Nq - 1)*cot(phi1)
    Ngamma = (Nq - 1)*np.tan(1.32*phi1)

        #Shape factors
    sq = 1 + B/L*sin(phi1)
    sc = (sq * Nq - 1)/(Nq - 1)
    sgamma = 1 - 0.3*B/L

        #Inclination factors - H parallel to L and L/B>2
    iq = 1 - H/(V+Aeff*c1*cot(phi1))
    ic = (iq*Nq-1)/(Nq-1)
    igamma = iq

    pmax_drained = (c1*Nc*sc*ic + sigmaq1*Nq*sq*iq + 0.5*gamma1*B*Ngamma*sgamma*igamma)
    V_cap_soil = pmax_drained     #kN/m2
    Vmax = (pmax_drained * Aeff)  #kN


#Rotational stability
    Q_passive =  0.5*gamma_sand*h**2 + (0.5*gamma_sand*h**2*np.sin(phi1))/
                          (np.cos((45*np.pi)/180+phi1/2)*np.sin((45*np.pi)/180-phi1))
    M_passive = 2/3 * h * Q_passive #*B #kNm
    M_cap_soil = M_passive
    return H_cap_soil, V_cap_soil, M_cap_soil
```

Figure K.20: Python module computing the resistance of the foundation for the dynamic design strategies.

K.5. GATES

K.5.1. STRENGTH OF THE GATES

```
def Gates_Strength(b_girder, t_steel):
    gamma_steel = 1                         #Safety factor steel
    fy = 355                                #N/mm2
    Wel = 1/6 * b_girder*1000 * t_steel**2    #mm3
    Mrd_gate = Wel * fy / gamma_steel / 10**6    #kNm
    return Mrd_gate

def Gates_BendingMoment(SLR, SS, H_gate, H_sill, b_girder):
    CC3 = 1.1
    L = 7
    Safetyfactor = 1.5 * CC3
    #Vertical girders only - Vertical moment
    p_block = Safetyfactor * 1025 * 9.81 * (H_sill + SLR + SS - L) /1000 #kpa = kN/m2
    p_triangle = Safetyfactor * 1025 * 9.81 * (H_sill + SLR + SS) /1000 #kpa

    M_block = 1/8 * p_block * L**2 #kNm/m
    x_triangle_max = L/np.sqrt(3)
    M_triangle = (p_triangle-p_block) *L*x_triangle_max/6 * (1 - x_triangle_max**2/L**2)  #kNm

    M_max_vert = M_block + M_triangle #kNm

    #With horizontal girders - Vertical moment
    spacing = 2.5 #m
    q_max_moment = p_block + (p_triangle - p_block)/2
    M_maxHG_vert = 1/10 * q_max_moment*(b_girder)**2


    return M_max_vert, M_maxHG_vert, p_triangle

def Gates_Deflection(b_girder, t_steel, p_triangle):
    alpha = 0.0138
    a = b_girder * 1000 #m to mm
    p = p_triangle / 1000 #kpa to N/mm2
    E = 210000 #N/mm2
    f_deflect = alpha * p * a**4 /(E * t_steel**3) #mm
    return f_deflect
```

Figure K.21: Python module computing maximum moment and deflection of the gates.

K.5.2. HEIGHT OF THE GATES

```
def Overtopping(H_gate, H_sill, Hs, SLR, SS):
    g = 9.81
    hs = H_sill + SS + SLR
    Rc = H_gate - hs
    Tp = 3.6*np.sqrt(Hs)      #The peak period of the waves
    Tm = Tp
    #Positive and zero freeboard
    if Rc >= 0:
        h_star = 1.35 * (hs/Hs) * (2*np.pi*hs/(g*Tm**2))
        if h_star<0.2:    #0.03 < h_star*R_c/Hm0 <= 1.0:
            q_overtopping = h_star**2*np.sqrt(g*hs**3) * 2.8*10**(-4) * (h_star*Rc/Hs)**(-3.1)
            #print('Calculated according to impulsive conditions')
        else:
            q_overtopping = np.sqrt(g*Hs**3) * 0.04*np.exp(-1.8*Rc/Hs)
            #print('Calculated according to non-impulsive conditions')
    #Negative freeboard
    if Rc < 0:
        q_overtopping = 0.54 * np.sqrt(g * abs(-Rc**3))        #In m3/s/m
    return q_overtopping
```

Figure K.22: Python module computing specific discharge overtopping or overflowing over the gates.

K.5.3. BUOYANCY OF THE GATES

```
def Buoyancy_upward(B_gate, B_MLK, H_sill, SS, SLR):
    rho_saltwater = 1025
    g = 9.81    #m/s2
    A = B_MLK * B_gate   #m2
    hss = SS + SLR

#The upward force - seaside
    Fb_left = (rho_saltwater * g * (hss + H_sill) * A/2)/10**6 #MN

#The upward force - seaside
    if SLR < 1.0:
        hwl_behind = 3.00
    if 1.0 <= SLR < 2.0:
        hwl_behind = 3.80
    if SLR >=2.0:
        hwl_behind = 4.55

    Fb_right = (rho_saltwater * g * (hwl_behind+H_sill) * A/2)/10**6 #MN

#The upward force - total
    Fb_tot = (Fb_left + Fb_right)  #kN

    return Fb_tot
```

Figure K.23: Python module computing the downward buoyancy force of the gate.

```
def Buoyance_downward(A1, A2, A3, B_gate, H_GateBottom, B_MLK, H_sill, SS, SLR):
    rho_saltwater = 1025
    g = 9.81    #m/s2
    A = B_MLK * B_gate   #m2

    if SLR < 1.0:
        hwl_behind = 3.00
    if 1.0 <= SLR < 2.0:
        hwl_behind = 3.80
    if SLR >=2.0:
        hwl_behind = 4.55

    Fw_cr = (rho_saltwater * g * (hwl_behind - H_GateBottom + H_sill) * A/2 )/10**6 #MN

    Fw_fill_1 = A1 * B_MLK * rho_saltwater * g
    Fw_fill_2 = A2 * B_MLK * rho_saltwater * g
    Fw_fill_3 = A3 * B_MLK * rho_saltwater * g
    Fw_fill = (Fw_fill_1 + Fw_fill_2 + Fw_fill_3)/10**6 #MN

    Fdown_empty = Fw_cr
    Fdown = Fw_cr + Fw_fill
    return Fdown, Fw_cr
```

Figure K.24: Python module computing the downward buoyancy force of the gate.

K.6. WAVES

K.6.1. WAVE CHARACTER

```
def Wave_character_sea(Hs, delta_H):
    g = 9.81
    if Hs/delta_H < 5:
        Tp = 3.6*np.sqrt(Hs)                        #Peak period of the significant wave heigh

    omega = 2*np.pi/Tp                             #Angular frequency of the waves [rad/s]

    #Shallow water
    L1 = Tp*np.sqrt(g*delta_H)                      #Wave length [m]
    if delta_H/L1 < 1/20:
        L = L1                                      #Wave length [m]
        c = L/Tp                                    #Wave celerity [m/s]
        #print('Shallow water')

    #Transitional water depth
    x = symbols('x')
    def transitional(x):
        return -(omega)**2 + g*x*(tanh(x*delta_H))#Wave length [m]

    n = lambdify(x, x-transitional(x)/diff(transitional(x),x))
    xi = 2.0
    cnt = 0
    while abs(transitional(xi)) > 10.0**(-10):
        cnt = cnt+1
        xi = n(xi)
    L2 = (2*np.pi)/xi

    if 1/20 < delta_H/L2 < 1/2:
        L = g*Tp**2/(2*np.pi)*np.tanh(xi*delta_H)   #Wave length [m]
        c = L/Tp                                    #Wave celerity [m/s]
        #print('Transitional water')

    #Deep water
    L3 = g*Tp**2/(2*np.pi)                         #Wave length [m]
    if delta_H/L3 > 1/2:
        L = g*Tp**2/(2*np.pi)                       #Wave length [m]
        c = L/Tp                                    #Wave celerity [m/s]
        #print('Deep water')

    k = 2*np.pi/L                                  #Wave number [-]
    a = Hs/2                                       #Amplitude at sea level [m]
    ab = Hs/(2*np.sinh(k*delta_H))                 #Amplitude at bottom [m]

    u_hat_b = omega * ab                            #Orbital velocity at the bottom [m/s]
    alpha_inc = 0                                  #Angle of attacking waves [degrees]
    phi_inc = (90+alpha_inc)/180*np.pi             #Angle between waves and current [rad]

    return L, k, c, u_hat_b, ab
```

Figure K.25: Python module computing the characteristics of the significant waves at the seaside.

```
def Wave_character_river(Hs_river, WL_river):
    g = 9.81
    if Hs_river/WL_river < 5:
        Tp = 3.6*np.sqrt(Hs_river)                          #Peak period of the significant wave height[s]

    omega = 2*np.pi/Tp                              #Angular frequency of the waves [rad/s]

    #Shallow water
    L1 = Tp*np.sqrt(g*WL_river)                      #Wave length [m]
    if WL_river/L1 < 1/20:
        L = L1                                      #Wave length [m]
        c = L/Tp                                    #Wave celerity [m/s]
        #print('Shallow water')

    #Transitional water depth
    x = symbols('x')
    def transitional(x):
        return -(omega)**2 + g*x*(tanh(x*WL_river))#Wave length [m]

    n = lambdify(x, x-transitional(x)/diff(transitional(x),x))
    xi = 2.0
    cnt = 0
    while abs(transitional(xi)) > 10.0**(-10):
        cnt = cnt+1
        xi = n(xi)
    L2 = (2*np.pi)/xi

    if 1/20 < WL_river/L2 < 1/2:
        L = g*Tp**2/(2*np.pi)*np.tanh(xi*WL_river)   #Wave length [m]
        c = L/Tp                                    #Wave celerity [m/s]
        #print('Transitional water')

    #Deep water
    L3 = g*Tp**2/(2*np.pi)                          #Wave length [m]
    if WL_river/L3 > 1/2:
        L = g*Tp**2/(2*np.pi)                       #Wave length [m]
        c = L/Tp                                    #Wave celerity [m/s]
        #print('Deep water')

    k = 2*np.pi/L                                   #Wave number [-]
    a = Hs_river/2                                    #Amplitude at sea level [m]
    ab = Hs_river/(2*np.sinh(k*WL_river))              #Amplitude at bottom [m]

    u_hat_b = omega * ab                             #Orbital velocity at the bottom [m/s]
    alpha_inc = 0                                   #Angle of attacking waves [degrees]
    phi_inc = (90+alpha_inc)/180*np.pi              #Angle between waves and current [rad]

    return L, k, c, u_hat_b, ab
```

Figure K.26: Python module computing the characteristics of the significant waves at the riverside.

```
def Waves_Sea_velocities(H_sill, delta_H, Hs, SS, SLR, u_c, dn50):
    g = 9.81
    #Induced by waves
    h0 = H_sill + SLR                    #Original water depth under the worst conditions

    #Determine wave length for hmax
    Lwave, kwave, c_wave, u_hat_b, ab = Wave_character_sea(Hs, delta_H)

    #Stone characteristics
    kr = 2*dn50 #Practical choice for statically stable protection - Schiereck [p.59]
    R = h0
    #Check validity of Chezy formula
    if ab >= 0.636*kr:
        cf = min(0.237*(ab/kr)**(-0.52),0.3)
        C = 18*np.log10(12*R/kr)        #[m0.5/s]
        #print('Conditions met')
    else:
        cf = 0.3
        C = 18*np.log10(12*R/kr)        #[m0.5/s]
    r0 = 1.2*np.sqrt(g)/C          #Schiereck [p.95]
    fc = C/40
    if fc > 1:                      #Schiereck [p.95]
        fc = 1
    alpha = max(1.5+ 5*r0*fc,2)    #Schiereck [p.95]
    psi_c = 0.055                           #Value at which particles are moving, 0.03 deemed too safe
    Delta = 1.585                           #Relative density

    #Shear velocities
    angle = 0                               #Angle of attack
    phi = (90 + angle)*np.pi/180            #Radian of attack

    #u_c = 2.6                               #Tidal velocity - http://www.wetwetwet.nl/stroomatlas/
    u_hat_b                                 #Orbital velocity at bottom
    u_star_c = np.sqrt(g)/C * u_c #Shear velocity due to current
    u_star_b = np.sqrt(cf/2) * u_hat_b #Shear velocity due to waves

    u_star_r = np.sqrt(u_star_c**2 + u_star_b**2 + 2*u_star_b*u_star_c*np.sin(phi))
    return u_star_r, alpha, r0, fc
```

Figure K.27: Python module computing the shear velocities over the bed protection due to waves on the seaside.

K.6.2. SIGNIFICANT WAVE HEIGHT

```
def Significant_Design_WaveHeight(U10, Fetch, Duration):
    g = 9.81
    H_inf = 0.24
    d_fetch = 25
    F_dash = (g * Fetch)/U10**2
    d_dash = (g * d_fetch)/U10**2
#The significant wave height estimation without data Voorendt [p.96]
    H_dash = H_inf *(np.tanh(0.343*d_dash**1.14) * tanh((4.41*10**(-4) * F_dash**0.79)
                                                        /(np.tanh(0.343*d_dash**1.14))))**0.572
    Hm0 = H_dash * U10**2 / g
    Hs = Hm0 #[m]

#The design wave height Voorendt [p.97]
    T_storm = Duration*3600
    T_wave = 8.4
    N = T_storm/T_wave

    Pr_H_Hd = 0.1
    Hs = Hm0
    Hd = np.sqrt(np.log(np.log((Pr_H_Hd - 1)*-1)/-N)/-2)*Hs
    print('The design wave height:', round(Hd,2))

    return Hs, Hd
```

Figure K.28: Python module computing the significant wave height.

K.6.3. WAVE IMPACT

```
def Wave_Impact_Sea(Hs, k_sea, B_MLK, delta_H):
    g = 9.81
    rho_saltwater = 1025
    WL = delta_H                #Is the water level at the center of the wave sinusoidal

    d1 = delta_H - 0.5*Hs
    p_maxA = 2*rho_saltwater*g*Hs    #N/m
    p_bottomB = p_maxA/cosh(k_sea*d1)  #N/m

    FtopA = 0.5*p_maxA*Hs #N/m
    FbottomB = (p_bottomB + p_maxA/2)*WL #N/m
    F_wavesgate = (FtopA+FbottomB)/1000 #*B_MLK #kN

    A_arm_bottom = Hs/3 + WL
    B_arm_bottom_rec = 0.5*WL
    B_arm_bottom_tri = 2/3*WL

    Ma_bottom = FtopA * A_arm_bottom
    Mb_bottom_rec = p_bottomB*WL * B_arm_bottom_rec
    Mb_bottom_tri = (p_maxA-p_bottomB)/2*WL * B_arm_bottom_tri

    return F_wavesgate, FtopA, p_maxA, p_bottomB
```

Figure K.29: Python module computing wave impact on the gate on the seaside of the barrier.

```
def Wave_Impact_River(Hs_river, k_river, B_MLK, WL_river, hwl_behind):
    g = 9.81
    rho_saltwater = 1025
    WL = hwl_behind       #Is the water level at the center of the wave sinusoidal

    d1 = WL - 0.5*Hs_river
    p_maxA = 2*rho_saltwater*g*Hs_river    #N/m
    p_bottomB = p_maxA/cosh(k_river*d1)  #N/m

    FtopA = 0.5*p_maxA*Hs_river #N/m
    FbottomB = (p_bottomB + p_maxA/2)*WL #N/m
    F_wavesgate = (FtopA+FbottomB)/1000 #*B_MLK #kN

    A_arm_bottom = Hs_river/3 + WL
    B_arm_bottom_rec = 0.5*WL
    B_arm_bottom_tri = 2/3*WL

    Ma_bottom = FtopA * A_arm_bottom
    Mb_bottom_rec = p_bottomB*WL * B_arm_bottom_rec
    Mb_bottom_tri = (p_maxA-p_bottomB)/2*WL * B_arm_bottom_tri

    return F_wavesgate, FtopA, p_maxA, p_bottomB
```

Figure K.30: Python module computing wave impact on the gate on the seaside of the barrier.